MECHANICAL FAILURE OF BONE AND ANTLER:

THE ACCUMULATION OF DAMAGE

Volume two, of two volumes

Andrew James Sedman

Thesis submitted for the degree of Doctor of Philosophy

Department of Biology, University of York

September 1993

TABLE OF CONTENTS

Volume II

APPENDIX 1

THE AJS/BBC DATA COLLECTION SYSTEM

All tensile, notch sensitivity and three-point-bending tests described within this thesis were performed using an Instron 1122 material testing machine. This machine, in the configuration available for this work, has a single pen chart recorder. This arrangement was used for determining the load applied to the three-point-bending specimens. However, the inertia of the pen makes this system unsuitable for the tensile testing of brittle materials such as bone.

During the initial stages of this thesis the mechanical responses of tensile specimens were recorded using a dual beam X-Y storage oscilloscope (manufactured by Tektronix). This was connected by way of amplifiers to load and deformation transducers (manufactured by Instron). This was the standard equipment and method used in this laboratory. This system permitted only limited amounts of data regarding the rate, or the time, of certain events to be recorded. (The method available was to record the stress and stain values on both traces, slightly displaced. One trace had an additional pulsed input of known frequency. This method was used by Currey (1975).) The data were obtained from the oscilloscope in the form of a photograph, examples of which are shown in figure 1.011. Clearly this system is unsatisfactory if the extension of a specimen during a long term creep test is required, or the rate of application of stress or strain during a tensile test is needed. I therefore undertook the design and manufacture of a data collection system that would provide at least stress, strain and time data.[1] I chose to build a digital data collection system for a number of reasons:

a) The data can easily be stored (in a number of different locations).

b) It is possible to use some degree of automated analysis. For example regression analysis can be used for the calculation of slopes.

c) Storing the data in digital form permits different permutations of the data to be easily plotted and examined. Rates of change of stress and strain can also be examined with ease. The data plots can also be normalised and superimposed.

d) At a more practical level it was perceived that building a digital system would be cheaper and easier than building an analogue one. For the same reasons the system was based around a BBC model B micro computer, which was available within the laboratory.

---

[1]I would like to express my thanks to Brian Adamson for his assistance, especially for his suggestions of ways to reduce the noise in the system.

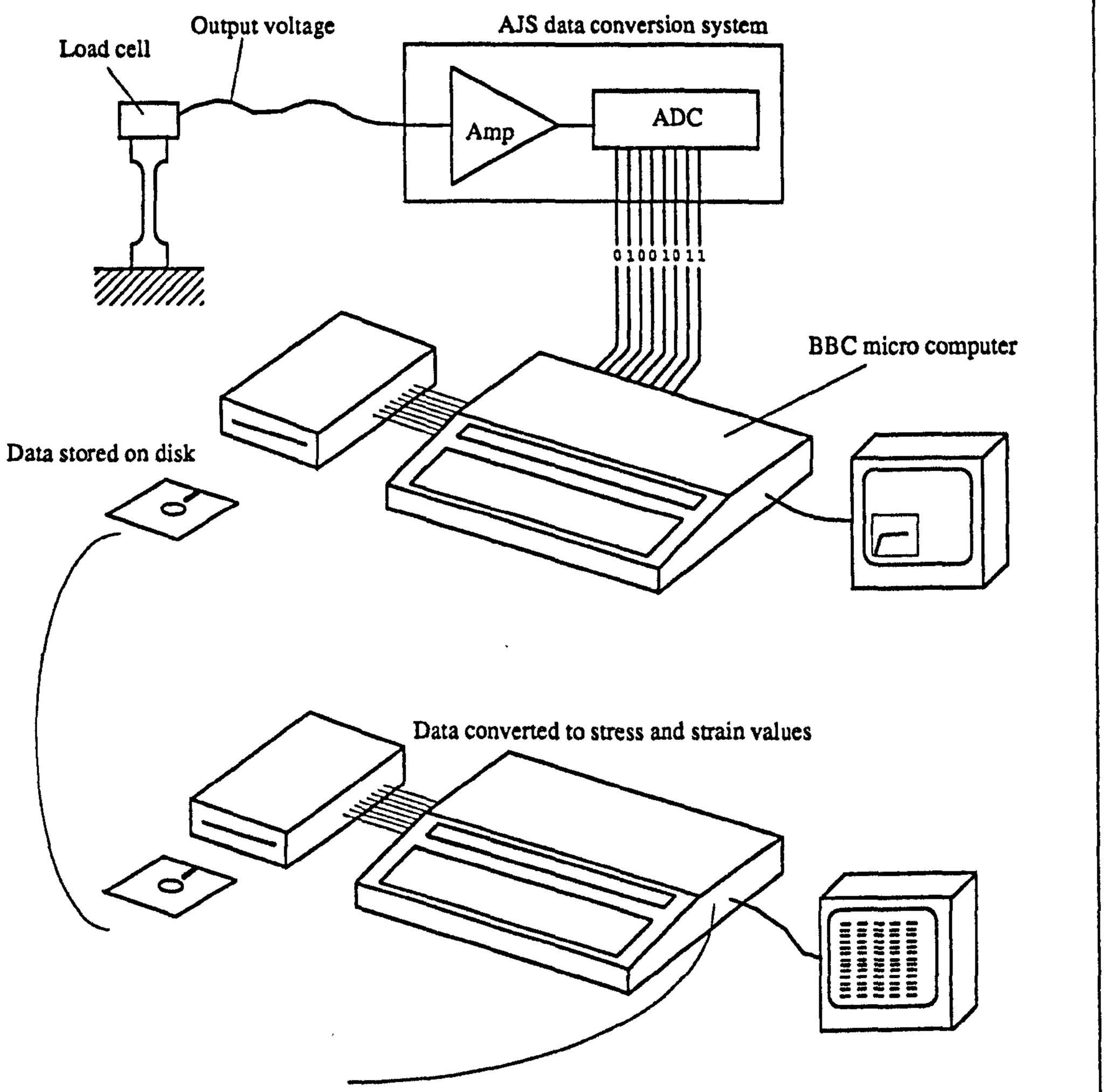

Figure A1.001

The basic stages in the collection of stress data by the BBC/AJS data collection system

The data collection system has two main components the BBC microcomputer and the data conversion system that I designed and built. The basic design of the data acquisition system can be explained by considering the stages the data pass through. These are listed below, using the load signal (channel 2) as an example. (The signal from the extensometer is treated in the same way.) This process is also shown diagrammatically in figure A1.001.

a) The load on the specimen is detected by a load cell. The change in the applied load is represented by a change in the output voltage of the transducer.[2]

b) The output voltage of the transducer is amplified so that its maximum expected range matches, or is less than, the maximum input voltage of the analogue-to-digital converter (ADC).

c) The size of the voltage, relative to the input range of the ADC, is converted into a binary number. The value of this number is also dependent on the number of steps or quantisation levels that range is divided into.

$$\text{Output number} = \frac{\text{Voltage input}}{\text{Voltage range}} \times \text{Number of quantisation levels}$$

d) ADC is prompted to produce a number (representing the amplified output voltage of the transducer) at certain intervals during the test. This number is then stored.

e) The stored numbers are converted into expressions of stress or strain. This is done by calibrating the system so that the size of the difference in the measured quantity represented by one quantisation level is known. This also requires that the first data points are recorded before any load is applied to the system, thus identifying one of the quantisation steps of the ADC as a zero level.

f) The data is then transferred to a VAX mainframe for permanent storage. Using programmes written for that computer the data is examined and various quantities, such as ultimate stress, determined.

The design of the AJS data conversion system is clearly more complicated than indicated in figure A1.001.[3] A number of design criteria were examined these can be summarised as.

a) How many transducers, or other recording channels were required?

b) How many quantisation levels should the ADC have? Normally the options are 256 or 4096 levels (an 8 of 12 bit converter).

c) How many ADCs were to be used: one for each transducer or a single one which sampled each of the transducers in turn?

d) If a single ADC was to be used, how were the errors resulting from sampling the different channels at different times to be avoided?

---

[2]Both the load cell and extensometers used in this work use strain gauges as the sensing elements, in the extensometer there are four active 120Ω gauges arranged in a Wheatstone bridge. Information on the excitation and output voltages are available in the form of a data sheet published by Instron.

[3]The initial design and prototypes were more complex than the system in the form it was used. Initially the gain of the amplifiers was under both manual and software control. When the input voltage to the ADC was approaching the maximum range of the chip the software instructed a multiplexer, which was in series with range of gain controlling resistors, to switch. However, the resistance of this system was not consistent. This resulted in unknown gains. The extra lines of programme slowed the data acquisition rate. Thus only pre-set gains where used in the final system.

e) If a single ADC was used, how would the multiplexer to be controlled? Similarly the ADC needs certain control signals.

f) How was the number produced by the ADC going to be transfered to, and stored in, the BBC micro?

The answers to these questions are interconnected. I needed at least two transducer inputs to the system, load and extension. I also wanted to record time data, but this was done by the computer, simply by noting the times at which the signals from the transducers were sampled. As part of my investigation was also to examine the optical changes in bone, and there was the possibility of using other transducers I decided to have four possible inputs built into the system. As the BBC micro is an 8 bit computer, the acquisition of data and its storage would be far simpler if an 8 bit ADC was used. However, this would give only 256 quantisation levels. Fortunately, an ADC supplied by Radio Spares (RS574AJ) can be used in a number of configurations, as a standard 12 bit or 8 bit converter or as a 12 bit converter wired so that only the upper 8 bit or the lower 4 bits are enabled at once. In the last configuration a 12 bit number can be sent, read and stored as two 8 bit numbers.[4] Later these numbers can be reconstructed to form the full 12 bit number again. I decided to use only one of this type of ADC, this decision was based on: the cost of the ADC; the more complex software control that would be needed to switch a digital rather than an analogue signal and the realisation that the time advantage of using a single ADC per channel was small. To avoid the problem of obtaining the values from the various transducers at different times a *sample-and-hold* chip was placed between the amplifier and the multiplexer for each channel. Thus the signal from each transducer could be sampled at the same (recorded) time. The voltage was maintained by the sample-and-hold chip until it had been converted to a digital signal. This requires that the sample-and-hold chips and the multiplexer were under the control of the BBC micro computer. I used the printer port for the outgoing control signals. The voltage level on a specific wire can be changed from high to low by writing the appropriate number to the memory location associated with the printer port. Similarly I used the computer's user port to read the digital output of the ADC. (As mentioned in a footnote above initially other control features were included, these are not reported here, but they did place further constrains on the design.) The data was stored in the BBC micro computer by writing it directly to memory. To enable sufficient data to be stored the memory was expanded using a 32K ram extension board (supplied by Watford Electronics).

---

[4]More accurately they are one 8 bit and one 4 bit number. However, they were both stored as individual bytes, or 8 bit numbers.

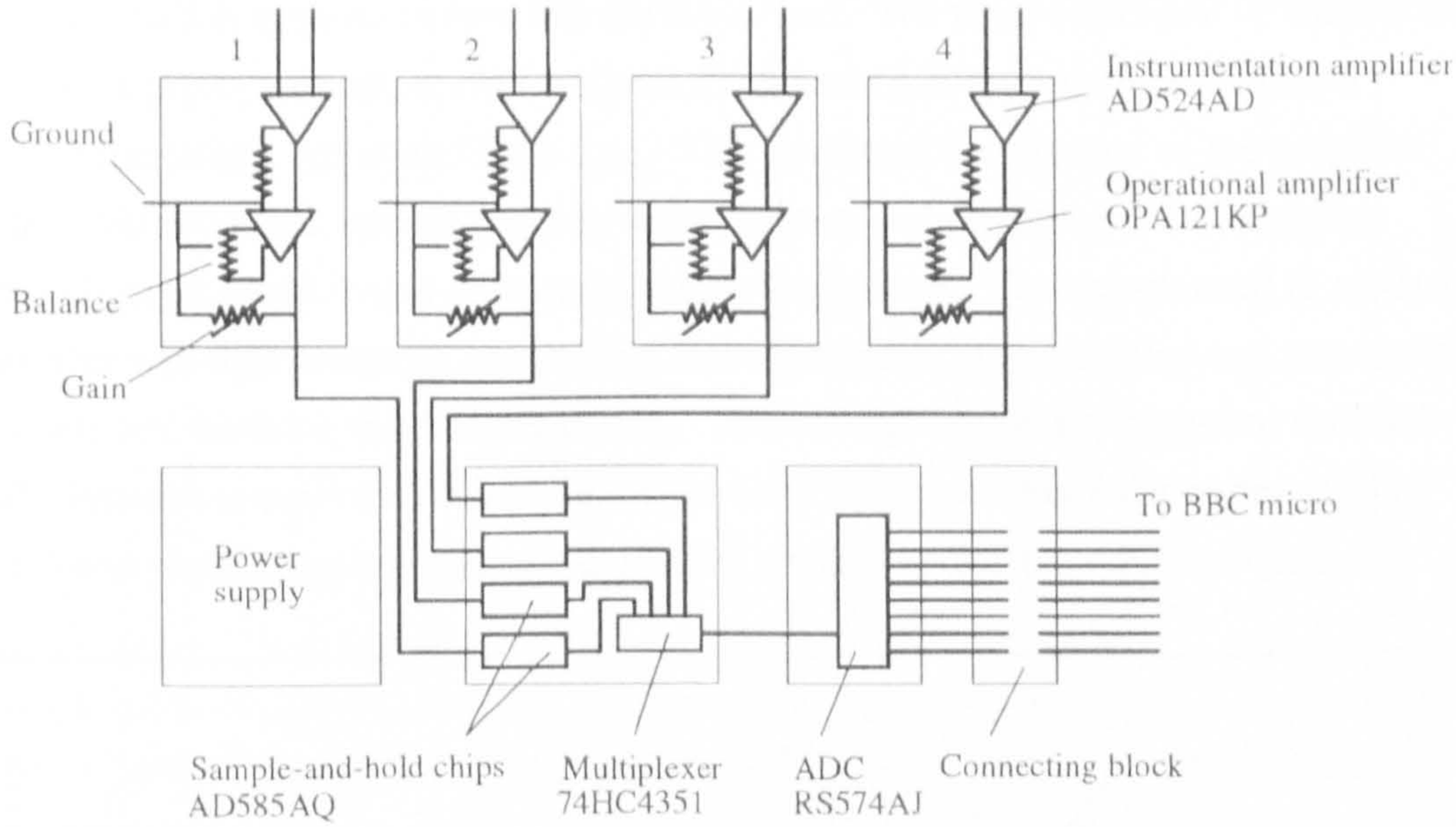

In this diagram a similar arrangement to that of the components of real equipment (shown in figure A1.003) has been used.

Figure A1.002

Schematic representation of the data conversion system in its original form

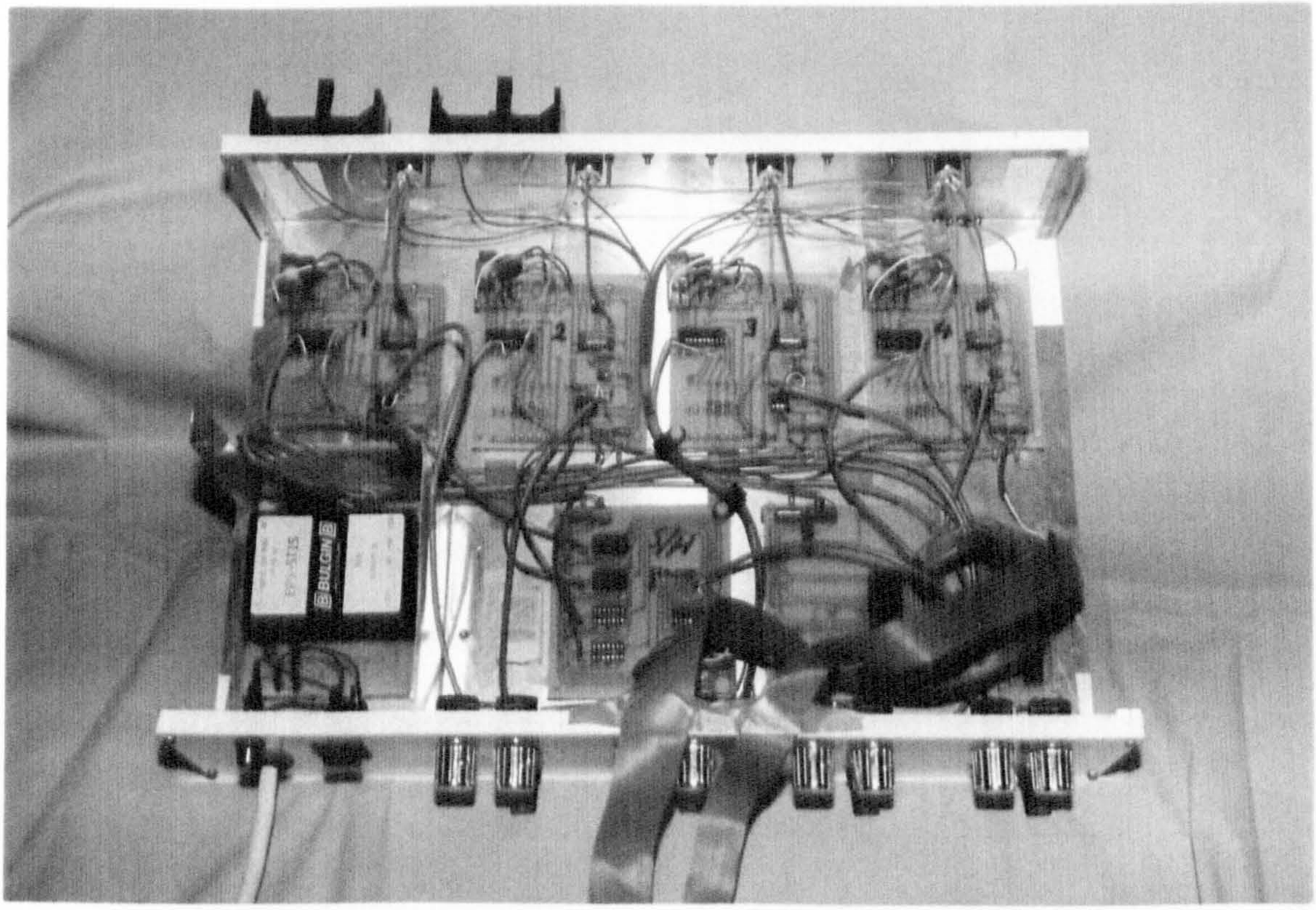

Figure A1.003

The data conversion system in its original form

A schematic representation of the data conversion system is given in figure A1.002, and a picture of the practical arrangement is given in figure A1.003. Some adaptations to this system were made during its use. The most important of these enabled the instant a photo was taken with a standard 35 mm SLR camera to be recorded alongside the stress, strain and time data. This involved the removal of the amplifier from the third channel, and its replace with a battery and capacitor. The capacitor became charged when it was connected across the battery. The switch used to make this connection was that normally controlling the flash gun.[5] The capacitor was in parallel with a resistor, hence it discharged slowly. The voltage across the capacitor was fed directly into the sample-and-hold chip of the third channel. When the output of this channel was plotted against time a clear spike marked each frame that was taken.

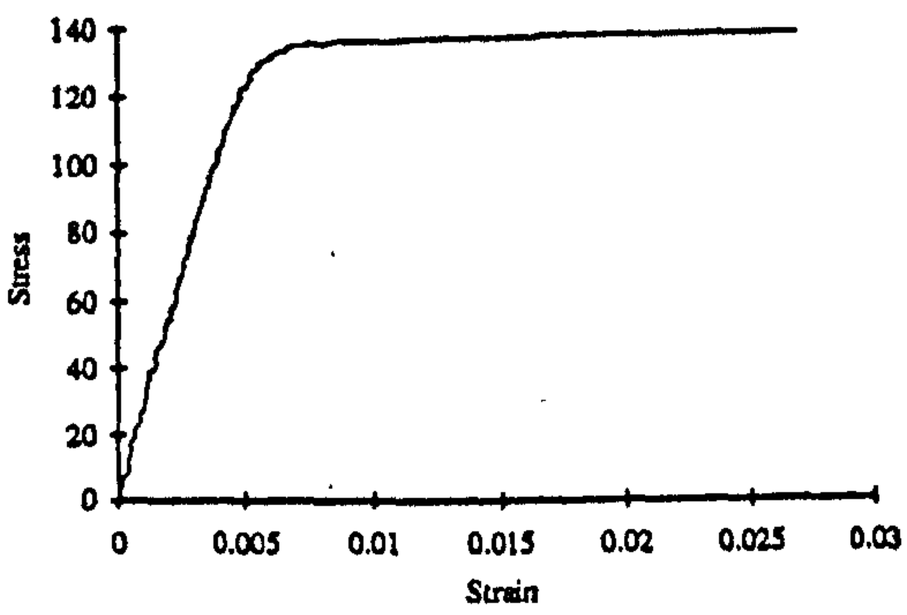

a)

Stress-strain plot
(Channel 2 and channel 1)

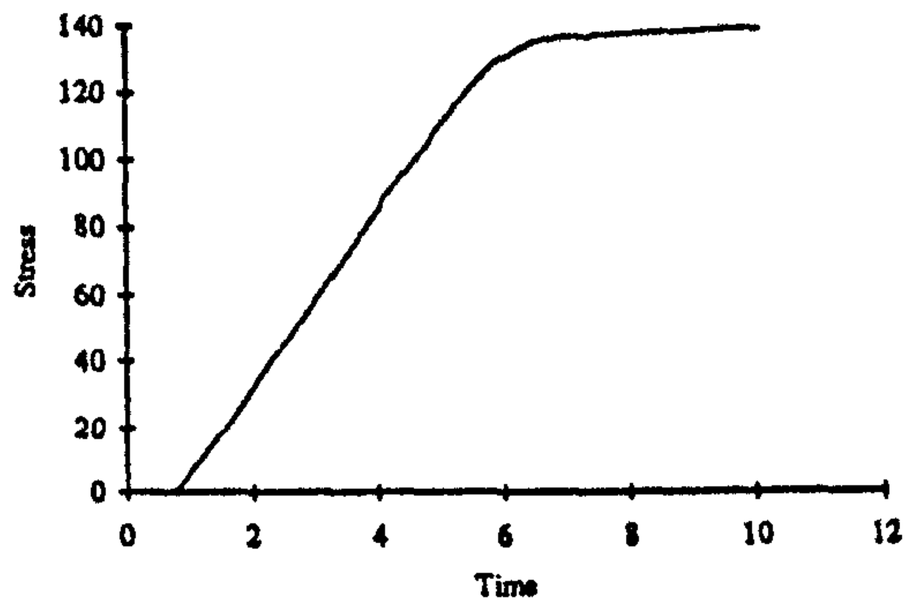

b)

Stress-time plot
(Channel 2 and computer data)

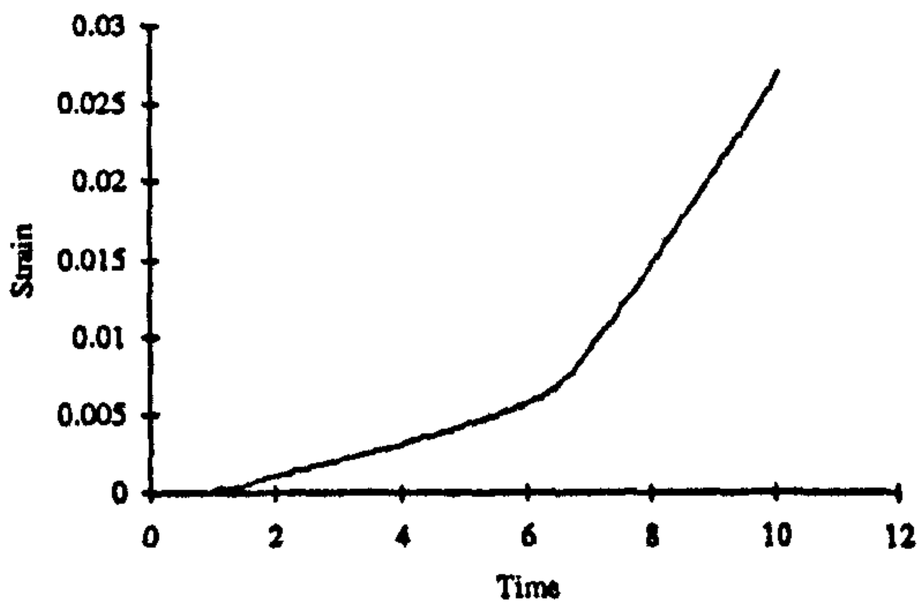

c)

Strain-time plot
(Channel 1 and computer data)

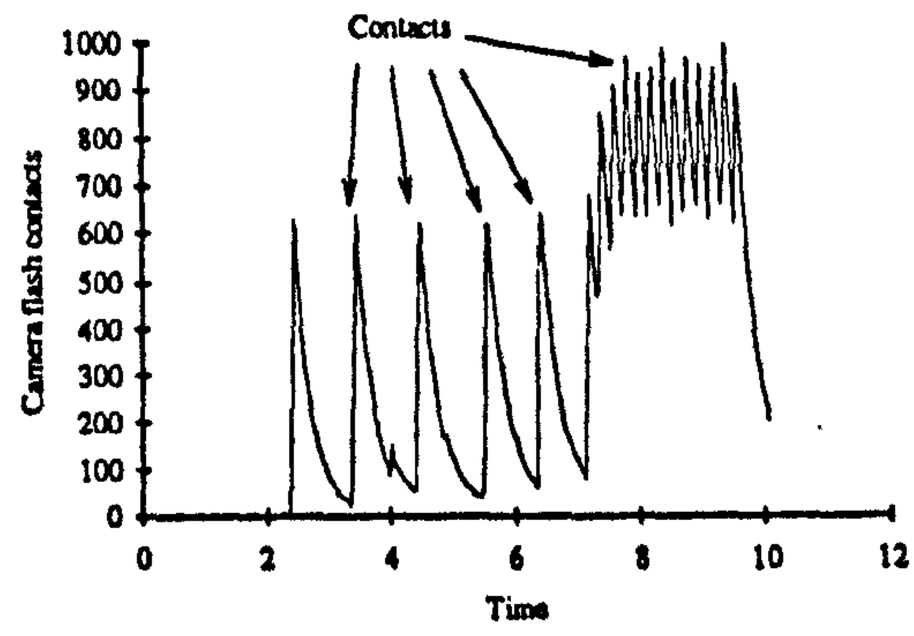

d)

Photo timing plot
(Channel 3 and computer data)

Plots of raw data obtained (up to the point of failure) obtained by the AJS/BBC data collection system. The data shown was obtained from a specimen of bovine femoral bone, 03/10/91/16. (This data is also used in chapter 8, where the spikes of figure d have been use to relate the photographic images with the mechanical behaviour shown in figures a, b and c.)

Figure A1.004

Plots of data obtained from the AJS/BBC data collection system after the system had been converted to obtain data on the timing of photographic recordings

[5]I thank Dr Peter Zioupos for suggesting this very successful arrangement.

There is no point in including all the programmes that were used to calibrate, collect and analyse the data. This is because the exact way the numbers are read from, or written to, the input and output ports of the computer is determined by the position of the wires. A full wiring diagram is not given here as such detail is considered excessive. However, one of the data acquisition programmes is included as an example. The other programmes will be described briefly, in the same order in which they were used.

The first programme used in a series of tests is the calibration programme. The aim of this programme is to determine the amount of the measured quantity that is represented by a quantisation level. This is achieved by a number of stages;

a) The equipment is set-up in the arrangement in which it will be used in the test, the correct load cell, specimen grips, extensometer and so on.

b) After the programme is started no further action is permitted for at least 10 minutes. This permits the electronics and transducers to warm-up and stabilise.

c) The operator is asked which channel is to be calibrated and its units. These units are arbitrary. In this study consistent units were used, in the case of the load cell newtons and for the extensometer millimetres. The programme then displays a small region of high resolution screen where the value read from the ADC for that channel is plotted against time.

d) The balance of the amplifiers is altered, if required, so the input value, shown pictorially on the computer monitor is in the required position.

e) The programme asks for a key to be pressed when the zero level is set. When this occurs 10 successive values are obtained from the ADC. The mean and standard deviation of these values are calculated, displayed and stored.

f) The operator is now asked to change the quantity measured by the transducer by a know amount. For example, more mass could be hung from the load cell. This amount is then entered into the computer in the units already chosen. The induced change was normally of a size that approach the full scale deflection. (The full scale deflection having already been set, by changing the gain of the amplifiers, to an appropriate level for the later tests by a similar process.)

g) On pressing another key, 10 values are obtain as in stage e.

h) The size of the change applied to the transducer is divided by the difference in the two mean quantisation levels. This gives a value of units per quantisation level.

i) Stages e to h are repeated five times. The zero level may be the same, by removing the mass, or increments in mass can be used (or the extension in the case of the extensometer).

j) The results of the five calibrations are then presented together with an overall mean value. It is this mean value that is used as the calibration factor. (The values from the five cycles were examined for consistency and any signs of drift.) All these results were then recorded.

The data acquisition programme used was dependant on the type of test and the number of channels that were in use. For example to get the maximum sampling rate the programme needs the minimum number of operations between successive samples. However, during a creep test such a high sampling rate would result in the memory becoming full before the tests had finished. (When two channels are sampled a maximum of about 2500 sets of data can be collected. With more channels in use the memory reaches its full capacity after storing fewer data sets.) Two basic programmes were used for tensile testing. The programme normally used, shown in figure A1.005, contains a procedure by which the operator can reduce the sampling rate by pressing a key (lines 412 and 600). The other programme used had this procedure and some other lines removed to get the highest possible sample rate with this system, about 38 Hz. The programme used for creep testing initially collected data at the fastest possible rate, in one for-next loop. The programme then collected data using a second programme loop, containing a delay that increased exponentially with each cycle. (The power term used was 1.001.)

The programme given in figure A1.005 is that used in the majority of the tensile tests described in this thesis. Lines 10 to 75 set-up the system, the graphics mode of the monitor (line 10) and the area of the screen this mode applies to (line 20). Within this region the output from the transducers is later plotted. Only part of the screen is used to reduce the amount of memory required to run the programme. The main body of the programme is in lines 90 to 415. This is a loop that is repeated 'FOR N% = 10000 TO 30450 STEP 8'. (The integer number N% is not only used as a step counter, but also indicates the memory location at which the numbers are stored.) The sample-and-hold chips, the multiplexer and ADC are triggered by line 120. Line 130 is a loop that repeats until the ADC signals that it has completed the conversion. The 12 bit number is then read and stored in two parts by lines 140 and 160. (Line 150 signals the ADC to supply the second number.) This process, bar the sampling, is now repeated for the second input in lines 170 to 210. Line 400 instructs the computer to store the time, starting at memory location N%+4. The time requires 4 bytes of storage space. (Hence the loop being in steps of 8 bytes.) Line 410 plots the point on the screen, channel 1 is used as the X-axis and channel 2 as the Y-axis. Line 411 prints the number of points that have been stored (this line was removed in some cases to increase the speed of the programme). Line 412 checks if a key has been pressed. The programme pauses at this line for T% multiples of 0.01 seconds. If no key has been pressed the programme is returned to the start of the loop by line 415. If the space bar has been pressed (ASCII value 32) the programme is stopped, a zero value is recorded in the byte where the next time value was to be placed (line 710). This zero is used by the programme the converts the data to stress and strain to mark the end of the data set. If '1', '2', '3', '4', '5', '6', '7', '8', or '9' are pressed then that number of hundredths of a second is added to the time the programme waits in line 412.

If '0' is pressed the sample frequency is returned to its original rate. When this loop is finished the execution of the programme moves onto line 580, and then to line 585. The latter line instructs the data stored in the computer's memory to be saved onto a disk, for later retrieval and convention.

```
 10 MODE0:T%=0
 20 VDU24,19;19;501;501;
 30 MOVE19,19
 40 PLOT21,19,501:PLOT21,501,501:PLOT21,501,19:PLOT21,19,19
 60 TIME=0
 70 ?&FE6C=14
 75 *FX 15,1
 90 FOR N% = 10000 TO 30450 STEP 8
120 ?&FE61=1:?&FE61=65:?&FE61=1:?&FE61=65
130 REPEAT:UNTIL?&FE6D=8
140 ?(N%)=?&FE60
150 ?&FE61=192
160 ?(N%+1)=?&FE60
170 ?&FE61=9:?&FE61=73:?&FE61=9:?&FE61=73
180 REPEAT:UNTIL?&FE6D=8
190 ?(N%+2)=?&FE60
200 ?&FE61=192
210 ?(N%+3)=?&FE60
400 !(N%+4)=TIME
410 PLOT69,(?(N%)-4.5)*2.5,(?(N%+2)-4.5)*2.5
411 PRINT TAB(0,0) "DATA  SET NUMBER ";(N%-10000)/8
412 U%=INKEY(T%)
415 IF U%= -1 THEN NEXT ELSE GOTO 600
580 PRINT"END OF DATA COLLECTION"
585 *SAVE DATA1 2710 7710
590 END
600 T%=T%+U%-48
605 *FX 15,1
606 IF U%=48 THEN T%=0
610 IF U%=32 THEN GOTO 700
620 NEXT
700 FOR I = 8 TO 16
710 ?(N%+I)=0
720 NEXT I
730 GOTO 580
```

Figure A1.005

The data collection programme used for tensile tests were stress, strain and time data were required

The data retrieval and conversion programme essentially works in reverse to the data collection programme. First the data is transferred back from disk to the memory locations it came from. Then the memory locations are read in order, the full numbers are reconstructed and the number associated with the initial zero level subtracted from them. These numbers are then multiplied by the calibration factors appropriate for the required output. This calibration factor is requested by the programme. If the values obtained from the calibration programme are used directly the output (in this case) will be expressed in units of Newtons and millimetres. Therefore, the calibration factor is corrected (by the dimensions of the specimen recorded at the time of testing) to produce data in the form of stress and strain. This is explained to the operator by the opening lines of the programme, shown in figure A1.006.

A number of features can be determined by simple examination of the raw data (represented in table A1.001). For example, the specimen failed between 1.15 and 1.18

seconds after the start of data collection. To obtain more measurements of certain mechanical properties the data was transferred to a VAX mainframe. There it was analysed using a programme linked to the Simpleplot graphics package.[6] This combination of programme and graphics package permits the data to be plotted and simple analysis performed. The main stages of this analysis are shown by a number of screen dumps presented in figures A1.007a to A1.007n. The raw data can also be imported into other plotting packages, or for data analysis.[7]

```
   10 MODE0:@%=&1040A
   20 PRINT "IF YOU ENTER THE CALIBRATION FACTOR FROM THE CALIBRATION PROGRAM THE DATA "
   30 PRINT "WILL BE CONVERTED TO THOSE UNITS.  THUS IF THE STRAIN AND NOT THE EXTENSION
IS"
   40 PRINT "REQUIRED THE CALIBRATION FACTOR SHOULD BE DIVIDED BY THE GAUGE LENGTH,"
   50 PRINT "LIKEWISE FOR OTHER INPUTS, LOAD/STRESS etc."
   70 PRINT "THE FIRST 4 POINTS ARE USED FOR FINDING THE ZERO LEVEL"
  120 INPUT "COMMENTS . . . ." C
  130 INPUT "WHAT IS THE CALIBRATION FACTOR FOR INPUT 1 ?" CF1
  140 INPUT "WHAT IS THE CALIBRATION FACTOR FOR INPUT 2 ?" CF2
        .                                .                                .
        .                                .                                .
        .                                .                                .
```

Figure A1.006

The opening lines of the data conversion programme for two channels

As each set of data is converted (in this example) to stress, strain and time it is saved onto disk as a text file. Table A1.001 contains a full set of data (for specimen 01/11/91/44, the results from which are contained in data set TB1. This example is used because the specimen was tested at a higher than normal cross-head speed thus the number of data points is small). The data is arranged in six columns in order they contain: strain (unitless), stress (in MPa), the third input (sometimes used for camera timing data, but not used in this example), fourth input (not used in this example), time (in seconds) and the last column indicates the row number.

---

[6]Produced by Bradford University Software Services Ltd.

[7]For example the one within the word processing programme used to write this thesis, Word for Windows 2 (Produced by the Microsoft Corporation). Most of the plots obtain from digital data obtain by the system described here that are presented in this thesis are plotted with this package. The data has also be read into Minitab for the fitting of mathematical models.

-5.500E-5	0.000E0	-1.000E0	-1.000E0	0.000E0	1
3.300E-5	0.000E0	-1.000E0	-1.000E0	3.000E-2	2
3.300E-5	0.000E0	-1.000E0	-1.000E0	6.000E-2	3
-1.100E-5	0.000E0	-1.000E0	-1.000E0	9.000E-2	4
3.300E-5	0.000E0	-1.000E0	-1.000E0	1.200E-1	5
-1.100E-5	1.808E-1	-1.000E0	-1.000E0	1.500E-1	6
1.210E-4	0.000E0	-1.000E0	-1.000E0	1.800E-1	7
-5.500E-5	0.000E0	-1.000E0	-1.000E0	2.100E-1	8
-5.500E-5	0.000E0	-1.000E0	-1.000E0	2.300E-1	9
1.870E-4	6.238E0	-1.000E0	-1.000E0	2.600E-1	10
4.290E-4	1.465E1	-1.000E0	-1.000E0	2.900E-1	11
8.250E-4	2.387E1	-1.000E0	-1.000E0	3.200E-1	12
9.570E-4	3.313E1	-1.000E0	-1.000E0	3.500E-1	13
1.441E-3	4.195E1	-1.000E0	-1.000E0	3.800E-1	14
1.595E-3	5.063E1	-1.000E0	-1.000E0	4.100E-1	15
1.969E-3	5.967E1	-1.000E0	-1.000E0	4.300E-1	16
2.277E-3	6.799E1	-1.000E0	-1.000E0	4.600E-1	17
2.585E-3	7.667E1	-1.000E0	-1.000E0	4.900E-1	18
2.937E-3	8.498E1	-1.000E0	-1.000E0	5.200E-1	19
3.201E-3	9.276E1	-1.000E0	-1.000E0	5.500E-1	20
3.641E-3	1.006E2	-1.000E0	-1.000E0	5.800E-1	21
3.707E-3	1.085E2	-1.000E0	-1.000E0	6.100E-1	22
4.169E-3	1.161E2	-1.000E0	-1.000E0	6.400E-1	23
4.411E-3	1.234E2	-1.000E0	-1.000E0	6.700E-1	24
4.873E-3	1.304E2	-1.000E0	-1.000E0	6.900E-1	25
5.269E-3	1.366E2	-1.000E0	-1.000E0	7.200E-1	26
5.753E-3	1.411E2	-1.000E0	-1.000E0	7.500E-1	27
6.633E-3	1.432E2	-1.000E0	-1.000E0	7.800E-1	28
7.909E-3	1.432E2	-1.000E0	-1.000E0	8.100E-1	29
9.361E-3	1.417E2	-1.000E0	-1.000E0	8.400E-1	30
1.090E-2	1.411E2	-1.000E0	-1.000E0	8.700E-1	31
1.248E-2	1.411E2	-1.000E0	-1.000E0	9.000E-1	32
1.391E-2	1.411E2	-1.000E0	-1.000E0	9.200E-1	33
1.532E-2	1.414E2	-1.000E0	-1.000E0	9.500E-1	34
1.673E-2	1.418E2	-1.000E0	-1.000E0	9.800E-1	35
1.796E-2	1.425E2	-1.000E0	-1.000E0	1.010E0	36
1.937E-2	1.431E2	-1.000E0	-1.000E0	1.040E0	37
2.069E-2	1.440E2	-1.000E0	-1.000E0	1.070E0	38
2.201E-2	1.449E2	-1.000E0	-1.000E0	1.100E0	39
2.324E-2	1.458E2	-1.000E0	-1.000E0	1.130E0	40
2.447E-2	1.469E2	-1.000E0	-1.000E0	1.150E0	41
2.582E-2	-3.255E0	-1.000E0	-1.000E0	1.180E0	42
5.158E-2	2.351E0	-1.000E0	-1.000E0	1.210E0	43
5.061E-2	2.983E0	-1.000E0	-1.000E0	1.240E0	44
5.026E-2	3.300E0	-1.000E0	-1.000E0	1.270E0	45
5.090E-2	2.712E0	-1.000E0	-1.000E0	1.300E0	46
5.065E-2	2.622E0	-1.000E0	-1.000E0	1.330E0	47
5.096E-2	2.803E0	-1.000E0	-1.000E0	1.350E0	48
5.092E-2	3.164E0	-1.000E0	-1.000E0	1.380E0	49
5.096E-2	3.074E0	-1.000E0	-1.000E0	1.410E0	50
5.074E-2	2.938E0	-1.000E0	-1.000E0	1.440E0	51
5.096E-2	2.893E0	-1.000E0	-1.000E0	1.470E0	52
5.090E-2	2.938E0	-1.000E0	-1.000E0	1.500E0	53
5.061E-2	2.983E0	-1.000E0	-1.000E0	1.530E0	54
5.092E-2	2.893E0	-1.000E0	-1.000E0	1.560E0	55
5.090E-2	2.712E0	-1.000E0	-1.000E0	1.580E0	56
5.074E-2	2.622E0	-1.000E0	-1.000E0	1.610E0	57
5.090E-2	2.622E0	-1.000E0	-1.000E0	1.640E0	58
5.090E-2	2.577E0	-1.000E0	-1.000E0	1.670E0	59
5.074E-2	2.622E0	-1.000E0	-1.000E0	1.700E0	60
5.070E-2	2.712E0	-1.000E0	-1.000E0	1.730E0	61
5.090E-2	2.803E0	-1.000E0	-1.000E0	1.760E0	62
5.070E-2	2.803E0	-1.000E0	-1.000E0	1.790E0	63
5.070E-2	2.712E0	-1.000E0	-1.000E0	1.810E0	64
5.074E-2	2.622E0	-1.000E0	-1.000E0	1.840E0	65
5.061E-2	2.622E0	-1.000E0	-1.000E0	1.870E0	66
5.061E-2	2.622E0	-1.000E0	-1.000E0	1.900E0	67
5.061E-2	2.622E0	-1.000E0	-1.000E0	1.930E0	68
-1.880E-2	-1.442E1	-1.000E0	-1.000E0	-2.000E-2	69

All the data sets sent to the VAX take the same format the two data columns not used here are filled with values of negative unity. This arrangement of data is that produced by the data conversion programme. The six columns of data in the order they are shown contain: strain, stress, camera timing data (not used here), fourth input (not used here), time in seconds, data line number. (Specimen 01/11/91/44, data stored as VID077.DAT)

Table A1.001

The full set of data as stored in the VAX for a specimen of bovine femoral bone

The data analysis programme (called Graph 3) asks for the name of the file where the data to be analysed is stored. In this example the data set used is that shown in table A1.001: VID077. (The date refers to the date of the last modification made to the programme.)

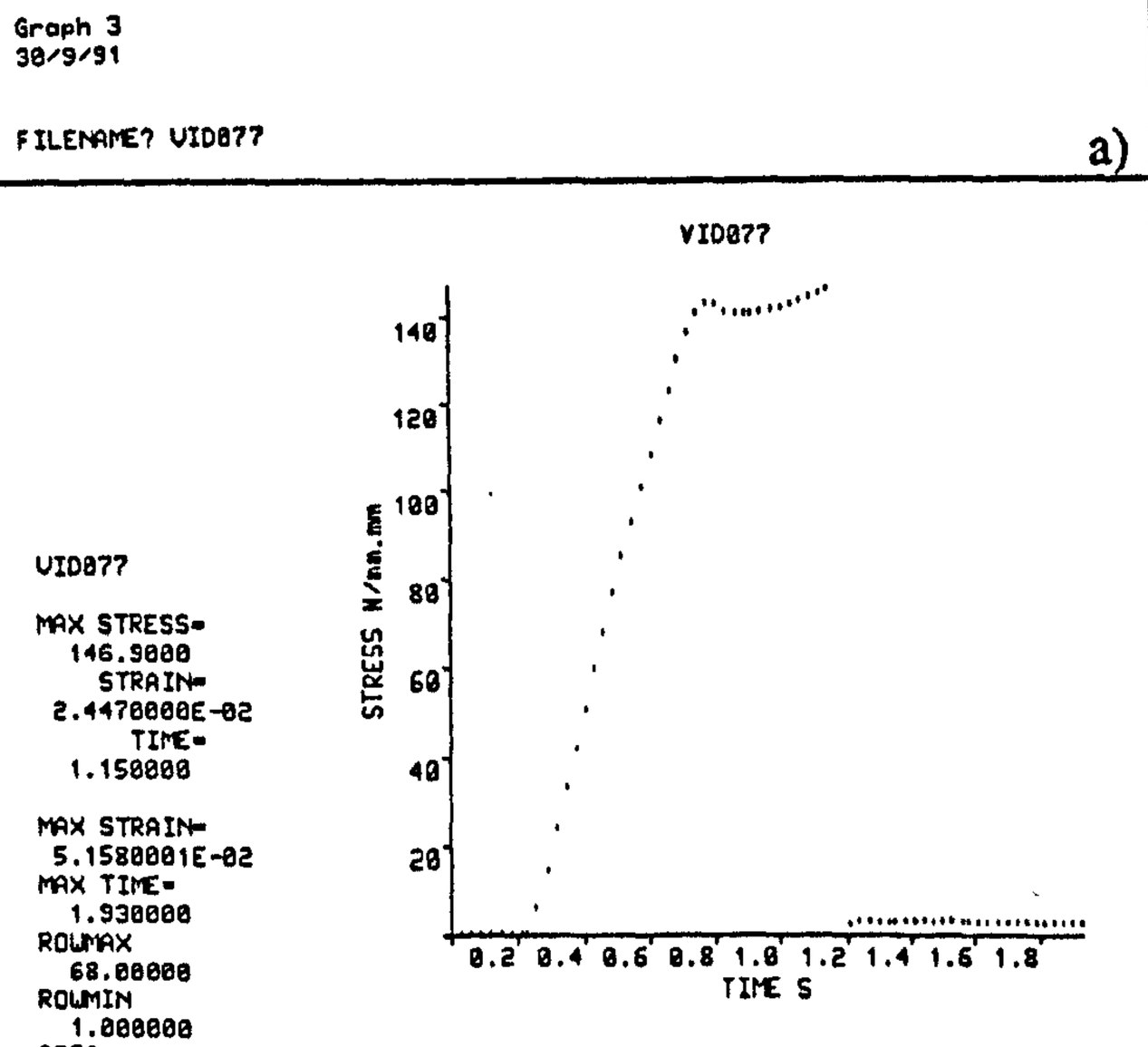

a)

The first plot produced is a stress-strain plot, and the axis labels are contained within the programme. The data values given are: the maximum stress, the strain and time when it occurred, the maximum strain, the time when it occurred, the last and first rows of data used and finally the area under the stress strain plot (by the trapezium rule).

b)

This plot is a strain-time plot. The data values given are the same as those above. This graph shows that these values have been obtained from the full data set and thus are not a true reflection of the mechanical behaviour.

c)

Figure 1.007 Continued below

Images of the computer screen at various stages of the data analysis programme

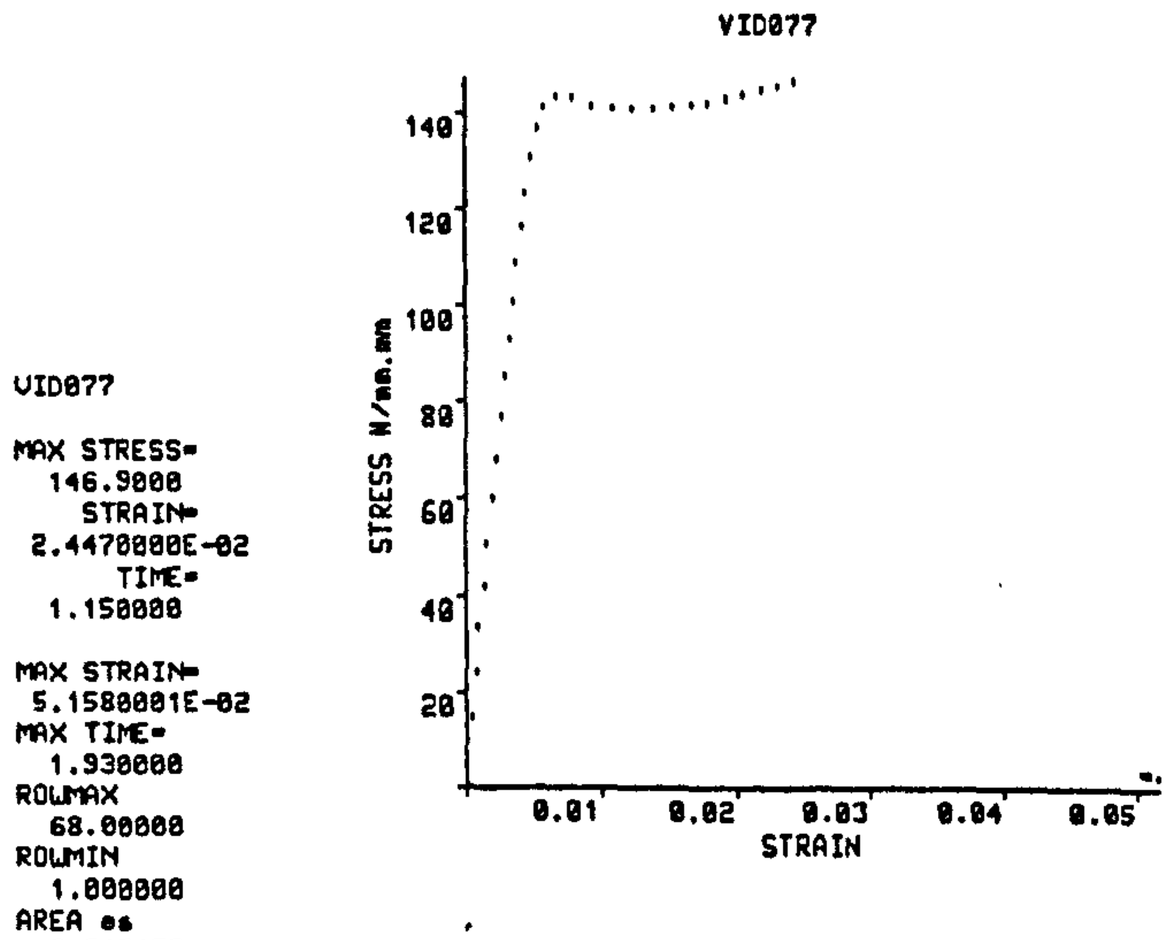

d)

This is a stress-time plot. The same comments made for the strain-time plot apply. Examination of the data obtained after the failure of the specimen can help to pinpoint errors. For example if the recorded load value was greater than that which could reasonably be attributed to that transmitted via the extensometer, the validity of the data would be questioned.

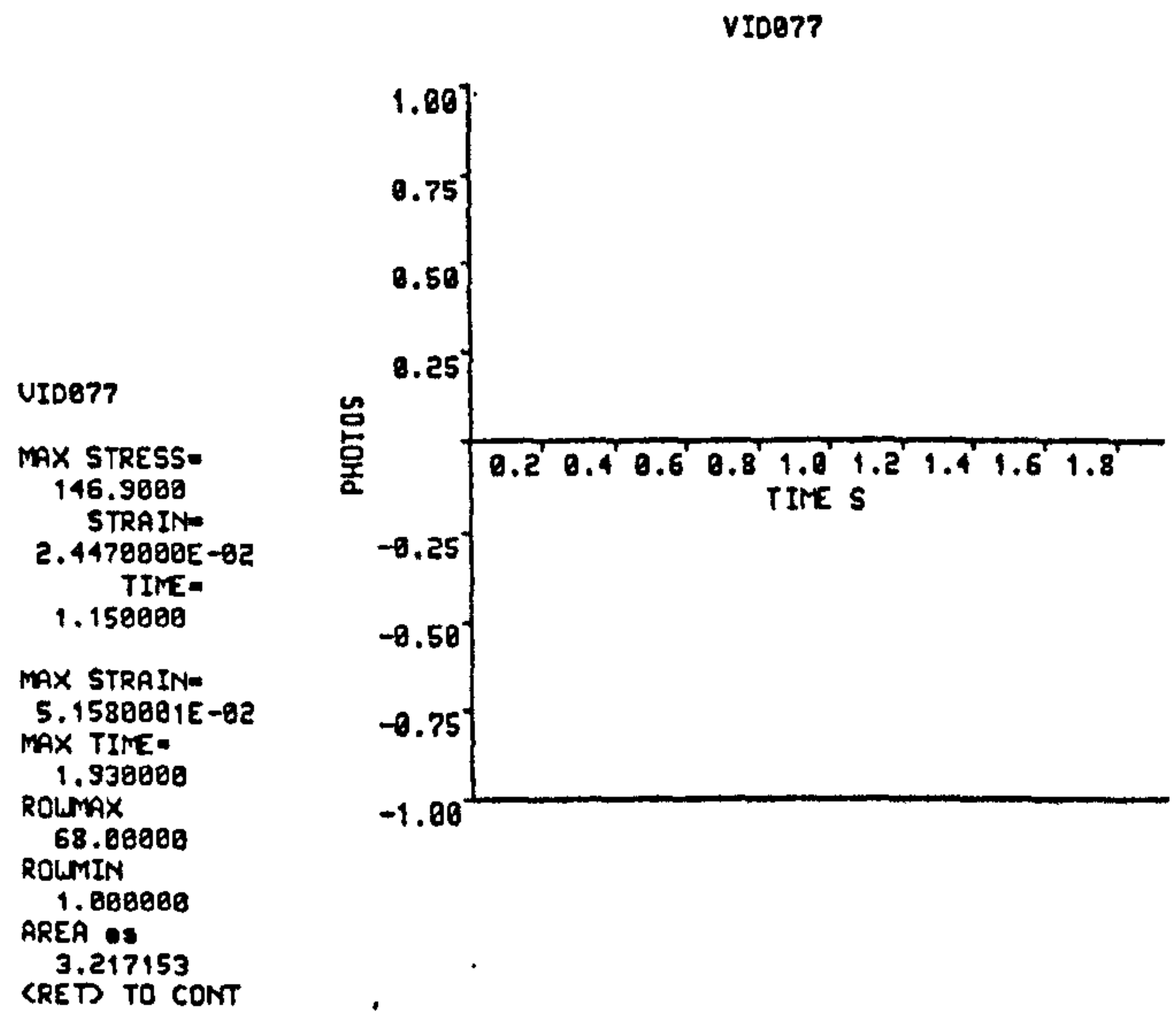

e)

The last plot automatically produced by the programme on the full set of data shows the output of the third channel. This channel is not used in this case so all the values are set to -1. When it is in use for recording the timing of photographs it contains the number obtained from the ADC for that channel. (See figure A1.004 for an example of its use.)

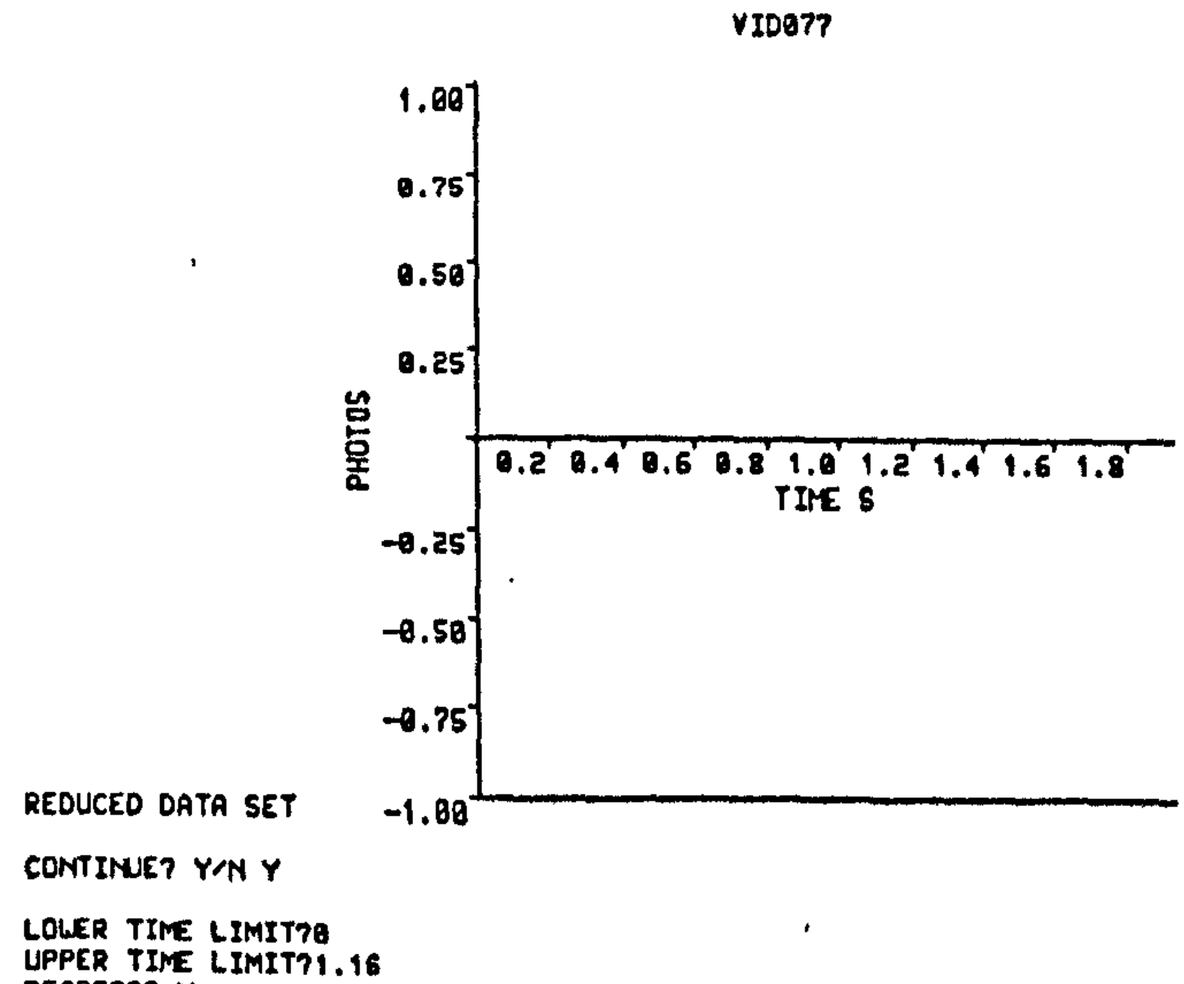

f)

The programme now enters an interactive stage or terminates depending on the operator's response, 'Y' or 'N'. If the operator enters 'Y' then the programme responds with a request for the lower and upper times of the data that are to be examined, in this case 0 and 1.16. The programme also asks if regression analysis is to be conduced on this data.

Figure 1.007 Continued from above and continued below

Images of the computer screen at various stages of the data analysis programme

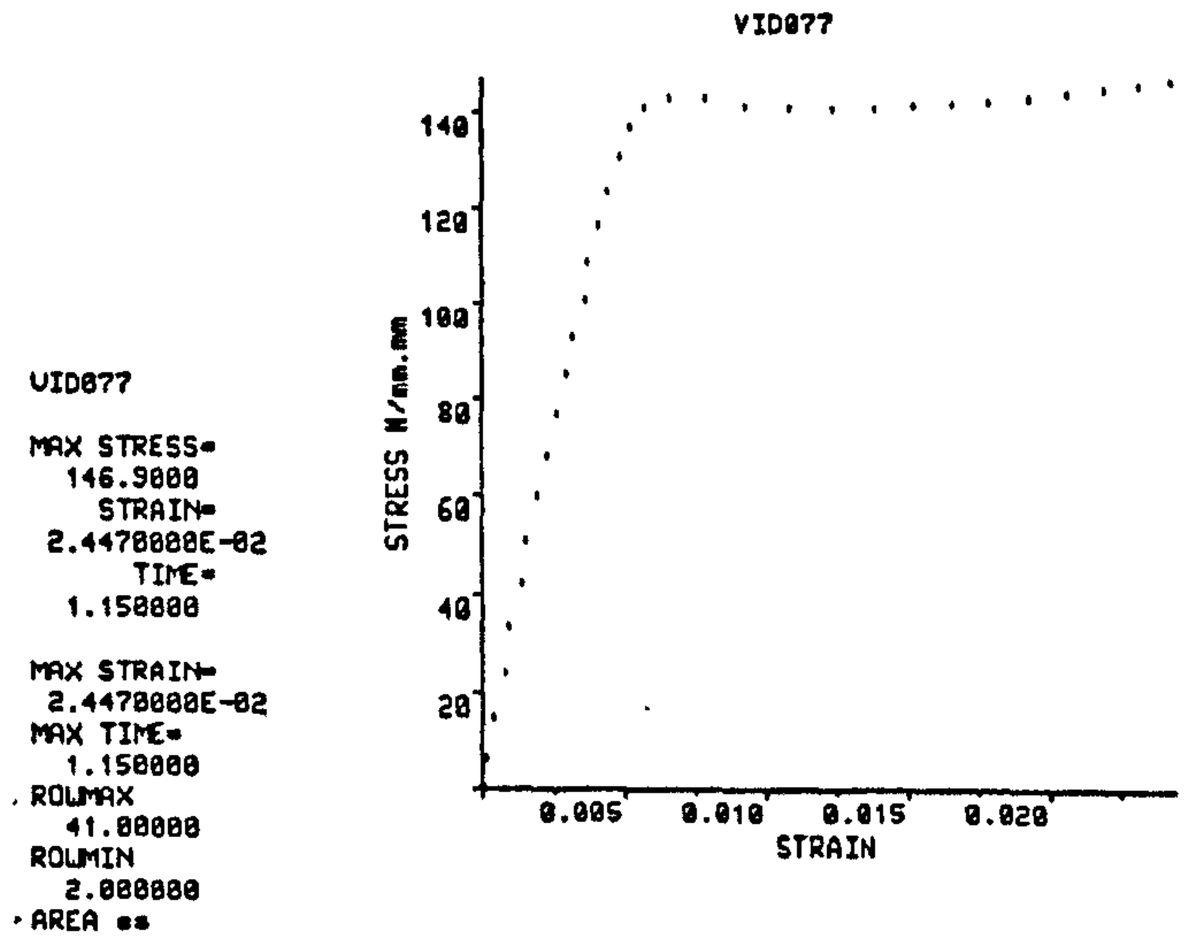

g)

This is a stress-strain plot of the reduced data set. The data values quoted and the area under the loading curve can now be interpreted as the correct values of these mechanical quantities.

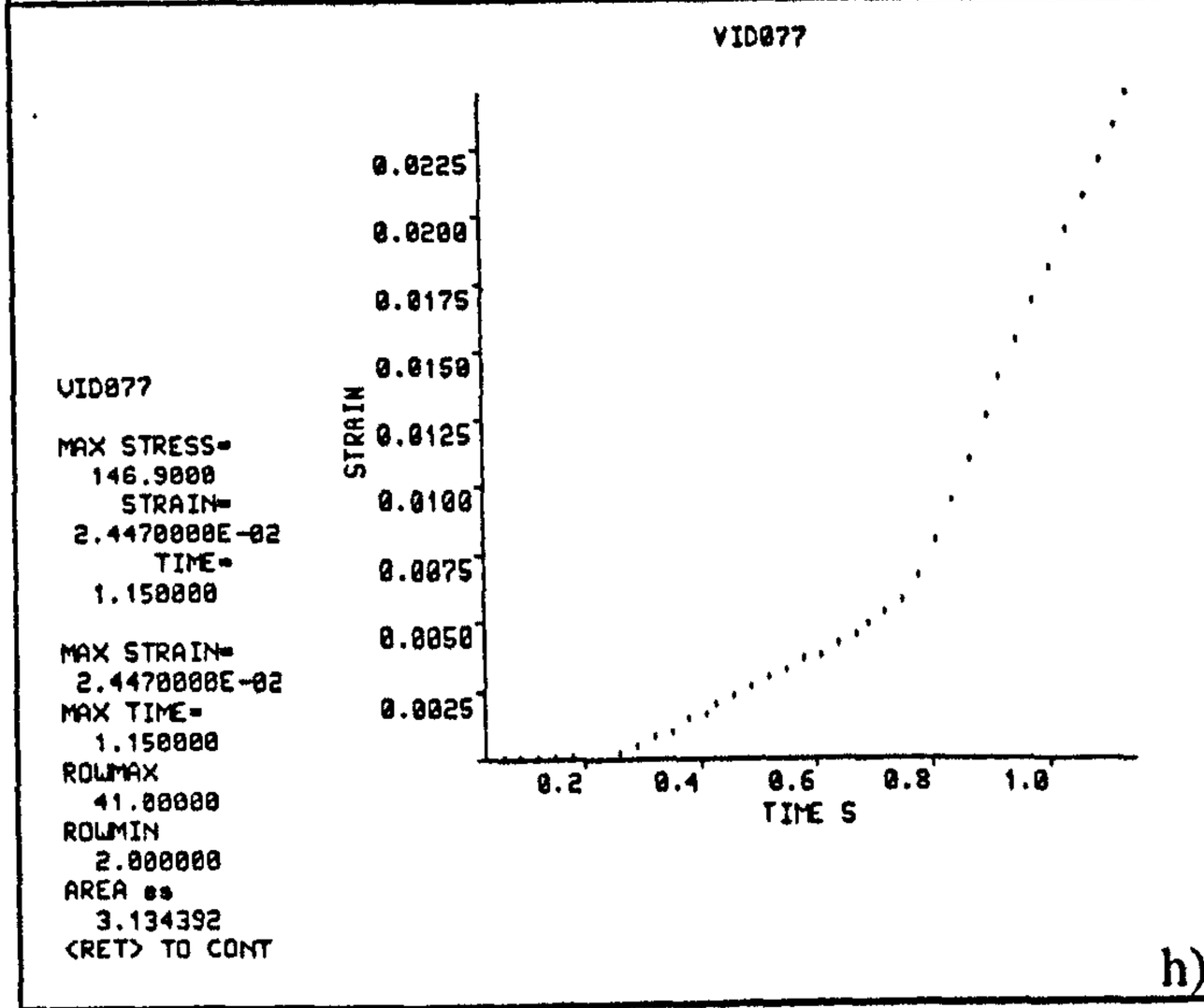

h)

Strain-time plot.

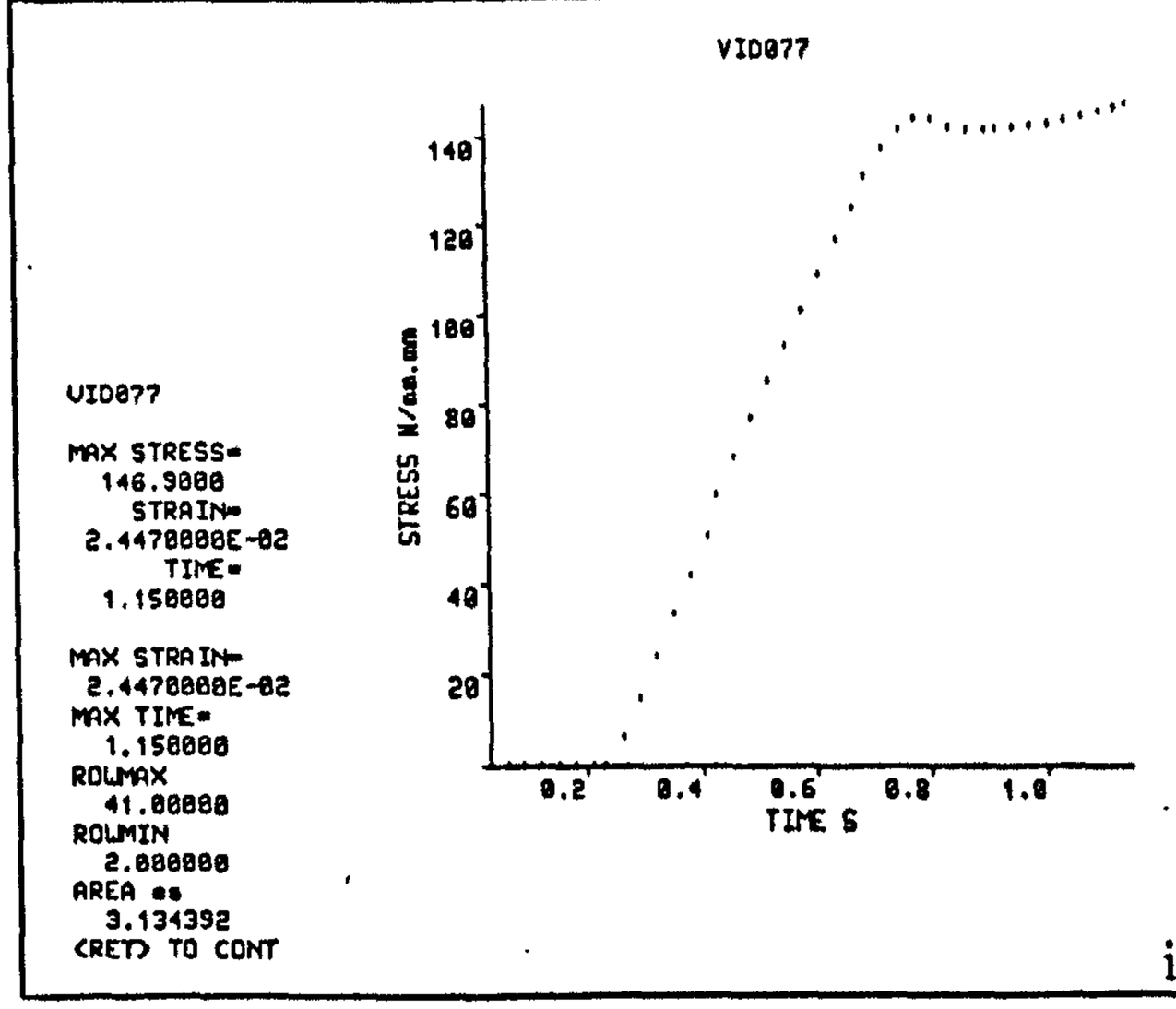

i)

Stress-time plot.

Figure 1.007 Continued from above and continued below

Images of the computer screen at various stages of the data analysis programme

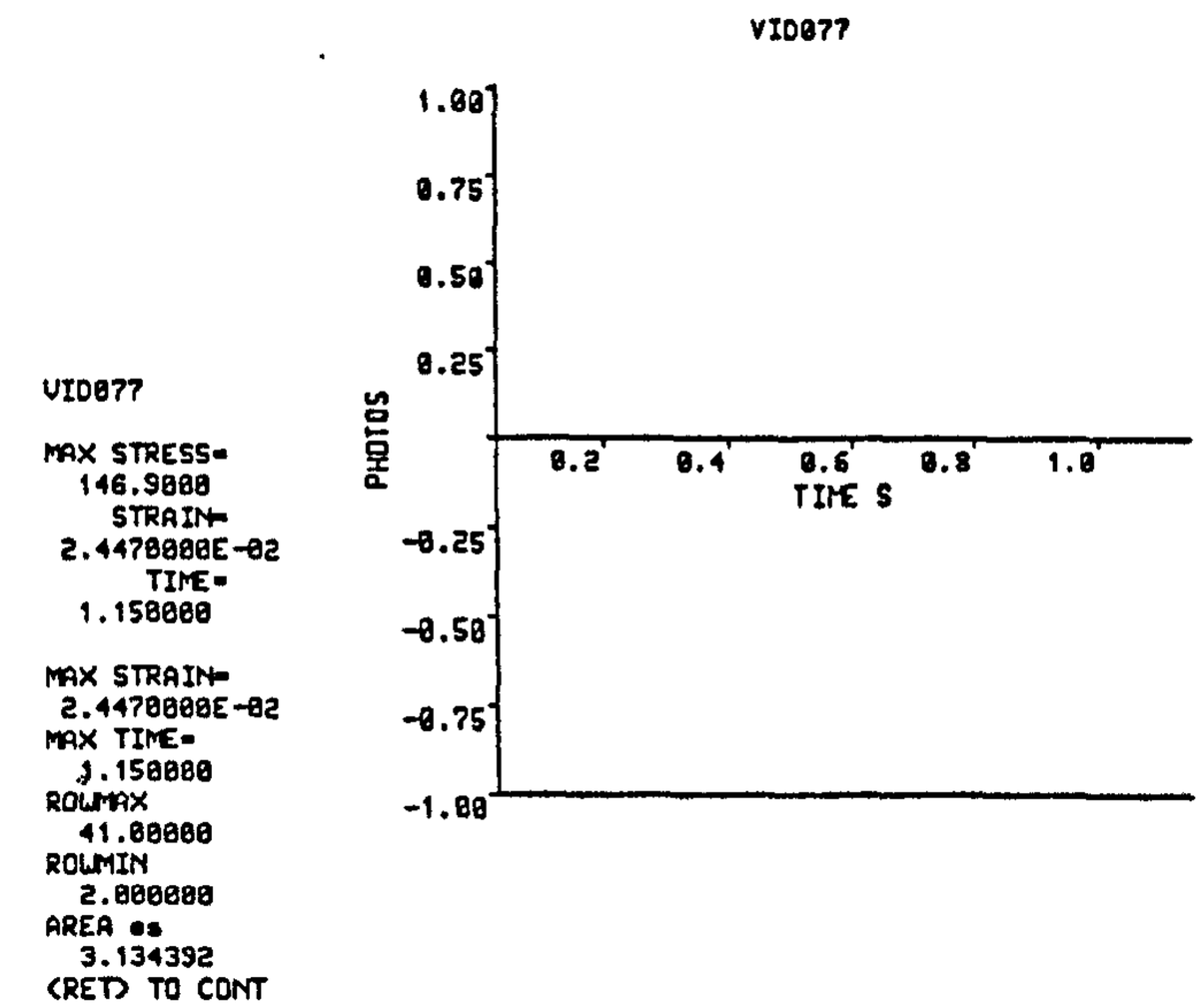

j)

Channel 3-time plot.

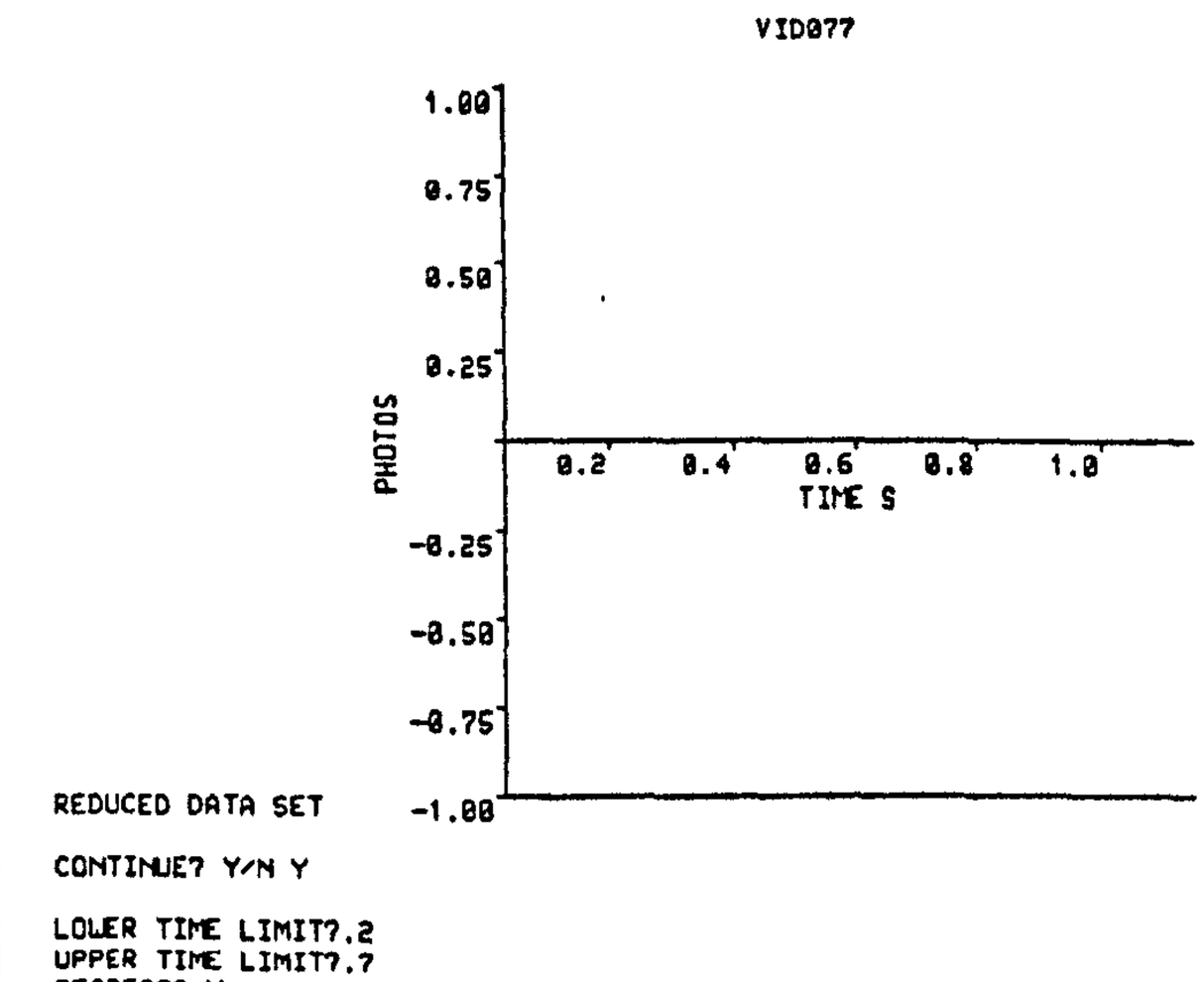

k)

The next interactive stage in reached. (The programme has looped back to the same line as figure A1.007f.) In this case a smaller range of data is examined that from 0.2 to 0.7 seconds into the test. Again the operator is asked if regression analysis is required. In this example the response is affirmative.

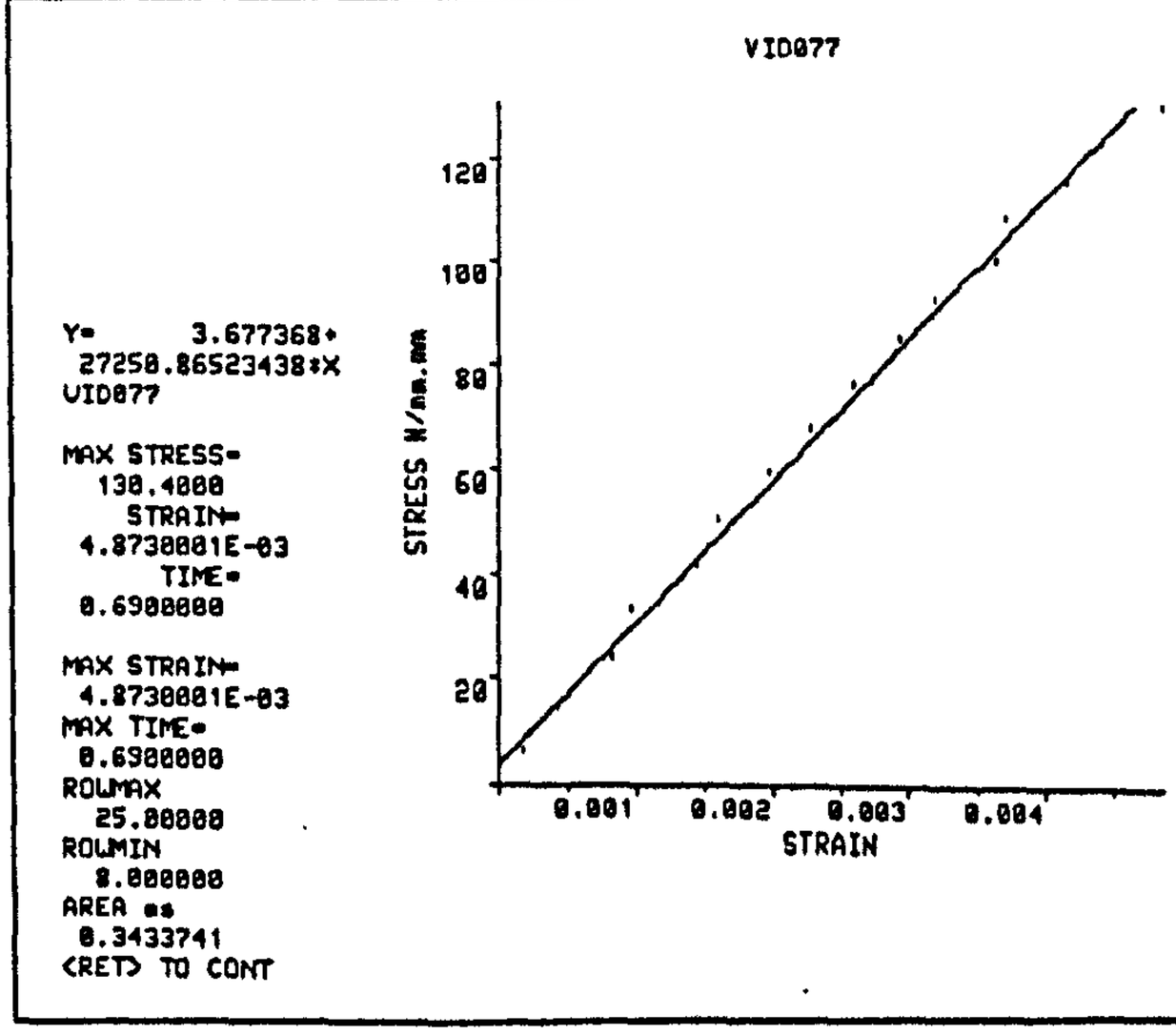

l)

This is a stress-strain plot for the reduced data set. The regression equation given is $Y = 3.677368 + 27250.86523438*X$. This implies that the material stiffness of this specimen is 27.25086523438 GPa. However, the values used for the analysis of the differences between specimens was that given rounded to the nearest MPa.

Figure 1.007 Continued from above and continued below

Images of the computer screen at various stages of the data analysis programme

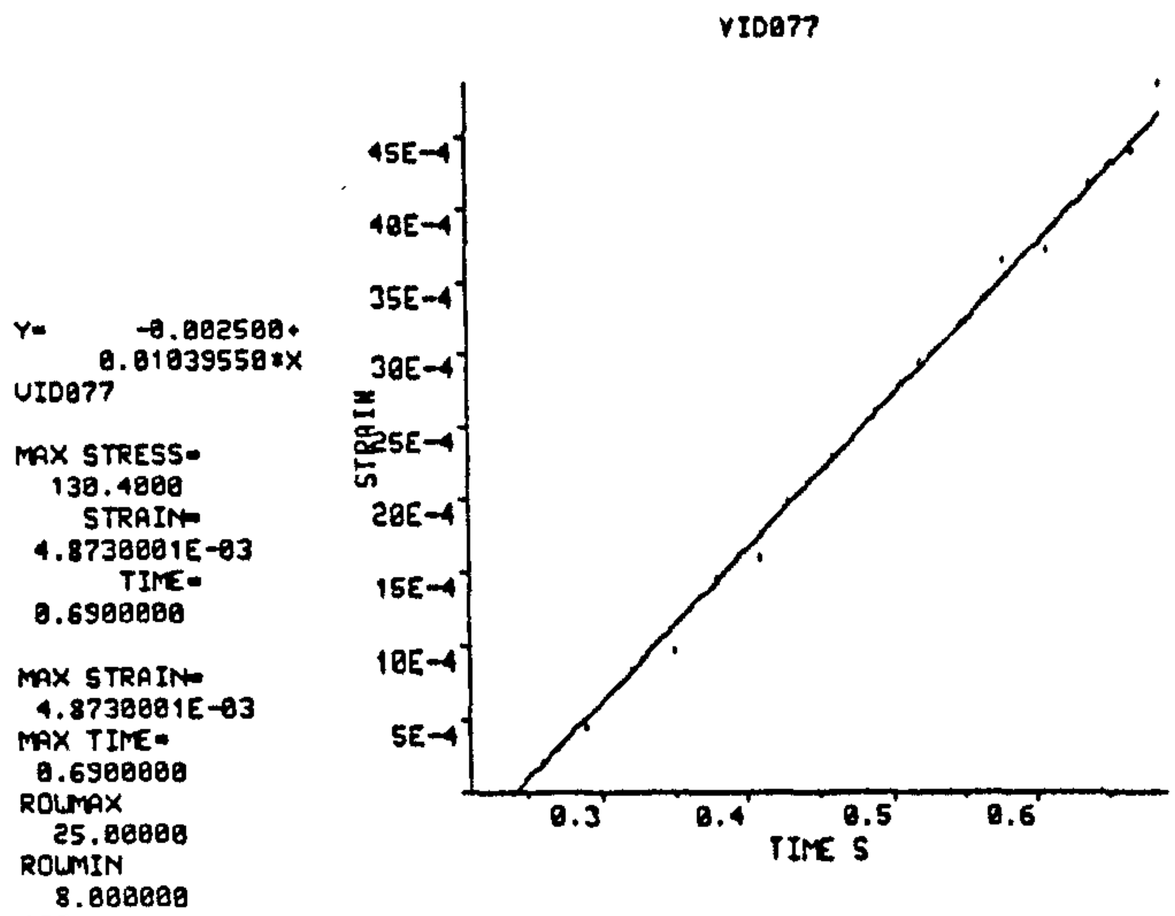

m)

The plot shown here is a strain-time plot. Therefore the slope of the regression line is the average strain rate exhibited by the gauge length during the period of the test examined. In this case the rate is about 0.01 s^{-1}.

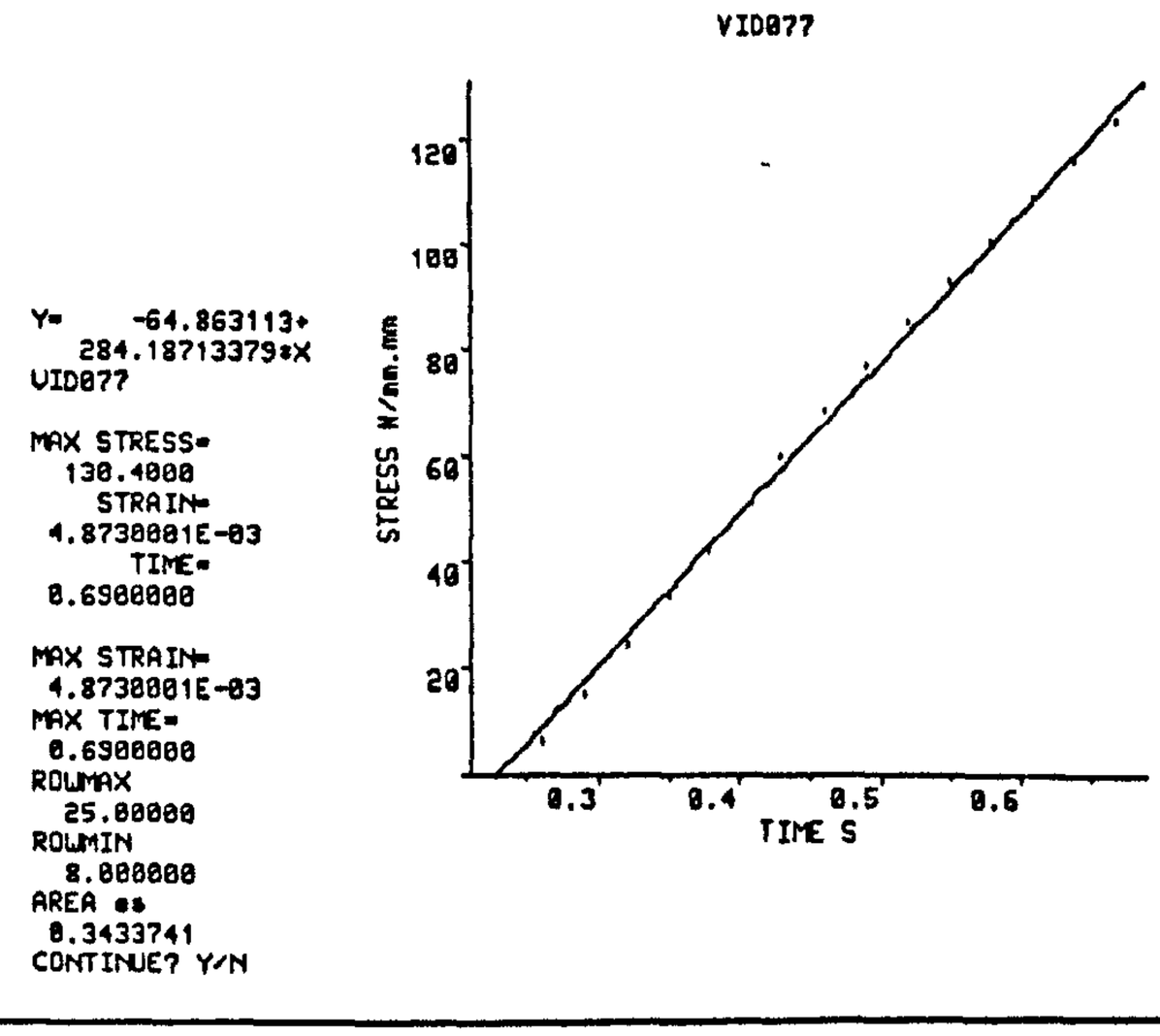

n)

This plot shows the values of stress plotted against time. Thus the slope of the regression line is the rate at which the stress was applied. This is related to the stiffness of the specimen and the cross-head speed used. However, this value was not used in the analysis presented here, although it did provide a check for the stiffness data that was used.

Figure 1.007 Continued from above

Images of the computer screen at various stages of the data analysis programme

APPENDIX 2

SPECIMEN PREPARATION FOR TENSILE, CREEP AND NOTCH SENSITIVITY TESTS

The specimens of bone and antler were prepared in a similar way. The main difference was that the initial sectioning of the antler was done in the dry state in which the antler was received, whereas the bovine bone was kept wet (or frozen) during all stages of the operation. In this description the photos show the preparation of specimens from a bovine femur. Where there is a variation between the methods of preparation or used for the antler specimens and that used for the bovine ones, this will be stated in a footnote. These differences normally arise from the different geometries of the two types of bone. Variation between the methods used for preparing the different types of specimens will also be included, either in the main text or in footnotes. At all stages of the operation and between operations the test material was immersed in water. The cutting operations, for which it had to be removed from the water bath, were completed as quickly as possible. Water was applied to the surface of the material with a pipette if there was no obvious dampness on the surface of the material.

The bovine bones (normally femurs) were obtained from local butchers. The butchered animals were normally 18 months old. The specimen preparation process was either started immediately or the material was stored in a freezer for preparation at a later data.[1] The preparation of the specimens will be described in a number of stages.

a) The first task was to clear, measure and draw the bone. The diaphysis was cleaned back to the first hard surface, and the epiphyses were exposed to the level of the articular cartilage. A line was drawn on the surface of the diaphysis and represented on the drawing.

b) Using a De Walt 3501 band saw with a 'skip tooth' blade (approximately 6tpi) two napkin rings of bone were removed from the central section of the diaphysis. (Figure A2.001) These napkin rings were about 50 mm in length. These were labelled and the more distal end marked.[2] Both ends of the napkin rings were then drawn round and the position of the line drawn on the side of the bone was marked on the drawing. A sketch of one side view of the napkin rings was also made.

c) The head of the femur was sectioned to examine the state of the epiphyseal plate: fused or unfused. (In all cases this was found to be unfused.)[3] (Figure A2.002).

---

[1]The antlers were stored in laboratory conditions.
[2]In the case of antler the more proximal end was marked.
[3]There is not equivalent sectioning operation for antler. However, the antlers were examined for evidence of velvet and casting. This gave some indication of maturity.

d) The napkin rings were sectioned longitudinally, and the marrow was removed. (Figure A2.003a.) They were then placed on top of the drawings of their outlines, and the internal detail added.[4]

e) The half napkin rings were sectioned longitudinally, producing rods of cortical bone. The distance between successive cuts was about 10 mm, but this depended on the size, radius of curvature and quality of the rings. (Figure A2.003b) The channel for the blood vessel noted in figure 1.001 can be seen in one of the sections shown in figure A2.003. Rods obtained from areas containing obvious blood vessels or muscle insertion points were rejected.

f) One edge of each rod was ground off so after further sectioning the orientation of the pieces of bone would be known. This edge was that seen in the bottom left-hand corner when the surface closest to the periosteum is viewed, and the bone is in its natural vertical (proximal-distal) orientation. Therefore I refer to this orientation as the *natural orientation.* (Figure A2.004a) Thus for bovine bone this edge is more distal.[5]

g) The external surface of the rods was then ground flat using carborundum paper. (Figure A2.004b). One of the adjoining surfaces was then ground flat and at 90° to the first. (Figure A2.004c.)

h) Slabs about 1.5 mm thick were then cut from the rod using the ground flat surface as a datum. These cuts were performed using a small table top band saw. (Figure A2.005.) The position of these slabs in the original bone was recorded by noting their position on the pictures of the napkin rings. Thus the positions and orientation of each specimen within the original structure are known. (However, this information has not been fully utilised in the work presented in this thesis, although during some of the initial analysis this variable was included.)

i) The slabs were then ground by hand, while immersed in water, using progressively finer carborundum paper until they were approximately 7 mm × 1.25 mm × 45 mm. If it was required to do so the datum corner was reground. (Figure A2.006.)

j) The rectangular slabs of material were tested in three-point-bending using an Instron 1122 machine (see figure A2.007). The specimen to be tested was positioned so it straddled a machined hole in a metal block, mounted centrally on an Instron compression load cell. The specimen was totally submerged in tap water. The compression surface was that which had been closest to the external surface of the original bone or antler.

k) The specimens were loaded to approximately 2 N. The cross-head speed used varied from test to test. The values are given in the main text. The load was recorded on the Instron's chart recorder, which was running at an appropriate speed to produce a line of suitable slope.

---

[4]The centre of the antlers contains a dense cancellous bone structure. This can not be remove in the same way that marrow can.
[5]For antler this edge is more proximal.

l) The straight portion of the loading curve (after the so-called *bedding-in* section, or initial non-linearity) was extrapolated to give the total deflection due to a load of 2 N.[6] This deflection comprises the sum of the deflection of the specimen being tested and the deflection of the loading equipment.

m) To account for the *machine deflection*, the system was loaded without a specimen and the recorded deflection (assumed to be due to the machine only) was subtracted from the measured deflections before the calculation of material stiffness was undertaken.

n) The equation used to calculate the material stiffness was that used to calculate the Young's modulus of a uniform rectangular beam of elastic material in three-point-bending. This equation is available in such books as Howatson *et al.* (1985).

$$E_b = \frac{P}{4\,\delta\,b}\left(\frac{L}{d}\right)^3$$

where: P is the load (in Newtons), L is the length of gauge section or the distance between the supports (in metres), δ is the vertical deflection at the centre of the gauge length (in metres) and E_b = Bending modulus, for an elastic material this is Young's modulus (in MPa)

o) The slabs of test material were machined into the familiar *dog-bone* shaped specimens. The waisted sections being of 4 or 5 mm in width. This operation was performed using an engraving machine with a milling tool. The tool is guided by a manually operated jig follower, thus with the appropriate jig specimens of different shapes, sizes or widths can be reproduced. See figures A2.008 to A2.010.

p) If the specimen was to be used in a tensile or creep test the preparation was completed by a final grind with a very fine carborundum paper and an inspection for any production induced flaws. If the specimen was to be used for notch sensitivity tests then there are a few more stages to be completed.

q) Two types of notch have been used in this study: ones with drilled tips and ones with cut tips. If a drilled tip was required then this operation was conducted first. A variety of drill sizes were used, but all at speeds of about 105 rad s^{-1} [1000 rpm]. (Figure A2.011.)

r) The notch was completed by cutting a slot from the edge of the specimen to this hole. (Figure A2.012.)

s) The final stage of the preparation was to give the specimen a slight grind on very fine carborundum paper to remove any burrs.

t) Before testing the dimensions of the notch were measured using a travelling microscope (with a graduated eye piece for the smaller dimensions). These measurements were performed on both sides of the specimen.[7]

---

[6]Total deflection = (distance on the chart) × (speed of cross-head/speed of chart)
[7]In some of the initial tests on antler these measurements were made on one side only.

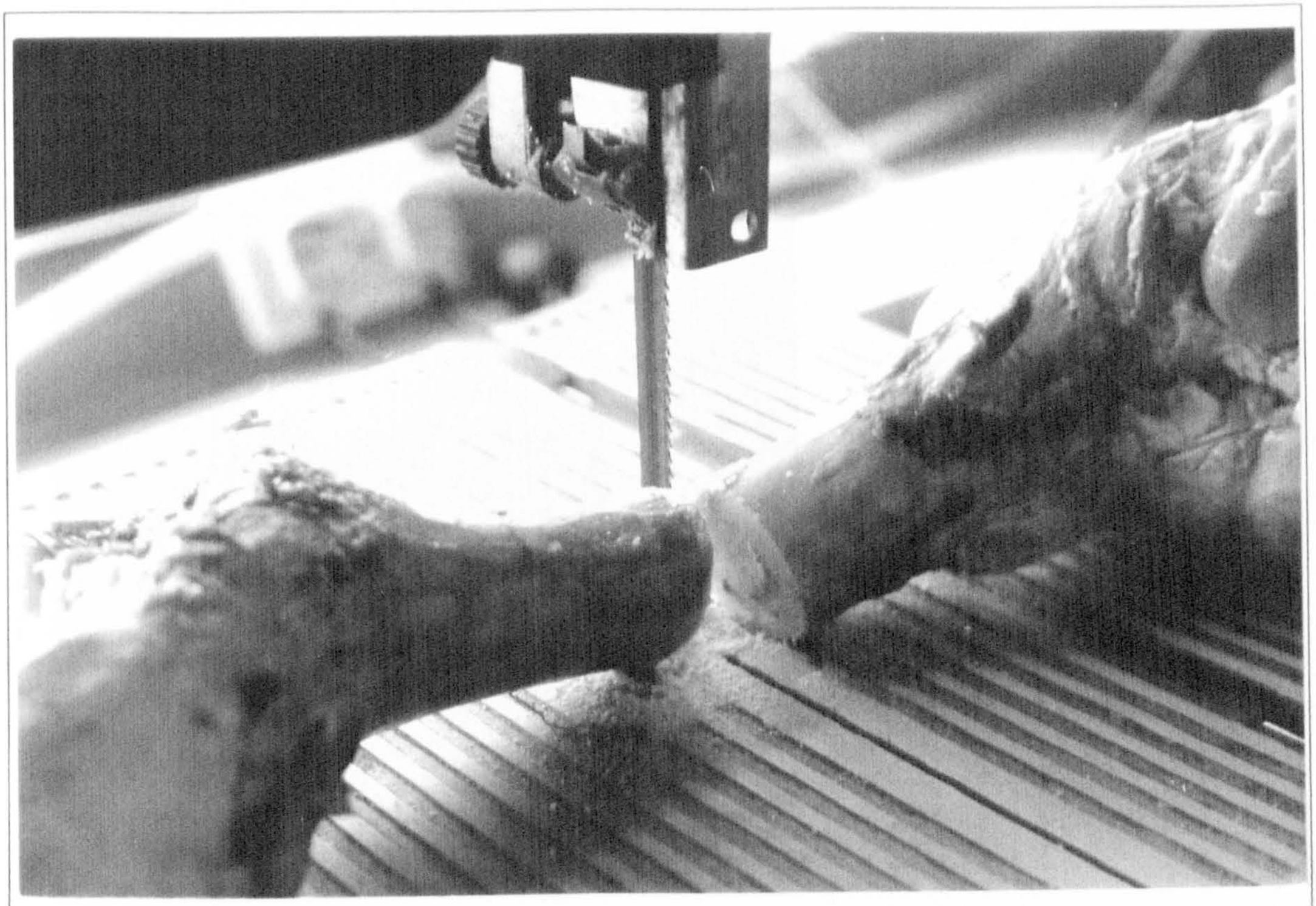

Figure A2.001

Initial sectioning of a bovine femur

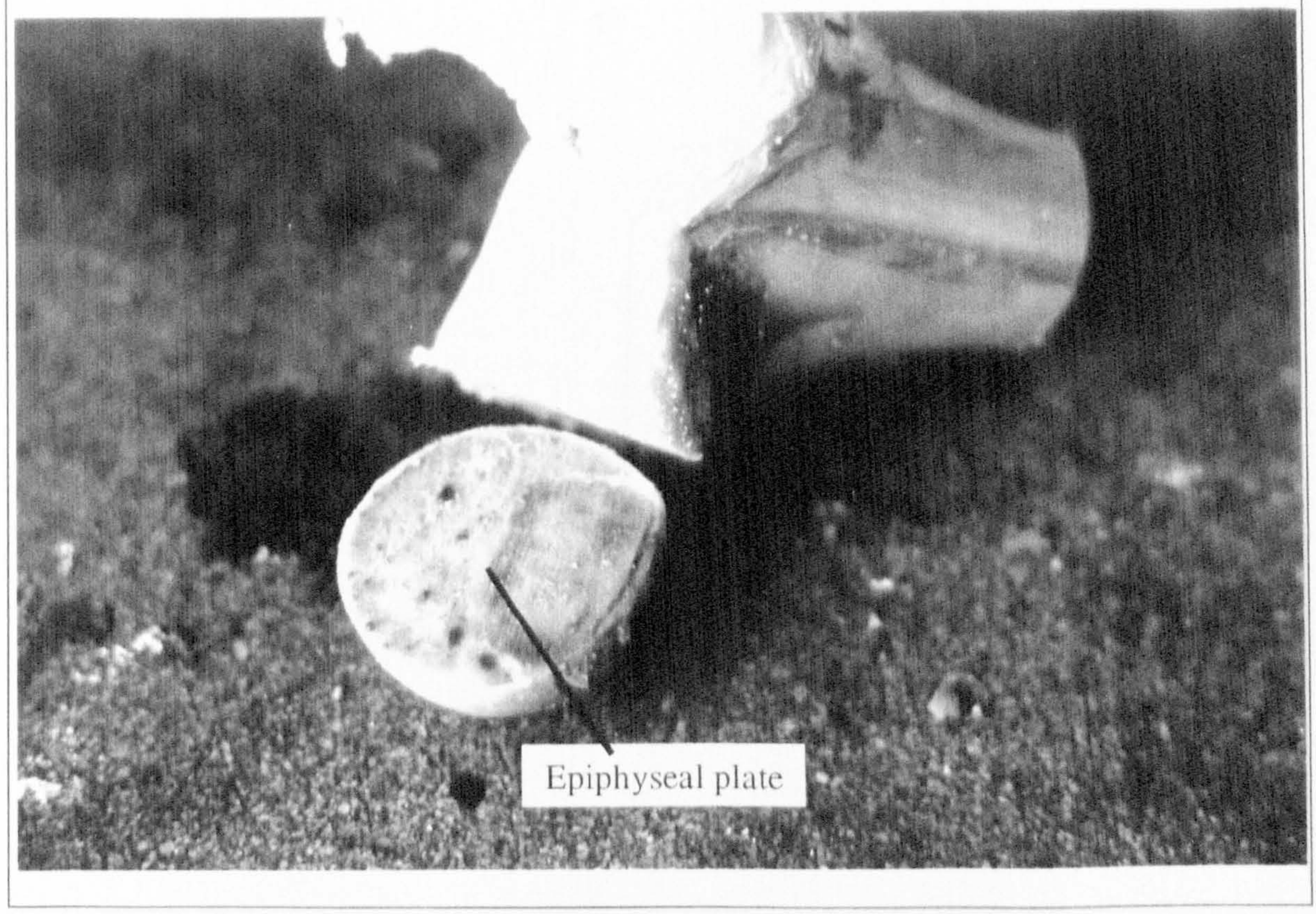

Figure A2.002

Section through the head of the bovine femur, for the examination of the epiphyseal plate

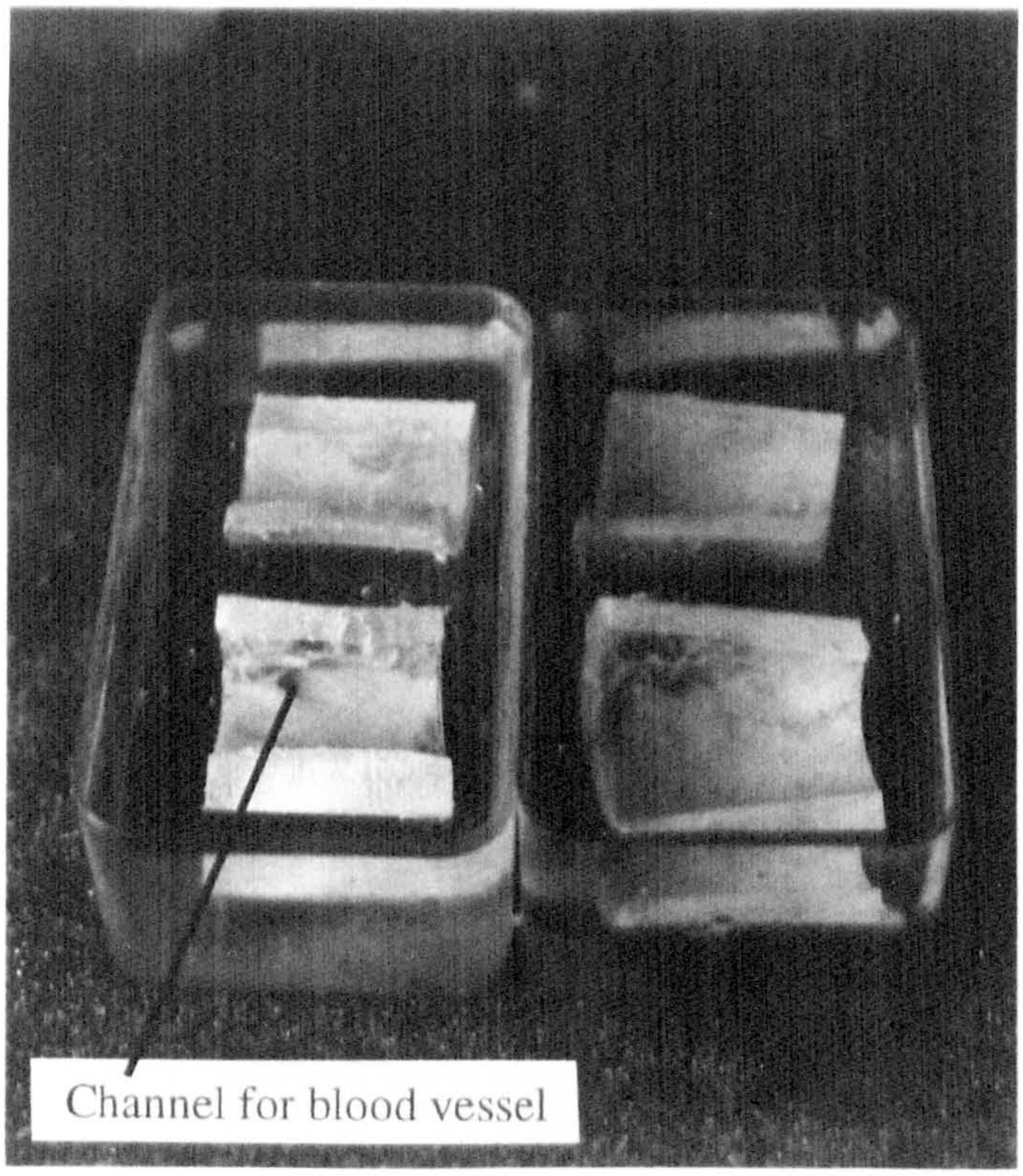

a

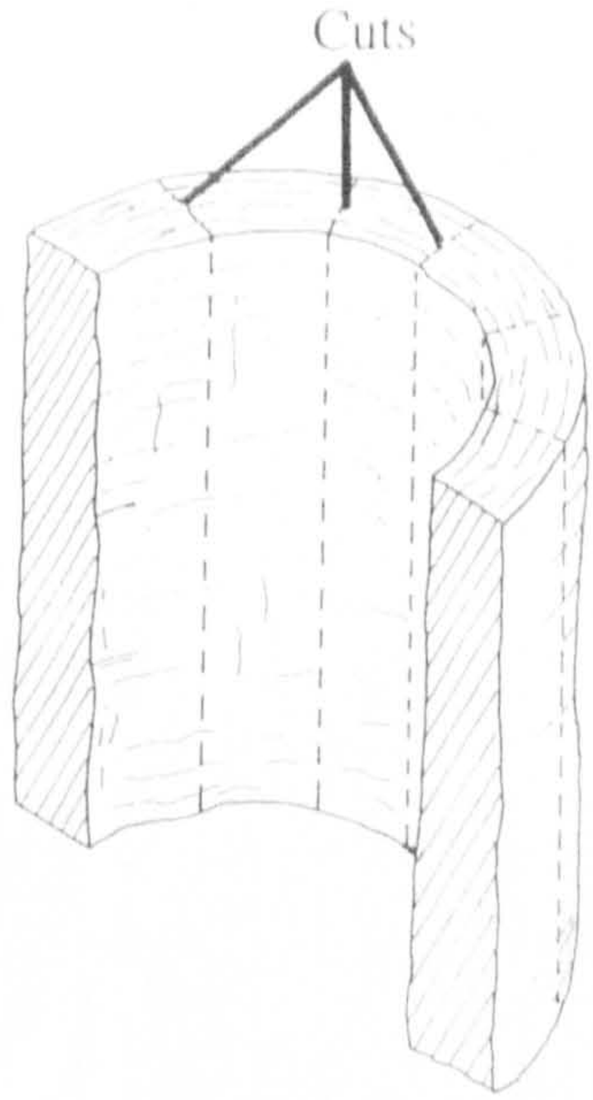

b

Figure A2.003

The sectioned napkin rings of bovine bone

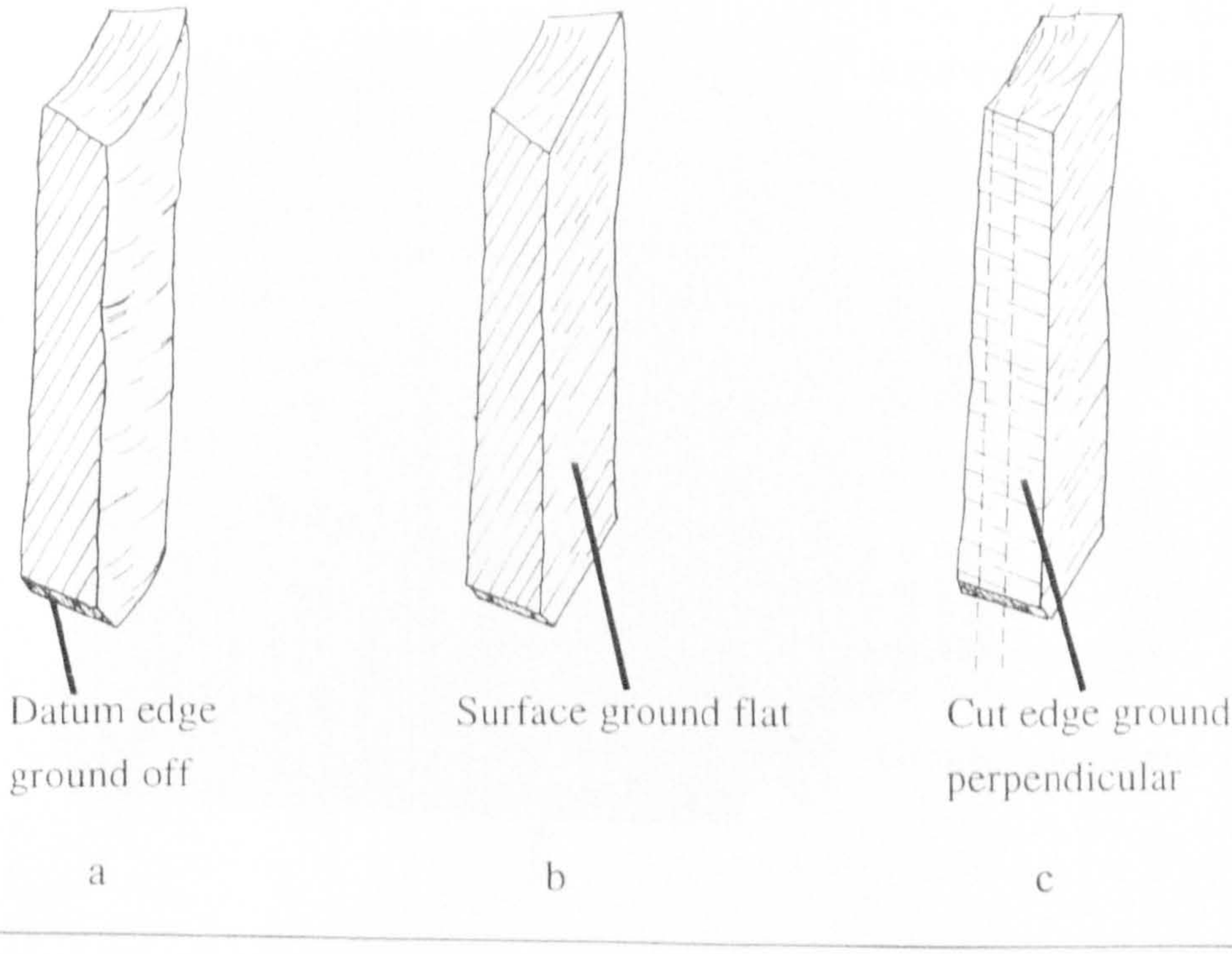

a b c

Figure A2.004

The preparation of the rods of bone

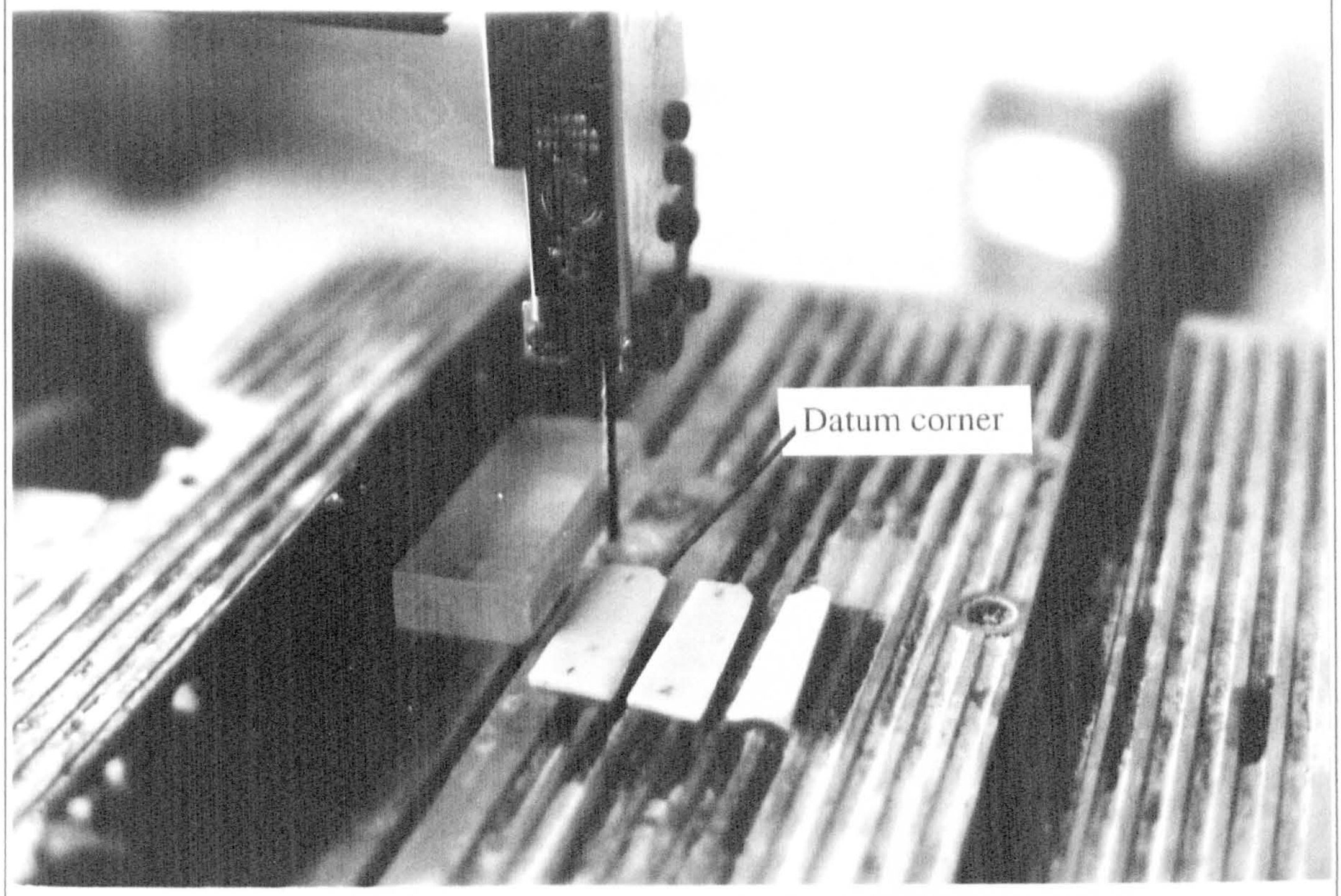

Figure A2.005

The sectioning of the rods of bone into slabs

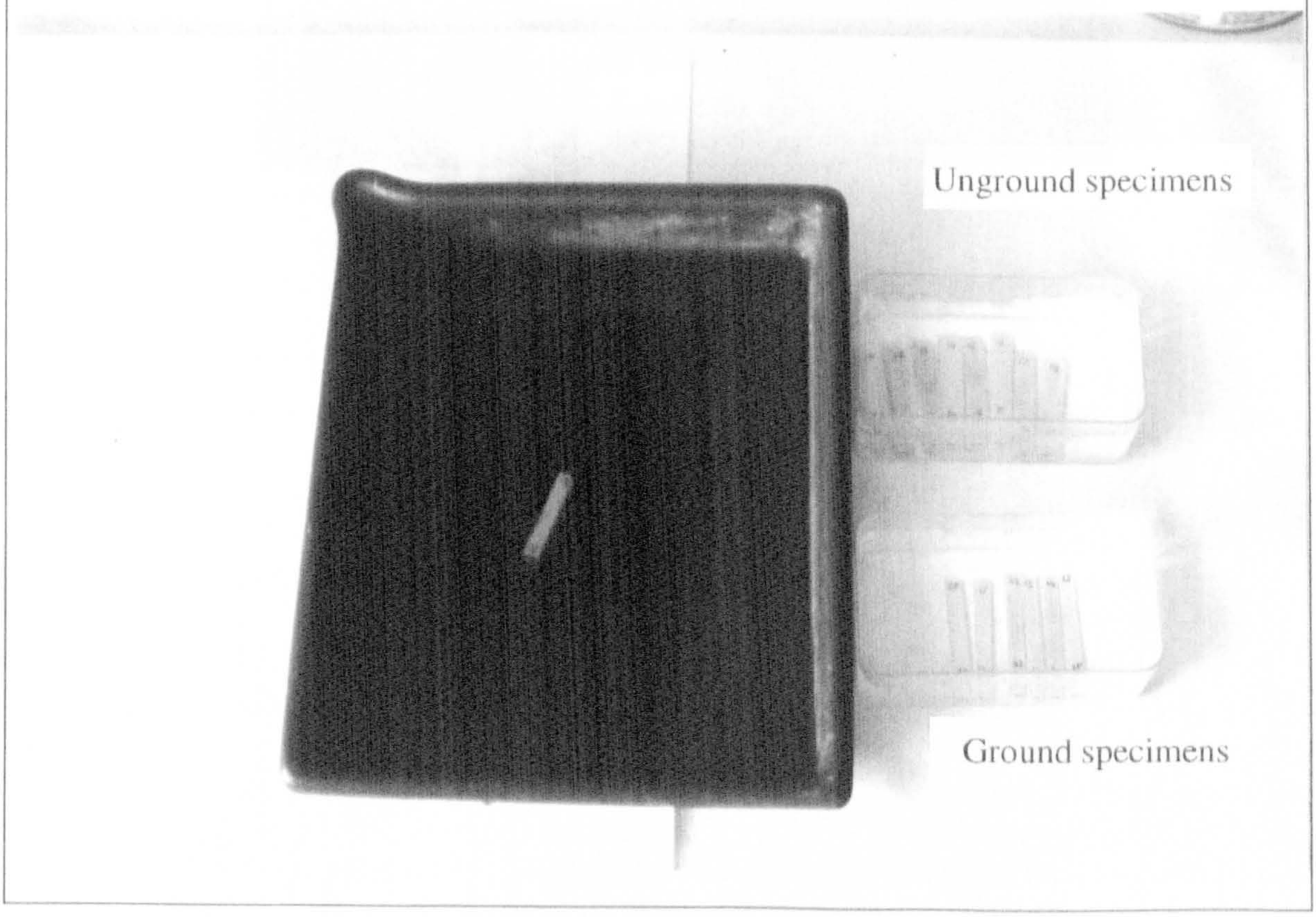

Figure A2.006

Grinding the slabs into regular shapes

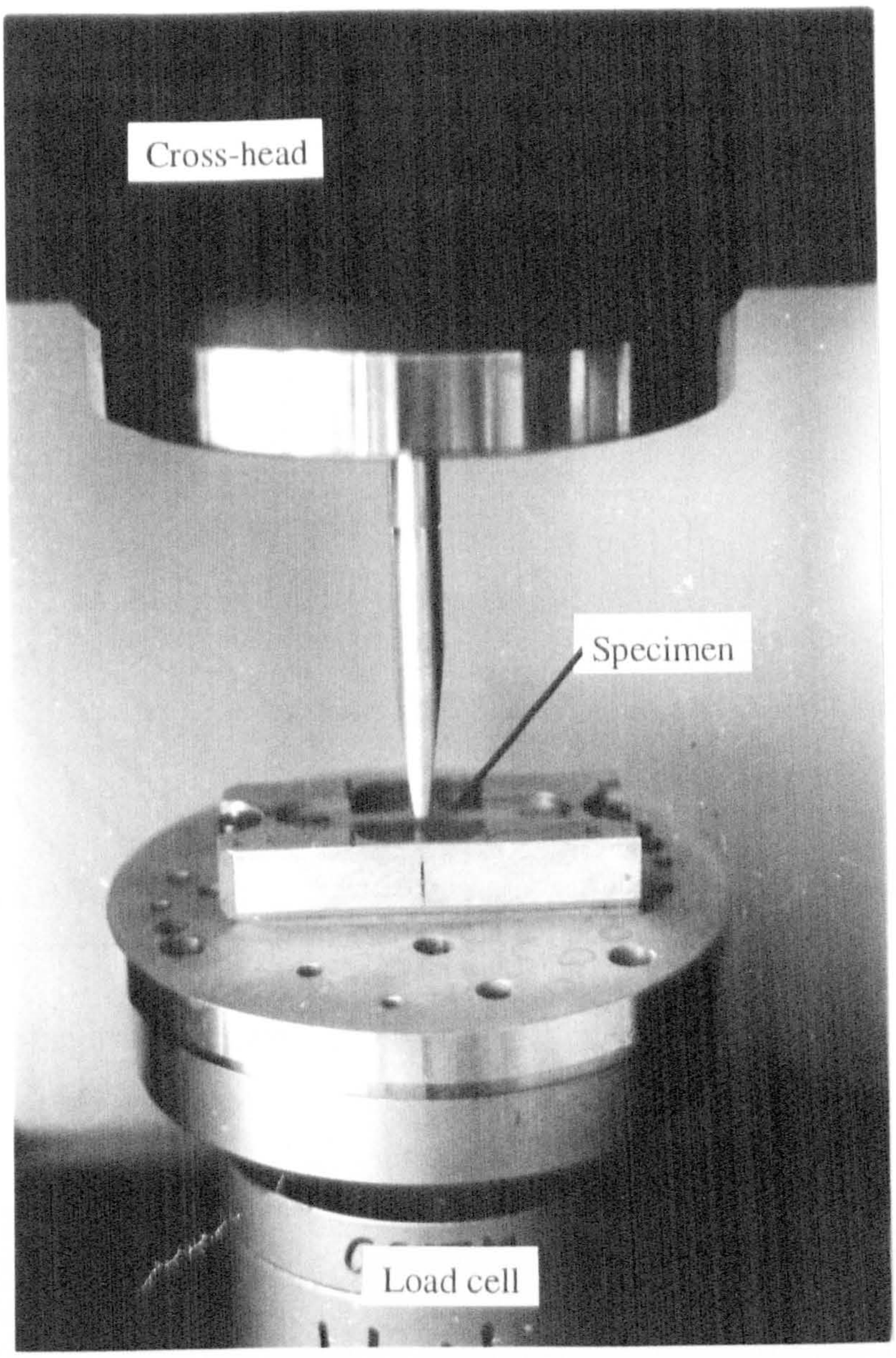

Figure A2.007

Three-point-bending of the slab of bovine bone

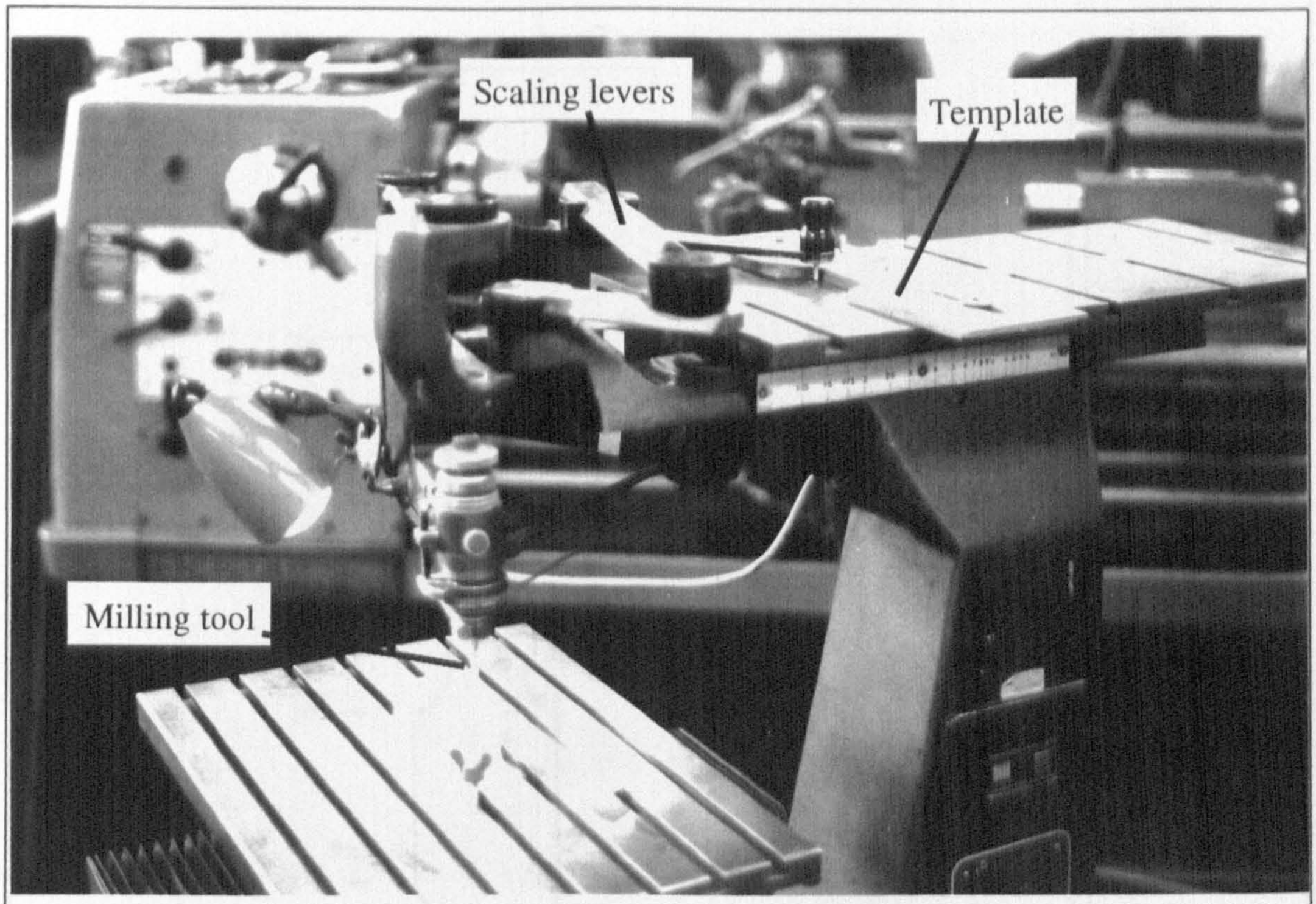

Figure A2.008

The engraving machine used to produce the waisted section of the specimens

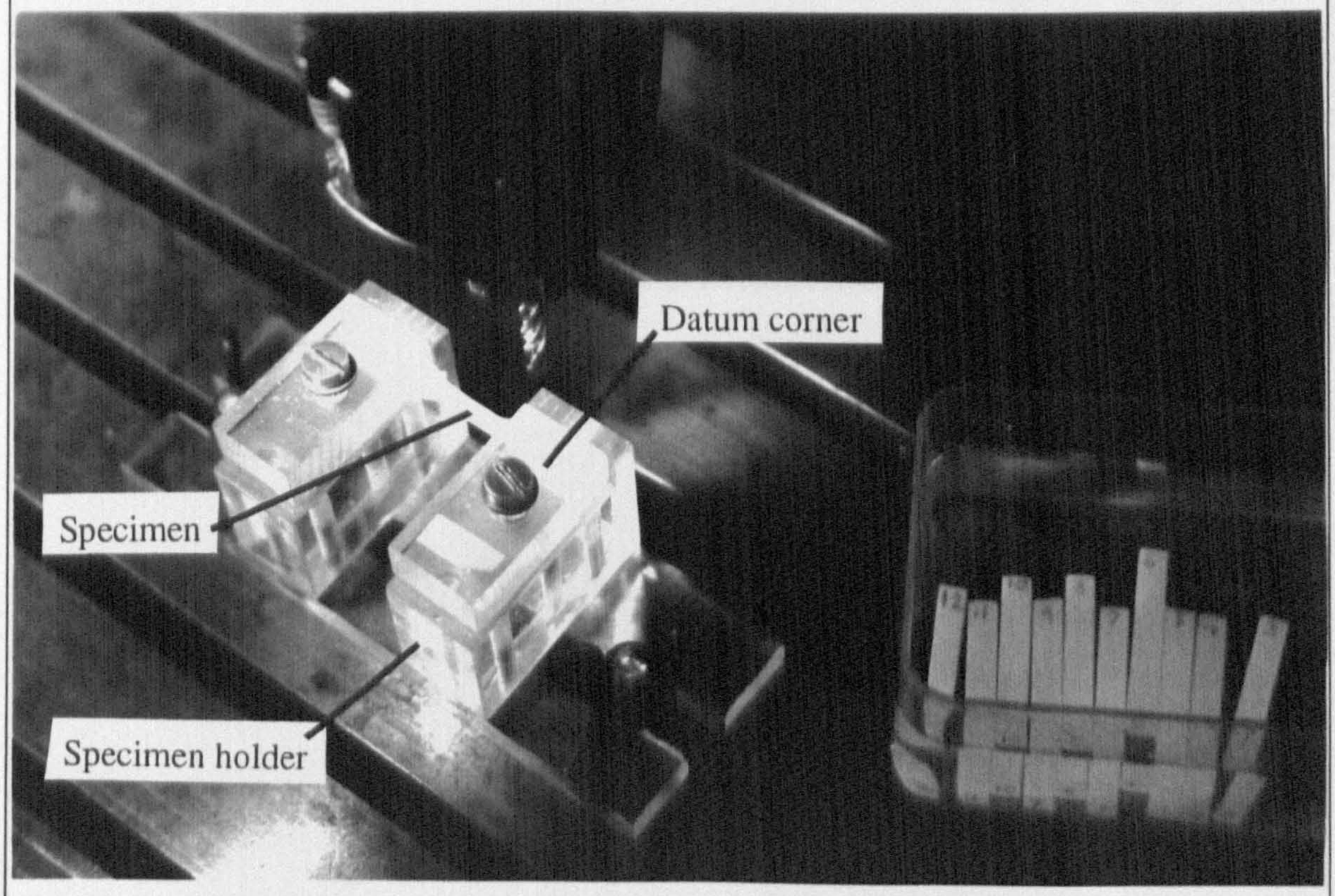

Figure A2.009

Detail of milling of the specimens

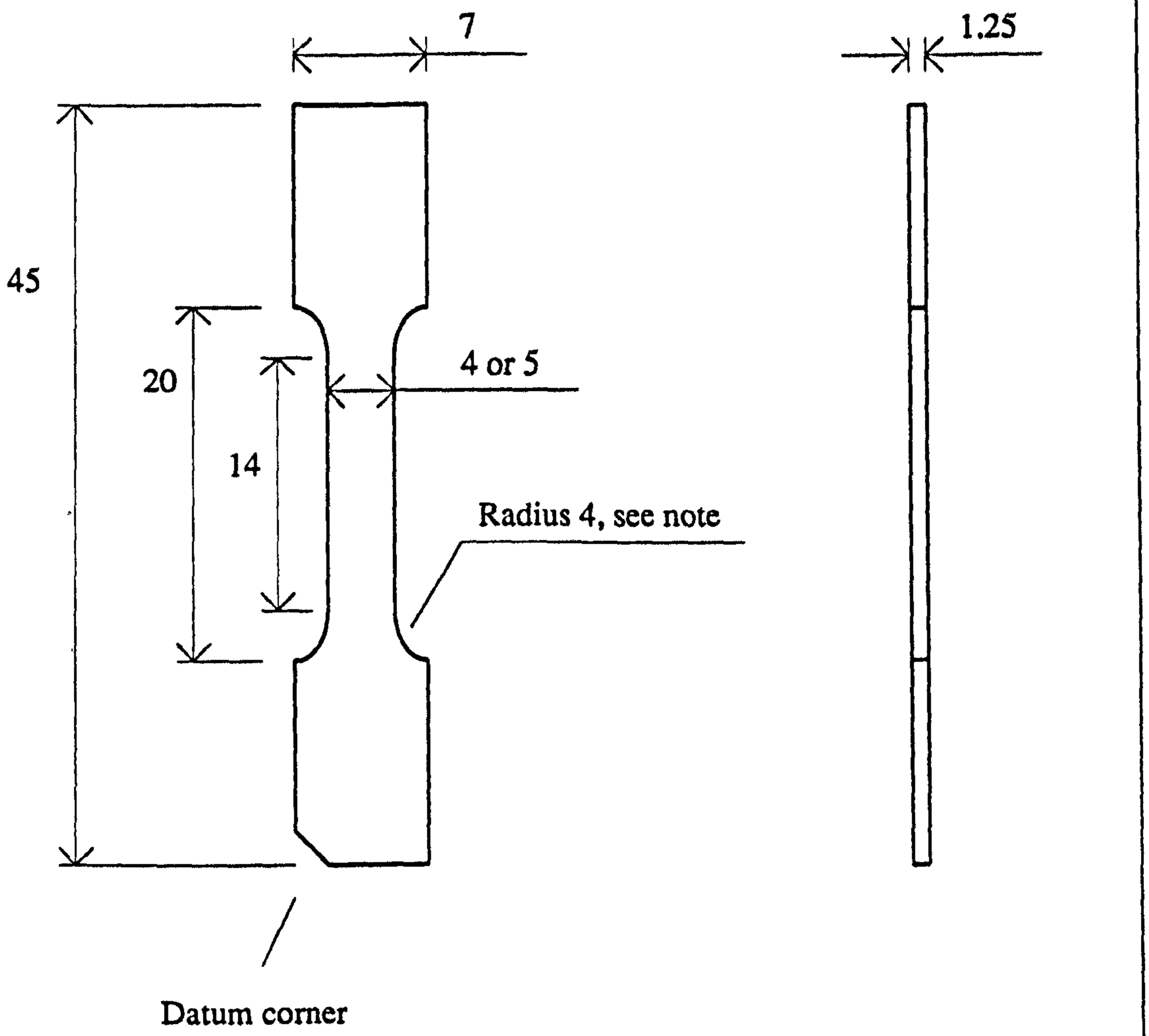

All dimensions in mm

Note: This is not a true radius, as the flare at the reduced cross-section is more gradual. The specimen is viewed in its *natural* orientation, the largest surface seen here was that closest to the surface of the original bone.

Figure A2.010

The basic shape and nominal dimensions of the tensile specimens

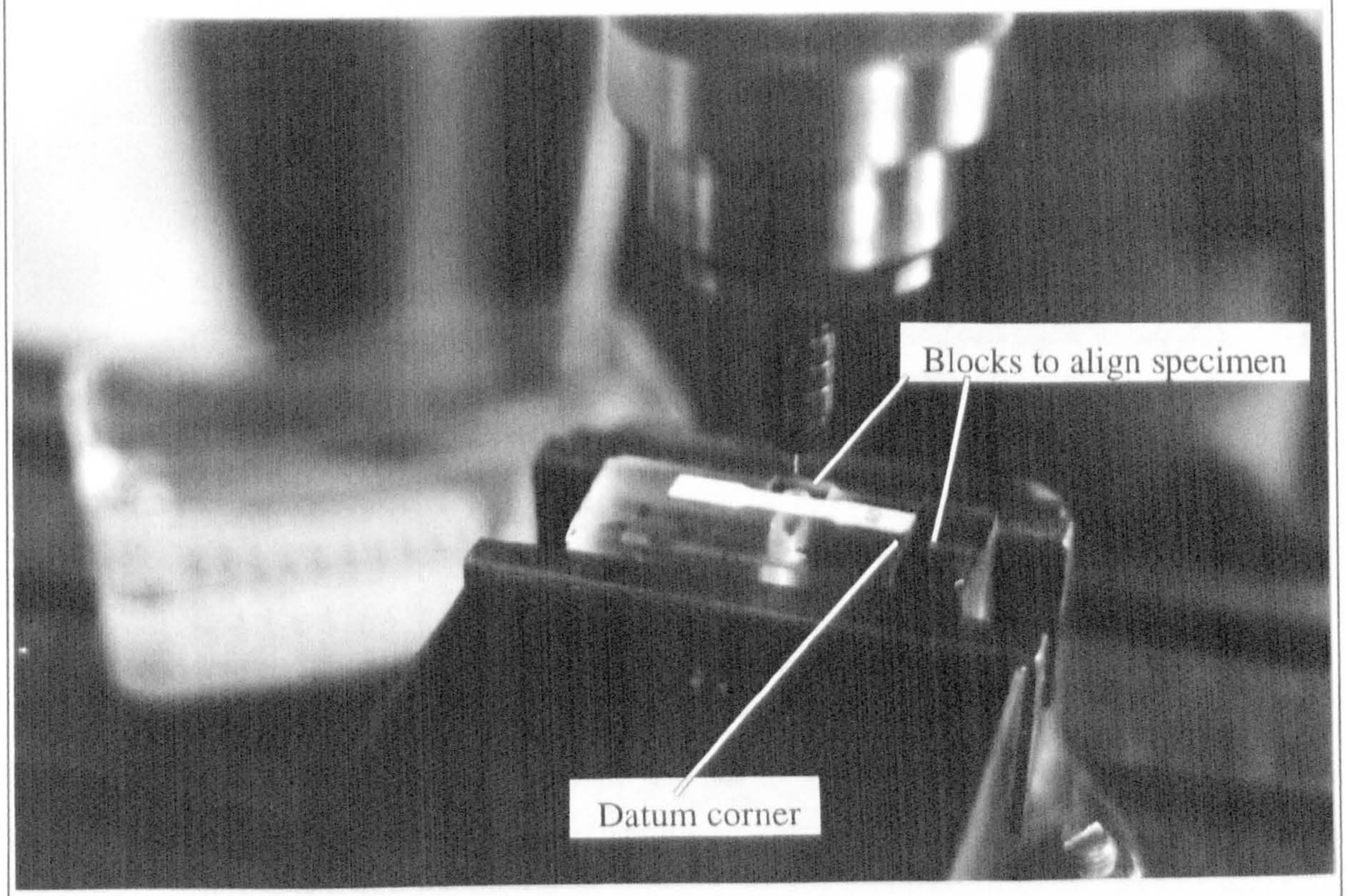

Figure A2.011

Drilling the tip radius of the notch

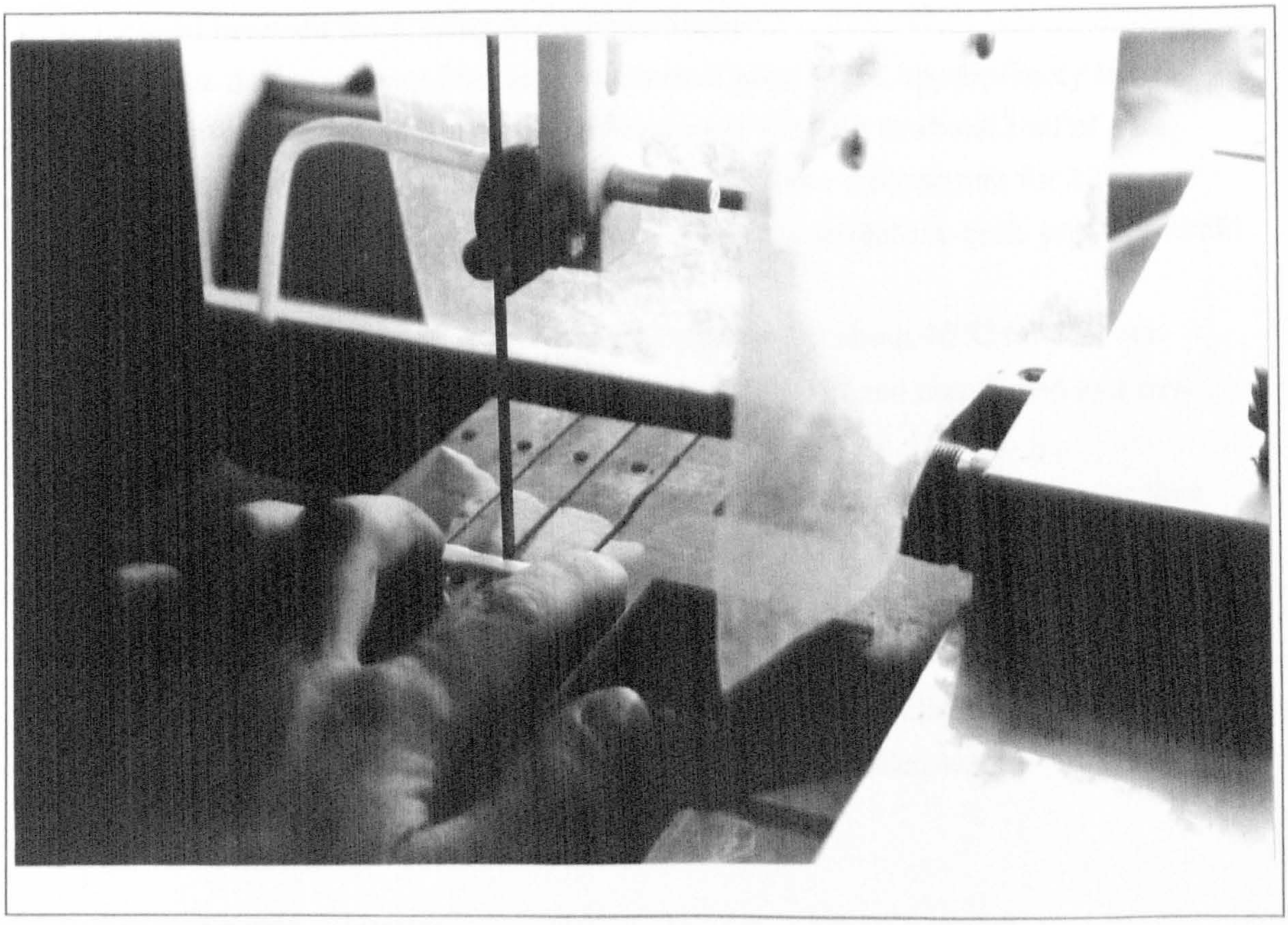

Figure A2.012

Cutting the notch using an Exakt diamond band saw

APPENDIX 3

CALCIUM DETERMINATION

The calcium content of the specimens was determined using a colorimetric method. This method is essentially the same as that which has been used in the laboratory for Professor John Currey for a number of years. For example see Currey (1988a). However, for the results presented in this thesis the final stage of calcium determination was performed using an automated analysis system.[1] It was considered that such a system would remove some of the variability due to human error.

The stages in the determination of the calcium content of bone are presented below. The term bone will be used, but the method equally applies to antler.

a) A small drill was used to obtain fine particles of bone. The holes were drilled in the material on the datum side of the fracture. (Thus the material was always more proximal than the fracture for the antler specimens, and more distal in the case of the bovine specimens.) During this operation the specimen was placed on a piece of weighing paper, so that the dust could be collected. Most of the material was obtained from the shoulder region of the specimen. Care was taken not to drill through the full depth of the specimen (and thus into the paper). The paper, drill and surrounding area were cleaned between the drilling of each specimen.

b) The dust was placed in clean flat bottom glass tubes, appropriately labelled.

c) To remove any fat the bone particles were tumbled in about 2 ml of a chloroform and methanol mixture. This was done at room temperature for 12 hours.

d) The tubes were left to stand for a few minutes so that the bone particles could settle. The solution was then pipetted off.

e) The remaining bone particles were then dried at about 40°C for 5 hours.

f) Approximately 0.006g of the dust was weight out and transferred to a new clean glass tube, appropriately labelled.

g) Approximately 1 ml of N/1 HCl was added to the tube. The tube was then stoppered and left for at least 12 hours (normally over night) to allow the bone to decalcify.

h) All the contents of the tube were transferred to a 50 ml volumetric flask. The tube was rinsed into the flask several times using deionised distilled water. The flask was then filled to approximately 15 ml using more deionised distilled water.

---

[1]I would like to thank Peter Humpherson and Kevin Brear for their assistance in setting up and calibrating the MIRA analysis system used in this study.

i) N/1 NaOH was added to the flask until the solution was neutralised. Neutralisation is signified by the formation of a cloudy precipitate. The amount of NaOH needed is approximately the same as the amount of HCl previously added.

j) HCl is added drop be drop. The flask is agitated between each addition. This process continues until the precipitate just clears.

k) The solution is made up to 50 ml using more deionised distilled water.

l) The tubes are then stoppered, or the solution transferred to other tubes for storage until it is analysed.

m) The concentration of calcium in the solution was determined by using o-cresolphthalein complexone. This was obtained in the form of a calcium testing kit from Boehringer Mannheim. The manufactures of this kit and Currey (1988c) refer to a paper by Sarkhar and Chauhan (1967) for the method. Basically this chemical forms a violet complex with calcium. The amount of this violet complex reflects the amount of calcium present.

n) The amount of the violet complex is determined by using MIRA analysis system. At the heart of this system is a photometer. Light is emitted from a flash tube and passes through an interference filter. The beam of light is then split. About 10% of the light falls directly on one photodiode, while the remaining 90% passes through the cuvet holding the sample solution before falling on another photodiode. The machine then compares the readings of absorbency obtained in this way with a previously stored calibration curve.

m) Once the concentration of the test solution has been obtain it is a simple matter to calculate the concentration of calcium in the mass of material from which that solution was made. The calculation is based on that in the instructions of the calcium determination kit and the mass of the bone from which the solution was made. In this case the calculation is simple: the reading from the MIRA divided by 20 times the mass of bone, will give the calcium content in mg g^{-1}.

It should be noted, as it was by Currey (1988a), that 'this process gives an estimate of the calcium content of dry bone; no attempt was made to measure the water content of bone'.

APPENDIX 4

HOW TO OBTAIN THE DATA SETS ANALYSED IN THIS THESIS

It is a capital mistake to theorise before one has data.

Sir Arthur Conan Doyle
Scandal in Bohemia

Data set	Main contents	Number of specimens
IA1	Impact energy, red deer antler	8
IB1	Impact energies, bovine femur	7
MA1	Calcium content, reindeer antler	78
MA2	Calcium content, red deer antler	110
MB1	Calcium content, bovine femur	37
TA1	Tensile test data, red deer antler	27
TB1	Tensile test data, bovine femur	30
CA1	Creep test data, reindeer antler	36
CB1	Creep test data bovine femur	33
CA2	Reduced data set from CA1	20
CB2	Reduced data set from CB1	15
NA1	Preliminary notch data, red deer antler	13
NA2	Preliminary notch sensitivity test data, (containing some tensile data), red deer antler	23
NA3	Notch sensitivity data (containing some resilience and tensile data), red deer antler	93
NA4	Notch sensitivity test data (whitened zone size), red deer antler	30
NA5	Notch sensitivity test data (cross-head speed), red deer antler	19
NB1	Notch sensitivity test data (containing some resilience and tensile data), bovine femoral bone	42
NB2	Notch sensitivity test data, bovine femoral bone	16
NB3	Notch sensitivity test data (containing some resilience and tensile data), bovine tibial and femoral bone	65

Table A4.001

Summery of the contents of the data sets used in this thesis

Due to the large size of the data sets used in this thesis I do not include lists of the raw data here as this would require many pages. However, I am happy to supply the data on disk (3.5 inch or 5.25 inch, MS-DOS) or in printed format. I suggest that the easiest way to contact my will be in writing, sending a blank disk if required, by way of one of the following addresses.

The Department of Biology
University of York
Heslington
York
YO1 5DD

93 Wainsford Road
Pennington
Lymington
Hants
SO41 8GG

APPENDIX 5

THE MATHEMATICAL REPRESENTATION OF VISCOELASTICITY

There are a number mathematical approaches that may be used to give a representation of linear viscoelastic behaviour for multiple step or non-step changes in stress or strain. One of which is based on the solution of the constitutive equations, giving the stress-strain-time relationships for step changes in stress or strain. These are then combined using Boltzmann's superposition principle. This approach enables the stress-strain-time relationship to be determined for a material subjected to a number of step changes, or differentiable non-step changes, of stress or strain. Another method is to obtain a direct solution of the equations for the loading conditions of interest. The application of this second approach is relatively easy for a limited range of loading conditions. The solution of the equations for step changes in stress or strain (as required by Boltzmann's superposition principle) and ramp changes by the second approach will be briefly outlined below. Further explanation of these approaches can be found in books such as that by Findley *et al.* (1989). Boltzmann's superposition principle is not examined in this thesis. This is because the stress-strain relationships for the loading conditions of interest here can be obtained directly.

The constitutive equation of a linear viscoelastic material may be expressed as a linear function of stress, strain and their time derivatives (as in equations 2.009 and 2.012). This can be represented by the following general expression, where $\sigma = \sigma(t)$ the variation of stress with time, and similarly $\varepsilon = \varepsilon(t)$ describes the variation of strain with time. (The dots indicate the derivatives with respect to time.)

$$f(\sigma, \dot{\sigma}, \ddot{\sigma}, \dddot{\sigma}, \ldots; \quad \varepsilon, \dot{\varepsilon}, \ddot{\varepsilon}, \dddot{\varepsilon}, \ldots) = 0 \qquad \text{(A5.001)}$$

This is commonly expressed in the more compact form of

$$P\sigma = Q\varepsilon \qquad \text{(A5.002)}$$

Where P and Q are linear differential operators with respect to time, Findley *et al.* express these mathematically as

$$P = \sum_{r=0}^{a} p_r \frac{\partial^r}{\partial t^r}, \qquad Q = \sum_{r=0}^{b} q_r \frac{\partial^r}{\partial t^r} \qquad \text{(A5.003))}$$

The differential operator form is expressed by the following equation

$$P\sigma = p_0\sigma + p_1\dot{\sigma} + p_2\ddot{\sigma} + \ldots + p_a\frac{\partial^a\sigma}{\partial t^a}$$

(A5.004)

$$= q_0\varepsilon + q_1\dot{\varepsilon} + q_2\ddot{\varepsilon} + \ldots + q_b\frac{\partial^b\varepsilon}{\partial t^b} = Q\varepsilon$$

There is no loss of generality if $p_0 = 1$. Taking the Laplace transform of the above equation results in the following equation.[1]

$$\hat{P}(s)\,\hat{\sigma}(s) = \left(p_0 + p_1 s + p_2 s^2 + \ldots + p_a s^a\right)\hat{\sigma}(s)$$

(A5.005))

$$= \left(q_0 + q_1 s + q_2 s^2 + \ldots + q_b s^b\right)\hat{\varepsilon}(s) = \hat{Q}(s)\,\hat{\varepsilon}(s)$$

where s is the transform variable. From this equation a more simple form of relationship can be expressed as follows.

$$\frac{\hat{Q}(s)}{\hat{P}(s)} = \frac{\hat{\sigma}(s)}{\hat{\varepsilon}(s)} \qquad \text{(A5.006)}$$

For the linear case p_r and q_r are, by definition, independent of stress and strain. By substituting the correct values into the terms in the above equations a description of idealised viscoelastic properties can be obtained. For example taking the simple three-element solid[2] the creep compliance J(t) (and the relaxation modulus Y(t)) can be calculated (remembering $p_0 = 1$) as follows

$$\sigma + p_1\dot{\sigma} = q_0\varepsilon + q_1\dot{\varepsilon} \qquad \text{(A5.007)}$$

This is the operator equation for the three parameter solid, changing this to the Laplace form gives the following equation

$$\hat{\sigma}(s) + p_1 s\,\hat{\sigma}(s) = q_0\,\hat{\varepsilon}(s) + q_1 s\,\hat{\varepsilon}(s) \qquad \text{(A5.008)}$$

Thus

---

[1]The application of a Laplace transform moves the differential equation from the time domain into a functional domain, in which it is expressed as an algebraic relationship. Use of algebraic manipulations permit the application of an inverse transformation, which returns the problem to the time domain, but in such a way that the original differential equation has been solved.

[2]The three-element solid is the mathematical representation of a Kelvin solid in series with a spring. I chose it as an example as it is commonly used to model bone: Sedlin (1965), Tennyson *et al.* (1972) and Tanabe *et al*, (1991a, b and c).

$$\hat{\sigma}(s)\,(1 + p_1 s) = \hat{\varepsilon}(s)\,(q_0 + q_1 s) \qquad \text{(A5.009)}$$

From the above equation it follows that

$$\hat{\sigma}(s) = \hat{\varepsilon}(s)\left[\frac{q_0 + q_1 s}{1 + p_1 s}\right] \qquad \text{(A5.010)}$$

and

$$\hat{\varepsilon}(s) = \hat{\sigma}(s)\left[\frac{1 + p_1 s}{q_0 + q_1 s}\right] \qquad \text{(A5.011)}$$

From this second equation the strain response to a step input of stress can be determined. This situation is the ideal creep test. The expression for the Laplace equivalent of a Heaviside step input of stress is given in equation A5.012. These and other equivalents are provided in standard tables. For example the books by Howatson *et al.* (1985) and Findley *et al.* (1989).

$$\sigma_0\, H(t) \Leftrightarrow \frac{\sigma_0}{s} \qquad \text{(A5.012)}$$

(Remembering that σ_0 is a constant and not a function of time.) Substituting this equation into equation A5.011 results in the following expression, which is for the strain during a creep test expressed in the functional domain.

$$\hat{\varepsilon}(s) = \frac{\sigma_0}{s}\left[\frac{1 + p_1 s}{q_0 + q_1 s}\right] \qquad \text{(A5.013)}$$

This equation is then expressed in partial fraction form, to enable the reverse transform to be completed (by use of the standard tables mentioned above).

$$\hat{\varepsilon}(s) = \sigma_0\left[\frac{1}{q_1 s\left(q_0/q_1 + s\right)} + \frac{p_1}{q_1\left(q_0/q_1 + s\right)}\right] \qquad \text{(A5.014)}$$

Using the convolution form of the inverse Laplace transform for two fractions of the right hand side of the equation, which are given below (equation A5.015), the strain response can be obtained.

$$\frac{1}{s\,(\alpha + s)} \Leftrightarrow \frac{1}{\alpha}\left(1 - e^{-\alpha t}\right) \qquad \text{and} \qquad \frac{1}{\alpha + s} \Leftrightarrow e^{-\alpha t} \qquad \text{(A5.015)}$$

Setting $q_0/q_1 = \alpha$, the strain response is expressed as follows

$$\varepsilon(t) = \sigma_0\left[\frac{1}{q_1}\left[\frac{q_1}{q_0}\left(1 - e^{-q_0 t/q_1}\right)\right] + \frac{p_1}{q_1} e^{-q_0 t/q_1}\right] \qquad \text{(A5.016)}$$

Consequently the creep compliance, $\varepsilon(t)/\sigma_0$, for a three-element solid is expressed as

$$J(t) = \left[\frac{1}{q_0}\left(1 - e^{-q_0 t/q_1}\right) + \frac{p_1}{q_1} e^{-q_0 t/q_1}\right] \qquad \text{(A5.017)}$$

Tables of such expressions for the creep compliance and relaxation modulus (and complex compliance) of a few simple models are provided in standard text books such as Findley *et al.* (1989) and Flügge (1975).

Taking equation A5.010 in place of A5.011 a similar procedure can be used to find the relaxation modulus. This process will result in the following equation

$$Y(t) = \left[q_0 - q_0 e^{-t/p_1} + \frac{q_1}{p_1} e^{-t/p_1}\right] \qquad \text{(A5.018)}$$

Equation A5.017 for the creep compliance and equation A5.018 for the stress relaxation modulus, can be expressed for the general case of a multiple parameter linear viscoelastic material. This could be achieved by using the same method on equation A5.005 or in place of equation A5.008. However, the solution is readily available in texts on the subject. The creep compliance and relaxation modulus can be expressed as follows; creep compliance is given by

$$J(t) = \frac{\varepsilon(t)}{\sigma_0} = C_0 + C_1 e^{-\alpha_1 t} + C_2 e^{-\alpha_2 t} + \ldots \qquad \text{(A5.019)}$$

The relaxation modulus is given by

$$Y(t) = \frac{\sigma(t)}{\varepsilon_0} = A_0 + A_1 e^{(-t/\tau_1)} + A_2 e^{(-t/\tau_2)} + \ldots \qquad \text{(A5.020)}$$

The basis for the derivation of the latter equation A5.020 can be found in Findley *et al.* These authors point out that experimentally it is usually easier to find the values of the coefficients (given above as A_0, A_1 and so on) rather than p_i and q_i. The coefficients in this equation can easily be derived for a linear viscoelastic solid, from stress and strain measurements taken during a stress relaxation or creep test. It is this approach, the experimental determination of the coefficients, which permits the mathematical representation of the behaviour of real materials. These equations can then be used to predict the material's behaviour under loading conditions, which are more likely to be encountered in real life.

Creep and stress relaxation are two aspects of the same behaviour. Therefore one is predictable from the other. This prediction is made possible by using the Laplace

transform of these quantities. In the function domain these two quantities are simply related by equation A5.021.[3]

$$\frac{\hat{\sigma}(s)}{\hat{\varepsilon}(s)} = s\,\hat{Y}(s) = \frac{1}{s\,\hat{J}(s)} \qquad \text{(A5.021)}$$

It was implied above that the determination of the coefficients of equation A5.019 or A5.020 from creep or stress relaxation tests is not a useful exercise in its own right. To benefit from this procedure these results need to be manipulated, to enable the prediction of the material's behaviour under more general or realistic loading histories. One such method for linear viscoelastic materials is Boltzmann's superposition principle, in which an irregular loading pattern is visualised as being made of distinct step changes in stress or strain. (If the loading pattern is differentiable the step size becomes infinitely small.) However, as mentioned above the Laplace transform method can also be used in situations other that the Heaviside step function. Thus if the values of the coefficients p_i and q_i have been determined for a material, (or a specific model, which incorporates a limited number of coefficients, is being tested) a prediction of behaviour under various loading conditions can be made. As a demonstration of this method the same material as used above, the three-element solid, will be subjected to a ramp input. In the first case the ramp input will be stress and in the second a strain. (These inputs can be viewed as idealised tensile tests.)

If the stress is applied at a constant rate $\dot{\sigma}$ the stress at any time is described by $\sigma(t) = \dot{\sigma}\,t$, where t is the time measured from the start of the load application. The appropriate Laplace transform for such a ramp function is given below.

$$\dot{\sigma}\,t \Leftrightarrow \frac{\dot{\sigma}}{s^2} \qquad \text{(A5.022)}$$

Taking equation A5.011, and substituting equation A5.022 (in the same way as above), results in the following equation.

$$\hat{\varepsilon}(s) = \frac{\dot{\sigma}}{s^2}\left[\frac{1 + p_1 s}{q_0 + q_1 s}\right] \qquad \text{(A5.023)}$$

This can be expanded to

---

[3]This form of analysis was the basis of an experiment I undertook before this study. The coefficients of Y(t) were obtained for a specimen of bovine bone and used to predict those of J(t). Predictions of strain during a creep test were then compared with experimentally obtained data. The difference in the strain values was < 5%. The coefficients were approximately $A_0 = 15$ GPa, $A_1 = 0.5$ GPa, $A_2 = 0.6$ GPa, $\tau_1 = 1400$ and $\tau_2 = 170$ where time was in seconds.

$$\hat{\varepsilon}(s) = \dot{\sigma}\left[\frac{1}{s^2\,(q_0 + q_1\,s)} + \frac{p_1\,s}{s^2\,(q_0 + q_1\,s)}\right] \qquad \text{(A5.024)}$$

This equation may then be expressed in partial fraction form as

$$\hat{\varepsilon}(s) = \dot{\sigma}\left[\frac{1}{q_1}\,\frac{1}{s^2\left(q_0/q_1 + s\right)} + \frac{p_1}{q_1}\,\frac{s}{s^2\left(q_0/q_1 + s\right)}\right] \qquad \text{(A5.025)}$$

Returning this equation back to the time domain[4] gives

$$\varepsilon(t) = \dot{\sigma}\left[\frac{1}{q_1}\left(\frac{q_1\,t}{q_0} - \left(\frac{q_1}{q_0}\right)^2\left(1 - e^{-q_0\,t/q_1}\right)\right) + \frac{p_1}{q_1}\left(\frac{q_1}{q_0}\left(1 - e^{-q_0\,t/q_1}\right)\right)\right] \qquad \text{(A5.026)}$$

which simplifies to

$$\varepsilon(t) = \dot{\sigma}\left[\frac{t}{q_0} + \left(\frac{p_1}{q_0} - \frac{q_1}{q_0^2}\right)\left(1 - e^{-q_0\,t/q_1}\right)\right] \qquad \text{(A5.027)}$$

or

$$\varepsilon(t) = \frac{\sigma(t)}{q_0} + \dot{\sigma}\left(\frac{q_0\,p_1 - q_1}{q_0^2}\right)\left(1 - e^{-q_0\,t/q_1}\right) \qquad \text{(A5.028)}$$

Clearly for a fixed stress rate the deviation from the time-independent linear response, $\varepsilon(t) = \sigma(t)/q_0$, increases with time (the value of the term in the extreme right hand parentheses changes from 0 at $t = 0$, to 1 at $t = \infty$). Similarly if some value of stress is considered, σ_1, then the strain exhibited by this solid can be shown to be dependent on the stress rate, in the following way.

$$\varepsilon_1 = \frac{\sigma_1}{q_0} + \dot{\sigma}\left(\frac{q_0\,p_1 - q_1}{q_0^2}\right)\left(1 - e^{\beta}\right) \qquad \text{(A5.029)}$$

where $\beta = -q_0\,\sigma_1/\dot{\sigma}\,q_1$ (by virtue of $t = \sigma_1/\dot{\sigma}$). As the stress rate increases the term within the extreme right hand parenthesis of equation A5.029 will tend towards zero. Thus at the highest stress rates the viscoelastic component of the deformation is very small. Obviously the exact proportion of the deformation that is time-dependent under such fixed conditions will be governed by the magnitude of the constants p_n and q_n. A

---

[4]By using $\frac{1}{s^2\,(\alpha + s)} \Leftrightarrow \frac{t}{\alpha} - \frac{1}{\alpha^2}\left(1 - e^{-\alpha t}\right)$ and $\frac{1}{s\,(\alpha + s)} \Leftrightarrow \frac{1}{\alpha}\left(1 - e^{-\alpha t}\right)$.

value of the secant compliance could be obtained from this equation, but this will not be done here.

The same approach (as used above for constant stress rate) can be used for a constant strain rate input $\varepsilon(t) = \dot{\varepsilon}\, t$. In this case the substitution is into equation A5.010.

$$\hat{\sigma}(s) = \frac{\dot{\varepsilon}}{s^2}\left[\frac{q_0 + q_1 s}{1 + p_1 s}\right] = \dot{\varepsilon}\left[\frac{q_0 + q_1 s}{s^2 (1 + p_1 s)}\right] \qquad \text{(A5.030)}$$

which becomes

$$\hat{\sigma}(s) = \dot{\varepsilon}\left[\frac{q_0}{s^2 (1 + p_1 s)} + \frac{q_1 s}{s^2 (1 + p_1 s)}\right] \qquad \text{(A5.031)}$$

Then representing this equation in partial fraction form gives

$$\hat{\sigma}(s) = \dot{\varepsilon}\left[\frac{q_0}{p_1}\,\frac{1}{s^2\left(1/p_1 + s\right)} + \frac{q_1}{p_1}\,\frac{s}{s^2\left(1/p_1 + s\right)}\right] \qquad \text{(A5.032)}$$

Returning to the time domain gives

$$\sigma(t) = \dot{\varepsilon}\left[\frac{q_0}{p_1}\left(\frac{p_1 t}{1} - \left(\frac{p_1}{1}\right)^2 \left(1 - e^{-t/p_1}\right)\right) + \frac{q_1}{p_1}\left(\frac{p_1}{1}\left(1 - e^{-p_1 t}\right)\right)\right]$$

(A5.033)

Equation A5.033 is the same as

$$\sigma(t) = \dot{\varepsilon}\left[\left(q_0 t - q_0 p_1 \left(1 - e^{-t/p_1}\right)\right) + q_1 \left(1 - e^{-t/p_1}\right)\right] \qquad \text{(A5.034)}$$

Thus

$$\sigma(t) = \dot{\varepsilon}\left[q_0 t + (q_1 - q_0 p_1)\left(1 - e^{-t/p_1}\right)\right] \qquad \text{(A5.035)}$$

Using the relationship of time and strain rate gives

$$\sigma(t) = \varepsilon(t)\, q_0 - \dot{\varepsilon}\,(q_0 p_1 - q_1)\left(1 - e^{-t/p_1}\right) \qquad \text{(A5.036)}$$

In this case the higher the strain rate the closer the relationship is to the time-independent one. Similar statements to those made above, regarding the departure from linearity, can also be applied to this equation.

APPENDIX 6

CREEP FRACTURE IN BONES WITH DIFFERENT STIFFNESSES: A PAPER BY MAUCH, CURREY AND SEDMAN

Erratum: Since the publication of this paper I have found that we made a typographical error in the preparation of the manuscript. Examination of the data shown in figure 2 and the values of the coefficients given in table 1A show a discrepancy in the results for specimens of bovine ulna. This discrepancy arises from the value of A being given as 15.5 when it should have been given as 11.5. As I reported in section 3.3.3, this erroneous value was then used to obtain the predictions of the time-to-rupture under a creep load of 100 MPa. The correct prediction is 1260 seconds, in place of 12.6×10^6 s. Thus giving a time that is about the same fraction of an hour as that previously given is of a year.

J. Biomechanics Vol. 25, No. 1, pp. 11–16, 1992.
Printed in Great Britain

0021-9290/92 $5.00 + .00
Pergamon Press plc

CREEP FRACTURE IN BONES WITH DIFFERENT STIFFNESSES

MARIANNE MAUCH, JOHN D. CURREY and ANDREW J. SEDMAN
Department of Biology, University of York, York YO1 5DD, U.K.

Abstract—Creep fracture experiments were used to examine the differences in time to fracture of bones with very different Young's moduli (bovine bone and red deer antler) and the implications of these differences for the 'cumulative-damage' model of Caler and Carter [*J. Biomechanics* 22, 625–635 (1989)] for bone fracture. Using normalised stress as the explanatory variable, the slopes of the distributions agreed quite well with that of Caler and Carter for human bone. However, antler took far longer to fracture at any given normalised stress than did bovine bone. Using stress alone as the explanatory variable, the relationships within each bone type almost disappeared. *Within* any bone type strain is the important determinant of time to fracture, but less mineralised bone takes much longer to fracture at any given strain, or normalised stress, which seems not to be in accord with the cumulative-damage model. The rate of damage accumulation in lightly mineralised bone at high strains (> 1%) is much less than that occurring in more heavily mineralised bone.

INTRODUCTION

Bone is not a completely brittle material. The tensile load–deformation curve of well-mineralised bone has two rather distinct parts: a nearly linearly elastic region, followed, after a short and quite well-defined transition zone, by a region in which the load increases rather little while the strain increases to about 2%, which is more than three times the strain at yield (Fig. 1A). An understanding of the fracture behaviour of bone requires an understanding of the processes occurring in the relatively long post-yield region.

Most metals, if they are unloaded and reloaded after they have undergone post-yield deformation, have a modulus of elasticity effectively the same as that they showed initially (Wyatt and Dew-Hughes, 1974). In bone, however, it seems that post-yield behaviour is characterised by microdamage in the form of tiny cracks which, at least initially, do not spread through the bone (Currey and Brear, 1974).

In 1985 Carter and Caler proposed a cumulative-damage model for the fracture of bone, derived from tests in cyclical fatigue loading, and also in monotonic tensile loading. Their idea was that bone fractured when it had suffered a certain amount of damage, and that the rate of damage accumulation was related to some high power of stress. According to their model, under *constant* stress, failure occurred at time T_B, where $T_B = A\sigma^{-B}$, A and B being empirically determined constants. The rate of damage accumulation dD/dt is given by

$$dD/dt = 1/(A\sigma^{-B}).$$

It follows that in a test involving monotonic loading to fracture, a low stress rate allows more time for damage to accumulate, at any particular stress, than will be available at a higher stress rate. Thus, low stress rates will produce lower strengths. Carter and Caler (1983, 1985) derived the following equation for the ultimate strength σ_{ult}:

$$\sigma_{ult} = [A(B+1)]^{1/(B+1)}\dot{\sigma}^{1/(B+1)},$$

where $\dot{\sigma}$ is the stress rate. The parameters A and B were determined from creep tests. Using six specimens, they determined the values of A and B for human femur at 36°C to be 3.02×10^{35} and 17.95, respectively, where stress is expressed in megapascals, and time in seconds. From this they estimated the stress rate dependence of bone strength to be given by

$$\sigma_{ult} = 87\dot{\sigma}^{0.053}.$$

If bone is assumed to be a linear material with a Young's modulus of 17 GPa, the above relationship translates approximately to $\sigma_{ult} = 147\dot{\varepsilon}^{0.055}$ (Carter and Caler, 1985). These predictions, resulting from creep tests, were found to be a fairly good fit to the results of strain rate experiments (Carter and Caler, 1985; Currey, 1989).

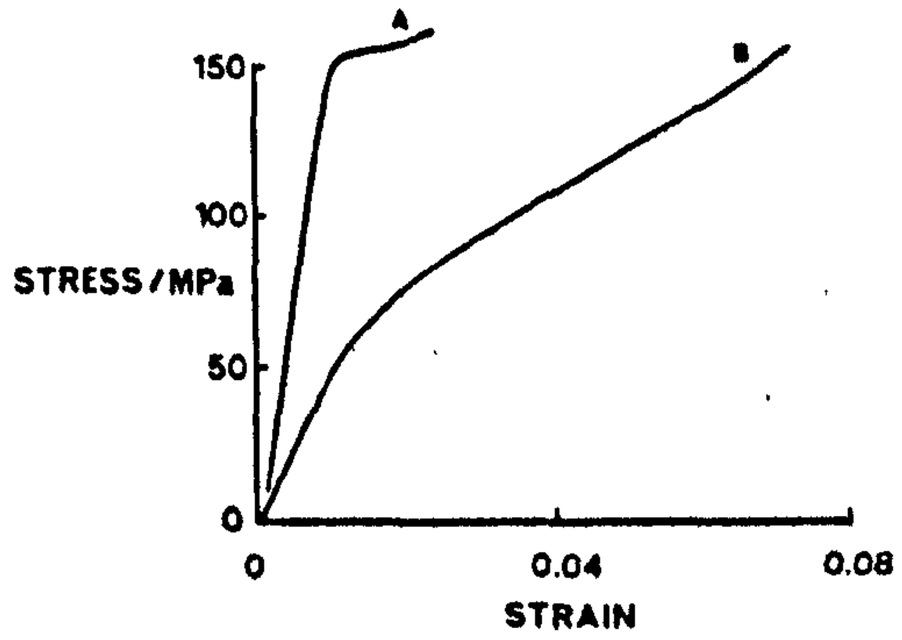

Fig. 1. Typical stress–strain curves. (A) 'Standard' bone such as is found in young cattle. (B) Antler.

Received in final form 12 *June* 1991.

In a later, somewhat more extended test, using 11 specimens and a greater range of time to rupture, Caler and Carter (1989) did not use stress (σ) but 'normalised' stress, which is stress/Young's modulus (σ/E). For specimens loaded in the linear region only, this is equivalent to strain. Caler and Carter found the exponent B to be about 16 for human cortical bone, that is, the rate of damage accumulation was proportional to $(\sigma/E)^{16}$.

An important implication of this model is that after yield the stress should not increase very much before failure. Because of the high value of B, the rate of damage accumulation is negligible at low stresses, but becomes very high once damage starts to accumulate at a measurable rate. If B is 16, and the damage accumulation rate is assumed to be unity at the stress at which the curve begins to bend over (which we arbitrarily call the yield stress), then the damage accumulation rate at 80% of yield stress is 0.03, at 90% it is 0.19, at 110% it is 4.6, and at 120% it is 18. Clearly, the specimen will fail very quickly as the stress rises above the level at which damage, as indicated by the bending over of the stress–strain curve, becomes apparent.

In 1989 Currey showed that reindeer antler (whose bone has a rather low degree of mineralisation and, therefore, a low Young's modulus) had a strain rate dependence of ultimate strength very similar to that found by Carter and Caler in human bone. It was reasonable, therefore, to assume that Carter and Caler's cumulative-damage model was applicable to antler as well as to cortical bone, and perhaps by extension to all compact bone.

However, there remained the difficulty that in antler there was a considerable increase in stress after the point of yield, the stress at failure being considerably greater than the stress at yield (Fig. 1B). For the reason given above this finding is difficult to accommodate with a model giving a value of 16 for the exponent B. A possible explanation would be that 'yield' in highly mineralised bone is a different phenomenon from 'yield' in antler. The difficulty mentioned above would disappear if yield in antler did not indicate the initiation of damage occurring at a high rate, but were some non-linear elastic or viscoelastic phenomenon. Then, of course, an explanation would be needed for the process of yield in antler itself.

The experiments of Currey (1989) showed that human bone and antler behaved similarly in regard to strain rate. However, there is a clear difference between antler and ordinary bone in their post-yield behaviour.

The purpose of this paper is to compare the creep-rupture behaviour of more and less highly mineralised bone (bovine and antler, red deer antler in this case) to determine whether they fall into the same general pattern, as would be implied by Carter and Caler's model and, if they differ, to determine what are the important variables affecting the creep-rupture behaviour of different types of bone.

MATERIALS AND METHODS

The specimens of bovine bone were obtained from ulnae that had been stored deep-frozen. The specimens were taken from the mid-shaft of two bones, and were taken from sites all round the bone. The antler specimens were taken from the base and from the tips of a normal hard antler of a red deer (*Cervus elaphus*). They had been stored dry. Drying and rewetting seems to have little effect on the mechanical properties of bone (Currey, 1988a). (Hereafter the specimens of bovine bone will be called 'bone', the bone from the red deer antler will be called 'antler'.)

It must be emphasised that antler is, in most respects except that it is lightly mineralised, like ordinary bone (Watkins, 1987). Although it grows extraordinarily quickly, it is *not* made of woven bone. It shows the standard fibrolamellar pattern characteristic of rapidly produced bone such as is found in the long bones of large herbivorous mammals (like bovines), and dinosaurs (Currey, 1987). That is, there are widely separated struts of parallel-fibred bone, with the space between filled in with highly oriented lamellar bone. Vincent (1990, p. 186) shows this very clearly. [Watkins (1987) uses the term 'osteonic' when describing antler; by this term he is referring to primary osteons, and not secondary osteons, or Haversian systems as they are often called (Currey, 1982).] Antler is also highly anisotropic, the general grain of the bone being along the length of the antler. Although some antler is highly porous, the specimens used in this study were nearly fully dense bone.

All test specimens were oriented so that their long axis was along the length of the bone or antler from which they came. The specimens were kept wet at all times during machining and until after testing, which was at room temperature. First, each specimen was rough-machined with a bandsaw, and then ground with medium and fine grit to a size of about $1.8 \times 7 \times 55$ mm. At this stage the Young's modulus of elasticity of the specimen was determined by three-point bending in an Instron 1122 table testing machine, using a gauge length of 45 mm. Young's modulus was calculated from the deflection of the mid-point, the deflection itself was determined from crosshead travel, allowance being made for machine compliance. Deformation rate was 1 mm min^{-1}. During this procedure great care was taken to ensure that the specimens were loaded only in the elastic region. We have found that there is a close relationship between Young's modulus as determined in bending and in tension (Currey, 1988b).

In this paper Young's modulus of elasticity is discussed as if it were a constant for a particular material. In fact, bone, like many other materials, is viscoelastic

and so the measured value of Young's modulus incorporates a viscous component and is to some extent a function of strain rate. However, the variation in strain rate in our experiments is small and will have had a negligible effect on the estimated values of Young's modulus.

The specimens were then machined into conventional tensile specimens, with 7 mm wide ends, leading by rounded shoulders to a central gauge length of 13 mm and a cross-section of 2.0 mm by 1.5 mm. After machining, the specimens were stored briefly in a refrigerator. They were allowed to reach room temperature before testing.

Creep fracture

The specimens were clamped by their expanded ends. Water-soaked tissue paper was wrapped round the specimens, and was itself wrapped round by adhesive tape. This prevented evaporation, only very occasional addition of water being needed. All specimens were found to be completely wet after fracture. Specimens were tested at room temperature, which varied from 20°C to 22°C in different experiments.

The load was applied to each tensile specimen by raising the crosshead of the tensile testing machine, which in turn caused the specimen to lift a predetermined weight via a lever. A preliminary set of tests indicated the values of σ/E to which the bones could be loaded without breaking immediately. Thereafter, four specimens were excluded from the results, one because it was found to have a large internal flaw, and three because they did not break (these are indicated in Figs. 2 and 3).

The stresses to which the specimens were subjected were chosen so as to obtain a wide range of times to fracture. The time course of the loading was followed by a pen recorder; the load on the specimen always increased smoothly. When the load was fully supported the crosshead was stopped. The time from the start of loading to full load varied slightly around 6 s, implying a strain rate of about $0.002\,s^{-1}$. Thereafter the load was constant, although it was monitored to ensure that it was so. The time to fracture, which did not include the loading time, was determined from the chart or, for longer-lasting experiments, from a digital clock activated by a microswitch. The set-up used in this experiment did not allow the determination of strain.

Since the loading to full load took about 6 s, times to fracture from the moment that the final load was reached were necessarily affected by any damage occurring during the loading period. However, as is shown above, it is improbable that much damage takes place until close to the final load. To allow for this initial damage to some extent, the time to fracture was taken to be the time from the moment the crosshead stopped, plus one second.

After fracture little holes were drilled in the central section of the specimens and the bone material so obtained was used to determine the calcium content of the specimens using the colorimetric method of Sarkhar and Chauhan (1967). Fracture surfaces of various specimens were examined in a scanning electron microscope.

RESULTS

Time to fracture as a function of stress

Figure 2 shows the results of the present experiments when stress (σ) is used as an explanatory variable. Clearly, there is no *overall* relationship between time to fracture and σ. The linear regression equations for the different bone types are given in Table 1A, along with equations from the human bone investigated by Caler and Carter. [Caler and Carter (1989) did not give the data that allow this analysis to be performed, and we are extremely grateful to Dr Dennis Carter for giving us a copy of their laboratory notebook to make the analysis possible.] The relationships for the non-human bone are very weak, and only that for antler base is significant. However, the distribution for the different types of bone (bovine and antler) are somewhat different, the points for the bovine bone lying to the right of those for the antler. That implies that, at any stress, the bovine bone will take longer to fracture than will the antler. Taking the regression equations at face value, they imply that if loaded to a stress of 100 MPa, the bovine bone would fracture in 12.6×10^6 s, the antler base in 63 s, and the antler tip in 8 s.

Time to failure as a function of σ/E

The results from the present experiments, and from Caler and Carter's experiment, are shown in Fig. 3. The linear equations describing the results are given in Table 1B. A test for homogeneity of slope gave no

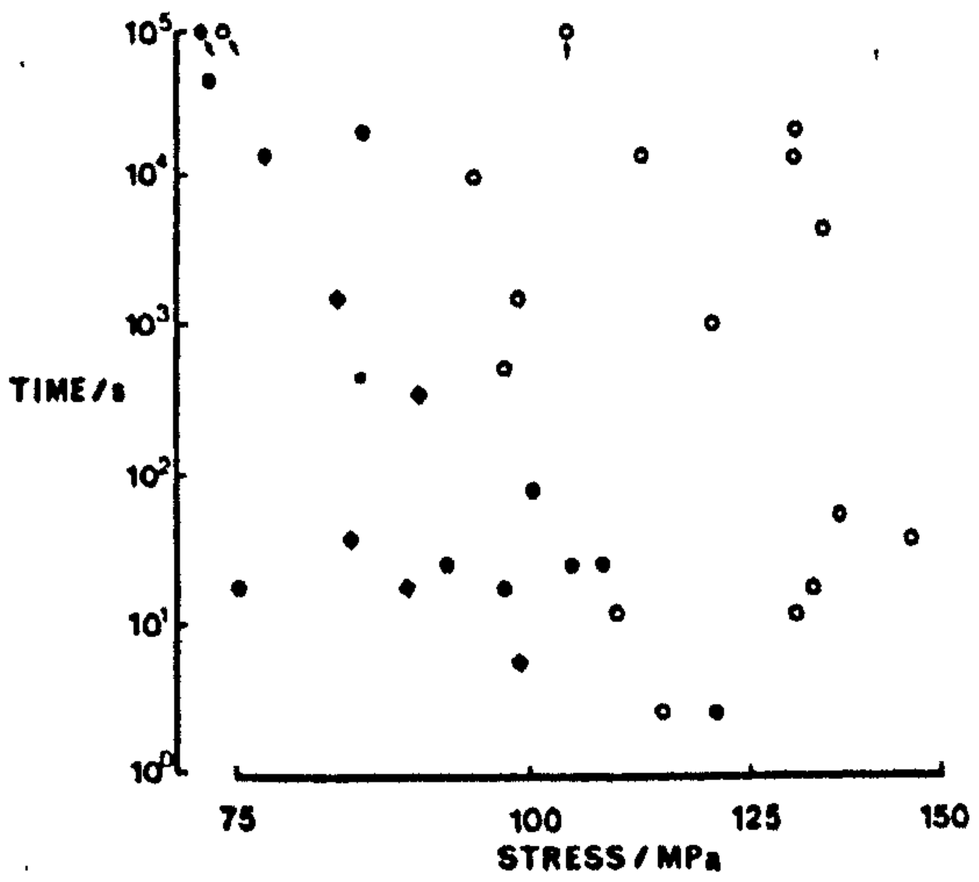

Fig. 2. Time to fracture as a function of stress. Symbols (which are repeated in the later figures): open circles: bovine; solid circles: antler base; solid lozenges: antler tip. The arrows indicate specimens that had not fractured after 100,000 s.

Table 1A. Values of the coefficients in the equation log (time to failure) = $A + B$ log (stress), time being measured in seconds, stress in MPa. s is the standard error of the estimated coefficients of the slope. Values for coefficients with non-significant t values in parentheses. The values for Caler and Carter's human bone experiment are derived from their published work (Caler and Carter, 1989) and from data made available to us by them

Tissue	N	A	B	s	t	P	R^2
Human femur	11	31.4	−15.2	0.75	6.55	<0.001	80.7
Bos ulna	14	15.5	(−4.2)	1.39	0.66	0.52	0.0
Antler base	10	31.6	−14.9	1.11	2.92	0.019	45.5
Antler tip	5	42.9	(−21.0)	0.85	1.39	0.211	27.4

Table 1B. As for Table 1A, except that the explanatory variable is (stress/Young's modulus), not stress alone

Tissue	N	A	B	s	t	P	R^2
Human femur	11	−36.3	−16.3	0.40	13.29	<0.001	94.1
Bos ulna	14	−34.6	−16.7	0.96	3.81	0.003	50.9
Antler base	10	−47.8	−26.9	1.08	3.06	0.015	48.2
Antler tip	5	−39.3	−21.0	0.33	5.83	0.010	89.2

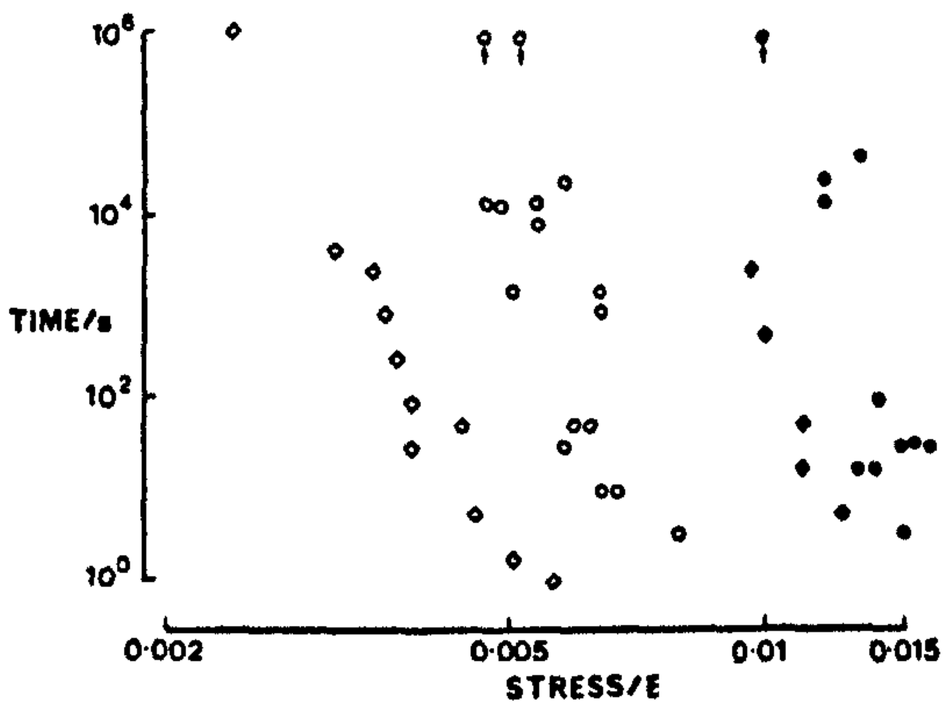

Fig. 3. Times to fracture as a function of (σ/E). Open lozenges: human bone, data of Caler and Carter. The arrows indicate the value of (σ/E) of specimens that had not fractured after 100,000 s.

Table 2A. Test for difference of slope. This was applied to all four regressions in which (stress/Young's modulus) was the explanatory variable

H0: Same slope (different intercepts)
H1: Different slopes (different intercepts)
$RSS_{H0} = 23.7$, $RSS_{H1} = 22.1$
$df_{H0} = 35$, $df_{H1} = 32$
Test statistic: $((RSS_{H0} - RSS_{H1})/(df_{H0} - df_{H1}))/(RSS_{H1}/df_{H1})$
$= 0.77$; 95% critical values $F_{3,32} = 2.9$
There is no evidence that the slopes are different.
Residual analysis suggests that normality assumptions are valid.

Table 2B. Test for difference of intercept. (The results of Caler and Carter are not included in this part of the analysis)

H0: Same intercepts (same slopes),
H1: Different intercepts (same slopes),
$RSS_{H0} = 43.9$ $RSS_{H1} = 21.9$
$df_{H0} = 27$ $df_{H1} = 25$
Test statistic: as above
$= 6.8$; 99% critical value $F_{2,25} = 5.57$
Reject H0, the intercepts are different.

The intercepts, having been forced all to have the same slope are:

Bos ulna:	17.55
Antler base:	24.29
Antler tip:	22.00

The test for the differences between the intercepts was based on Sheffe's multiple confidence intervals for all contrasts. All intercepts were significantly different from each other at the 0.01 level.

evidence that the slopes are different from each other (Table 2A).

Comparing the results of Caler and Carter from the human femur with ours from the bovine bone, it is clear that the bovine ulna specimens took, at any particular value of σ/E, a much longer time to fracture than the human specimens. However, this difference is not important. Compared with the experiments of Carter and Caler, our experimental methods involved different specimen temperatures; whereas the experiment of Caler and Carter was carried out near body temperature, our experiments were carried out at room temperature. It would be surprising if the fracture process were not in some way temperature-sensitive.

Of course, apart from temperature there are several other differences between Caler and Carter's methods and ours: the geometry of the specimens was somewhat different, Young's modulus was determined by different methods, and the strain rates used for initial loading were different. Whether these factors produced any further differences between the results is difficult to say. It is not perhaps important, because our results showed the same *general* relationships as

shown by Carter and Caler, and the purpose of the present experiments is not to compare our results with theirs, but to attempt to assess the significance of our own results for an understanding of fracture in bone.

All our experiments were carried out at virtually the same temperature. The regression analysis provides no good reason for supposing that the slopes are different. Nevertheless, although the scatter about the lines for the bovine ulna and the antler base is rather large, the differences in their *position* are real, that is, all three sets of points are differently placed along the X-axis (Table 2B).

The difference between the relatively highly mineralised, high Young's modulus bovine bone and the antlers is striking. For example, if a loading of σ/E of 0.006 is applied to the bones, the equations predict that the bovine ulna will fail in about 320 s, the antler tip in 260 d, and the antler base in 29,000 yr. These are much larger differences between the bones than those seen when stress alone was the explanatory variable; furthermore, it is now the antler which has the greater predicted fracture time.

Figures 4(a) and (b) show the scatterplots for the data of Caler and Carter using σ and σ/E as explanatory variables. The fit is less good in the former case ($R^2 = 80.7$ and 94.1% for the two explanatory variables, respectively), but the negative relationship is still clear.

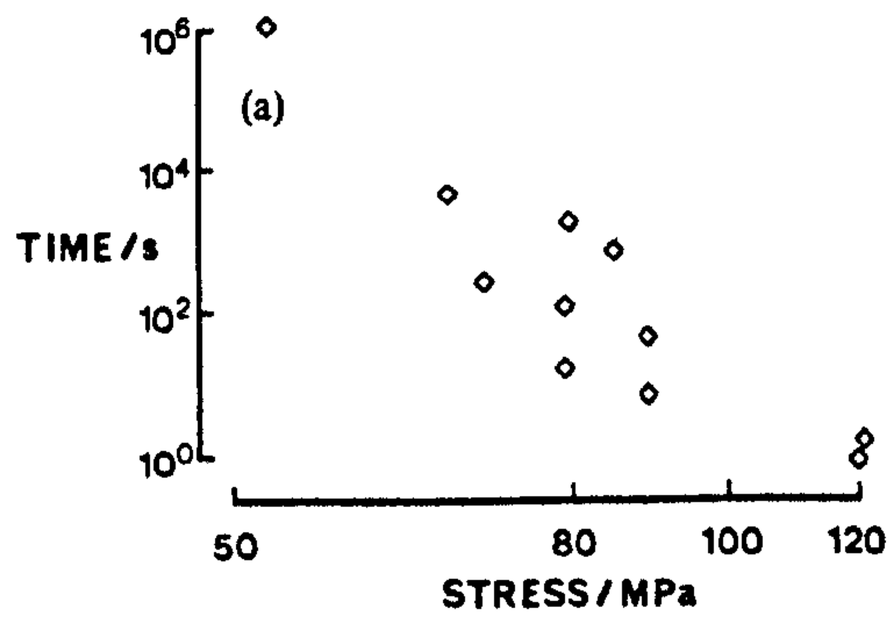

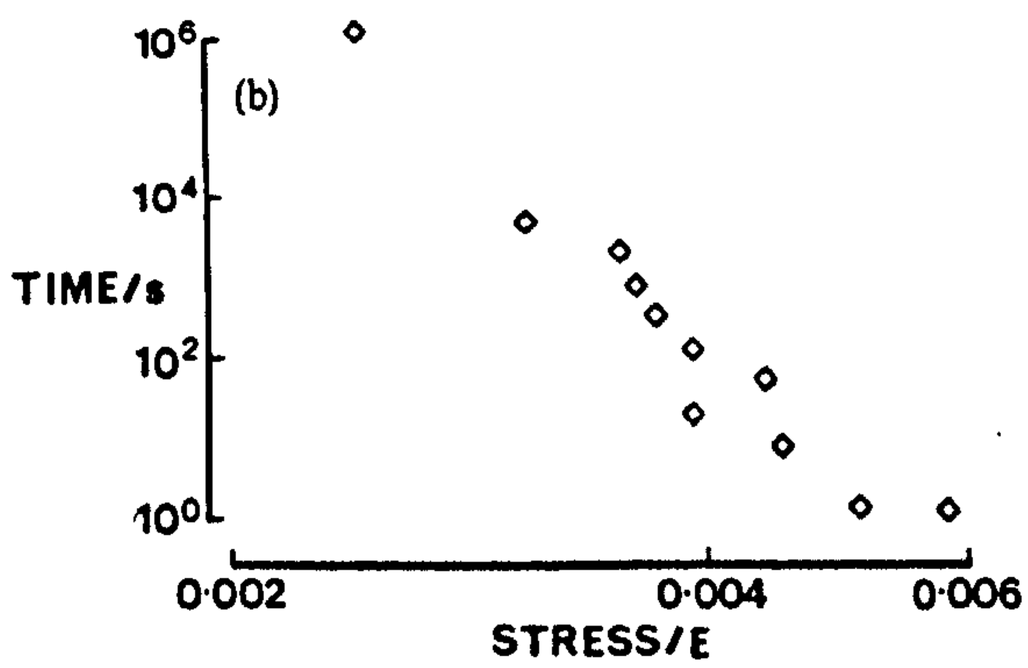

Fig. 4. (a) Human bone, time to fracture as a function of stress. Data of Carter and Caler. (b) Human bone, time to fracture as a function of (σ/E).

Fracture surface and calcium content

Caler and Carter (1989) examined the fracture surface of some of their specimens. In general, specimens that had been loaded to a low normalised stress, and which therefore took a long time to fracture, showed a rough fracture surface at a fine level, but a macroscopically rather flat surface. Specimens that bore a high load, and fractured within a second or so, showed a flatter surface at all levels of magnification (Caler and Carter, 1989, Figs 4 and 5). Our bovine specimens had an appearance similar to those of Caler and Carter, although some of our specimens that failed after a long time had two regions, one extremely rough, and the other much smoother. Presumably, the rough region is where the specimen started to fail, over a long time, and the smoother region is where the crack travelled much more quickly immediately prior to failure.

In marked contrast, the antler specimens were always very rough, whether they had fractured at once or after many hours. There was no obvious difference between the surfaces of the specimens at each end of the time scale. In general, antler fracture surfaces were much rougher at higher magnifications than were the bovine specimens, whatever the time before fracture. Although this roughness is likely to be associated with toughness, it does not in itself give insight into the creep behaviour of antler as opposed to bovine bone.

Figure 5 shows the values of Young's modulus and calcium content of the specimens, and also the relationship between them. The antlers have both a lower Young's modulus and lower calcium content than the bovine bone. The relationship between the two properties is in accord with the general relationship reported previously by Currey (1988b). In particular, rather small differences in calcium content are associated with very large differences in a mechanical property. Variation in Young's modulus is to a very large extent determined by variation in calcium content or mineral.

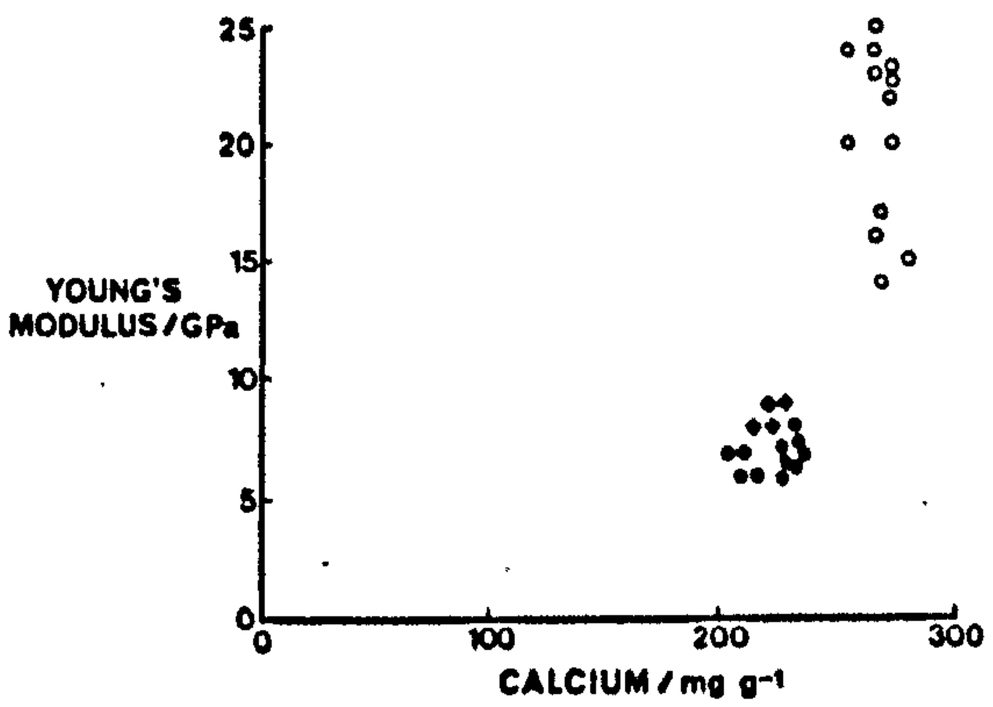

Fig. 5. Young's modulus as a function of calcium content (milligrams of calcium per gram of dry bone). The lower set of points are all antler, the upper set all bovine. Note the strongly non-proportional relationship.

DISCUSSION

These results show that there are great differences in the creep-rupture properties of red deer antler compared with 'ordinary' bone. All types of bone and antler show a reduction in the time to failure as σ/E is increased. The relationships are not clean, and there is no evidence that the *slopes* of the lines are different. Naturally, the fact that there is no statistical evidence that the slopes are different does not mean that they are the same; indeed, the relatively high values of s (the standard error) and low values for R^2 imply that the calculated values for the slopes should be treated with reserve. However, whether the slopes are or are not different, their positions certainly are. Antler takes far longer to rupture at any given value of σ/E than does bone. On the other hand, if stress is taken as the explanatory variable, the evidence for a negative relationship between time to failure and stress is much weaker, and disappears in the case of bovine bone.

Figure 2 shows that, in bones taken as a whole, there is no relationship between stress and time to fracture. There is, however, a clear indication that the more highly mineralised bone survives longer at any stress than the less mineralised antler bone. Since the data of Caler and Carter for human bone, and our own data for each separate type of bone, show that there is indeed a clear relationship between time to fracture and σ/E (which is effectively some measure of the initial strain) the problem is: why is there no relationship *overall*? At the moment there is no answer to this. However, a probable explanation may relate to the nature of the changes taking place in bone and antler during large strains. We propose that the relatively highly mineralised bovine bone is incapable of undergoing strains of more than about 0.005 without suffering damage. If the load producing such a strain is maintained, more damage is continually incurred. On the other hand, the more lightly mineralised bone found in antler seems able to undergo considerably larger strains before significant damage starts to accumulate (albeit at lower *stresses* than those causing irreversible changes in bovine bone).

Observations in our laboratory indicate that this is indeed the case. On loading bovine bone to a strain of about 0.005 the yield point is reached. If the bone is loaded further, then on reloading after unloading the compliance is found to have increased, indicating that damage has occurred. In contrast to this, antler can be loaded to a strain of about 0.02 before increased compliance is detectable on reloading after unloading. It may be that the antler undergoes 'damage' of some kind that heals on unloading.

The cumulative-damage model of Caler and Carter supposes that damage accumulates as some high power of stress or, assuming that the material is linear, of strain. The experiments reported in this paper show, first, that it is strain, not stress, that is the important variable and, second, that bones of different degrees of mineralisation show markedly different responses to strain: strain that would cause a highly mineralised specimen to accumulate damage at a very high rate leaves less mineralised bone unaffected. Although the cumulative-damage model is in many ways very satisfactory, to be comprehensive it needs to take into account the markedly differing responses to strain of bones of different degrees of mineralisation. Experiments on bone material with mineralisation intermediate between those of antler and bovine bone should give insight into this phenomenon.

Acknowledgement—AJS was supported by an SERC Studentship. J. Byrne, of the University of York Computer Service, provided statistical advice.

REFERENCES

Caler, W. E. and Carter, D. R. (1989) Bone creep-fatigue damage accumulation. *J. Biomechanics* **22**, 625–635.
Carter, D. R. and Caler, W. E. (1983) Cycle-dependent and time-dependent bone fracture with repeated loading. *J. biomech. Engng* **105**, 166–170.
Carter, D. R. and Caler, W. E. (1985) A cumulative damage model for bone fracture. *J. orthop. Res.* **3**, 84–90.
Currey, J. D. (1982) 'Osteons' in the biomechanical literature. *J. Biomechanics* **15**, 717.
Currey, J. D. (1987) The evolution of the mechanical properties of amniote bone. *J. Biomechanics* **20**, 1035–1044.
Currey, J. D. (1988a) The effects of drying and rewetting on some mechanical properties of compact bone. *J. Biomechanics* **21**, 439–441.
Currey, J. D. (1988b) The effect of porosity and mineral content on the Young's modulus of elasticity of compact bone. *J. Biomechanics* **21**, 131–139.
Currey, J. D. (1989) Strain rate dependence of the mechanical properties of reindeer antler and the cumulative damage model of bone fracture. *J. Biomechanics* **22**, 469–475.
Currey, J. D. and Brear, K. (1974) Tensile yield in bone. *Calcif. Tissue Res.* **15**, 173–179.
Sarkhar, B. C. and Chauhan, U. P. S. (1967) A new method for determining micro quantities of calcium in biological materials. *Anal. Biochem.* **20**, 155–156.
Vincent, J. (1990) *Structural Biomaterials*. Princeton University Press, Princeton, NJ.
Watkins, M. R. (1987) The development of a tough artificial composite based on antler bone. Ph.D. thesis, University of Reading, U.K.
Wyatt, O. H. and Dew-Hughes, D. (1974) *Metals, Ceramics and Polymers*. Cambridge University Press, Cambridge.

APPENDIX 7

THE NON-CONSTANT STRAIN RATE EXHIBITED BY AN OPEN LOOP MATERIALS TESTING MACHINE

In a number of sections of this thesis I have stated that the measured value of various mechanical properties and the rate at which stress and strain are applied to the specimen could be determined to a small degree by what I have referred to as a machine-specimen interaction. I have attributed this interaction to the use of an open loop testing machine.[1] Due to the very nature of such a control loop there is no mechanism by which the machine can monitor the difference between the required testing rate and that experienced by the specimen. The main contributory factors to this error are the deflections that occur outside the gauge length of the specimen. I will now explain the effect of such machine deflections on the quantities investigated in this thesis. This explanation will be based of the examination of an analogy of a tensile test. Some comments of how this effect may effect other forms of test are presented at the end of this appendix.

For the experiments conducted for this thesis an Instron 1122 materials testing machine was used. This is an open loop, screw-driven, machine. The main elements of this type of machine are shown in figure A7.001. The specimen is clamped in one fixed and one movable jaw. A load monitoring system is placed between one of the jaws and the main frame of the machine. The movable jaw is that which is fixed to the cross-head. The cross-head is supported by two stout screw threads. When the screw threads are rotated the cross-head will move relative to the fixed jaw. Hence the specimen will be stretched or squashed. The load is monitored during this deformation process. By rotating the screw-threads faster or slower the rate at which the cross-head moves can be altered. The Instron 1122 machine is provided with a number of pre-set speeds of these screw threads.

I stated above that the Instron 1122 test of machine uses open-loop control. From comments within the main body of this thesis it will be inferred that this machine may not give a constant extension under load or extension rate, because the machine defects. (The load-cell deforms, the jaws stretch, the cross-head bends, the screw threads shorten and all the joints between these parts open or close depending on the direction of the load.) Clearly the load experienced by the specimen gauge length is also transmitted

---

[1]In a closed-loop, or feed-back, control system the deformation rate is measured, using an extensometer for example. The measured rate is compared with the required rate. The machine then speeds-up or slows-down according on the error between these two values.

through all the structures outside the gauge length.[2] Thus the degree to which these structures deform will depend on how stiff they are, and on the size of the applied load. A machine that deforms only a small amount is commonly referred to as a hard machine and one that deforms a lot as a soft machine. The consequences of machine deflections can be explained by using a spring model (similar to that by Freudenthal, 1950). I will examine a static case first where an extension has been applied to the system, one turn of the screw thread for example. The gauge length of the specimen, L_s, is modelled by one spring and all the structures outside it by another, see figure A7.002.

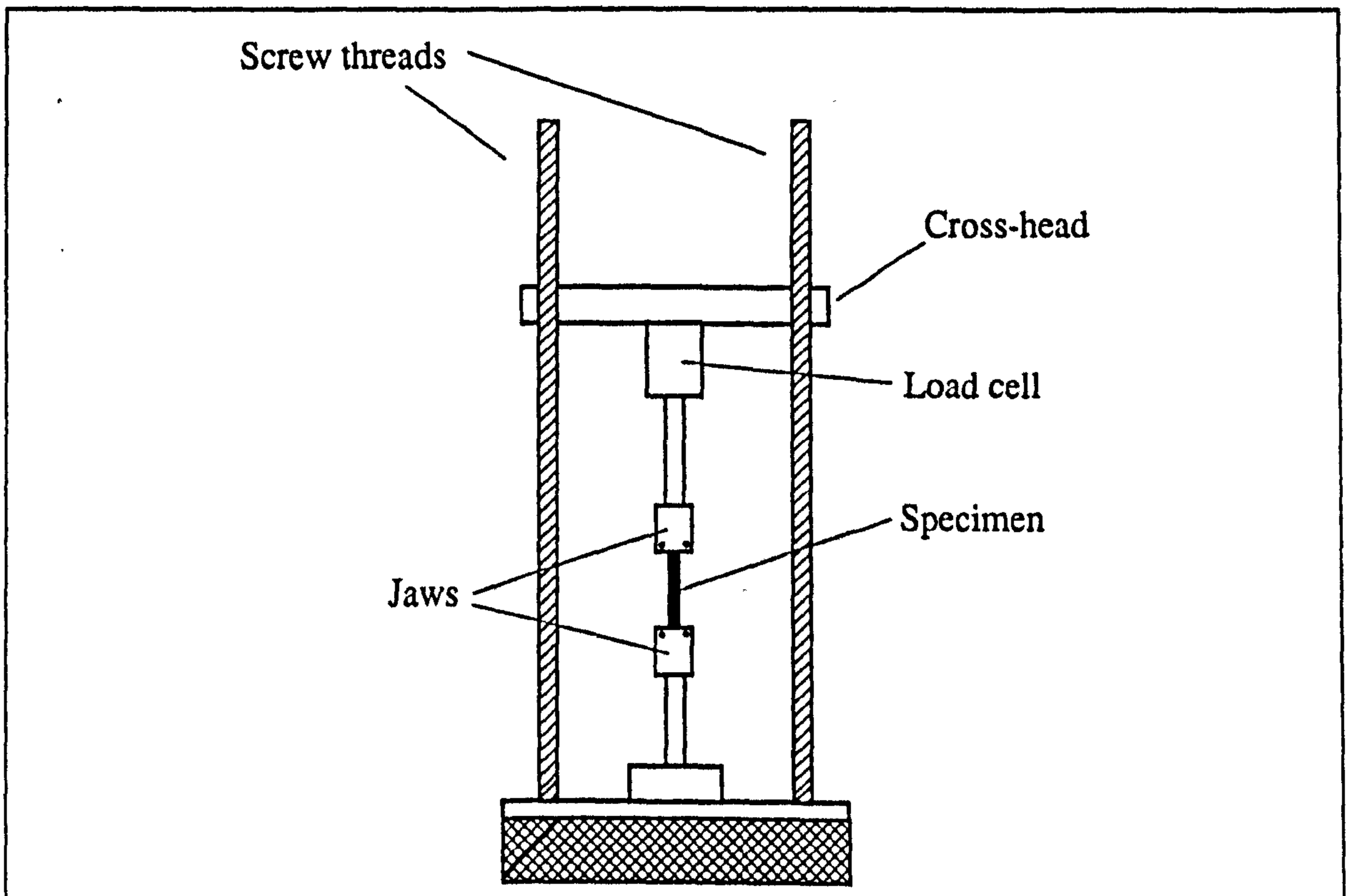

Figure A7.001

Basic parts of an open-loop, screw-driven, materials testing machine

In figure A7.002 two images of the same model are shown one with the system unloaded and the other with it loaded. The lengths of the various parts are given the following symbols: L_W is the length of the whole analogue system, L_M is the length of the machine analogue and L_s is the length of the specimen analogue. Rotating the screw threads (by say one revolution) will extend the whole system by ΔL_W. As a result of this extension a force, P, will be experienced by the specimen and the machine (and in the

[2]In this initial analysis all structures outside the gauge length are considered as being part of the testing machine. Later the effect of the portion of the specimen that falls between the gauge length and the machine will be included in the analysis.

real machine monitored by the load cell). This force will result in extensions of the specimen and (deflections in) the machine, expressed as ΔL_S and ΔL_M.

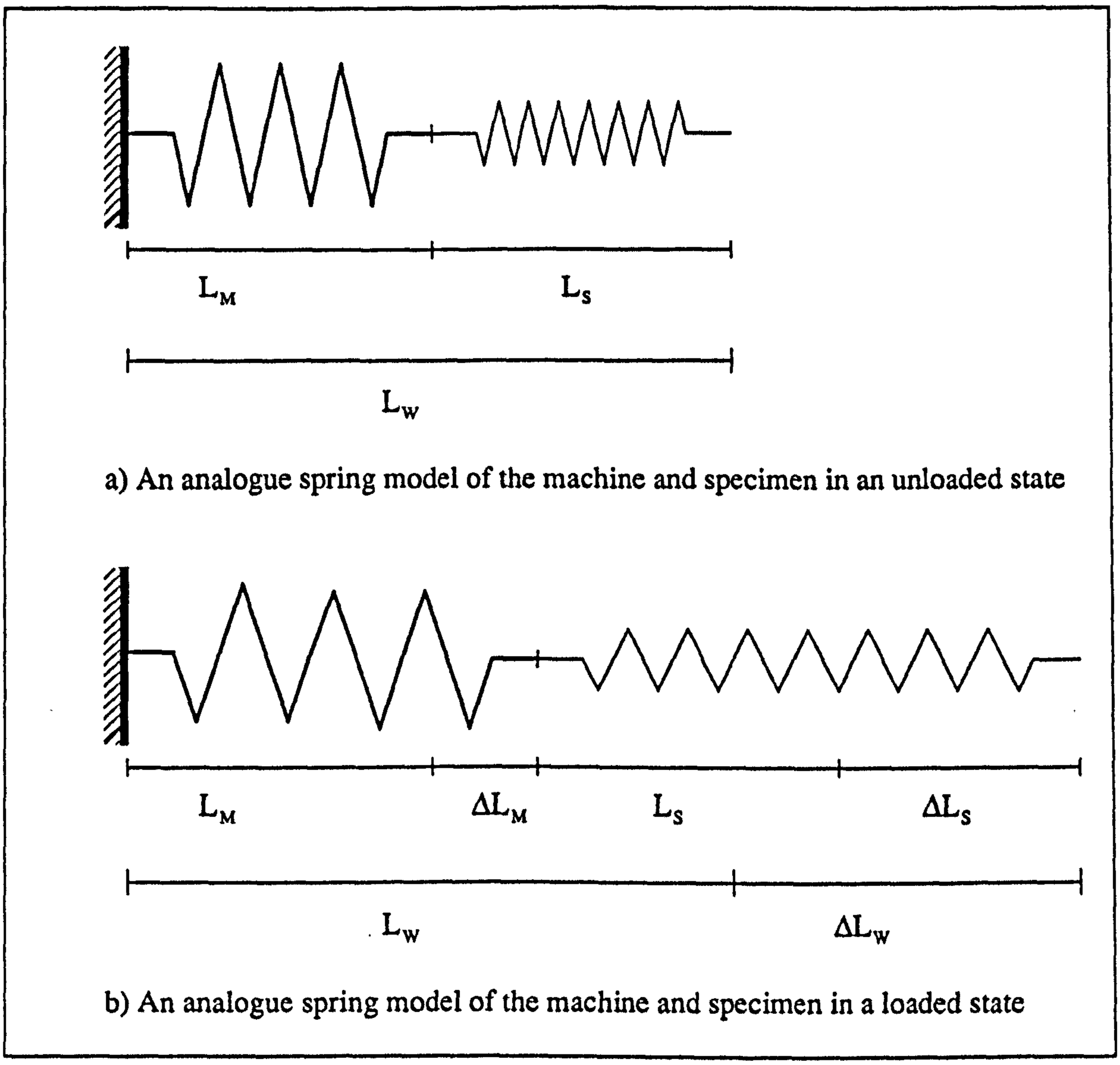

a) An analogue spring model of the machine and specimen in an unloaded state

b) An analogue spring model of the machine and specimen in a loaded state

Figure A7.002

Spring model of specimen-machine interaction

The various deflections of the spring analogies in figure A7.002 can be related mathematically. If the stiffnesses of the springs are expressed as the load experienced by the spring divided by the extension that load causes, then the stiffness of the machine can be expressed as

$$K_M = \frac{P}{\Delta L_M} \qquad \text{(A7.001)}$$

and that of the specimen as

$$K_S = \frac{P}{\Delta L_S} \qquad \text{(A7.002))}$$

The deflection of the whole system can be expressed as

$$\Delta L_W = \Delta L_M + \Delta L_S \qquad \text{(A7.003))}$$

Thus

$$\Delta L_W = \frac{P}{K_M} + \frac{P}{K_S} \qquad \text{(A7.004)}$$

Since the load on both parts of the system is the same equation A7.004 can be re-expressed as

$$\Delta L_W = \frac{P(K_S + K_M)}{K_M K_S} \qquad \text{(A7.005)}$$

Thus from equation A7.002

$$\Delta L_S = \frac{\Delta L_W K_M}{(K_S + K_M)} \qquad \text{(A7.006)}$$

Therefore if the stiffness of the specimen is infinite the specimen will not extend and all the deflection will be in the machine. Similarly if the specimen is infinitely compliant (its extension requiring no load) the machine will not deform and all the extension will be experienced by the specimen. The effect of a harder machine is perhaps made clearer by rearranging the above equation.

$$\frac{\Delta L_S}{\Delta L_W} = \frac{K_M}{(K_S + K_M)} \qquad \text{(A7.007)}$$

This expression shows that if a stiffer test machine was used the extension of the specimen would be close to that recorded for the full system. If the test machine were infinitely rigid, the extension of the specimen could be calculated directly from the cross-head movement. However, no machine is infinitely rigid. There are a number of ways to circumvent the problem with the type of machine used here. First, the deflection of the machine can be determined and this value subtracted from the recorded deflection of the whole system. (This method was used in the three-point-bending tests performed for this thesis.) Second, a direct measuring device, such as an extensometer can be used. (This method of measuring the extension of tensile specimens was used in this work and is the standard procedure within the lab where they were performed.) Thus the extension of the specimen can be obtained without the error due to machine deflection. However, machine deflections have another effect: a non-constant extension rate.

A more realistic case can be considered, where the screw threads are turned at a constant rate, rather than a single step. The extension rates can be derived in a similar way to the deflections above. Giving the following equation

$$\frac{d L_s}{d t} = \frac{d L_w}{d t} \frac{K_M}{(K_s + K_M)} \qquad \text{(A7.008)}$$

where

$\frac{d L_w}{d t}$ is the extension rate of the system, determined by the screw-thread speed,

$\frac{d L_s}{d t}$ is the extension rate of the specimen's gauge length.

Thus from equation A7.008 it can be seen that the more compliant a specimen is the closer its extension rate is to the machine's. The extension rate is clearly dependent on the specimen stiffness. Specimens may exhibit different stiffnesses for a number of reasons, two of which are

a) Size: a specimen that has a larger cross-sectional area will be stiffer, and thus deform more slowly.

b) Variation in material properties: this variation may be between specimens or within the same specimen at different times. Specimens made of different materials may have different stiffnesses. The more compliant one will be extended more quickly.

The first reason for different specimen stiffnesses can generally be avoided. It is this second point that is a cause of concern in this study, as antler is a more compliant material than bone. However, what is of more significance is the variation in the specimen's stiffness during a test. In this study I am concerned with the processes that are occurring in the material as it enters and passes through the knee region of the tensile loading curve. Unfortunately it is when the material enters this phase of the test that it becomes more compliant. If the spring analogy is accepted this would imply that the strain rate experienced by the specimen after the knee region is greater than that before it. This is clearly demonstrated by the results I obtained using the AJS/BBC data collection system, an example of which is shown in figure A7.004.

So far I have referred to extension or deformation rates, whereas the literature refers to strain rates (see chapter 3). The reason for my wording is that the strain rate is dependent on a number of other variables. It will be remembered that strain is a normalisation of extension (I consider only engineering strain here). Thus an extension of 0.1 mm in a gauge length of 10 mm gives a strain of 0.01, but in a length of 15 mm it will give a strain of 0.0067. Therefore the strain rate obtained when using an open loop controlled machine is also dependent on the length of the specimen. Using the above equation this can be expressed as

$$\varepsilon_s = \frac{\Delta L_s}{L_s} = \frac{\Delta L_w K_M}{L_s (K_s + K_M)} \qquad \text{(A7.009)}$$

If it can be assumed that the strain rate is uniform over the full length of the specimen, then

$$\dot{\varepsilon}_s = \frac{d L_s}{L_s \, d t} = \frac{d L_w}{d t} \, \frac{K_M}{L_s (K_s + K_M)} \qquad \text{(A7.010)}$$

It can be seen that the strain rate, like the extension rate, is a function of the machine and specimen stiffnesses. There is no simple way to overcome this interaction in an open loop machine.

Unfortunately this situation is further complicated when the method used to measure strain is considered. Commonly an extensometer or strain gauge is placed across part of the reduced cross-section of the specimen. This situation is demonstrated in figure 7.003.

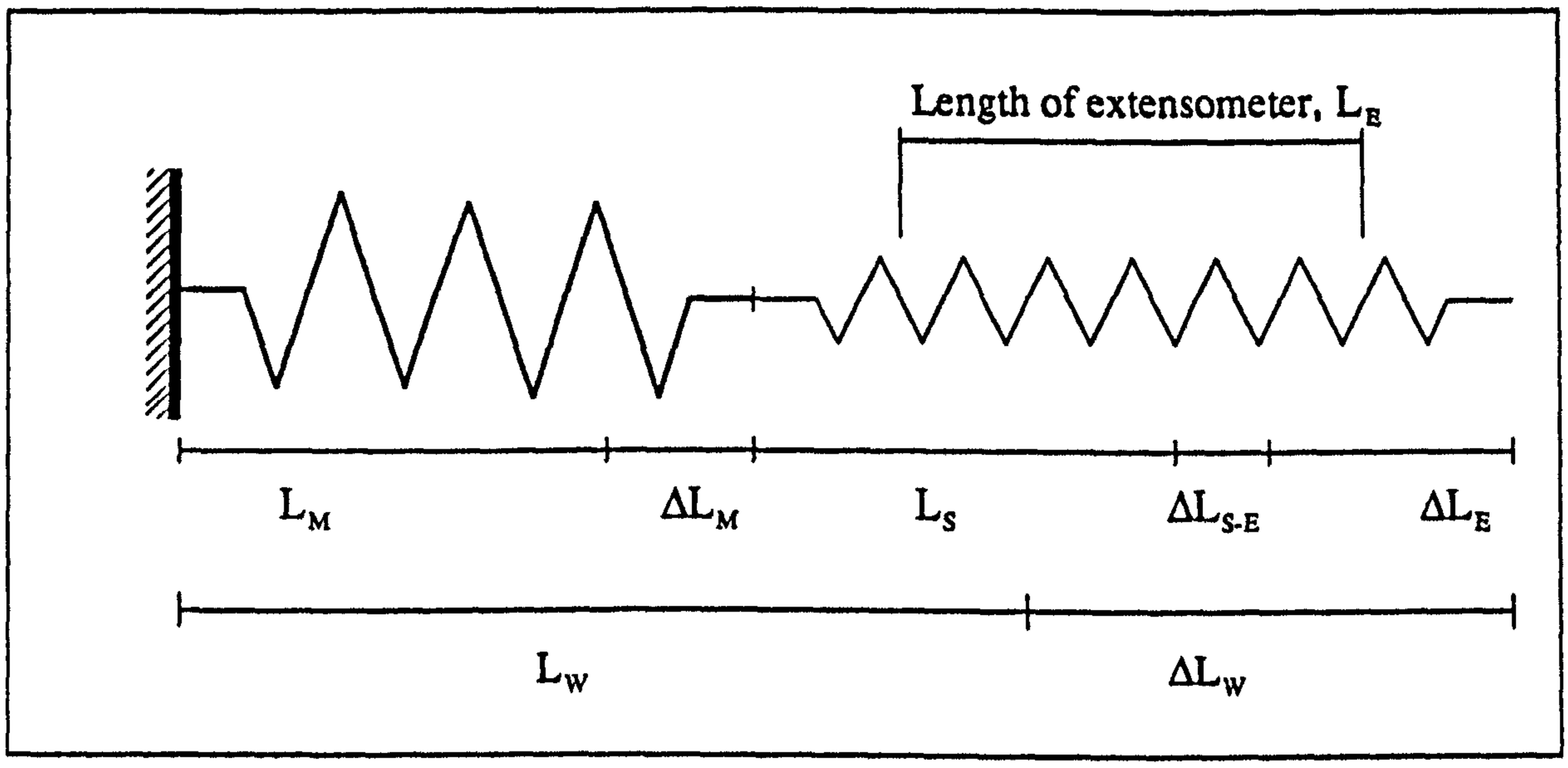

Figure A7.003

A spring analogue of the specimen and testing machine, showing the gauge length over which the extension is measured

By considering figure A7.003 considering the previous analogies and discussion, two points are raised: first, if the machine is assumed to be hard, then the strain rate should be approximated using the whole length of the specimen and the cross-head speed, rather than the length over which strain is measured. This is because some extension will occur out side the measured length, ΔL_{S-E}. Second, the smaller the gauge length is, in proportion to the length of the specimen, the more compliant the machine will appear to be. (This can be visualised by dividing the specimen's spring analogue into two sections.) Thus the extension rate in the gauge length is smaller than that for the whole specimen, but its nominal strain rate is the same.

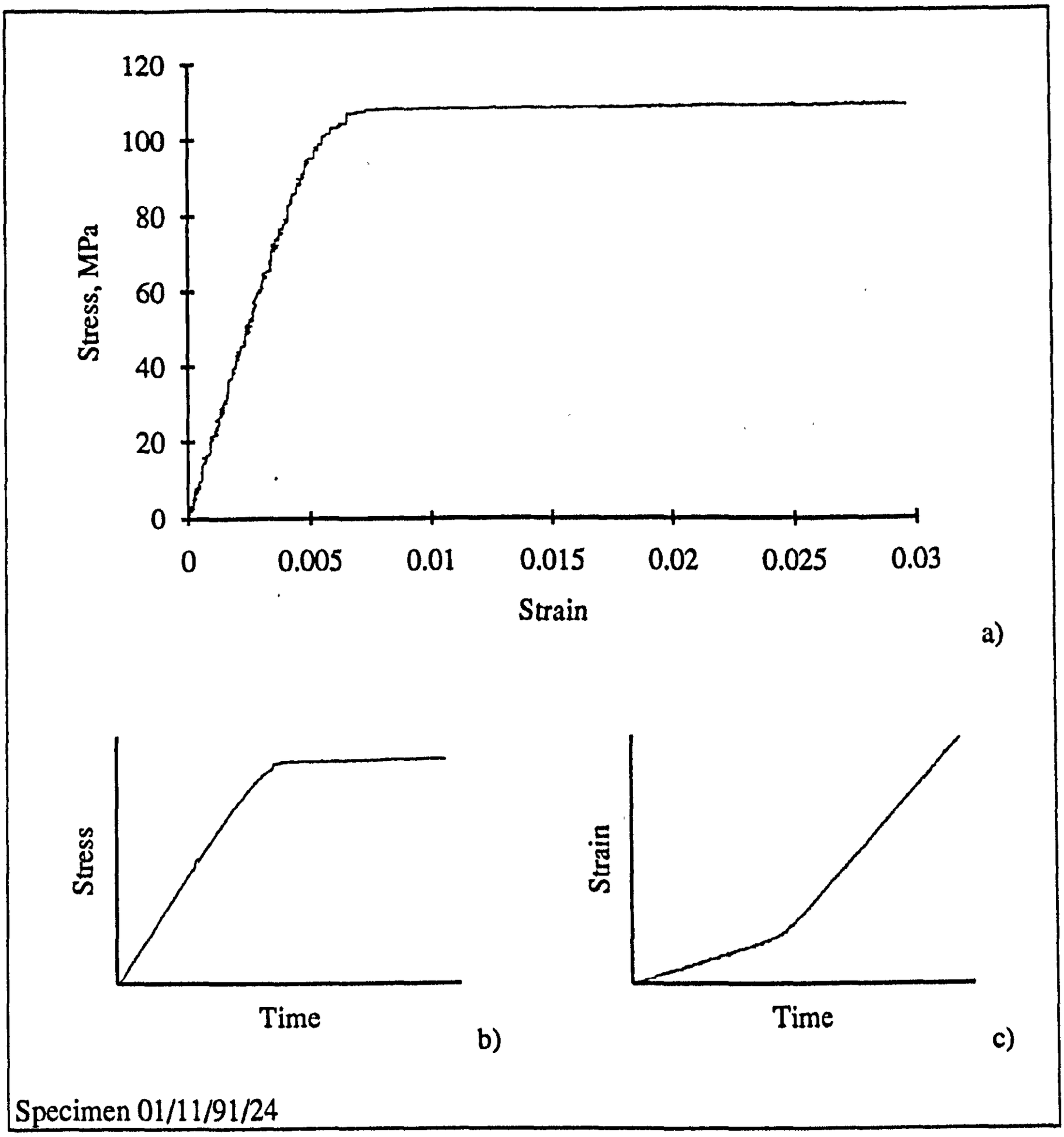

Figure A7.004

Stress-strain (a), stress-time (b) and strain-time (c) relationships for a specimen of bovine femoral bone

The observation that the extension rate of a specimen is dependent its own stiffness, has implications when examining time-dependent properties. One of the properties of bone that has been used as a basis of a description of its visco-elastic nature is the observed increase in material stiffness with strain rate. However, with the machine specimen interaction described here such an increase in material stiffness will result in a lower strain rate. Thus the true effect is likely to be greater than the one observed using such an open-loop machine.

Figure A7.004 clearly shows that the strain rate does change when the specimen stiffness changes. (This plot shows one of the more extreme cases, where the reduction

in the specimen's stiffness is quite severe.) This results shows that it is incorrect to assign a single extension, loading or strain rate to such a test conducted on such an open-loop machine. The change in strain rate may also affect on the shape of the knee region. From examination of the model I constructed based on a statement made by Fondrk *et al.* (see section 3.3.3.2) the effect of the non-constant strain rate on the shape of the knee region can be postulated. As the strain rate increases, on the specimen entering the knee region, the load required for it to attain the flat region of the curve is slightly increased. This may produce a more gentle curve.

So far in this appendix I have stated (and shown) that the open loop test machine used in this study in unable to produce a constant stress or strain rate during a tensile test in which the specimen exhibits an increase in compliance. I have also proposed a model to explain this fact. I would now like to consider the effect this may have on some of the other properties measured in this and other types of test.

a) Failure in a tensile test or fracture in a notch sensitivity test is likely to be accelerated, due to the energy stored within the test machine. This energy storage is a result of its deflection under load. (See chapters 5 and 6.)

b) The strain rate at the notch tip in a SEN specimen will be greater than that measured over the gauge length of about 10 mm. The reduced section has an effect similar to introducing a small but more compliant spring into the analogy presented in figure A7.003.

APPENDIX 8

THE J INTEGRAL

The J integral is a technique used in EPFM, but it has a basis in the ideas of NLEFM. As pointed out by Atkins and Mai (1988), there may not be a difference between the curvature induced in the *loading* section of a load extension plot, produced by irreversible plastic flow and that produced by non-linear elasticity. The variation caused by the different physical processes only becomes apparent on *unloading* the material. This technique is included as an appendix, because although not used in this thesis, with hindsight I consider that this technique is appropriate for the determination of fracture parameters for both antler and bone. This method can account for plastic deformation assuming that the material is not unloaded. Therefore as there is no apparent difference between a plastic and damage response until the material is unloaded, this situation is also encompassed by the J integral.

In section 5.2.2.2 (on the modern interpretation of the energy approach) the following equation was introduced:

$$U_t = U_o + U_e + U_s - F \qquad \text{(A8.001)}$$

where

U_t = The total energy of the system

U_o = The elastic energy of the loaded system without a crack

U_e = The energy released due to the crack

U_s = The surface energy due to the crack

F = The external work supplied to the system.

In the analysis presented in that section linear elastic behaviour was considered. However, (as pointed out by Ewalds and Wanhill) equation A8.001 remains valid for as long as the behaviour remains elastic (linear or non-linear). An important consequence of this is that under certain conditions non-linear elastic behaviour can be used to model the plastic behaviour of a material. This condition is that no unloading may occur in any part of the body (that is not behaving elasticity). If the material is not unloaded it is irrelevant if the energy supplied to it is recoverable (elastic) or not (plastic).

Assuming that the above equation remains valid, it will be possible to derive the conditions for instability. In the LEFM case this derivation produces the potential energy release rate, G, (see equation 5.014) the equivalent in the case considered here is J.

Atkins and Mai refer to this as *the potential energy release rate for non-linear elastic cracking*. This process results in the equation

$$J = - \frac{dU_e}{da} \qquad \text{(A8.002)}$$

Ewalds and Wanhill (1986) use a slightly different nomenclature and derivation, as they group the potential energy terms together, $U_p = U_o + U_e - F$, and do not assume the external work is zero. Thus their equation

$$J = - \frac{dU_p}{da} \qquad \text{(A8.003)}$$

contains 'all the energy terms that may contribute to nonlinear elastic behaviour'.

Ewalds and Wanhill note that during crack growth the region around the newly formed crack is unloaded, and thus (for the reasons given above) it may be expected that J is only applicable up to the point of fracture initiation in a situation where plasticity occurs. However, they report that some success in using the J integral to characterise crack growth has been claimed. They then present a more detailed examination of this approach, this will be passed over here.

The original test method to find J_{IC} was a graphical one. Ewalds and Wanhill (1986) illustrate the method with diagrams similar to figures A8.001 to A8.003, presented here. The procedure is as follows:

a) Load-displacement diagrams are obtained for a number of specimens pre-cracked to different lengths (figure A8.001). The area bounded by the load-displacement curve and the displacement axis, represents the energy supplied to the specimen (per unit thickness, as a thin specimen will require less load for the same displacement as a thick one). If the system is assumed to be elastic this is the same as the potential energy within the specimen.

b) The value of energy determined from figure A8.001 is recorded for each specimen at a number of constant values of displacement. These energy values are then plotted against crack length, see figure A8.002.

c) The negative slopes of the energy-crack length curves of figure A8.002 are plotted against displacement for the various crack lengths in figure A8.003. This represents the required quantity, as

$$- \frac{dU_p}{da} = J \qquad \text{(A8.004)}$$

d) If the displacement at crack initiation is known for a particular initial crack length, this can be plotted of the graph (figure A8.003) and the corresponding value of the potential energy release rate for non-elastic cracking obtained. Ideally the values obtained from the various initial crack lengths should be identical. Lack of consistency

in the graphical obtained values of J_{IC} could imply that this quantity is an inappropriate criterion for crack extension for the material concerned. However, there are many possibilities for errors in this method of its derivation. Ewalds and Wanhill (1986) report some of these possible errors.

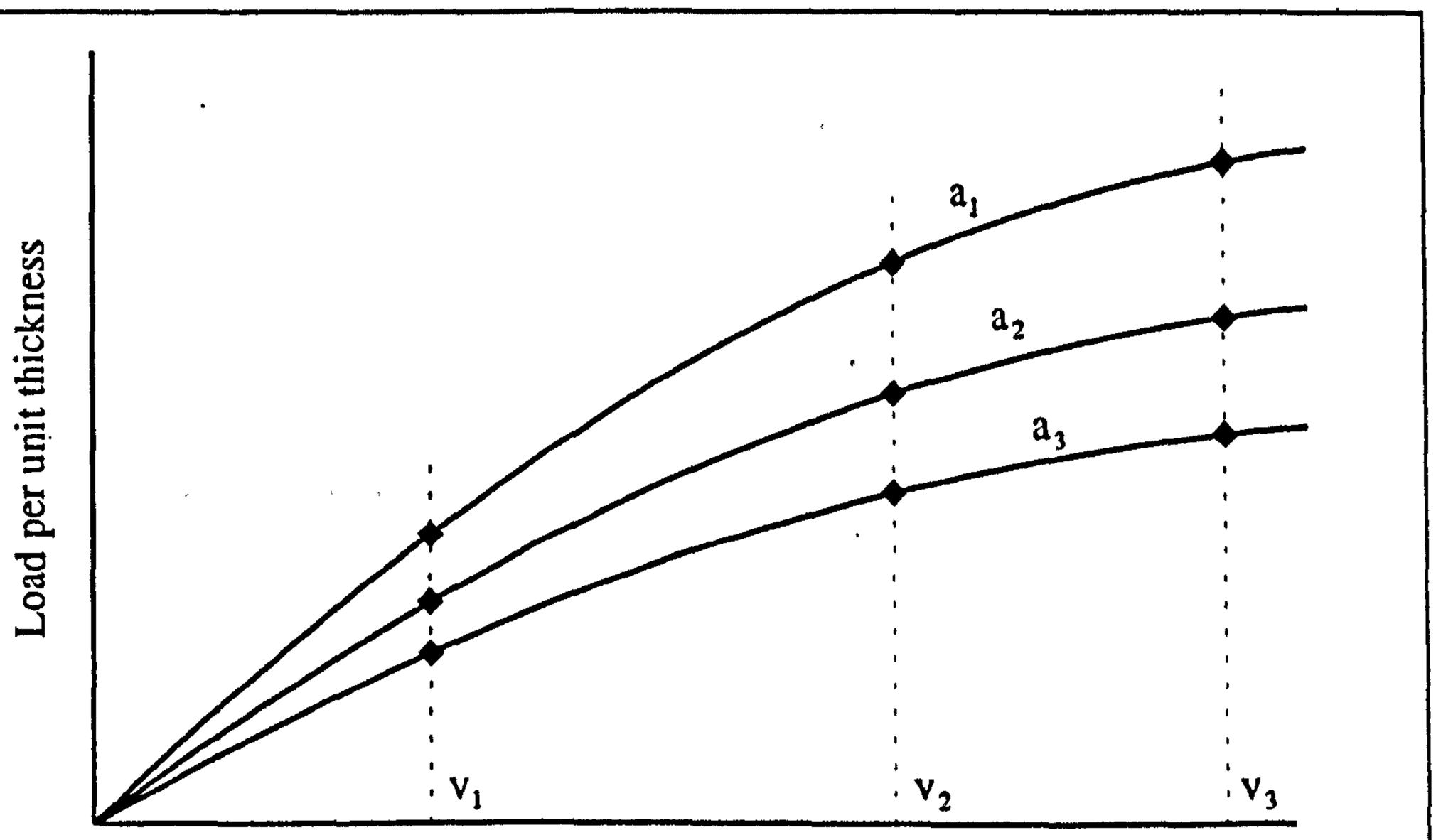

Idealised load-displacement diagrams for specimens containing different crack lengths a_1, a_2 and a_3, from which the energy per unit thickness (area under the curve) is determined at various displacements v_1, v_2 and v_3

Figure A8.001 After Ewalds and Wanhill (1986)

Idealised load-displacement diagrams for specimens containing different crack lengths

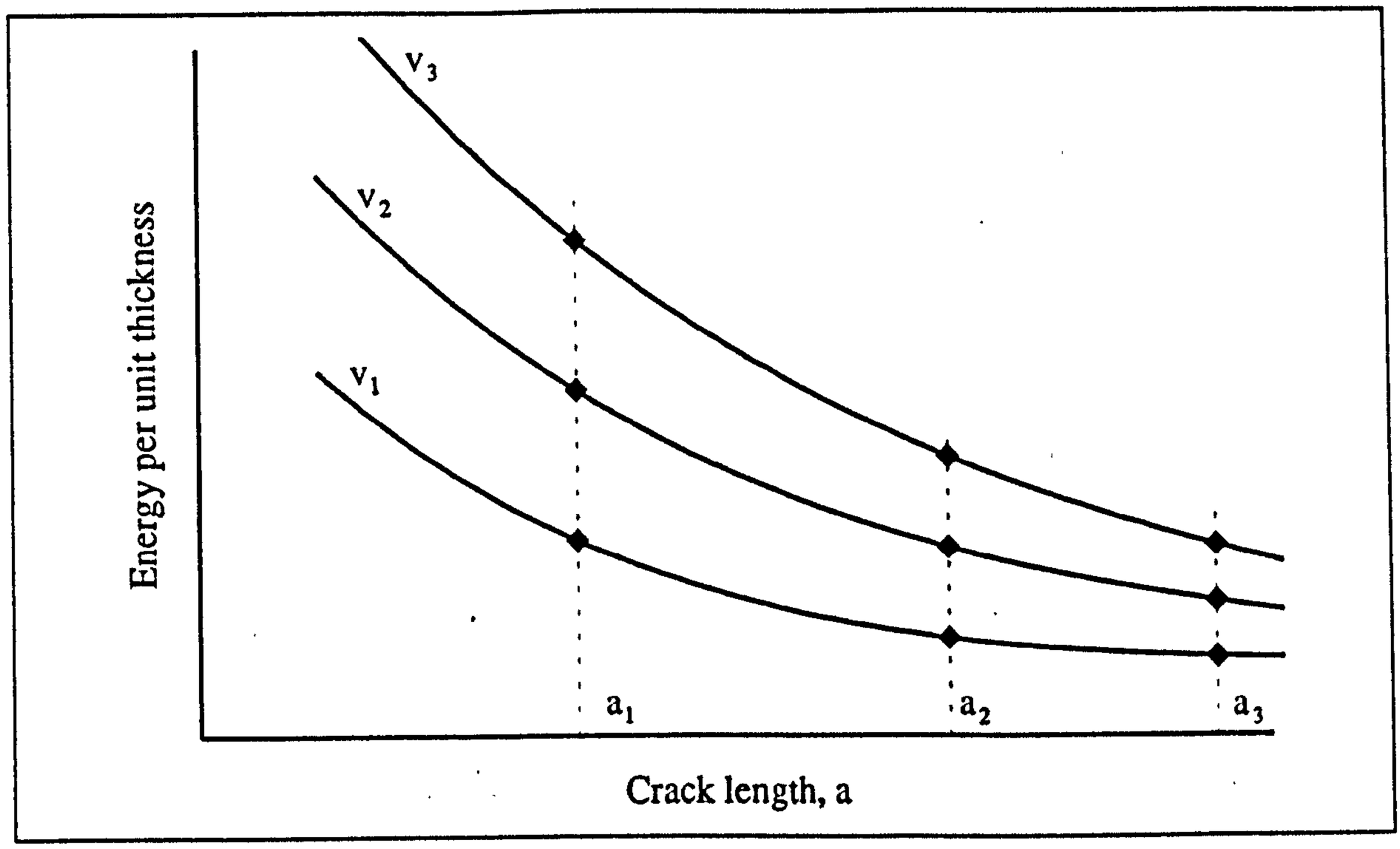

Figure A8.002 After Ewalds and Wanhill (1986)

Idealised energy-crack length diagrams

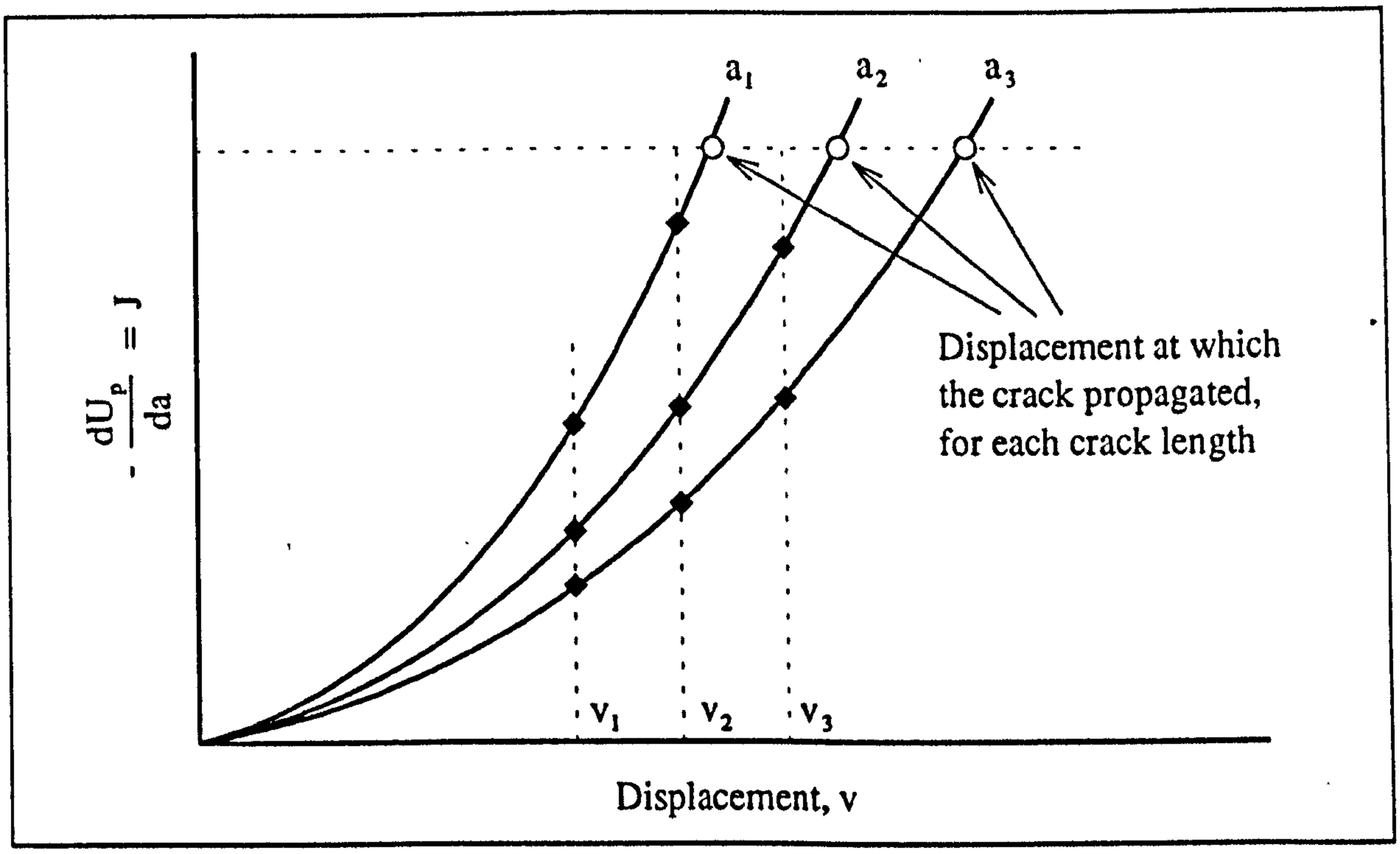

Figure A8.003 After Ewalds and Wanhill (1986)

Determination of the potential energy release rate for non-linear elastic cracking

APPENDIX 9

TABLES OF REGRESSION EQUATIONS FOR CHAPTER 4

This appendix contains the regression equations of the tensile and creep data that is used as the basis of chapter 4. The data sets are presented in appendix 4. The equations are presented in the form in which they were obtained from Minitab, the statistical package used for the analysis. The Student's t values of the constant and variables are presented below the appropriate quantity. (An explanation of quantities in parentheses or square brackets is given in chapter 4.) The R^2 values quoted is that adjusted for the degrees of freedom as supplied by Minitab. Appendix 12 contains a table relating the value of Student's t to the degrees of freedom and the probability or level of significance. However, were appropriate this information has been given for the specific equations referred to in chapter 4.

To assist with the correlation of the tables presented here and the text and figures in chapter 4 each table is numbered, it also contains the number of the figure in which the main variables are plotted. To the same ends this appendix is divided into sections using the same titles as in chapter 4. These titles are preceded by the section number (in parentheses) that corresponds to the relevant section in chapter 4.

(4.2.6.5.) RESULTS: THE EFFECT OF CROSS-HEAD SPEED ON MATERIAL STIFFNESS

Type of specimens	Regression equations and t values of the data shown in figure 4.010. (Data sets TA1 and TB1)	R^2 %	
27 Antler	$E_t = 6.85 - 0.107 \ln(\dot{x})$ t: 4.34 - 0.74	0.0 (8.0)	*a*
27 Antler	$E_t = -0.52 + 0.061 \ln(\dot{x}) + 0.814 E_b$ t: - 0.30 0.59 5.30	51.2 (60.1)	*b*
27 Antler	$\ln(E_t) = 1.85 - 0.0194 \ln(\dot{x})$ t: 9.14 - 1.06	0.5 (8.4)	*c*
27 Antler	$\ln(E_t) = -6.72 + 0.0036 \ln(\dot{x}) + 1.15 \ln(E_b)$ t: - 1.44 0.28 5.63	55.3 (63.3)	*d*
30 Bone	$E_t = 30.8 + 0.819 \ln(\dot{x})$ t: 14.08 4.00	34.1 (33.8)	*e*
30 Bone	$E_t = 13.5 + 0.601 \ln(\dot{x}) + 0.731 E_b$ t: 3.55 3.84 5.00	64.5 (64.2)	*f*
30 Bone	$\ln(E_t) = 3.47 + 0.0365 \ln(\dot{x})$ t: 34.54 3.87	32.6 (31.5)	*g*
30 Bone	$\ln(E_t) = 1.31 + 0.0265 \ln(\dot{x}) + 0.681 \ln(E_b)$ t: 3.17 3.78 5.28	65.6 (65.2)	*h*
Units: E_t, GPa. $\dot{x}$, m s^{-1}. E_b, GPa.			

Table A9.001

Regression equations of the relationship of the material stiffness in tension for specimens of antler and bovine bone to the cross-head speed of the test

(4.2.6.6.) RESULTS: THE EFFECT OF CROSS-HEAD SPEED ON KNEE STRESS

Type of specimens	Regression equations and t values of the data shown in figure 4.012. (Data sets TA1 and TB1)	R^2 %	
27 Antler	$\sigma_K = 103 + 3.33 \ln(\dot{x})$ t: 10.21 3.65	32.2 (29.8)	*a*
27 Antler	$\sigma_K = 54.4 + 4.44 \ln(\dot{x}) + 5.35 E_b$ t: 5.01 6.94 5.67	69.8 (68.6)	*b*
27 Antler	$\ln(\sigma_K) = 4.67 + 0.0447 \ln(\dot{x})$ t: 31.30 3.31	27.7 (24.9)	*c*
27 Antler	$\ln(\sigma_K) = -2.74 + 0.0623 \ln(\dot{x}) + 0.877 \ln(E_b)$ t: -8.35 6.86 6.13	70.6 (69.4)	*d*
30 Bovine bone	$\sigma_K = 179 + 6.23 \ln(\dot{x})$ t: 12.82 4.75	42.7 (42.5)	*e*
30 Bovine bone	$\sigma_K = 60.5 + 4.73 \ln(\dot{x}) + 5.03 E_b$ t: 2.68 5.11 5.81	73.6 (73.5)	*f*
30 Bovine bone	$\ln(\sigma_K) = 5.27 + 0.0527 \ln(\dot{x})$ t: 41.31 4.41	38.8 (38.1)	*g*
30 Bovine bone	$\ln(\sigma_K) = 2.39 + 0.0393 \ln(\dot{x}) + 0.909 \ln(E_b)$ t: 4.81 4.69 5.89	72.2 (72.1)	*h*
Units: σ_K, MPa. $\dot{x}$, m s^{-1}. E_b, GPa.			

Table A9.002

The relationship of knee stress to the cross-head speed of the test for specimens of bone and antler.

Type of specimens	Regression equations and t values of the data shown in figure 4.012. (Data sets TA1 and TB1)	R^2 %	
27 Antler	$\ln(\sigma_K) = 3.63 + 0.0556 \ln(\dot{x}) + 0.560 \ln(E_t)$ t: 17.58 6.05 5.71	68.0 (70.3)	*a*
27 Antler	$\ln(\sigma_K) = 2.94 + 0.00612 \ln(\dot{x}) + 0.291 \ln(E_t) + 0.544 \ln(E_b)$ t: 9.23 7.24 2.18 2.68	74.6 (74.6)	*b*
30 Bovine bone	$\ln(\sigma_K) = 1.91 + 0.0173 \ln(\dot{x}) + 0.968 \ln(E_t)$ t: 3.44 1.78 6.13	73.5 (72.6)	*c*
30 Bovine bone	$\ln(\sigma_K) = 1.61 + 0.0237 \ln(\dot{x}) + 0.590 \ln(E_t) + 0.507 \ln(E_b)$ t: 3.13 2.58 2.89 2.60	78.1 (77.6)	*d*
Units: σ_K, MPa. $\dot{x}$, m s^{-1}. E_t, GPa. E_b, GPa.			

Table A9.003

The relationship of knee stress to the cross-head speed and the tensile stiffness

Type of specimens	Regression equations and t values of the data shown in figure 4.012. (Data sets TA1 and TB1)	R^2 %	
27 Antler	$\sigma_K = 61.3 + 31552\ \dot{x}$ t: 27.32 5.09	48.9 (46.8)	*a*
27 Antler	$\sigma_K = 12.9 + 34609\ \dot{x} + 4.24\ E_b$ t: 1.33 7.80 5.07	74.3 (73.3)	*b*
27 Antler	$\sigma_K = 34.7 + 29089\ \dot{x} + 3.37\ E_t$ t: 4.80 5.76 3.79	66.7 (68.0)	*c*
27 Antler	$\sigma_K = 14.1 + 33558\ \dot{x} + 0.80\ E_t + 3.59\ E_b$ t: 1.41 7.02 0.64 2.72	73.7 (73.1)	*d*
30 Bovine bone	$\sigma_K = 104 + 49924\ \dot{x}$ t: 30.46 5.95	54.3 (52.7)	*e*
30 Bovine bone	$\sigma_K = 18.4 + 36216\ \dot{x} + 4.29\ E_b$ t: 1.01 5.22 4.75	74.1 (73.2)	*f*
30 Bovine bone	$\sigma_K = 19.7 + 24309\ \dot{x} + 4.02\ E_t$ t: 1.08 2.89 4.65	73.6 (72.6)	*g*
30 Bovine bone	$\sigma_K = -0.8 + 25809\ \dot{x} + 2.43\ E_t + 2.70\ E_b$ t: -0.04 3.35 2.42 2.54	78.1 (77.2)	*h*
Units: σ_K, MPa. $\dot{x}$, m s^{-1}. E_t, GPa. E_b, GPa.			

Table A9.004

Knee stress and cross-head speed: non logarithmic relationships

(4.2.6.7.) RESULTS: THE EFFECT OF CROSS-HEAD SPEED ON ULTIMATE STRESS

Type of specimens	Regression equations and t values of the data shown in figure 4.013. (Data sets TA1 and TB1)	R^2 %	
27 Antler	$\sigma_{ult} = 167 + 6.31 \ln(\dot{x})$ t: 11.84 4.92	47.2 (45.6)	*a*
27 Antler	$\sigma_{ult} = 106 + 7.70 \ln(\dot{x}) + 6.76 E_b$ t: 6.22 7.66 4.56	70.5 (69.4)	*b*
27 Antler	$\ln(\sigma_{ult}) = 5.20 + 0.0575 \ln(\dot{x})$ t: 38.09 4.65	44.2 (42.4)	*c*
27 Antler	$\ln(\sigma_{ult}) = 3.57 + 0.0723 \ln(\dot{x}) + 0.739 \ln(E_b)$ t: 10.70 7.83 5.08	72.0 (71.0)	*d*
30 Bovine bone	$\sigma_{ult} = 182 + 6.49 \ln(\dot{x})$ t: 12.53 4.74	42.6 (43.0)	*e*
30 Bovine bone	$\sigma_{ult} = 54.7 + 4.87 \ln(\dot{x}) + 5.42 E_b$ t: 2.43 5.27 6.28	75.8 (76.2)	*f*
30 Bovine bone	$\ln(\sigma_{ult}) = 5.29 + 0.0542 \ln(\dot{x})$ t: 40.19 4.39	38.7 (38.4)	*g*
30 Bovine bone	$\ln(\sigma_{ult}) = 2.24 + 0.0400 \ln(\dot{x}) + 0.963 \ln(E_b)$ t: 4.53 4.80 6.25	74.0 (74.4)	*h*
	Re-analysing using the material stiffness during the test		
27 Antler	$\ln(\sigma_{ult}) = 4.30 + 0.0669 \ln(\dot{x}) + 0.488 \ln(E_t)$ t: 21.39 7.50 5.11	72.2 (72.5)	*i*
27 Antler	$\ln(\sigma_{ult}) = 3.75 + 0.0713 \ln(\dot{x}) + 0.281 \ln(E_t) + 0.417 \ln(E_b)$ t: 11.50 8.20 2.05 2.00	74.6 (74.6)	*j*
30 Bovine bone	$\ln(\sigma_{ult}) = 1.80 + 0.0175 \ln(\dot{x}) + 1.00 \ln(E_t)$ t: 3.17 1.76 6.21	73.8 (73.1)	*k*
30 Bovine bone	$\ln(\sigma_{ult}) = 1.48 + 0.0246 \ln(\dot{x}) + 0.583 \ln(E_t) + 0.566 \ln(E_b)$ t: 2.86 2.68 2.85 2.90	79.4 (79.2)	*l*
Units: σ_{ult}, MPa. $\dot{x}$, m s^{-1}. E_t, GPa. E_b, GPa.			

Table A9.005

Relationships of the ultimate stress to the cross-head speed and material stiffness

Type of specimens	Regression equations and t values of the data shown in figure 4.013. (Data sets TA1 and TB1)	R^2 %	
27 Antler	$\sigma_{ult} = 89.0 + 58522\ \dot{x}$ t: 31.0 7.48	67.9 (66.5)	*a*
27 Antler	$\sigma_{ult} = 33.2 + 62045\ \dot{x} + 4.89\ E_b$ t: 2.51 10.21 4.27	81.0 (80.2)	*b*
27 Antler	$\sigma_{ult} = 60.9 + 55917\ \dot{x} + 3.57\ E_t$ t: 6.15 8.08 2.92	75.3 (75.4)	*c*
27 Antler	$\sigma_{ult} = 33.5 + 61864\ \dot{x} + 0.14\ E_t + 4.77\ E_b$ t: 2.43 9.36 0.08 2.62	80.2 (79.3)	*d*
30 Bovine bone	$\sigma_{ult} = 104 + 52818\ \dot{x}$ t: 29.84 6.16	56.0 (54.6)	*e*
30 Bovine bone	$\sigma_{ult} = 12.0 + 38047\ \dot{x} + 4.63\ E_b$ t: 0.68 5.63 5.25	77.4 (76.8)	*f*
30 Bovine bone	$\sigma_{ult} = 16.9 + 26289\ \dot{x} + 4.17\ E_t$ t: 0.91 3.08 4.75	75.2 (74.2)	*g*
30 Bovine bone	$\sigma_{ult} = -6.5 + 28002\ \dot{x} + 2.35\ E_t + 3.09\ E_b$ t: -0.36 3.72 2.39 2.98	80.8 (80.1)	*h*
Units: σ_{ult}, MPa. $\dot{x}$, m s^{-1}. E_t, GPa. E_b, GPa.			

Table A9.006

Non-logarithmic relationships of the ultimate stress to the cross-head speed and material stiffness

(4.2.6.8.) RESULTS: THE EFFECT OF CROSS-HEAD SPEED ON KNEE STRAIN

Type of specimens	Regression equations and t values of the data shown in figure 4.015. (Data sets TA1 and TB1)	R^2 %	
27 Antler	$\varepsilon_K = 0.0121 + 0.000417 \ln(\dot{x})$ t: 10.72 4.08	37.6 (44.8)	*a*
27 Antler	$\varepsilon_K = 0.0163 + 0.000320 \ln(\dot{x}) - 0.000468 E_b$ t: 10.88 3.63 - 3.59	57.7 (64.2)	*b*
27 Antler	$\ln(\varepsilon_K) = - 4.32 + 0.0544 \ln(\dot{x})$ t: - 29.42 4.09	37.7 (45.3)	*c*
27 Antler	$\ln(\varepsilon_K) = - 2.94 + 0.0418 \ln(\dot{x}) - 0.629 \ln(E_b)$ t: - 6.90 3.55 - 3.39	56.1 (63.4)	*d*
30 Bovine bone	$\varepsilon_K = 0.00576 + 0.000076 \ln(\dot{x})$ t: 14.49 2.04	9.8 (6.9)	*e*
30 Bovine bone	$\varepsilon_K = 0.00457 + 0.000061 \ln(\dot{x}) - 0.00005 E_b$ t: 4.92 1.60 1.42	12.9 (9.8)	*f*
30 Bovine bone	$\ln(\varepsilon_K) = - 5.16 + 0.0143 \ln(\dot{x})$ t: - 66.26 1.97	9.0 (6.1)	*g*
30 Bovine bone	$\ln(\varepsilon_K) = - 5.75 + 0.0116 \ln(\dot{x}) + 0.185 \ln(E_b)$ t: - 12.95 1.55 1.34	11.5 (8.4)	*h*
27 Antler	$\ln(\varepsilon_K) = - 3.31 + 0.0438 \ln(\dot{x}) - 0.546 \ln(E_t)$ t: - 16.07 4.79 - 5.59	71.8 (72.1)	*i*
27 Antler	$\ln(\varepsilon_K) = - 3.30 + 0.0437 \ln(\dot{x}) - 0.544 \ln(E_t) - 0.005 \ln(E_b)$ t: - 9.09 4.53 - 3.57 - 0.02	70.5 (71.0)	*j*
30 Bovine bone	$\ln(\varepsilon_K) = - 4.96 + 0.0165 \ln(\dot{x}) - 0.059 \ln(E_t)$ t: - 9.49 1.79 - 0.39	6.2 (3.2)	*k*
30 Bovine bone	$\ln(\varepsilon_K) = - 5.22 + 0.0222 \ln(\dot{x}) - 0.400 \ln(E_t) + 0.457 \ln(E_b)$ t: - 10.63 2.54 - 2.05 2.46	20.9 (19.2)	*l*
Units: ε_K, unitless. $\dot{x}$, m s^{-1}. E_t, GPa. E_b, GPa.			

Table A9.007

The relationship of the knee strain for specimens of bovine femoral bone and red deer antler to the cross-head speed of the test and the material stiffness of the specimen

Type of specimens	Regression equations and t values of the data shown in figure 4.015. (Data sets TA1 and TB1)	R^2 %	
27 Antler	$\varepsilon_K = 0.00720 + 2.22\ \dot{x}$ t: 21.38 2.39	15.3 (25.4)	*a*
27 Antler	$\varepsilon_K = 0.0137 + 1.82\ \dot{x} - 0.000565\ E_b$ t: 8.47 2.46 - 4.06	47.7 (55.9)	*b*
27 Antler	$\varepsilon_K = 0.0125 + 2.72\ \dot{x} - 0.000675\ E_t$ t: 15.69 4.88 - 6.88	70.3 (69.9)	*c*
27 Antler	$\varepsilon_K = 0.0127 + 2.68\ \dot{x} - 0.000656\ E_t - 0.000027\ E_b$ t: 10.05 4.44 - 4.19 - 0.16	69.1 (68.8)	*d*
30 Bovine bone	$\varepsilon_K = 0.00483 + 0.640\ \dot{x}$ t: 46.00 2.47	14.9 (11.8)	*e*
30 Bovine bone	$\varepsilon_K = 0.00407 + 0.518\ \dot{x} + 0.000038\ E_b$ t: 5.48 1.82 1.03	15.1 (11.9)	*f*
30 Bovine bone	$\varepsilon_K = 0.00562 + 0.881\ \dot{x} - 0.000038\ E_t$ t: 7.60 2.58 - 1.08	15.4 (12.2)	*g*
30 Bovine bone	$\varepsilon_K = 0.00484 + 0.937\ \dot{x} - 0.000098\ E_t + 0.000102\ E_b$ t: 6.37 2.95 - 2.36 2.34	27.5 (24.7)	*h*
Units: ε_K, unitless. $\dot{x}$, m s^{-1}. E_t, GPa. E_b, GPa.			

Table A9.008

The relationship of knee strain to cross-head speed

(4.2.6.9.) RESULTS: THE EFFECT OF CROSS-HEAD SPEED ON ULTIMATE STRAIN

Type of specimens	Regression equations and t values of the data shown in figure 4.016. (Data sets TA1 and TB1)	R^2 %	
27 Antler	$\varepsilon_{ult} = 0.148 + 0.00609 \ln(\dot{x})$ t: 16.06 7.32	66.9 (67.2)	*a*
27 Antler	$\varepsilon_{ult} = 0.126 + 0.00658 \ln(\dot{x}) + 0.00237 E_b$ t: 8.94 7.93 1.94	70.2 (70.3)	*b*
27 Antler	$\ln(\varepsilon_{ult}) = -1.71 + 0.0761 \ln(\dot{x})$ t: -14.59 7.18	66.0 (66.1)	*c*
27 Antler	$\ln(\varepsilon_{ult}) = -2.33 + 0.0818 \ln(\dot{x}) + 0.283 \ln(E_b)$ t: -5.95 7.57 1.66	68.2 (68.2)	*d*
30 Bovine bone	$\varepsilon_{ult} = 0.0354 + 0.00181 \ln(\dot{x})$ t: 3.99 2.17	11.4 (9.9)	*e*
30 Bovine bone	$\varepsilon_{ult} = -0.0083 + 0.00126 \ln(\dot{x}) + 0.00185 E_b$ t: -0.43 1.58 2.49	25.2 (23.4)	*f*
30 Bovine bone	$\ln(\varepsilon_{ult}) = -3.36 + 0.0935 \ln(\dot{x})$ t: -6.21 1.84	7.7 (4.9)	*g*
30 Bovine bone	$\ln(\varepsilon_{ult}) = -10.9 + 0.0600 \ln(\dot{x}) + 2.27 \ln(E_b)$ t: -3.70 1.25 2.56	22.9 (20.4)	*h*
Units: ε_{ult}, unitless. $\dot{x}$, m s^{-1}. E_t, GPa. E_b, GPa.			

Table A9.009

The relationship of the ultimate strain to the cross-head speed and the material stiffness measured in bending

27 Antler	$\ln(\varepsilon_{ult}) = -1.85 + 0.0776 \ln(\dot{x}) + 0.076 \ln(E_t)$ t: -7.49 7.07 0.65	65.2 (64.8)	*a*
27 Antler	$\ln(\varepsilon_{ult}) = -2.43 + 0.0823 \ln(\dot{x}) - 0.149 \ln(E_t) + 0.453 \ln(E_b)$ t: -5.93 7.57 -0.87 1.74	67.9 (70.0)	*b*
30 Bovine bone	$\ln(\varepsilon_{ult}) = -5.97 + 0.0660 \ln(\dot{x}) + 0.75 \ln(E_t)$ t: -1.66 1.04 0.73	6.1 (2.9)	*c*
30 Bovine bone	$\ln(\varepsilon_{ult}) = -8.04 + 0.111 \ln(\dot{x}) - 1.92 \ln(E_t) + 3.58 \ln(E_b)$ t: -2.46 1.90 -1.48 2.89	26.2 (24.5)	*d*
Units: ε_{ult}, unitless. $\dot{x}$, m s^{-1}. E_t, GPa. E_b, GPa.			

Table A9.010

The relationship of the ultimate strain to the cross-head speed and the material stiffness in bending and tension

(4.2.6.10.) RESULTS: THE EFFECT OF CROSS-HEAD SPEED ON THE FINAL SLOPE

Type of specimens	Regression equations and t values of the data shown in figure 4.019. (Data sets TA1 and TB1)	R^2 %	
27 Antler	$S = 0.533 + 0.00546 \ln(\dot{x})$ t: 7.63 0.86	0.0 (0.0)	*a*
27 Antler	$S = 0.480 + 0.00667 \ln(\dot{x}) + 0.00583 E_b$ t: 4.20 0.99 0.59	0.0 (0.0)	*b*
27 Antler	$\ln(S) = -0.652 + 0.0100 \ln(\dot{x})$ t: -4.60 0.76	0.0 (0.0)	*c*
27 Antler	$\ln(S) = -0.951 + 0.0127 \ln(\dot{x}) + 0.136 \ln(E_b)$ t: -1.92 0.93 0.63	0.0 (0.0)	*d*
11 Bovine bone	$S = 0.467 + 0.0190 \ln(\dot{x})$ t: 1.28 0.59	0.0 (0.0)	*e*
11 Bovine bone	$S = 0.601 + 0.0157 \ln(\dot{x}) - 0.0082 E_b$ t: 0.93 0.43 -0.26	0.0 (0.0)	*f*
11 Bovine bone	$\ln(S) = 0.17 + 0.175 \ln(\dot{x})$ t: 0.10 1.13	2.6 (5.2)	*g*
11 Bovine bone	$\ln(S) = -0.55 + 0.180 \ln(\dot{x}) + 0.26 \ln(E_b)$ t: -0.06 1.02 0.08	0.0 (3.1)	*h*
Units: S, GPa. $\dot{x}$, m s^{-1}. E_t, GPa. E_b, GPa.			

Table A9.011

The relationship of the final slope to the cross-head speed and the material stiffness in bending

27 Antler	$\ln(S) = -1.18 + 0.0155 \ln(\dot{x}) + 0.285 \ln(E_t)$ t: -4.28 1.27 2.18	11.7 (8.8)	*a*
27 Antler	$\ln(S) = -0.612 + 0.0109 \ln(\dot{x}) + 0.505 \ln(E_t) - 0.443 \ln(E_b)$ t: -1.32 0.88 2.60 -1.50	16.0 (16.6)	*b*
11 Bovine bone	$\ln(S) = 7.5 + 0.174 \ln(\dot{x}) - 2.41 \ln(E_t)$ t: 0.68 1.09 -0.67	0.0 (18.1)	*c*
11 Bovine bone	$\ln(S) = 6.2 + 0.220 \ln(\dot{x}) - 4.04 \ln(E_t) + 2.26 \ln(E_b)$ t: 0.52 1.20 -0.87 0.58	0.0 (6.5)	*d*
Units: S, GPa. $\dot{x}$, m s^{-1}. E_t, GPa. E_b, GPa.			

Table A9.012

The relationship of the final stiffness to the cross-head speed and the material stiffness in bending and tension

(4.2.6.11.) RESULTS: THE EFFECT OF CROSS-HEAD SPEED ON ULTIMATE DAMAGE

Type of specimens	Regression equations and t values of the data shown in figure 4.021. (Data sets TA1 and TB1)	R^2 %	
27 Antler	$D_t = 0.835 - 0.00053 \ln(\dot{x})$ t: 31.51 [22.68] - 0.22 [- 1.22]	0.0 (15.3) [1.8]	*a*
27 Antler	$D_t = 0.742 + 0.00159 \ln(\dot{x}) + 0.0103 E_b$ t: 20.38 [15.91] 0.74 [- 0.08] 3.26 [5.17]	25.1 (42.7) [51.6]	*b*
27 Antler	$\ln(D_t) = - 0.181 - 0.00074 \ln(\dot{x})$ t: - 5.69 [- 5.20] - 0.25 [- 1.22]	0.0 (14.9) [1.9]	*c*
27 Antler	$\ln(D_t) = - 0.468 - 0.00187 \ln(\dot{x}) + 0.130 \ln(E_b)$ t: - 4.96 [- 7.12] 0.72 [- 0.02] 3.17 [5.19]	23.9 (41.8) [51.8]	*d*
30 Bovine bone	$D_t = 0.805 + 0.0256 \ln(\dot{x})$ t: 3.96 [24.20] 1.34 [30.5]	2.7 (0.0) [30.5]	*e*
30 Bovine bone	$D_t = - 0.263 + 0.0121 \ln(\dot{x}) + 0.00452 E_b$ t: - 0.60 [9.45] 0.68 [3.50] 2.70 [5.23]	20.6 (17.6) [64.2]	*f*
30 Bovine bone	$\ln(D_t) = - 0.331 + 0.0448 \ln(\dot{x})$ t: - 0.58 [- 4.17] 0.84 [3.62]	0.0 (0.0) [29.4]	*g*
30 Bovine bone	$\ln(D_t) = - 7.48 + 0.0115 \ln(\dot{x}) + 2.26 \ln(E_b)$ t: - 2.44 [- 6.27] 0.22 [3.45] 2.37 [5.34]	13.2 (10.0) [64.4]	*h*
Units: D_t, unitless. $\dot{x}$, m s^{-1}. E_b, GPa.			

Table A9.013

The relationship of the ultimate damage to the cross-head speed and the material stiffness in bending

27 Antler	$\ln(D_t) = -0.395 + 0.00150 \ln(\dot{x}) + 0.116 \ln(E_t)$ t: -8.55 [-27.58] 0.73 [-0.78] 5.27 [19.81]	49.9 (53.4) [94.1]	*a*
27 Antler	$\ln(D_t) = -0.389 + 0.00145 \ln(\dot{x}) - 0.118 \ln(E_t) - 0.0049 \ln(E_b)$ t: -4.77 0.67 3.46 -0.09 [-15.51] [-0.77] [12.85] [-0.15]	47.7 (51.8) [93.9]	*b*
30 Bovine bone	$\ln(D_t) = -3.62 + 0.0101 \ln(\dot{x}) + 0.95 \ln(E_t)$ t: -0.96 [-33.81] 0.15 [-0.96] 0.88 [30.48]	0.0 (0.0) [97.9]	*c*
30 Bovine bone	$\ln(D_t) = -5.52 + 0.0510 \ln(\dot{x}) - 1.49 \ln(E_t) + 3.27 \ln(E_b)$ t: -1.54 0.80 -1.05 2.41 [-32.73] [-0.75] [20.69] [0.60]	13.6 (10.5) [97.9]	*d*
Units: D_t, unitless. $\dot{x}$, m s^{-1}. E_t, GPa. E_b, GPa.			

Table A9.014

The relationship of the ultimate damage to the cross-head speed and the material stiffness in bending and tension

Type of specimens	Regression equations and t values of the data shown in figure 4.022. (Data sets TA1 and TB1)	R^2 %	
27 Antler	$D_b = 0.888 - 0.00010 \ln(\dot{x})$ t: 56.06 - 0.07	0.0 (0.0)	*a*
27 Antler	$D_b = 0.838 + 0.00105 \ln(\dot{x}) + 0.00553 E_b$ t: 36.94 0.78 2.81	18.5 (15.6)	*b*
27 Antler	$\ln(D_b) = - 0.119 - 0.00010 \ln(\dot{x})$ t: - 6.66 - 0.06	0.0 (0.0)	*c*
27 Antler	$\ln(D_b) = - 0.261 + 0.00119 \ln(\dot{x}) + 0.0648 \ln(E_b)$ t: - 4.74 0.78 2.70	16.9 (14.1)	*d*
30 Bovine bone	$D_b = 0.655 + 0.0156 \ln(\dot{x})$ t: 2.68 0.68	0.0 (0.0)	*e*
30 Bovine bone	$D_b = - 0.701 - 0.0015 \ln(\dot{x}) + 0.0574 E_b$ t: - 1.36 - 0.07 2.90	19.4 (16.4)	*f*
28 Bovine bone	$\ln(D_b) = - 0.161 + 0.0597 \ln(\dot{x})$ t: - 0.28 1.13	1.0 (0.0)	*g*
28 Bovine bone	$\ln(D_b) = - 8.27 + 0.0136 \ln(\dot{x}) + 2.52 \ln(E_b)$ t: - 2.81 0.27 2.79	21.5 (18.7)	*h*
Units: D_b, unitless. $\dot{x}$, m s^{-1}. E_b, GPa.			

Table A9.015

The relationship of the ultimate damage to the cross-head speed and the material stiffness in bending

27 Antler	$\ln(D_b) = -0.136 + 0.00008 \ln(\dot{x}) + 0.0093 \ln(E_t)$ t: -3.60 0.05 0.52	0.0 (0.0)	*a*
27 Antler	$\ln(D_b) = -0.297 + 0.00138 \ln(\dot{x}) - 0.0530 \ln(E_t) + 0.126 \ln(E_b)$ t: -5.67 1.00 -2.42 3.77	30.9 (38.4)	*b*
30 Bovine bone	$\ln(D_b) = -3.88 + 0.0199 \ln(\dot{x}) + 1.07 \ln(E_t)$ t: -1.07 0.31 1.04	1.3 (0.0)	*c*
30 Bovine bone	$\ln(D_b) = -6.22 + 0.0564 \ln(\dot{x}) - 1.80 \ln(E_t) + 3.83 \ln(E_b)$ t: -1.90 0.96 -1.34 2.91	14.0 (20.8)	*d*
Units: D_b, unitless. $\dot{x}$, m s^{-1}. E_t, GPa. E_b, GPa.			

Table A9.016

The relationship of the ultimate damage to the cross-head speed and the material stiffness in bending and tension

(4.2.6.12.) RESULTS: THE EFFECT OF CROSS-HEAD SPEED ON WORK INPUT

Type of specimens	Regression equations and t values, for the data shown in figure 4.023. (Data sets TA1 and TB1)	R^2 %	
27 Antler	$W = 16.2 + 0.896 \ln(\dot{x})$ t: 10.43 6.36	60.2 (60.5)	*a*
27 Antler	$W = 9.44 + 1.05 \ln(\dot{x}) + 0.748 E_b$ t: 5.05 9.56 4.62	78.1 (78.3)	*b*
27 Antler	$\ln(W) = 3.20 + 0.130 \ln(\dot{x})$ t: 14.27 6.40	66.6 (60.8)	*c*
27 Antler	$\ln(W) = 0.688 + 0.153 \ln(\dot{x}) + 1.14 E_b$ t: 1.18 9.52 4.51	77.8 (78.2)	*d*
30 Bovine bone	$W = 5.09 + 0.319 \ln(\dot{x})$ t: 4.13 2.76	18.6 (18.6)	*e*
30 Bovine bone	$W = -1.63 + 0.234 \ln(\dot{x}) + 0.284 E_b$ t: -0.62 2.18 2.84	35.0 (34.5)	*f*
30 Bovine bone	$\ln(W) = 1.79 + 0.162 \ln(\dot{x})$ 2.34 2.25	12.3 (9.7)	*g*
30 Bovine bone	$\ln(W) = -10.2 + 0.106 \ln(\dot{x}) + 3.78 \ln(E_b)$ -2.64 1.63 3.15	33.5 (31.3)	*h*
Units: W, MJ m^{-3}. $\dot{x}$, m s^{-1}. E_b, GPa.			

Table A9.017

The statistical relationship between the work or area under the curve and the cross-head speed of the tensile test on specimens of bone and antler

27 Antler	$\ln(W) = 2.03 + 0.142 \ln(\dot{x}) + 0.633 \ln(E_t)$ t: 5.18 8.17 3.40	72.3 (71.1)	*a*
27 Antler	$\ln(W) = 0.790 + 0.153 \ln(\dot{x}) + 0.152 \ln(E_t) + 0.970 \ln(E_b)$ t: 1.29 9.34 0.59 2.48	77.2 (77.2)	*b*
30 Bovine bone	$\ln(W) = -4.69 + 0.0934 \ln(\dot{x}) + 1.87 \ln(E_t)$ t: - 0.94 1.06 1.31	14.5 (11.5)	*c*
30 Bovine bone	$\ln(W) = -7.63 + 0.157 \ln(\dot{x}) - 1.93 \ln(E_t) + 5.09 \ln(E_b)$ t: - 1.70 1.96 - 1.08 2.99	34.0 (32.1)	*d*
Units: W, MJ m^{-3}. $\dot{x}$, m s^{-1}. E_t, GPa. E_b, GPa.			

Table A9.018

The statistical relationship between the work or area under the curve and the cross-head speed of the tensile test on specimens of bone and antler, with reference to the material stiffness in tension

The following tables are for the regression equations derived from the data obtained from creep tests on specimens of bone and antler. The equation presented is that obtained from analysis of either data set CA2 or CB2. The former contains antler data and the latter that from bovine bone. These data sets are comprised of a core of data from samples for which values of nearly all the variables examine are available. The R^2 values in parentheses are those obtained when the same regression was performed on the full set of data the number of specimens examined in this case is also presented in parentheses.

(4.3.7.1.) LOGARITHMS OF CREEP STRESS, $\ln(\sigma_0)$, AND TIME-TO-RUPTURE, $\ln(t_R)$

Type of specimens	Regression equations and t values, for the data shown in figure 4.034. (Data sets CA2 and CB2 [CA1 and CB1])	R^2 %	
CA2 20 (28)	$\ln(t_R) = 45.4 - 9.35 \ln(\sigma_0)$ t: 3.98 - 3.42	36.0 (43.8)	*a*
CA2 12 (16)	$\ln(t_R) = 45.0 - 9.06 \ln(\sigma_0) - 3.16 \ln(E_t)$ t: 2.51 - 2.08 - 1.80	50.4 (57.7)*	*b*
CA2 20 (28)	$\ln(t_R) = 27.5 - 9.66 \ln(\sigma_0) + 3.6 \ln(Ca)$ t: 0.33 - 3.06 0.22	32.4 (43.5)	*c*
CB2 15 (25)	$\ln(t_R) = 25.1 - 4.28 \ln(\sigma_0)$ t: 1.17 - 0.91	0.0 (4.7)	*d*
CB2 15 (25)	$\ln(t_R) = 26.5 - 5.49 \ln(\sigma_0) + 1.32 \ln(E_b)$ t: 1.20 - 1.03 0.53	0.0 (6.5)	*e*
CB2 15 (24)	$\ln(t_R) = 26.4 - 4.35 \ln(\sigma_0) + 0.26 \ln(E_t)$ t: 1.02 - 0.85 0.06	0.0 (7.8)	*f*
CB2 15 (25)	$\ln(t_R) = - 136 - 6.11 \ln(\sigma_0) + 30.5 \ln(Ca)$ t: - 0.92 - 1.23 1.11	0.4 (0.7)	*g*
Units: t_R, s. σ_0, MPa. E_t, GPa. E_b, GPa. Ca, mg g^{-1}			

Table A9.019

Relationship of the time-to-rupture and the creep stress

(4.3.7.2.) CREEP STRESS, σ_0, AND TIME-TO-RUPTURE, $\ln(t_R)$

Type of specimens	Regression equations and t values, for the data shown in figure 4.036. (Data sets CA2 and CB2 [CA1 and CB1])	R^2 %	
CA2 20 (28)	$\ln(t_R) = 15.4 - 0.137\ \sigma_0$ t: 5.49 - 3.23	33.2 (41.4)	*a*
CA2 12 (16)	$\ln(t_R) = 17.8 - 0.137\ \sigma_0 - 1.87\ E_t$ t: 4.46 - 2.15 - 1.66	45.3 (53.3)	*b*
CA2 20 (28)	$\ln(t_R) = 14.8 - 0.138\ \sigma_0 + 0.0034\ Ca$ t: 0.95 - 2.88 0.04	29.3 (40.3)	*c*
CB2 15 (25)	$\ln(t_R) = 10.0 - 0.0459\ \sigma_0$ t: 2.15 - 0.93	0.0 (4.5)	*d*
CB2 15 (25)	$\ln(t_R) = 9.49 - 0.0688\ \sigma_0 - 0.113\ E_b$ t: 2.00 - 1.23 0.89	0.0 (9.8)	*e*
CB2 15 (24)	$\ln(t_R) = 10.2 - 0.0452\ \sigma_0 - 0.010\ E_t$ t: 1.71 - 0.85 - 0.06	0.0 (6.9)	*f*
CB2 15 (25)	$\ln(t_R) = - 19.3 - 0.0655\ \sigma_0 + 0.121\ E_t$ t: - 0.73 - 1.26 1.13	1.2 (0.4)	*g*
Units: t_R, s. σ_0, MPa. E_t, GPa. E_b, GPa. Ca, mg g^{-1}			

Table A9.020

Statistical relationship of time-to-rupture to the creep stress

(4.3.7.3.) LOGARITHM OF STRESS AND LOGARITHM OF ELONGATION AT RUPTURE: PART 1, $\ln(\sigma_0)$ AND $\ln(\varepsilon_R)$

Type of specimens	Regression equations and t values, for the data shown in figure 4.037. (Data sets CA2 and CB2 [CA1 and CB1])	R^2 %	
CA2 20 (31)	$\ln(\varepsilon_R) = -3.59 + 0.247 \ln(\sigma_0)$ t: -2.00 0.58	0.0 (7.0)	*a*
CA2 12 (16)	$\ln(\varepsilon_R) = -5.89 + 0.848 \ln(\sigma_0) - 0.249 \ln(E_t)$ t: -3.16 1.87 -1.36	14.6 (5.9)	*b*
CA2 20 (31)	$\ln(\varepsilon_R) = -1.6 + 0.281 \ln(\sigma_0) - 0.39 \ln(Ca)$ t: -0.13 0.57 -0.15	0.0 (4.9)	*c*
CB2 15 (26)	$\ln(\varepsilon_R) = -16.8 + 2.68 \ln(\sigma_0)$ t: -3.65 2.64	29.9 (18.7)	*d*
CB2 15 (26)	$\ln(\varepsilon_R) = -16.9 + 2.77 \ln(\sigma_0) - 0.094 \ln(E_b)$ t: -3.51 2.37 -0.18	24.2 (24.9)	*e*
CB2 15 (26)	$\ln(\varepsilon_R) = -13.0 + 3.25 \ln(\sigma_0) - 1.92 \ln(E_t)$ t: -2.96 3.52 -2.23	46.4 (45.4)	*f*
CB2 15 (26)	$\ln(\varepsilon_R) = -9.0 + 2.77 \ln(\sigma_0) - 1.49 \ln(Ca)$ t: -0.27 2.48 -0.24	24.4 (33.6)	*g*
Units: ε_R, unitless. σ_0, MPa. E_t, GPa. E_b, GPa. Ca, mg g^{-1}			

Table A9.021

Relationship of strain at rupture to the creep stress and material stiffness

(4.3.7.4.) LOGARITHM OF STRESS AND LOGARITHM OF ELONGATION AT RUPTURE: PART 2, $\ln(\sigma_0)$ AND $\ln(\varepsilon_{0\rightarrow R})$

Type of specimens	Regression equations and t values, for the data shown in figure 4.038. (Data sets CA2 and CB2 [CA1 and CB1])	R^2 %	
CA2 20 (31)	$\ln(\varepsilon_{0\rightarrow R}) = -2.80 - 0.121 \ln(\sigma_0)$ t: -1.73 -0.31	0.0 (0.0)	*a*
CA2 12 (16)	$\ln(\varepsilon_{0\rightarrow R}) = -4.93 + 0.213 \ln(\sigma_0) + 0.293 \ln(E_t)$ t: -1.63 0.32 1.11	0.1 (0.0)	*b*
CA2 20 (31)	$\ln(\varepsilon_{0\rightarrow R}) = 13.7 + 0.171 \ln(\sigma_0) - 3.31 \ln(Ca)$ t: 1.25 0.41 -1.52	2.1 (0.0)	*c*
CB2 15 (23)	$\ln(\varepsilon_{0\rightarrow R}) = -25.7 + 4.50 \ln(\sigma_0)$ t: -3.15 -2.50	27.4 (23.2)	*d*
CB2 15 (23)	$\ln(\varepsilon_{0\rightarrow R}) = -26.3 + 5.02 \ln(\sigma_0) - 0.566 \ln(E_b)$ t: -3.12 2.47 -0.60	23.6 (26.5)	*e*
CB2 15 (23)	$\ln(\varepsilon_{0\rightarrow R}) = -20.5 + 5.27 \ln(\sigma_0) - 2.59 \ln(E_t)$ t: -2.44 2.97 -1.57	34.8 (26.1)	*f*
CB2 15 (23)	$\ln(\varepsilon_{0\rightarrow R}) = 16.0 + 4.97 \ln(\sigma_0) - 7.9 \ln(Ca)$ t: 0.28 2.56 -0.73	24.7 (30.4)	*g*
Units: $\varepsilon_{0\rightarrow R}$, unitless. σ_0, MPa. E_t, GPa. E_b, GPa. Ca, mg g^{-1}			

Table A9.022

Creep strain, creep stress and material stiffness

(4.3.7.5.) LOGARITHM OF STRESS AND LOGARITHM OF ELONGATION AT RUPTURE: PART 3, $\ln(\sigma_0)$ AND $\ln(\varepsilon_{1*\rightarrow R})$

Type of specimens	Regression equations and t values, for the data shown in figure 4.039. (Data sets CA2 and CB2 [CA1 and CB1])	R^2 %	
CA2 20 (30)	$\ln(\varepsilon_{1*\rightarrow R}) = -11.8 + 1.61 \ln(\sigma_0)$ t: - 2.16 1.23	2.6 (8.6)	*a*
CA2 12 (15)	$\ln(\varepsilon_{1*\rightarrow R}) = -22.0 + 3.90 \ln(\sigma_0) + 1.13 \ln(E_t)$ t: - 3.14 2.29 1.64	51.3 (55.7)	*b*
CA2 20 (30)	$\ln(\varepsilon_{1*\rightarrow R}) = 45.1 + 2.62 \ln(\sigma_0) - 11.4 \ln(Ca)$ t: 1.22 1.85 - 1.56	9.8 (8.4)	*c*
CB2 15 (20)	$\ln(\varepsilon_{1*\rightarrow R}) = -34.9 + 6.46 \ln(\sigma_0)$ t: - 3.27 2.74	31.8 (36.9)	*d*
CB2 15 (20)	$\ln(\varepsilon_{1*\rightarrow R}) = -35.5 + 7.07 \ln(\sigma_0) - 0.66 \ln(E_b)$ t: - 3.22 2.64 - 0.53	27.8 (37.9)	*e*
CB2 15 (20)	$\ln(\varepsilon_{1*\rightarrow R}) = -28.8 + 7.36 \ln(\sigma_0) - 3.05 \ln(E_t)$ t: - 2.56 3.11 - 1.39	37.1 (47.7)	*f*
CB2 15 (20)	$\ln(\varepsilon_{1*\rightarrow R}) = 24.5 + 7.14 \ln(\sigma_0) - 11.3 \ln(Ca)$ t: 0.33 2.82 - 0.80	29.8 (38.6)	*g*
Units: $\varepsilon_{1*\rightarrow R}$, unitless. σ_0, MPa. E_t, GPa. E_b, GPa. Ca, mg g^{-1}			

Table A9.023

Approximate creep strain, creep stress and material stiffness

(4.3.7.6.) LOGARITHM OF STRESS AND LOGARITHM OF ELONGATION AT RUPTURE: PART 4, $\ln(\sigma_0)$ AND $\ln(\varepsilon_{1*\rightarrow 3})$

Type of specimens	Regression equations and t values, for the data shown in figure 4.040. (Data sets CA2 and CB2 [CA1 and CB1])	R^2 %	
CA2 20 (26)	$\ln(\varepsilon_{1*\rightarrow 3}) = -11.6 + 1.54 \ln(\sigma_0)$ t: - 2.06 1.14	1.6 (13.6)	*a*
CA2 12 (15)	$\ln(\varepsilon_{1*\rightarrow 3}) = -23.6 + 4.30 \ln(\sigma_0) + 1.13 \ln(E_t)$ t: - 3.68 2.76 1.80	59.9 (61.2)	*b*
CA2 20 (26)	$\ln(\varepsilon_{1*\rightarrow 3}) = 45.8 + 2.56 \ln(\sigma_0) - 11.5 \ln(Ca)$ t: 1.21 1.75 - 1.53	8.4 (24.4)	*c*
CB2 14 (17)	$\ln(\varepsilon_{1*\rightarrow 3}) = -27.1 + 4.75 \ln(\sigma_0)$ t: - 3.63 2.90	36.2 (36.0)	*d*
CB2 14 (17)	$\ln(\varepsilon_{1*\rightarrow 3}) = -27.3 + 4.92 \ln(\sigma_0) - 0.158 \ln(E_b)$ t: - 3.45 2.51 - 0.18	30.6 (36.5)	*e*
CB2 14 (17)	$\ln(\varepsilon_{1*\rightarrow 3}) = -20.0 + 5.94 \ln(\sigma_0) - 3.73 \ln(E_t)$ t: - 3.30 4.58 - 3.16	63.6 (67.1)	*f*
CB2 14 (17)	$\ln(\varepsilon_{1*\rightarrow 3}) = -44.8 + 4.50 \ln(\sigma_0) + 3.4 \ln(Ca)$ t: - 0.79 2.38 0.31	31.0 (38.3)	*g*
Units: $\varepsilon_{1*\rightarrow 3}$, unitless. σ_0, MPa. E_t, GPa. E_b, GPa. Ca, mg g^{-1}			

Table A9.024

Steady state creep strain, creep stress and material stiffness

(4.3.7.8.) ELONGATION AT RUPTURE AND THE LOGARITHM OF THE TIME-TO-RUPTURE: PART 1, ε_R AND $\ln(t_R)$

Type of specimens	Regression equations and t values, for the data shown in figure 4.041. (Data sets CA2 and CB2 [CA1 and CB1])	R^2 %	
CA2 20 (29)	$\ln(t_R) = 10.2 - 47.6\,\varepsilon_R$ t: 5.55 - 2.12	15.6 (11.8)	*a*
CA2 12 (17)	$\ln(t_R) = 16.5 - 65.6\,\varepsilon_R - 3.14\,E_t$ t: 4.33 - 1.91 - 2.79	41.2 (25.2)	*b*
CA2 20 (29)	$\ln(t_R) = 26.8 - 46.2\,\varepsilon_R - 0.0787\,Ca$ t: 1.63 - 2.05 - 1.01	15.7 (8.4)	*c*
CB2 15 (29)	$\ln(t_R) = 6.79 - 102\,\varepsilon_R$ t: 5.93 - 1.06	0.9 (0.0)	*d*
CB2 15 (29)	$\ln(t_R) = 5.33 - 112\,\varepsilon_R + 0.067\,E_b$ t: 1.91 - 1.12 0.58	0.0 (1.8)	*e*
CB2 15 (29)	$\ln(t_R) = 10.2 - 125\,\varepsilon_R - 0.110\,E_t$ t: 1.95 - 1.20 - 0.67	0.0 (16)	*f*
CB2 15 (29)	$\ln(t_R) = -18.1 - 118\,\varepsilon_R + 0.098\,Ca$ t: - 0.69 - 1.20 0.95	0.1 (0.0)	*g*
Units: t_R, s. ε_R, unitless. E_t, GPa. E_b, GPa. Ca, mg g^{-1}			

Table A9.025

Relationship of the time-to-rupture and the rupture strain

(4.3.7.9.) ELONGATION AT RUPTURE AND THE LOGARITHM OF THE TIME-TO-RUPTURE: PART 2, $\varepsilon_{0\rightarrow R}$ AND $\ln(t_R)$

Type of specimens	Regression equations and t values, for the data shown in figure 4.043. (Data sets CA2 and CB2 [CA1 and CB1])	R^2 %	
CA2 20 (26)	$\ln(t_R) = 6.47 - 1.4\ \varepsilon_{0\rightarrow R}$ t: 2.75 - 0.02	0.0 (12.5)	*a*
CA2 12 (16)	$\ln(t_R) = 11.5 - 62.1\ \varepsilon_{0\rightarrow R} - 2.26\ E_t$ t: 3.86 - 0.68 - 1.58	21.2 (35.8)	*b*
CA2 20 (26)	$\ln(t_R) = 30.1 - 31.4\ \varepsilon_{0\rightarrow R} - 0.106\ Ca$ t: 1.44 - 0.47 - 1.14	0.0 (11.1)	*c*
CB2 15 (21)	$\ln(t_R) = 6.44 - 107\ \varepsilon_{0\rightarrow R}$ t: 7.25 - 1.02	0.3 (0.0)	*d*
CB2 15 (21)	$\ln(t_R) = 5.05 - 116\ \varepsilon_{0\rightarrow R} + 0.062\ E_b$ t: 1.83 - 1.06 0.53	0.0 (0.0)	*e*
CB2 15 (21)	$\ln(t_R) = 9.52 - 128\ \varepsilon_{0\rightarrow R} - 0.102\ E_t$ t: 1.89 - 1.14 - 0.62	0.0 (5.8)	*f*
CB2 15 (21)	$\ln(t_R) = -17.9 - 122\ \varepsilon_{0\rightarrow R} + 0.095\ Ca$ t: - 0.68 - 1.15 0.92	0.0 (0.0)	*g*
Units: t_R, s. $\varepsilon_{0\rightarrow R}$, unitless. E_t, GPa. E_b, GPa. Ca, mg g^{-1}			

Table A9.026

Relationship of the time-to-rupture and the creep strain

(4.3.7.10.) ELONGATION AT RUPTURE AND THE LOGARITHM OF THE TIME-TO-RUPTURE: PART 3, $\varepsilon_{l*\rightarrow R}$ AND $\ln(t_R)$

Type of specimens	Regression equations and t values, for the data shown in figure 4.044. (Data sets CA2 and CB2 [CA1 and CB1])	R^2 %	
CA2 20 (25)	$\ln(t_R) = 8.16 - 225\ \varepsilon_{l*\rightarrow R}$ t: 9.93 - 2.46	21.0 (38.5)	*a*
CA2 12 (15)	$\ln(t_R) = 9.46 - 360\ \varepsilon_{l*\rightarrow R} - 0.72\ E_t$ t: 6.68 - 3.32 - 0.68	62.8 (63.2)	*b*
CA2 20 (25)	$\ln(t_R) = 32.3 - 242\ \varepsilon_{l*\rightarrow R} - 0.113\ Ca$ t: 2.08 - 2.73 - 1.55	26.8 (41.1)	*c*
CB2 15 (18)	$\ln(t_R) = 6.37 - 113\ \varepsilon_{l*\rightarrow R}$ t: 7.40 - 0.97	0.0 (14.5)	*d*
CB2 15 (18)	$\ln(t_R) = 4.60 - 138\ \varepsilon_{l*\rightarrow R} + 0.082\ E_b$ t: 1.68 - 1.12 0.69	0.0 (12.6)	*e*
CB2 15 (18)	$\ln(t_R) = 8.71 - 125\ \varepsilon_{l*\rightarrow R} - 0.079\ E_t$ t: 1.79 - 1.03 - 0.49	0.0 (10.7)	*f*
CB2 15 (18)	$\ln(t_R) = -23.2 - 152\ \varepsilon_{l*\rightarrow R} + 0.116\ Ca$ t: - 0.86 - 1.27 1.10	3.1 (13.8)	*g*
Units: t_R, s. $\varepsilon_{l*\rightarrow R}$, unitless. E_t, GPa. E_b, GPa. Ca, mg g^{-1}			

Table A9.027

Time-to-rupture and approximate creep strain

(4.3.7.11.) ELONGATION AT RUPTURE AND THE LOGARITHM OF THE TIME-TO-RUPTURE: PART 4, $\varepsilon_{1*\rightarrow 3}$ AND $\ln(t_R)$

Type of specimens	Regression equations and t values, for the data shown in figure 4.046. (Data sets CA2 and CB2 [CA1 and CB1])	R^2 %	
CA2 20 (26)	$\ln(t_R) = 8.17 - 229\ \varepsilon_{1*\rightarrow 3}$ t: 10.55 - 2.65	24.1 (27.9)	*a*
CA2 12 (15)	$\ln(t_R) = 9.57 - 334\ \varepsilon_{1*\rightarrow 3} - 0.80\ E_t$ t: 6.57 - 3.16 - 0.75	60.8 (63.8)	*b*
CA2 20 (26)	$\ln(t_R) = 33.5 - 248\ \varepsilon_{1*\rightarrow 3} - 0.119\ Ca$ t: 2.22 - 3.00 - 1.68	31.1 (34.3)	*c*
CB2 15 (18)	$\ln(t_R) = 6.44 - 137\ \varepsilon_{1*\rightarrow 3}$ t: 7.76 - 1.13	1.9 (18.0)	*d*
CB2 15 (18)	$\ln(t_R) = 4.83 - 154\ \varepsilon_{1*\rightarrow 3} + 0.072\ E_b$ t: 1.78 - 1.21 0.63	0.0 (15.0)	*e*
CB2 15 (18)	$\ln(t_R) = 9.50 - 161\ \varepsilon_{1*\rightarrow 3} - 0.102\ E_t$ t: 1.94 - 1.24 - 0.63	0.0 (13.3)	*f*
CB2 15 (18)	$\ln(t_R) = -22.0 - 171\ \varepsilon_{1*\rightarrow 3} + 0.112\ Ca$ t: - 0.84 - 1.37 1.08	5.4 (16.2)	*g*
Units: t_R, s. $\varepsilon_{1*\rightarrow 3}$, unitless. E_t, GPa. E_b, GPa. Ca, mg g^{-1}			

Table A9.028

Time-to-rupture and steady state creep strain

(4.3.7.13.) LOGARITHM OF CREEP STRESS AND THE LOGARITHM OF ELONGATION RATE: PART 1, $\ln(\dot{\varepsilon}_{1\bullet\rightarrow3})$ AND $\ln(\sigma_0)$

Type of specimens	Regression equations and t values, for the data shown in figure 4.047. (Data sets CA2 and CB2 [CA1 and CB1])	R^2 %	
CA2 20 (31)	$\ln(\dot{\varepsilon}_{1\bullet\rightarrow3}) = -43.2 + 10.9 \ln(\sigma_0)$ t: - 2.84 2.99	29.5 (35.4)	*a*
CA2 12 (15)	$\ln(\dot{\varepsilon}_{1\bullet\rightarrow3}) = -54.8 + 13.4 \ln(\sigma_0) + 4.29 \ln(E_t)$ t: - 2.49 2.50 1.99	58.9 (66.1)	*b*
CA2 20 (31)	$\ln(\dot{\varepsilon}_{1\bullet\rightarrow3}) = 32 + 12.2 \ln(\sigma_0) - 15.1 \ln(Ca)$ t: 0.30 2.94 - 0.70	27.4 (35.9)	*c*
CB2 14 (17)	$\ln(\dot{\varepsilon}_{1\bullet\rightarrow3}) = -30.1 + 7.28 \ln(\sigma_0)$ t: - 1.37 1.50	8.8 (15.4)	*d*
CB2 14 (17)	$\ln(\dot{\varepsilon}_{1\bullet\rightarrow3}) = -30.4 + 7.42 \ln(\sigma_0) - 0.14 \ln(E_b)$ t: - 1.30 1.28 - 0.05	0.5 (14.7)	*e*
CB2 14 (17)	$\ln(\dot{\varepsilon}_{1\bullet\rightarrow3}) = -24.2 + 8.28 \ln(\sigma_0) - 3.16 \ln(E_t)$ t: - 0.99 1.60 - 0.67	4.4 (39.4)	*f*
CB2 14 (17)	$\ln(\dot{\varepsilon}_{1\bullet\rightarrow3}) = 18 + 7.97 \ln(\sigma_0) - 9.3 \ln(Ca)$ t: 0.11 1.43 - 0.29	1.2 (20.8)	*g*
Units: $\dot{\varepsilon}_{1\bullet\rightarrow3}$, $\mu\varepsilon\ s^{-1}$. σ_0, MPa. E_t, GPa. E_b, GPa. Ca, mg g^{-1}			

Table A9.029

Steady state creep rate and creep stress

(4.3.7.14.) LOGARITHM OF CREEP STRAIN AND THE LOGARITHM OF ELONGATION RATE: PART 2, $\ln(\dot{\varepsilon}_{1*\rightarrow R})$ AND $\ln(\sigma_0)$

Type of specimens	Regression equations and t values, for the data shown in figure 4.048. (Data sets CA2 and CB2 [CA1 and CB1])	R^2 %	
CA2 20 (25)	$\ln(\dot{\varepsilon}_{1*\rightarrow R}) = -43.4 + 11.0 \ln(\sigma_0)$ t: -2.93 3.09	31.0 (40.2)	*a*
CA2 12 (15)	$\ln(\dot{\varepsilon}_{1*\rightarrow R}) = -53.2 + 13.0 \ln(\sigma_0) + 4.29 \ln(E_t)$ t: -2.36 2.37 1.94	56.4 (64.5)	*b*
CA2 20 (25)	$\ln(\dot{\varepsilon}_{1*\rightarrow R}) = 31 + 12.3 \ln(\sigma_0) - 15.0 \ln(Ca)$ t: 0.30 3.04 -0.72	29.0 (39.0)	*c*
CB2 15 (18)	$\ln(\dot{\varepsilon}_{1*\rightarrow R}) = -46.2 + 10.7 \ln(\sigma_0)$ t: -1.64 1.73	12.4 (20.0)	*d*
CB2 15 (18)	$\ln(\dot{\varepsilon}_{1*\rightarrow R}) = -48.3 + 12.6 \ln(\sigma_0) - 1.98 \ln(E_b)$ t: -1.66 1.78 -0.61	7.9 (23.4)	*e*
CB2 15 (18)	$\ln(\dot{\varepsilon}_{1*\rightarrow R}) = -39.5 + 11.7 \ln(\sigma_0) - 3.31 \ln(E_t)$ t: -1.25 1.76 -0.54	7.3 (35.1)	*f*
CB2 15 (18)	$\ln(\dot{\varepsilon}_{1*\rightarrow R}) = 174 + 13.2 \ln(\sigma_0) - 41.8 \ln(Ca)$ t: 0.90 2.03 -1.15	14.5 (32.0)	*g*
Units: σ_0, MPa. $\dot{\varepsilon}_{1*\rightarrow R}$, $\mu\varepsilon\ s^{-1}$. E_t, GPa. E_b, GPa. Ca, $mg\ g^{-1}$			

Table A9.030

Approximate creep rate and creep stress

(4.3.7.15.) LOGARITHM OF CREEP STRESS AND THE LOGARITHM OF ELONGATION RATE: PART 3, $\ln(\dot{\varepsilon}_{0\rightarrow R})$ AND $\ln(\sigma_0)$

Type of specimens	Regression equations and t values, for the data shown in figure 4.049. (Data sets CA2 and CB2 [CA1 and CB1])	R^2 %	
CA2 20 (26)	$\ln(\dot{\varepsilon}_{0\rightarrow R}) = -34.4 + 9.22\ln(\sigma_0)$ t: - 2.93 3.28	33.9 (43.9)	*a*
CA2 20 (16)	$\ln(\dot{\varepsilon}_{0\rightarrow R}) = -35.5 + 9.27\ln(\sigma_0) + 3.45\ln(E_t)$ t: - 1.91 2.05 1.89	51.3 (60.1)	*b*
CA2 20 (26)	$\ln(\dot{\varepsilon}_{0\rightarrow R}) = 0.0 + 9.83\ln(\sigma_0) - 6.9\ln(Ca)$ t: 0.00 3.04 - 0.41	30.8 (42.4)	*c*
CB2 15 (18)	$\ln(\dot{\varepsilon}_{0\rightarrow R}) = -37.0 + 8.78\ln(\sigma_0)$ t: - 1.44 1.55	9.2 (20.0)	*d*
CB2 15 (18)	$\ln(\dot{\varepsilon}_{0\rightarrow R}) = -39.0 + 10.5\ln(\sigma_0) - 1.89\ln(E_b)$ t: - 1.48 1.63 - 0.64	4.9 (23.4)	*e*
CB2 15 (18)	$\ln(\dot{\varepsilon}_{0\rightarrow R}) = -31.3 + 9.62\ln(\sigma_0) - 2.85\ln(E_t)$ t: - 1.09 1.59 - 0.51	3.7 (35.1)	*f*
CB2 15 (18)	$\ln(\dot{\varepsilon}_{0\rightarrow R}) = 166 + 11.1\ln(\sigma_0) - 38.4\ln(Ca)$ t: 0.94 1.87 - 1.17	11.6 (32.0)	*g*
Units: $\dot{\varepsilon}_{0\rightarrow R}$, $\mu\varepsilon\ s^{-1}$. σ_0, MPa. E_t, GPa. E_b, GPa. Ca, mg g^{-1}			

Table A9.031

Creep strain and average stress rate

(4.3.7.17.) LOGARITHM OF TIME-TO-RUPTURE AND THE LOGARITHM OF ELONGATION RATE: PART 1, $\ln(t_R)$ AND $\ln(\dot{\varepsilon}_{1\bullet\rightarrow3})$

Type of specimens	Regression equations and t values, for the data shown in figure 4.050. (Data sets CA2 and CB2 [CA1 and CB1])	R^2 %	
CA2 20 (26)	$\ln(t_R) = 8.14 - 0.762 \ln(\dot{\varepsilon}_{1\bullet\rightarrow3})$ t: 49.72 - 15.96	93.0 (95.6)	*a*
CA2 12 (15)	$\ln(t_R) = 7.84 - 0.744 \ln(\dot{\varepsilon}_{1\bullet\rightarrow3}) + 0.184 \ln(E_t)$ t: 38.29 - 13.46 0.33	96.5 (97.8)	*b*
CA2 20 (26)	$\ln(t_R) = 55.9 - 0.749 \ln(\dot{\varepsilon}_{1\bullet\rightarrow3}) - 8.92 \ln(Ca)$ t: 2.41 - 16.87 - 2.06	94.1 (96.6)	*c*
CB2 14 (17)	$\ln(t_R) = 7.68 - 0.773 \ln(\dot{\varepsilon}_{1\bullet\rightarrow3})$ t: 22.32 - 7.99	82.8 (88.5)	*d*
CB2 14 (17)	$\ln(t_R) = 5.79 - 0.786 \ln(\dot{\varepsilon}_{1\bullet\rightarrow3}) + 0.617 \ln(E_b)$ t: 2.22 - 7.83 0.73	83.8 (87.8)	*e*
CB2 14 (17)	$\ln(t_R) = 14.4 - 0.780 \ln(\dot{\varepsilon}_{1\bullet\rightarrow3}) - 1.95 \ln(E_t)$ t: 2.68 - 8.22 - 1.23	83.6 (89.2)	*f*
CB2 14 (17)	$\ln(t_R) = -60.3 - 0.784 \ln(\dot{\varepsilon}_{1\bullet\rightarrow3}) + 12.3 \ln(Ca)$ t: - 1.09 - 8.23 1.23	83.5 (87.7)	*g*
Units: t_R, s. $\dot{\varepsilon}_{1\bullet\rightarrow3}$, $\mu\varepsilon\ s^{-1}$. E_t, GPa. E_b, GPa. Ca, mg g^{-1}			

Table A9.032

Time-to-rupture and the steady state creep rate

(4.3.7.18.) LOGARITHM OF TIME-TO-RUPTURE AND THE LOGARITHM OF ELONGATION RATE: PART 2, $\ln(t_R)$ AND $\ln(\dot{\varepsilon}_{1\bullet\rightarrow R})$

Type of specimens	Regression equations and t values, for the data shown in figure 4.053. (Data sets CA2 and CB2 [CA1 and CB1])	R^2 %	
CA2 20 (25)	$\ln(t_R) = 8.19 - 0.772 \ln(\dot{\varepsilon}_{1\bullet\rightarrow R})$ t: 48.22 - 15.55	92.7 (95.9)	*a*
CA2 12 (15)	$\ln(t_R) = 7.82 - 0.741 \ln(\dot{\varepsilon}_{1\bullet\rightarrow R}) + 0.110 \ln(E_t)$ t: 38.10 - 13.41 0.20	96.5 (97.7)	*b*
CA2 20 (25)	$\ln(t_R) = 54.3 - 0.759 \ln(\dot{\varepsilon}_{1\bullet\rightarrow R}) - 8.61 \ln(Ca)$ t: 2.25 - 16.21 - 1.91	93.6 (96.4)	*c*
CB2 15 (18)	$\ln(t_R) = 7.35 - 0.656 \ln(\dot{\varepsilon}_{1\bullet\rightarrow R})$ t: 27.63 - 9.21	85.7 (89.0)	*d*
CB2 15 (18)	$\ln(t_R) = 5.59 - 0.658 \ln(\dot{\varepsilon}_{1\bullet\rightarrow 3}) + 0.563 \ln(E_b)$ t: 2.13 - 9.03 0.67	85.1 (88.5)	*e*
CB2 15 (18)	$\ln(t_R) = 10.9 - 0.657 \ln(\dot{\varepsilon}_{1\bullet\rightarrow R}) - 1.06 \ln(E_t)$ t: 1.93 - 9.00 - 0.63	85.0 (88.4)	*f*
CB2 15 (18)	$\ln(t_R) = -37.7 - 0.649 \ln(\dot{\varepsilon}_{1\bullet\rightarrow R}) + 8.0 \ln(Ca)$ t: - 0.67 - 8.91 0.80	85.3 (88.3)	*g*
Units: t_R, s. $\dot{\varepsilon}_{1\bullet\rightarrow R}$, $\mu\varepsilon\ s^{-1}$. E_t, GPa. E_b, GPa. Ca, mg g^{-1}			

Table A9.033

Time-to-rupture and approximate creep rate

(4.3.7.19.) LOGARITHM OF TIME-TO-RUPTURE AND THE LOGARITHM OF ELONGATION RATE: PART 3, $\ln(t_R)$ AND $\ln(\dot{\varepsilon}_{0\rightarrow R})$

Type of specimens	Regression equations and t values, for the data shown in figure 4.054. (Data sets CA2 and CB2 [CA1 and CB1])	R^2 %	
CA2 20 (26)	$\ln(t_R) = 10.4 - 0.982 \ln(\dot{\varepsilon}_{0\rightarrow R})$ t: 89.42 - 38.53	98.7 (97.9)	*a*
CA2 12 (16)	$\ln(t_R) = 10.2 - 0.961 \ln(\dot{\varepsilon}_{0\rightarrow R}) + 0.132 \ln(E_t)$ t: 69.10 - 25.29 0.44	99.0 (97.0)	*b*
CA2 20 (26)	$\ln(t_R) = 28.3 - 0.973 \ln(\dot{\varepsilon}_{0\rightarrow R}) - 3.35 \ln(Ca)$ t: 2.75 - 39.38 - 1.74	98.9 (97.9)	*c*
CB2 15 (21)	$\ln(t_R) = 7.82 - 0.749 \ln(\dot{\varepsilon}_{0\rightarrow R})$ t: 29.89 - 10.72	89.1 (86.7)	*d*
CB2 15 (21)	$\ln(t_R) = 6.64 - 0.749 \ln(\dot{\varepsilon}_{0\rightarrow R}) + 0.375 \ln(E_b)$ t: 2.86 - 10.42 0.51	88.4 (86.0)	*e*
CB2 15 (21)	$\ln(t_R) = 11.7 - 0.750 \ln(\dot{\varepsilon}_{0\rightarrow R}) - 1.15 \ln(E_t)$ t: 2.38 - 10.57 - 0.79	88.7 (85.9)	*f*
CB2 15 (21)	$\ln(t_R) = -25.3 - 0.742 \ln(\dot{\varepsilon}_{0\rightarrow R}) + 5.96 \ln(Ca)$ t: - 0.51 - 10.28 0.67	88.6 (86.6)	*g*
Units: t_R, s. $\dot{\varepsilon}_{0\rightarrow R}$, $\mu\varepsilon\ s^{-1}$. E_t, GPa. E_b, GPa. Ca, mg g^{-1}			

Table A9.034

Time-to-rupture and the steady state creep rate

Type of specimens	Regression equations and t values, for the data shown in figure 4.055. (Data sets CA2 and CB2 [CA1 and CB1])	R^2 %	
CA2 20 (26)	$t_R = 1563 + 1056\,(1/\dot{\varepsilon}_{1*\rightarrow 3})$ t: 1.80 1.95	12.9 (18.5)	*a*
CA2 12 (15)	$t_R = 3833 + 721\,(1/\dot{\varepsilon}_{1*\rightarrow 3}) - 1815\,E_t$ t: 2.32 2.85 - 1.90	65.8 (68.0)	*b*
CA2 20 (26)	$t_R = 85094 + 1366\,(1/\dot{\varepsilon}_{1*\rightarrow 3}) - 396\,Ca$ t: 3.79 3.25 - 3.73	49.2 (49.7)	*c*
CB2 14 (17)	$t_R = 321 + 1932\,(1/\dot{\varepsilon}_{1*\rightarrow 3})$ t: 0.91 2.33	25.4 (30.7)	*d*
CB2 14 (17)	$t_R = -441 + 2034\,(1/\dot{\varepsilon}_{1*\rightarrow 3}) + 31.6\,E_b$ t: - 0.27 2.30 0.49	20.3 (27.9)	*e*
CB2 14 (17)	$t_R = 760 + 1952\,(1/\dot{\varepsilon}_{1*\rightarrow 3}) - 15.5\,E_t$ t: 0.31 2.24 - 0.18	18.8 (25.8)	*f*
CB2 14 (17)	$t_R = -18406 + 2287\,(1/\dot{\varepsilon}_{1*\rightarrow 3}) + 72.8\,Ca$ t: - 1.21 2.65 1.23	28.4 (33.5)	*g*
Units: t_R, s. $1/\dot{\varepsilon}_{1*\rightarrow 3}$, s^{-1}. E_t, GPa. E_b, GPa. Ca, mg g^{-1}.			

Table A9.035

Statistical relationship of time-to-rupture and the reciprocal of the steady state creep rate

(4.3.8.5.) THE NTDF MODEL APPROACH: PART 1 NORMALISED BY BENDING STIFFNESS

Type of specimens	Regression equations and t values, for the data shown in figure 4.057. (Data set CB2 [CB1])	R^2 %	
CB2 15 (25)	$\ln(t_R) = -2.0 - 1.40 \ln(\sigma_0/E_b)$ t: - 0.15 - 0.57	0.0 (3.5)	*a*
CB2 15 (25)	$\ln(t_R) = -11.5 - 5.49 \ln(\sigma_0/E_b) - 4.17 \ln(E_b)$ t: - 0.66 - 1.03 - 0.86	0.0 (6.5)	*b*
CB2 15 (24)	$\ln(t_R) = 0.4 - 1.38 \ln(\sigma_0/E_b) - 0.70 \ln(E_t)$ t: 0.02 - 0.54 - 0.15	0.0 (0.6)	*c*
CB2 15 (25)	$\ln(t_R) = -84 - 0.79 \ln(\sigma_0/E_b) + 15.4 \ln(Ca)$ t: - 0.51 - 0.28 - 0.50	0.0 (0.9)	*d*
Units: t_R, s. σ_0/E_b, unitless. E_t, GPa. E_b, GPa. Ca, mg g^{-1}			

Table A9.036

Time-to-rupture and the normalised stress

Type of specimens	Regression equations and t values, for the data shown in figure 4.057. (Data set CB2 with the outlying point removed)	R^2 %	
CB2 14	$\ln(t_R) = -43.6 - 8.86 \ln(\sigma_0/E_b)$ t: - 2.07 - 2.34	25.6	*a*
CB2 14	$\ln(t_R) = -43.5 - 8.75 \ln(\sigma_0/E_b) + 0.16 \ln(E_b)$ t: - 1.97 - 1.74 0.03	18.8	*b*
CB2 14	$\ln(t_R) = -43.5 - 8.85 \ln(\sigma_0/E_b) - 0.04 \ln(E_t)$ t: - 1.62 - 2.23 - 0.993	18.8	*c*
CB2 14	$\ln(t_R) = -164 - 8.27 \ln(\sigma_0/E_b) + 22.3 \ln(Ca)$ t: - 1.15 - 2.13 0.86	23.9	*d*
Units: t_R, s. σ_0/E_b, unitless. E_t, GPa. E_b, GPa. Ca, mg g^{-1}			

Table A9.037

Time-to-rupture and the normalised stress

(4.3.8.6.) THE NTDF MODEL APPROACH: PART 2 NORMALISED BY TENSILE STIFFNESS

Type of specimens	Regression equations and t values, for the data shown in figure 4.059. (Data sets CA2 and CB2 [CA1 and CB1])	R^2 %	
CA2 12 (16)	$\ln(t_R) = 16.2 + 3.30 \ln(\sigma_0/E_t)$ t: 2.16 1.38	7.6 (8.1)	*a*
CA2 12 (16)	$\ln(t_R) = -17.6 - 9.06 \ln(\sigma_0/E_t) - 12.2 \ln(E_t)$ t: - 1.44 - 2.08 - 3.10	50.4 (57.7)	*b*
CA2 12 (16)	$\ln(t_R) = -119 + 3.02 \ln(\sigma_0/E_t) + 25.1 \ln(Ca)$ t: - 0.60 1.21 0.68	2.4 (1.8)	*c*
CB2 15 (24)	$\ln(t_R) = -6.3 - 2.10 \ln(\sigma_0/E_t)$ t: - 0.29 - 0.55	0.0 (9.3)	*d*
CB2 15 (24)	$\ln(t_R) = -10.0 - 2.40 \ln(\sigma_0/E_t) + 0.63 \ln(E_b)$ t: - 0.37 - 0.58 0.26	0.0 (5.5)	*e*
CB2 15 (24)	$\ln(t_R) = -5.5 - 4.35 \ln(\sigma_0/E_t) - 4.09 \ln(E_t)$ t: - 0.25 - 0.85 - 0.69	0.0 (7.8)	*f*
CB2 15 (24)	$\ln(t_R) = -156 - 3.19 \ln(\sigma_0/E_t) + 25.8 \ln(Ca)$ t: - 0.94 - 0.79 0.91	0.0 (5.0)	*g*
Units: t_R, s. σ_0/E_b, unitless. E_t, GPa. E_b, GPa. Ca, mg g^{-1}			

Table A9.038

Time-to-rupture and the normalised stress

(4.3.8.7.) THE NTDF MODEL APPROACH: PART 3 INSTANTANEOUS STRAIN

Type of specimens	Regression equations and t values, for the data shown in figure 4.060. (Data sets CA2 and CB2 [CA1 and CB1])	R^2 %	
CA2 20 (27)	$\ln(t_R) = 1.50 - 1.49 \ln(\varepsilon_0)$ t: 0.59 - 1.97	13.2 (27.6)	*a*
CA2 12 (16)	$\ln(t_R) = -9.70 - 6.24 \ln(\varepsilon_0) - 7.29 \ln(E_t)$ t: - 1.79 - 3.24 - 4.76	66.1 (62.3)	*b*
CA2 20 (27)	$\ln(t_R) = 81.5 - 1.39 \ln(\varepsilon_0) - 14.9 \ln(Ca)$ t: 0.91 - 1.82 - 0.89	12.2 (26.3)	*c*
CB2 15 (21)	$\ln(t_R) = -15.0 - 3.70 \ln(\varepsilon_0)$ t: - 0.78 - 1.07	1.1 (25.2)	*d*
CB2 15 (21)	$\ln(t_R) = -25.2 - 4.69 \ln(\varepsilon_0) + 1.47 \ln(E_b)$ t: - 0.97 - 1.21 0.61	0.0 (21.1)	*e*
CB2 15 (21)	$\ln(t_R) = -10.1 - 5.08 \ln(\varepsilon_0) - 3.78 \ln(E_t)$ t: - 0.49 - 1.29 - 0.76	0.0 (21.1)	*f*
CB2 15 (21)	$\ln(t_R) = -172 - 4.57 \ln(\varepsilon_0) + 27.5 \ln(Ca)$ t: - 1.12 - 1.29 1.03	1.6 (21.1)	*g*
Units: t_R, s. ε_0, unitless. E_t, GPa. E_b, GPa. Ca, mg g^{-1}			

Table A9.039

Time-to-rupture and the instantaneous strain

(4.3.8.8.) THE NTDF MODEL APPROACH: PART 4 STEADY STATE INSTANTANEOUS STRAIN

Type of specimens	Regression equations and t values, for the data shown in figure 4.061. (Data sets CA2 and CB2 [CA1 and CB1])	R^2 %	
CA2 20 (26)	$\ln(t_R) = -0.54 - 2.61 \ln(\varepsilon_i^*)$ t: - 0.12 - 1.53	6.6 (14.1)	*a*
CA2 12 (15)	$\ln(t_R) = -3.22 - 4.50 \ln(\varepsilon_i^*) - 5.76 \ln(E_t)$ t: - 0.42 - 1.43 - 3.05	40.2 (55.0)	*b*
CA2 20 (26)	$\ln(t_R) = 94.6 - 2.51 \ln(\varepsilon_i^*) - 17.7 \ln(Ca)$ t: 1.03 - 1.47 - 1.04	7.0 (15.5)	*c*
CB2 15 (18)	$\ln(t_R) = 0.9 - 0.88 \ln(\varepsilon_i^*)$ t: 0.09 - 0.46	0.0 (2.0)	*d*
CB2 15 (18)	$\ln(t_R) = 0.7 - 0.87 \ln(\varepsilon_i^*) + 0.11 \ln(E_b)$ t: 0.06 - 0.44 0.05	0.0 (0.0)	*e*
CB2 15 (18)	$\ln(t_R) = 6.8 - 1.53 \ln(\varepsilon_i^*) - 2.80 \ln(E_t)$ t: 0.44 - 0.65 - 0.51	0.0 (10.4)	*f*
CB2 15 (18)	$\ln(t_R) = -93 - 0.59 \ln(\varepsilon_i^*) + 17.2 \ln(Ca)$ t: - 0.60 - 0.29 0.61	0.0 (5.8)	*g*
Units: t_R, s. ε_i^*, unitless. E_t, GPa. E_b, GPa. Ca, mg g^{-1}			

Table A9.040

Time-to-rupture and the steady state instantaneous strain

APPENDIX 10

ANALYSIS OF NOTCH SENSITIVITY TESTS ON SPECIMENS OF ANTLER WITH SHARP AND BLUNT NOTCHES

This appendix contains some analysis of the results obtained from 23 specimens of red deer antler (NA2). Two of these specimens were un-notched, 9 of them had notches terminating in a drilled hole, and the remaining twelve had notches that were sharpened with a razor blade. The analysis of the fracture behaviour of these specimens is presented here rather than in the main text because the majority of the findings are repeated in the analysis of larger and more well designed experiments (their design being based on these tests).

One aim of these tests is to establish whether there is a difference in the fracture behaviour of specimens containing notches of different tip radii. Two cases are examined: notches that have been sharpened by a razor blade and ones where the tip has been drilled. Another aim of these tests was to develop, or examine, various equations that could be used to analyse this and later data sets. The experimental procedure is explained in the main text (section 7.3.1).

A10.1. RESULTS

A10.1.1. RESULTS: FAILURE STRESS OF THE UN-NOTCHED SPECIMENS

The two un-notched antler specimens failed at stresses of 83.7 and 81.3 MPa, and had knee stresses of about 50 MPa. The 23 notched specimens failed at a mean stress of 53.1 MPa (s.d. 13.6) the range of these values being 31.7 to 77.7 MPa. Thus it can be assumed that in the notched specimens the stress in the bulk of the material, away from the notch, will be approximately equal to the knee stress of that specimen. As antler exhibits an increasing stress in the post-knee region, this result implies that there is only a limited amount of post-knee behaviour. Therefore, the assumption of linear elasticity, although inaccurate, was be used as a first approximation.

A10.1.2. RESULTS: FAILURE STRESS AND NOTCH LENGTH

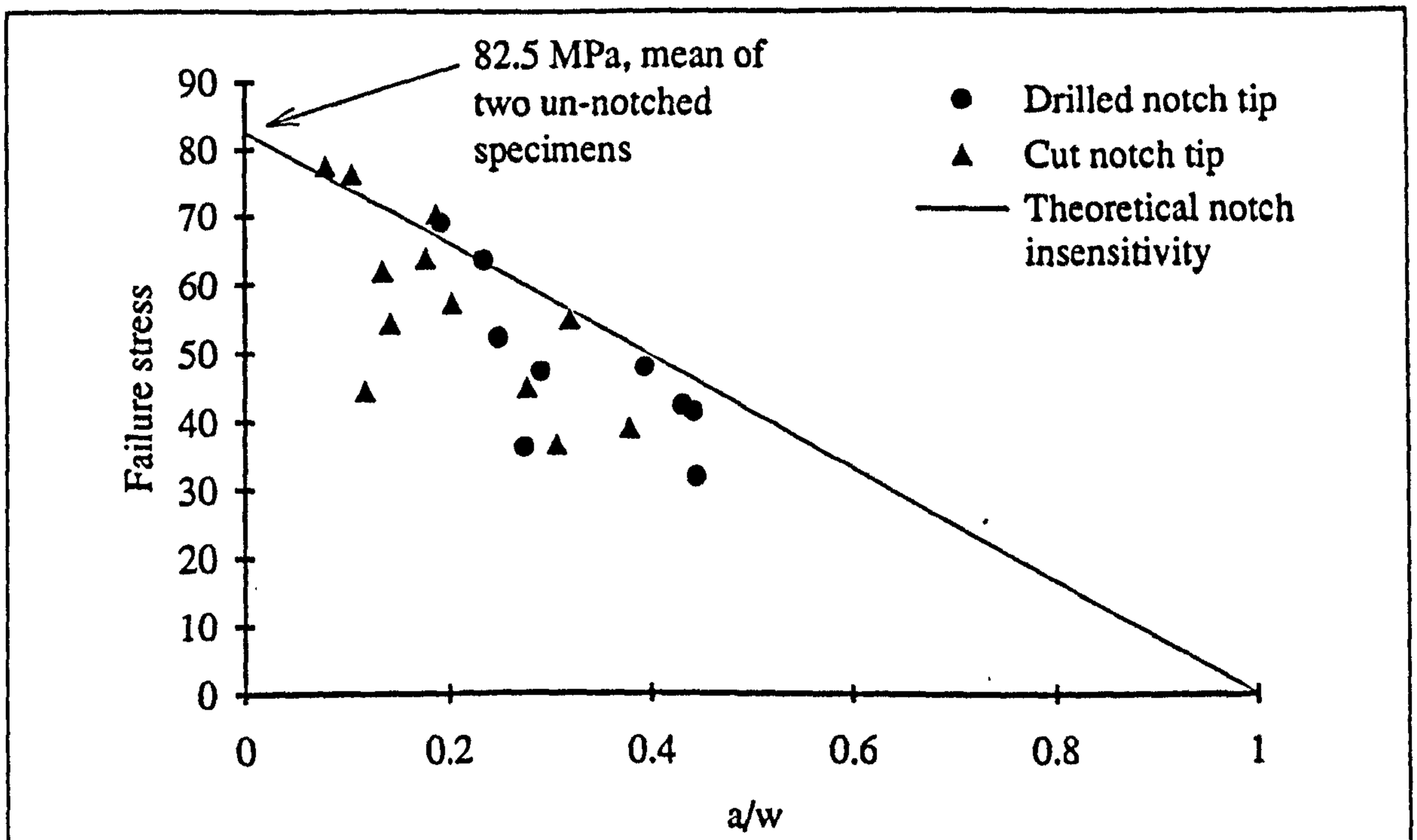

Units:

σ_f Failure stress, MPa.

a/w Ratio of notch length to specimen width, unitless.

Figure A10.001

The relationship of failure stress to a/w for SEN specimens of red deer antler, and the theoretical line for a notch insensitive material (Data set NA2)

One qualitative demonstration of notch sensitivity, or notch insensitivity, is to plot the failure stress against the ratio of notch length to specimen width (σ_f and a/w) as shown in figure 7.006.[1] If the material is completely notch insensitive, the data points will fall in a straight line drawn between the failure stress of un-notched specimens and the value of 1 on the a/w axis. This is because in a notch insensitive material the stress in the reduced section is, by definition, due only to the applied load and the cross sectional area of material, (Hull, 1981; also implied by Atkins and Mai, 1988) For a notch sensitive material the data points will fall below this line, forming a curve with the same end points, the more notch sensitive the material the more the curve will diverge from the linear line. It appears from figure A10.001 that for the data obtained in these tests (NA2) that there is a reasonable case for questioning the notch sensitivity of antler. This method can be made more rigorous by using regression analysis. The two models investigated

[1]Another similar method, outlined by Hull (1981), is to plot the ligament stress (load/cross-sectional area of the reduced section) against the notch length. The notch insensivie material will, ideally, produce a horizontal plot. The ligament stress for such a material being a constant.

are that of the notch insensitive material and the classically notch sensitive linear elastic material. This technique enables the ability to explain the data obtained, by use of theoretical classical notch sensitive and notch insensitive equations, to be assessed. Such an assessment is the aim of the next part of this section.

As mentioned above for a notch insensitive material σ_f is directly related to a/w. In the case where w is constant this relationship can be expressed as one between σ_f and a only. For a classically notch sensitive material the failure stress is directly related to $a^{-0.5}$. Therefore it is these two relationships that I will examine first.

Type of antler specimens	Regression equations and t values, for the failure stress and three geometric quantities of SEN specimens of red deer antler	R^2 %	
12 cut 9 drilled	σ_f = 76.1 - 23.1 a t: 15.12 - 4.99	54.4	*a*
12 cut	σ_f = 77.3 - 25.8 a t: 10.91 - 3.17	45.1	*b*
9 drilled	σ_f = 78.2 - 23.7 a t: 7.44 - 2.99	49.8	*c*
12 cut 9 drilled	σ_f = 75.9 - 89.1 (a/w) t: 15.14 - 4.97	54.2	*d*
12 cut	σ_f = 77.4 - 101 (a/w) t: 10.91 - 3.17	45.1	*e*
9 drilled	σ_f = 78.0 - 91.6 (a/w) t: 7.46 - 2.99	49.8	*f*
12 cut 9 drilled	σ_f = 14.7 + 1.11 $a^{-0.5}$ t: 1.77 4.79	52.3	*g*
12 cut	σ_f = 17.3 + 1.03 $a^{-0.5}$ t: 1.34 3.15	44.8	*h*
9 drilled	σ_f = - 13.8 + 2.13 $a^{-0.5}$ t: - 0.78 3.53	58.8	*i*
Units: σ_f, MPa. w, mm. a, mm. $a^{-0.5}$, $m^{-0.5}$.			

Table A10.001

The relationship of failure stress to various geometrical quantities, equations based on notch-insensitivity and LEFM

Table A10.001 gives some of the results from the regression analysis, on both the full set of notched specimens and just on those sharpened with a razor blade. This shows very little change in the R^2 value when the σ_f was regressed against a or $a^{-0.5}$, the values falling respectively from 54.4% (*a*) to 52.3% (*g*) for the full set of data, and 45.1% (*b*) to 44.8% (*h*) for the cut notches. This method has made no reliable distinction as to which of these relationships explains the failure stress of these specimens most accurately. It is noticeable that the significance of each of the various length terms is similar. There is some variation but this is not consistent between the three groups of specimens tested.

Changing the explanatory variable from a in equations *a*, *b* and *c* (of table A10.003) to a/w in equations *d*, *e* and *f*, does not improve the regressions. However, the normalisation of the notch length in this way is useful in visualising the meaning of these equations. This is because it highlights an obvious limitation of these linear relationships; as a/w approaches unity the predicted failure stress becomes negative. Ideally the constant and the coefficient should have the same value.

It was found in the analysis of data set NA1 that the material stiffness of the specimens, was an important predictor of the failure stress. Thus the regression equations represented in the table A10.001 have been repeated using the material stiffness measured in three-point-bending as another explanatory variable. These modified equations are given in table A10.002 below. All the relationships in table A10.002 have a higher R^2 than the equivalent relationship where the material stiffness is not taken into account (table A10.001). However, these equations still do not answer the question of which geometrical factor more fully explains the variation in failure stress, and thus indicating the notch sensitivity or otherwise of the material. For each geometrical variable that is considered for the whole set of data about one quarter of the variability in failure stress still remains unexplained. However, when only the drilled specimens are considered at least 95% of the variability is explained in each case. The reason for this difference is unknown.

Type of antler specimens	Regression equations and t values, for the failure stress and various geometrical quantities and the material stiffness, of SEN specimens of red deer antler.	R^2 %	
12 cut 9 drilled	σ_f = 48.8 - 23.6 a + 3.34 E_b t: 6.25 - 6.82 3.99	74.4	*a*
12 cut	σ_f = 55.4 - 28.2 a + 2.90 E_b t: 4.60 - 3.98 2.11	59.2	*b*
9 drilled	σ_f = 33.5 - 18.8 a + 4.52 E_b t: 5.21 - 7.33 8.09	95.1	*c*
12 cut 9 drilled	σ_f = 48.6 - 91.2 (a/w) + 3.33 E_b t: 6.19 - 6.76 3.95	74.1	*d*
12 cut	σ_f = 55.5 - 111 (a/w) + 2.90 E_b t: 4.61 - 3.97 2.11	59.2	*e*
9 drilled	σ_f = 33.3 - 72.4 (a/w) + 4.52 E_b t: 5.15 - 7.26 8.02	95.0	*f*
12 cut 9 drilled	σ_f = - 18.1 + 1.18 $a^{-0.5}$ + 3.64 E_b t: - 1.94 7.19 4.51	76.3	*g*
12 cut	σ_f = - 12.6 + 1.15 $a^{-0.5}$ + 3.06 E_b t: - 0.74 4.12 2.27	61.0	*h*
9 drilled	σ_f = - 33.9 + 1.61 $a^{-0.5}$ + 4.14 E_b t: - 4.86 7.02 6.95	94.7	*i*
Units: σ_f, MPa. E_b, GPa. w, mm. a, mm. $a^{-0.5}$, $m^{-0.5}$.			

Table A10.002

Regression equations relating failure stress and notch length, with and without taking material stiffness into account

In this section the fit of experimental data to some theoretical relationships between the failure stress and the notch length of SEN specimens of antler have been examined. This analysis has not determined if the function of the notch length that best explains the variation in the failure stress is, a, a/w or $a^{-0.5}$. Therefore, the material can not easily be classified as notch insensitive or classically notch sensitive (by the definitions used here). The material appears to fall in the region between these extremes of behaviour, the failure stress being related to some other power function or multiple (for example) of notch length. If this is the case the material would be notch sensitive, but to a lesser degree than the classically notch sensitive materials, such as glass. The

derivation of such a power, if it exists, could be achieved by examination of the data in logarithmic form. This has not been done here as these equations are examined in a later section where another form of analysis is examined (section 7.3.2.5 on Purslow's approach).

This section has highlighted the large influence that the material stiffness has on the failure stress in the presence of a notch. The influence of the material stiffness on the failure stress of antler is a recurrent theme in this research.

A10.1.3. RESULTS: CRITICAL STRESS INTENSITY FACTORS, $K^{\bullet}_{IQ}$

In the initial tests it appeared that the use of the pin-jointed shape correction factor increased the relationship between the measured stress intensity factor and the geometry of the specimen. Therefore, I will now investigate the effect of using the un-flexing shape correction factor, as defined above (section 7.2.5.1).

The mean values of the various stress intensity factors, investigated here, are given in table A10.003. The uncorrected value is the smallest, and that with the pin-jointed correction factor is the greatest. Clearly, if any reliance is to be placed on the experimentally determined values of the SIF being the true critical stress intensity value, the appropriate shape correction factor needs to be found, or the value of the stress intensity factor should be treated with extreme scepticism.

Type of antler specimens	K^{I}_{IQ} mean (s.d.)	K^{U}_{IQ} mean (s.d.)	K^{P}_{IQ} mean (s.d.)	
12 cut 9 drilled	2.77 (0.48)	3.48 (0.67)	4.49 (1.4)	*a*
12 cut	2.66 (0.49)	3.24 (0.65)	3.82 (1.11)	*b*
9 drilled	2.92 (0.45)	3.79 (0.59)	5.38 (1.38)	*c*

Units:

K^{I}_{IQ} *Infinite-sheet* critical stress intensity factor, MPa $m^{0.5}$.

K^{U}_{IQ} *Un-flexing* critical stress intensity factor, MPa $m^{0.5}$.

K^{P}_{IQ} *Pin-jointed* critical stress intensity factor, MPa $m^{0.5}$.

Table A10.003

Values of the various stress intensity factors as used in LEFM, applied to notched specimens of red deer antler (Data set NA2)

The relationships of the critical stress intensity factors and the material stiffness (measured in three-point-bending) are shown in table A10.004 *a-f.* Clearly, as the equation for the stress intensity factor changes from K^{I}_{IQ} to K^{U}_{IQ} then to K^{P}_{IQ} (*infinite sheet* to *un-flexing* then to *pin-jointed*) its correlation with the bending stiffness decreases. This is the same trend as that which was displayed in the initial tests (data set NA1), but in the this data set (NA2) any effect due to different radii can be avoided by comparison of the twelve results from the razor blade sharpened notches alone. When this is done the same trend is seen.

Type of antler specimens	Regression equations and t values, of the relationship between various stress intensity factors and the material stiffness measured in three-point-bending	R^2 %	
12 cut 9 drilled	$K^{I}_{IQ} = 1.21 + 0.187\ E_b$ t: 3.43 4.49	48.9	*a*
12 cut	$K^{I}_{IQ} = 1.42 + 0.150\ E_b$ t: 2.72 2.42	30.5	*b*
9 drilled	$K^{I}_{IQ} = 0.898 + 0.238\ E_b$ t: 2.89 6.64	84.3	*c*
12 cut 9 drilled	$K^{U}_{IQ} = 1.54 + 0.233\ E_b$ t: 2.79 3.61	37.6	*d*
12 cut	$K^{U}_{IQ} = 1.66 + 0.192\ E_b$ t: 2.30 2.25	27.0	*e*
9 drilled	$K^{U}_{IQ} = 1.45 + 0.276\ E_b$ t: 2.36 3.90	63.9	*f*
12 cut 9 drilled	$K^{P}_{IQ} = 2.08 + 0.290\ E_b$ t: 1.46 1.74	9.2	*g*
12 cut	$K^{P}_{IQ} = 1.72 + 0.255\ E_b$ t: 1.27 1.60	12.3	*h*
9 drilled	$K^{P}_{IQ} = 3.09 + 0.271\ E_b$ t: 1.28 0.97	0.0	*i*
Units: K^{I}_{IQ}, MPa $m^{0.5}$.	K^{U}_{IQ}, MPa $m^{0.5}$.	K^{P}_{IQ}, MPa $m^{0.5}$.	E_b, GPa.

Table A10.004

The relationship of three forms of stress intensity factor and the material stiffness of red deer antler (Data set NA2)

The relationships of the critical stress intensity factors, $K^{\bullet}_{IQ}$, to the ratio of notch length to specimen width, a/w, are shown in table A10.005. These regression equations show the same trend as in the initial tests (set NA1), the R^2 value for the cut notches increasing from 1.5% to 20.6% and then 64.4% in its relationship with a/w. The R^2 value for the relationship of these two variables, E_b and a/w, is 0.0%. This result reinforces the finding above that a relationship between the critical stress intensity factor and the specimen geometry is produced, not removed, by the inclusion of not only the pin-jointed shape correction factor, but also by the un-flexing sheet correction factor: the less restrained the specimen is assumed to be the greater the correlation between $K^{\bullet}_{IQ}$ and the geometrical quantity a/w. This implies, if this approach is valid, that the shape correction factor may not be within the region bounded by the two forms of correction factor considered here. The uncorrected form of the critical stress intensity factor appears to be more independent of the specimen geometry than, those that contain a correction. This may be taken as evidence that the equations considered here, are not applicable to this specimen geometry or this material.

As would be expected (from the expressions that describe the shape correction factors, and the plot of these relationships) if there is initially only a limited correlation of the experimentally determined stress intensity factor with a/w, introducing these correction factors induces such a correlation. This finding again confirms one of the tentative conclusions based on the first set of data (NA1).

Type of antler specimens	Regression Equations and t values, of the relationships of three forms of the critical stress intensity factor and the geometrical quantity a/w	R^2 %	
12 cut 9 drilled	K^I_{IQ} = 2.51 + 1.02 (a/w) t: 9.70 1.10	1.0	*a*
12 cut	K^I_{IQ} = 2.33 + 1.62 (a/w) t: 6.98 1.08	1.5	*b*
9 drilled	K^I_{IQ} = 3.20 - 0.85 (a/w) t: 5.57 - 0.51	0.0	*c*
12 cut 9 drilled	K^U_{IQ} = 2.68 + 3.10 (a/w) t: 8.46 2.73	24.5	*d*
12 cut	K^U_{IQ} = 2.52 + 3.55 (a/w) t: 6.27 1.96	20.6	*e*
9 drilled	K^U_{IQ} = 3.40 + 1.21 (a/w) t: 4.56 0.55	0.0	*f*
12 cut 9 drilled	K^P_{IQ} = 1.71 + 10.9 (a/w) t: 4.27 7.56	73.7	*g*
12 cut	K^P_{IQ} = 1.91 + 9.47 (a/w) t: 4.15 4.57	64.4	*h*
9 drilled	K^P_{IQ} = 1.75 + 11.1 (a/w) t: 1.63 3.51	58.6	*i*
Units: K^I_{IQ}, MPa $m^{0.5}$.	K^U_{IQ}, MPa $m^{0.5}$.	K^P_{IQ}, MPa $m^{0.5}$.	a/w, unitless

Table A10.005

Regression equations showing the relationships between various calculated values of the stress intensity factor and the ratio of notch length to specimen width

A10.1.4. RESULTS: PURSLOW'S APPROACH

Type of antler specimens	Regression equations and t values obtained by application of Purslow's original equation (*a to c*) and a modified form that considers material stiffness (*d to f*)	R^2 %	
12 cut 9 drilled	$\ln(\sigma_f) = 3.38 - 0.381 \ln(a/w)$ t: 27.20 - 4.76	52.0	*a*
12 cut	$\ln(\sigma_f) = 3.41 - 0.356 \ln(a/w)$ t: 16.76 - 3.11	44.0	*b*
9 drilled	$\ln(\sigma_f) = 3.15 - 0.601 \ln(a/w)$ t: 13.45 - 3.07	51.3	*c*
12 cut 9 drilled	$\ln(\sigma_f) = 2.24 - 0.412 \ln(a/w) + 0.524 \ln(E_b)$ t: 8.98 - 7.57 4.87	78.1	*d*
12 cut	$\ln(\sigma_f) = 2.43 - 0.406 \ln(a/w) + 0.427 \ln(E_b)$ t: 5.87 - 4.31 2.54	63.8	*e*
9 drilled	$\ln(\sigma_f) = 1.85 - 0.494 \ln(a/w) + 0.669 \ln(E_b)$ t: 8.24 - 6.28 6.28	92.5	*f*
Units: σ_f, MPa. E_b, GPa. w, mm. a, mm			

Table A10.006

Regression equations from the Purslow theory applied to Antler (Set NA2)

The regression equations based on Purslow's approach have a lower predictive power than those based on the idea that the material is notch insensitive. As in the previous cases, the addition of the material stiffness as a predictor vastly improves the predictive power of the regression equations.

A13.1.5. Results: the effect of drill or sharpened notch tips and tip radii

One-way analysis of variance was performed on the residuals of all the above regression equations (and some additional ones) that were derived for the 21 notch specimens. The two groups used were: the specimens where the notch tip was cut and those were it was drilled. Examination of the *p* values, or significance level of the difference between these groups, showed that in only three cases was the value below 0.5. These where considerably lower than 0.5, all being less than 0.2. The equations in which the residuals were significantly different all came from table A10.004, relating the critical

stress intensity factor to the material stiffness. Thus it appears that the notch tip may affect the SIF. However, the effect of the form of the notch tip may be slightly different from how it appears. The reason for its apparent effect could be due to a significant difference in the notch lengths of the two groups ($p = 0.010$). As a result of the correlation between the notch length and the form of the notch tip, those regressions that contain the notch length as an explanatory variable also take into account (to some degree) the form of the notch tip. This has the effect of reducing the dependence of the residuals on the type of notch. This observation clouds the findings slightly. However, the regression equations of the data from the specimens possessing notches with a drilled end of different radii shown in tables A10.007 and A10.008) are not, generally, those expected by applying the Inglis equation (5.001) or LEFM. The Inglis equation predicts that, if everything else stays constant, the failure stress will decrease when the notch tip radius decreases. The theory of LEFM suggests that an increase in notch tip radius will result in an increase in the calculated stress intensity factor. Therefore, the slight effect that does exist is contrary to that which is predicted. Thus I consider that this effect is an artefact, and the form of the notch tip does not effect the fracture behaviour.

Type of antler specimens	Regression equations and t values	R^2 %	
9 drilled	$\sigma_f = 97.1 - 14.6\ a - 1825\ \rho^{0.5}$ t: 9.66 - 2.23 - 2.81	74.7 (49.8)	*a*
9 drilled	$\sigma_f = 97.0 - 56.1\ (a/w) - 1826\ \rho^{0.5}$ t: 9.65 - 2.23 - 2.81	74.7 (49.8)	*b*
9 drilled	$\sigma_f = 36.9 + 1.33\ a^{-0.5} - 1639\ \rho^{0.5}$ t: 1.48 2.33 - 2.43	75.7 (58.8)	*c*
9 drilled	$\sigma_f = 47.8 - 16.4\ a + 3.75\ E_b - 642\ \rho^{0.5}$ t: 6.09 - 7.46 6.97 - 2.33	97.2 (95.1)	*d*
9 drilled	$\sigma_f = 47.7 - 63.1\ (a/w) + 3.75\ E_b - 644\ \rho^{0.5}$ t: 6.00 - 7.34 6.87 2.30	97.1 (95.0)	*e*
9 drilled	$\sigma_f = -14.2 + 1.42\ a^{-0.5} + 3.55\ E_b - 544\ \rho^{0.5}$ t: - 1.00 5.92 5.38 - 1.56	95.7 (94.7)	*f*
Units: σ_f, MPa. $\rho^{0.5}$, $m^{0.5}$. w, mm. a, mm. $a^{-0.5}$, $m^{-0.5}$.			
Comments: The R^2 % in parentheses is that obtained without the tip radius variable			

Table A10.007

Regression equations relating failure stress and notch length, with and without taking material stiffness into account

Type of antler specimens	Regression equations and t values	R^2 %	
9 drilled	$K_{IQ}^{I} = 1.35 + 0.216\,E_b - 15.9\,\rho^{0.5}$ t: 1.91 4.48 - 0.72	83.2 (84.3)	*a*
9 drilled	$K_{IQ}^{U} = 1.00 + 0.298\,E_b + 15.6\,\rho^{0.5}$ t: 0.69 3.03 0.35	58.7 (63.9)	*b*
9 drilled	$K_{IQ}^{P} = -1.73 + 0.505\,E_b + 168\,\rho^{0.5}$ t: - 0.33 1.40 1.02	0.0 (0.0)	*c*
9 drilled	$K_{IQ}^{I} = 4.14 + 0.91\,(a/w) - 90.6\,\rho^{0.5}$ t: 6.73 0.59 - 2.28	31.0 (0.0)	*d*
9 drilled	$K_{IQ}^{U} = 4.60 + 3.46\,(a/w) - 116\,\rho^{0.5}$ t: 5.71 1.71 - 2.22	29.9 (0.0)	*e*
9 drilled	$K_{IQ}^{P} = 3.46 + 14.3\,(a/w) - 164\,\rho^{0.5}$ t: 2.91 4.80 - 2.13	72.5 (58.6)	*f*
9 drilled	$\ln(\sigma_f) = 1.56 - 0.376\,\ln(a/w) - 0.224\,\ln(\rho)$ t: 1.81 - 1.83 1.89	64.4 (51.3)	*g*
9 drilled	$\ln(\sigma_f) = 1.62 - 0.455\,\ln(a/w) + 0.618\,\ln(E_b) - 0.0468\,\ln(\rho)$ t: 3.92 - 4.54 4.57 - 0.68	91.8 (92.5)	*h*

Units: K_{IQ}^{*}, MPa $m^{0.5}$. $\rho^{0.5}$, $m^{0.5}$. σ_f, MPa. ρ, mm. E_b, GPa.
w, mm. a, mm.

Comments: The R^2 % in parentheses is that obtained without the tip radius variable

Table A10.008

Regression equations from the Purslow theory applied to Antler (Set NA2)

APPENDIX 11

PRESENTATION GIVEN AT EIGHTH MEETING OF THE EUROPEAN SOCIETY OF BIOMECHANICS

Some of the images described in chapter 8 were presented at the eighth meeting of the European Society of Biomechanics, in Rome, 21-24 June 1992. This appendix contains copies of the meeting abstract, the figures presented at the meeting as slides, and a description of the video used in the presentation. This video is also presented in this thesis, bound separately.[1]

---

[1]I would like to thank John Aldworth, of the University of York's audio-visual unit, for his technical assistance in the editing of this video.

Optical changes as an indicator of mechanical damage in bone and antler

A.J. Sedman, J.D. Currey and P. Zioupos

Department of Biology, University of York, York, England

To aid understanding and communication standard words are used to describe bone, such as; elastic, brittle, plastic, anelastic, visco-elastic. The definition of these words being previously established and defined in the fields of engineering or material science.

It is now accepted that bone is not elastic, or even elastic-plastic, but exhibits time-dependence. The stiffness of bone increases at higher strain, or loading, rates and it exhibits "creep", thus the term visco-elastic is often used. This description implies a reversible process, with no permanent change in the mechanical properties. But if bone is loaded past its 'yield' point, then unloaded, upon reloading a reduced stiffness will be recorded, (Burstein et al., 1973). Thus a visco-elastic characterisation of the mechanical properties is also inaccurate.

The authors, and other workers, are approaching this problem from different directions, and converging on another explanation of the mechanical properties of bone. This is "damage", an idea originally developed to explain creep of metals at high temperatures. It can be viewed as the density of cracks or cavities within the structure. In the basic theory, the damage state can be expressed in terms of "effective area reduction". This can be represented by a variable that changes from D=0 when the material is undamaged to D=1 after fracture. The structure will fail when the damage has reached a level such that the remaining material is unable to sustain the loads upon it. If the structural stiffness of the specimen is calculated in the normal way, the variable can be expressed as a function of the reduction in stiffness. This idea is consistent with cyclic test results.

One method used to apply these ideas to bone is creep and/or fatigue tests. Fondrk et al. (1988) note that creep strain is produced at a constant rate, thus indicating damage takes time to accumulate. Caler and Carter (1989) used damage to explain creep and fatigue results and produced a "cumulative damage model". This approach was used for bone and antler, (antler being bone with a lower mineral content), by Mauch et al. (1992). Another method is to examine the bone for flaws that could explain the reduced stiffness. This has been done using stain (Currey and Brear, 1973). They noted that wet tensile specimens become opaque, having previously been translucent, when yielding occurred. This supports the idea that damage takes the form of tiny cracks within the material. For an increased number of such interfaces will result in a greater scattering of light.

We have conducted experiments to combine these approaches. The results support the damage theory. Changes in the optical properties of both bovine femur and red deer antler were recorded during tensile and basic fracture mechanics tests, by a 35 mm camera and high speed video, 1000 frames s^{-1}. The tests were performed at 37C, within a water bath. Single edge notch specimens were used for the fracture mechanics tests. In tensile tests the occurrence, extent and intensity of whitening being strongly related to the yielding of the material. Specimens that fail at a lower value of ultimate strain exhibit a less uniform change in translucency. When the specimen fails or the stress is removed, the appearance of the bone returns towards its initial state. This process is not instantaneous; and is consistent with the time needed to recover "non-elastic" strain obtained in a loading-unloading test. This effect is clearly seen in notched specimens; the damaged volume is initially concentrated at the tip of the notch, then around the crack front. In some cases the material through which the crack has passed, and has thus been relieved of stress, exhibits a reduction in whitening. We assume this to be the collapsing of the internal flaws. This results in a bright spot moving across the specimen. In other specimens the damage appears across the whole section before any crack is observed. In antler the time between crack initiation and failure is a few seconds, but bone failed within 0.001 seconds. In antler the crack direction was more varied and the surface less regular. The effects are demonstrated on a short video film.

The aim of this work is to develop the ideas of damage, as applied to bone and antler. The optical changes were used as an indication of the damage state. The optical results obtained during the single edge notch tests help to explain the scatter in the results, as they show that damage is occurring in a larger volume than the crack tip, so more energy is being used than that required to produce the two new surfaces.

References

Burstein, A. H., Reilly, D. T., and Frankel, V. H. (1973) Failure Characteristics of Bone and Bone Tissue. Perspectives in Biomedical Engineering (Edited by Kenedi, R. M.), pp. 131-134. MacMillan, London.

Caler, W. E. and Carter, D. R. (1989) Bone Creep-Fatigue Damage Accumulation, *J. Biomechanics* 22, 625-635.

Currey, J. D. and Brear, K. (1974) Tensile Yield in Bone, *Calc. Tiss. Res.* 15, 173-179.

Fondrk, M., Bahniuk, E., Davy, D. T. and Michaels, C. (1988) Some Viscoplastic Characteristics of Bovine and Human Cortical Bone, *J. Biomechanics* 21, 623-630.

Mauch, M., Currey, J. C. and Sedman, A. J. (1992) Creep Fracture in Bones with Different Stiffnesses, *J. Biomechanics* 25, 11-16

A11.2. DESCRIPTION OF THE VIDEO AND AN OUTLINE OF THE ACCOMPANYING TALK

This description of the video is based on the notes for the accompanying talk presented in Rome.[2] Reference to the slides as they were used in the talk is also included. The timing of these slides relative to the video is indicated their position in the text. Arrows and other comments have been added to the slides. These are to help identify features that were indicated by use of a pointer during the presentation. Within this appendix the important aspects of the video recording will be demonstrated by using annotated prints of a few video images. (The quality of some of these images is poor as they were obtained from the edited VHS copy of the tests rather than the master copy.)

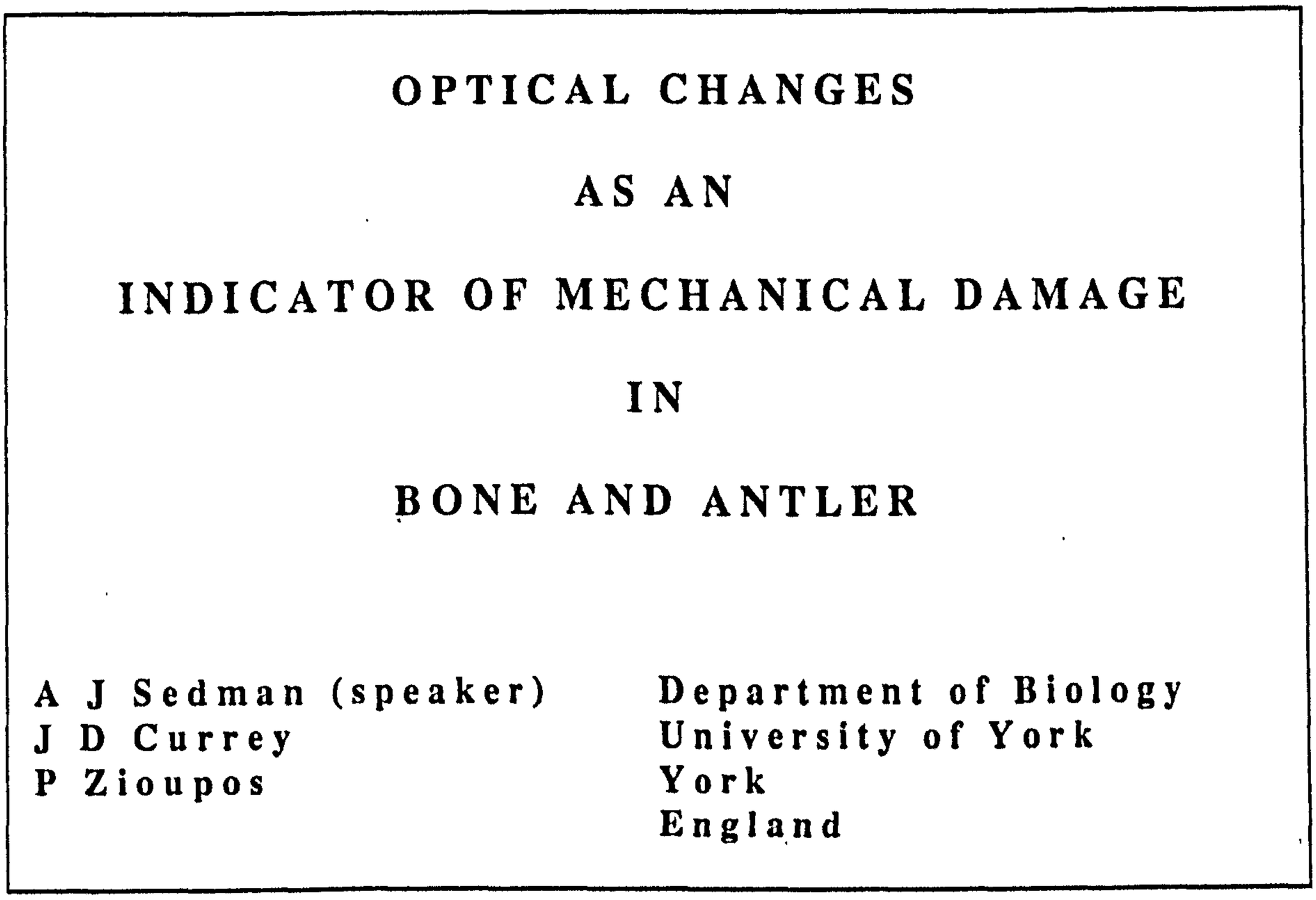

Figure A11.001

Slide 0: introductory slide

I began my talk by stating that the optical effects I was going to described in the talk and demonstrate using a video recording are only one part of a larger project investigating the yield and fracture behaviour of bone. This work is in the form of a comparative study, using bovine femoral bone and red deer antler. Antlers are essentially bones of lower than normal mineral content. These two materials have evolved to fulfil different biological functions, and hence have different mechanical properties.

---

[2]I gave this talk before deciding to adopt the nomenclature of knee stress and knee strain. Thus the term yield was used in a way that I now consider to be wrong.

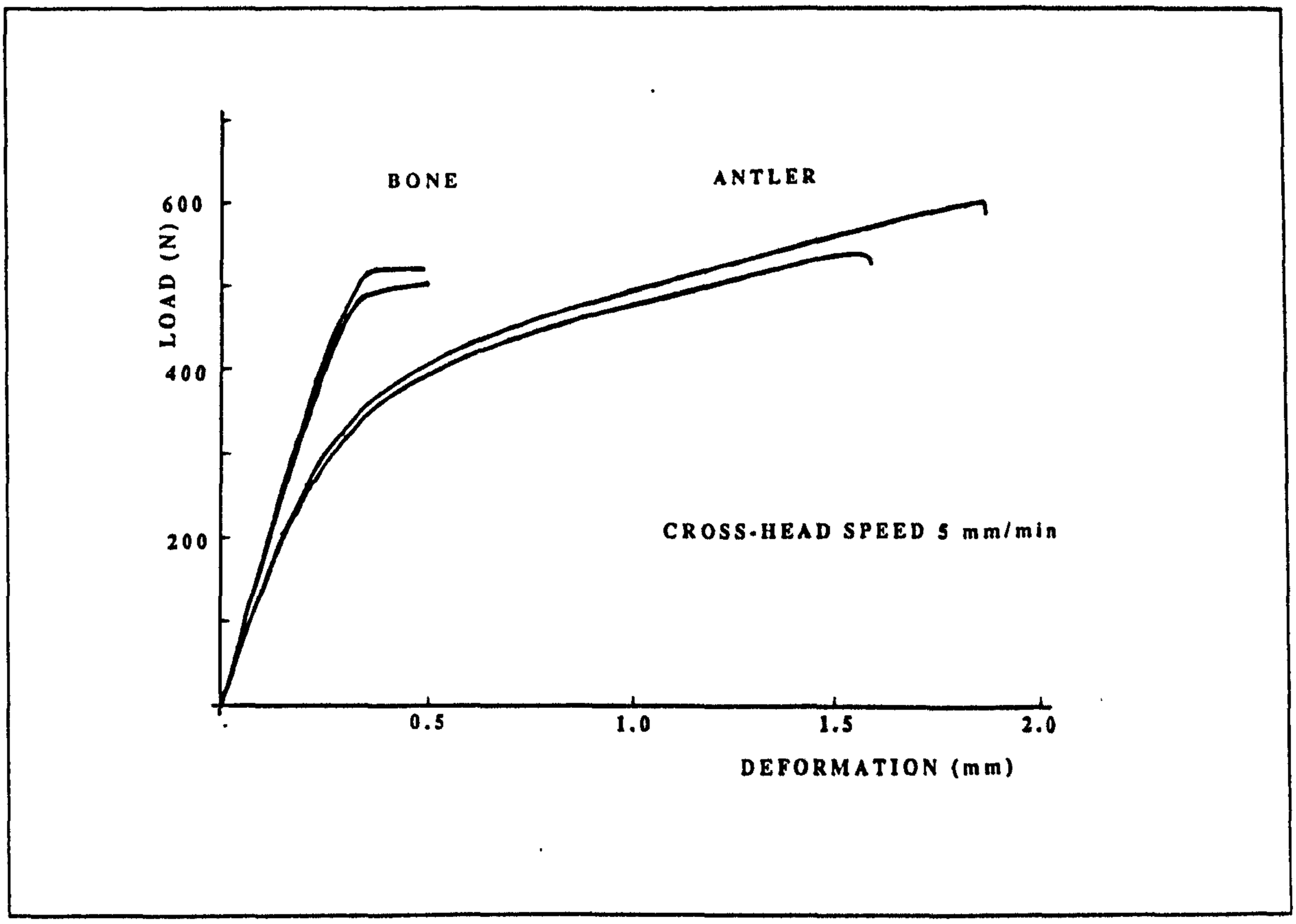

Figure A11.002

Slide 1: load-extension curves of bovine femoral bone and red deer antler

The response of both materials to mechanical loading was shown using in slide 1 (figure A11.002). I pointed out this is not an idealised graph, but like all the other slides used in the presentation it displays the loading curves obtained from the tests shown in the video presentation.[3] I used the term *yield* to identify the region of the loading curve where the slope decreases. This region is well defined in bone, but less so in antler.

I stated that a number of theories have been used to explain the mechanical response of bone to tensile loading. These include descriptions of the material as *elastic and brittle* or *elastic-plastic* depending on the amount of *post-yield strain.* These classifications fail to take into account the observed time dependant properties, so the theory of *visco-elasticity* has been adopted by some workers, but this theory has little to say about the yield and post-yield region.

A more recent approach to the mechanical response of bone, is based on the theory of *continuum damage mechanics* developed by Kachanov (1958) for steel at high

---

[3]The plots were obtained by tracing the chart output. The unloading part of the plot was traced from the other side of the paper to obtain a load deformation plot in place of a load time plot. The values of deformation are for the whole system not just for the gauge length of the specimen.

temperatures, but now widely used in the analysis of composites. Damage can be viewed as a reduction in the effective cross-sectional area of the material due to the accumulation of flaws, thus if damage is accumulated the effective stress and hence the strain will increase. This is equivalent to an increase in material compliance. This increase in compliance has been observed in bone (slide 2) and antler (slide 3).

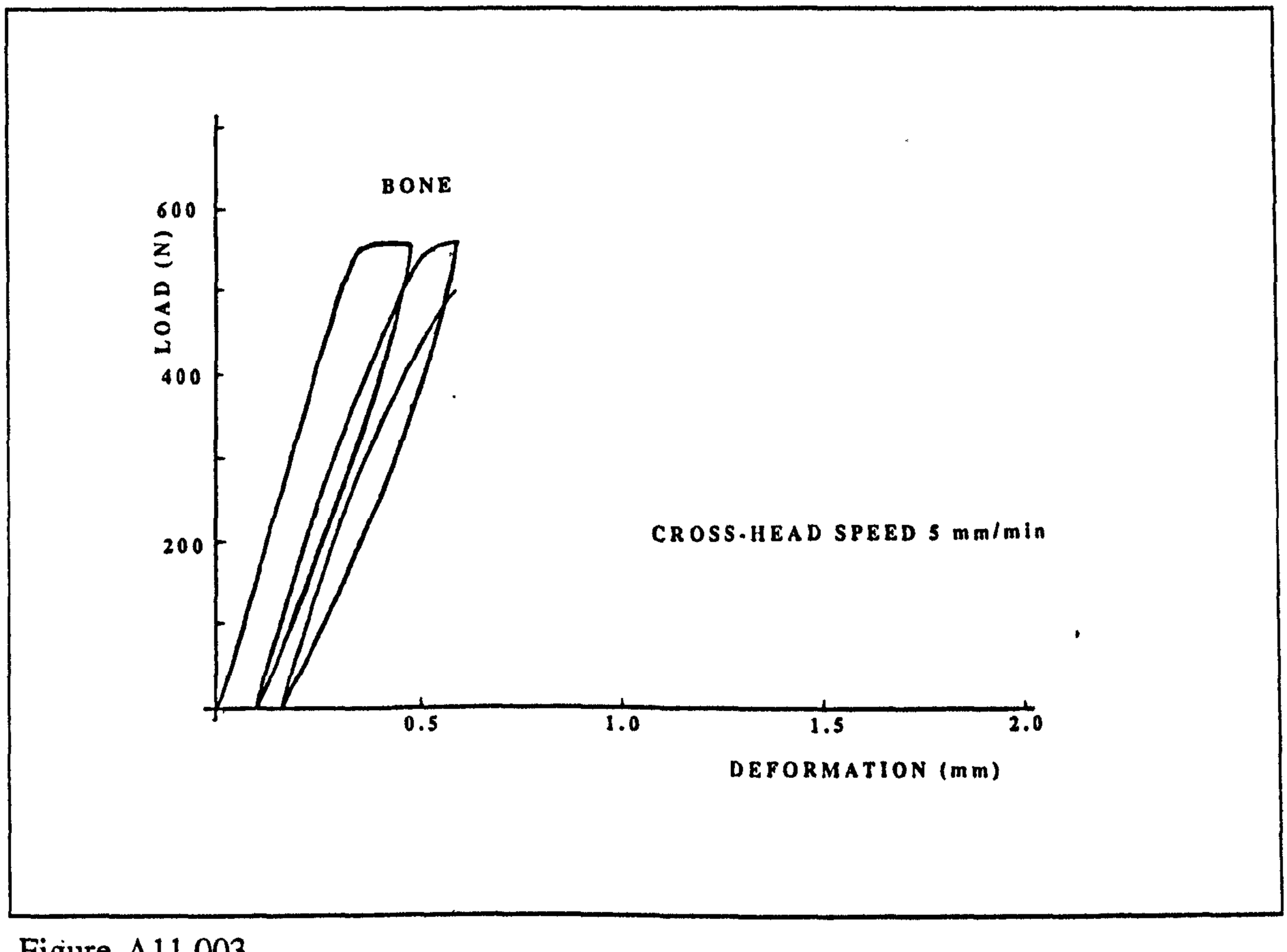

Figure A11.003

Slide 2: the reduction in stiffness of bovine bone subjected to loading-unloading tests

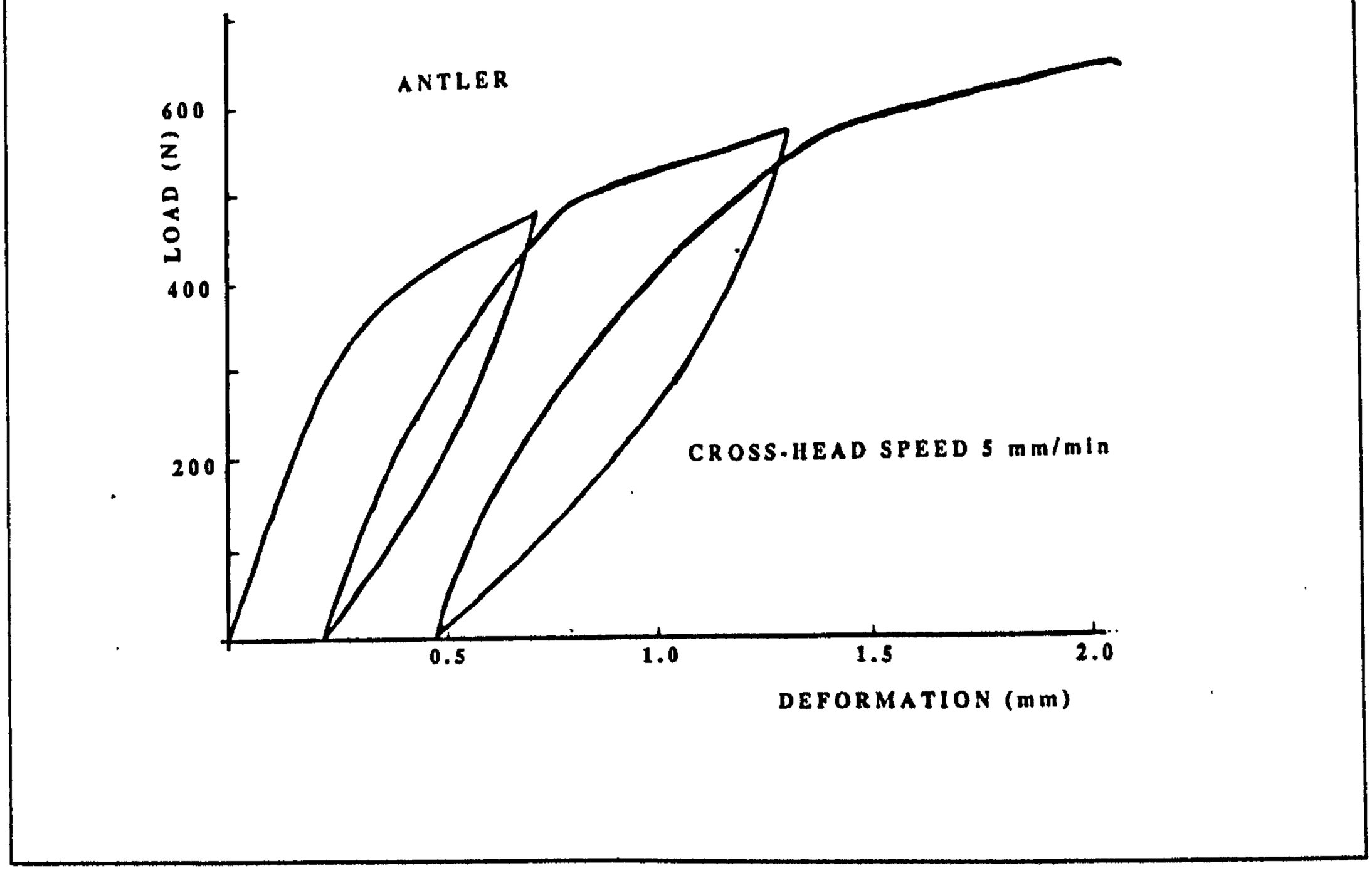

Figure A11.004

Slide 3: the reduction in stiffness of antler subjected to loading-unloading tests

The increase in compliance is not very clear in the case of bovine bone (slide 2, above), but is more noticeable in the case of antler. (This is due to the higher stiffness of bone combined with the use of only one experimental arrangement, to give more easily comparable images.)

The rate at which damage accumulates is proportional to the normalised stress raised to a power of more than 10. Thus a long time at a low stress can cause a similar amount of damage as a short time at a high stress. This theory can model the change in stiffness with strain rate and the variation in the value of yield stress, failure stress and post yield strain.

The damage in bone and antler takes the form of small cracks, the greater the damage the higher the crack density. These cracks form additional interfaces within the material that will reflect light, so if the specimen is viewed from the same side as it is illuminated the damaged areas will appear to whiten. Thus the whitening of a specimen or a region of it indicates that it is undergoing some damage process. (At this point in the talk the video was started.)

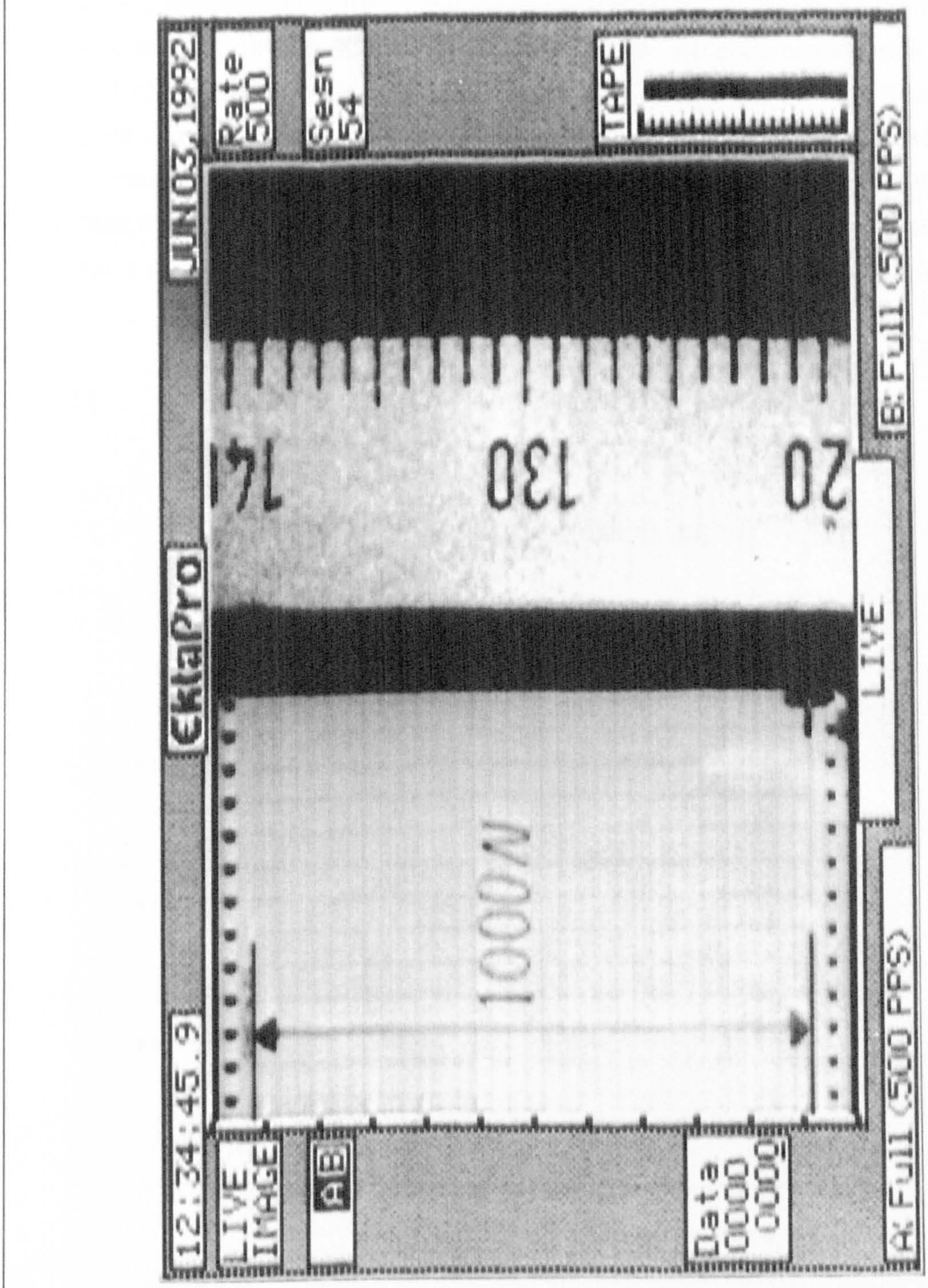

Figure A11.005

Outline of video image 1 (session 54): chart and scale

The first set of images seen on playing the video introduces the visual arrangement used for the tests. On the left side of the picture a chart recorder is shown, the full scale deflection of which is 1000 N. On the right a rule is shown where the test specimens will be seen in the forthcoming images. The graduations of this rule are in millimetres. All the images shown in the video are replayed at the same speed at which

they were recorded. (A frame rate of 500 frames per second was used so further analysis of the events could be performed.) All the specimens shown on this video were tested using a cross-head speed of 8.33×10^{-5} m s^{-1} [5 mm min^{-1}] and are contained in a water bath at 37°C. The chart speed is 8.33×10^{-3} m s^{-1} [0.5 m min^{-1}]. (One confusing aspect of the forth-coming video images is the appearance of objects after fracture. Most of these are air bubbles, they *float* downwards because the camera was mounted up-side down (due to physical restrictions). However, in the second set of images (session 36) a fragment is produced during fracture, this consequently *falls* to the top of the image.)

A11.2.1 TENSILE AND LOADING-UNLOADING TESTS

A11.2.1.1 TENSILE TESTS: BOVINE FEMORAL BONE

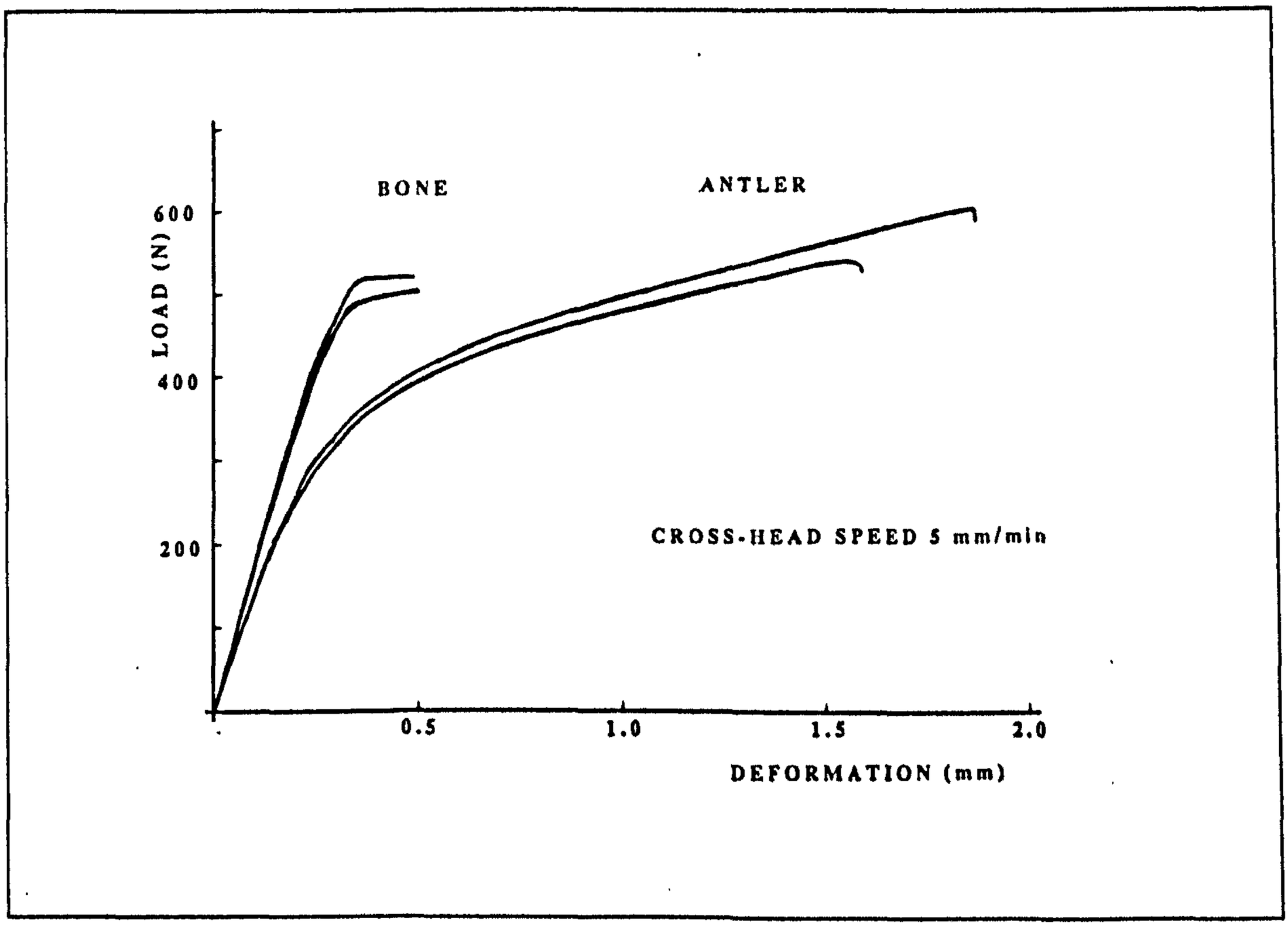

Figure A11.006

Slide 4: load-extension curves of bovine bone and antler

The images of the tensile testing of bovine bone shown here are from sessions numbered 36 and 71. The load-time plots for these tests and those of antler were also displayed on a slide as the video was being shown.

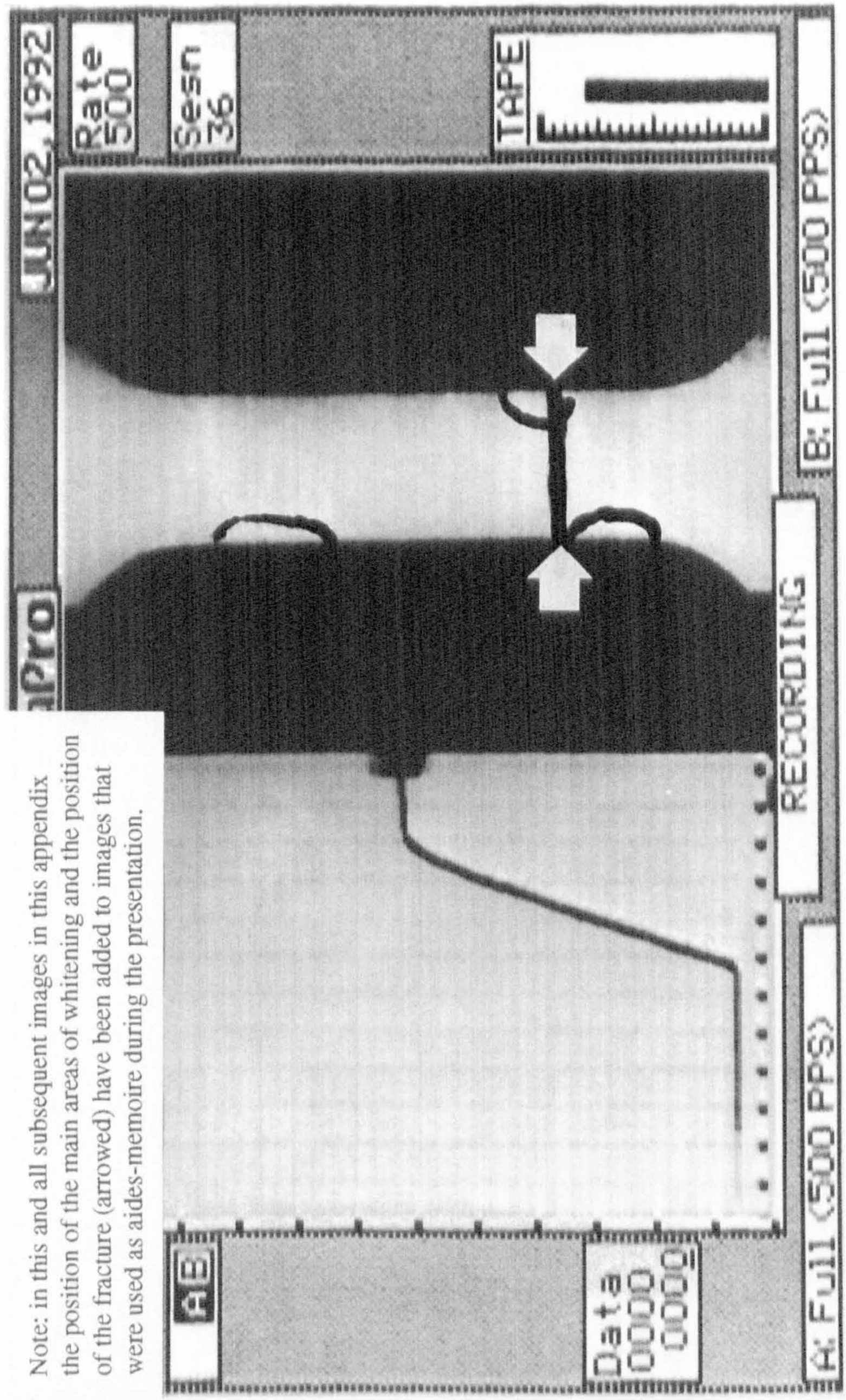

Note: in this and all subsequent images in this appendix the position of the main areas of whitening and the position of the fracture (arrowed) have been added to images that were used as aides-memoire during the presentation.

Figure A11.007

Outline of video image 2 (Session 36): tensile test of bovine bone

Whitening is seen as the loading line curves over, indicating a connection between these two events. The specimen finally fractures where the whitening first appeared. A similar result is shown in the next test, also a tensile test of bovine bone.

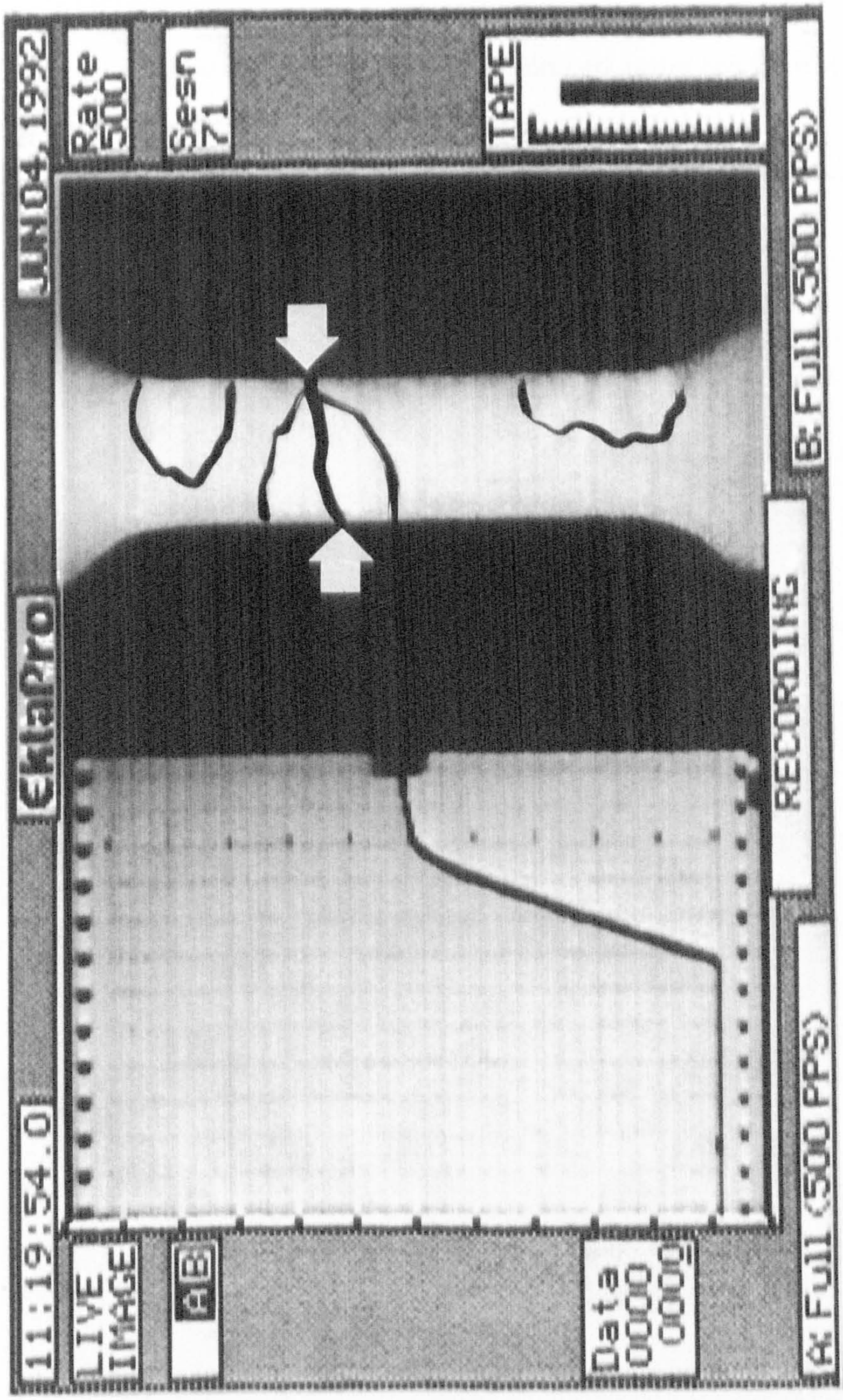

Figure A11.008

Outline of video image 3 (Session 71): tensile test of bovine bone

A11.2.1.2. TENSILE TESTS: ANTLER

The images that show the effect of tensile loading on antler are from sessions numbered 67 and 68.

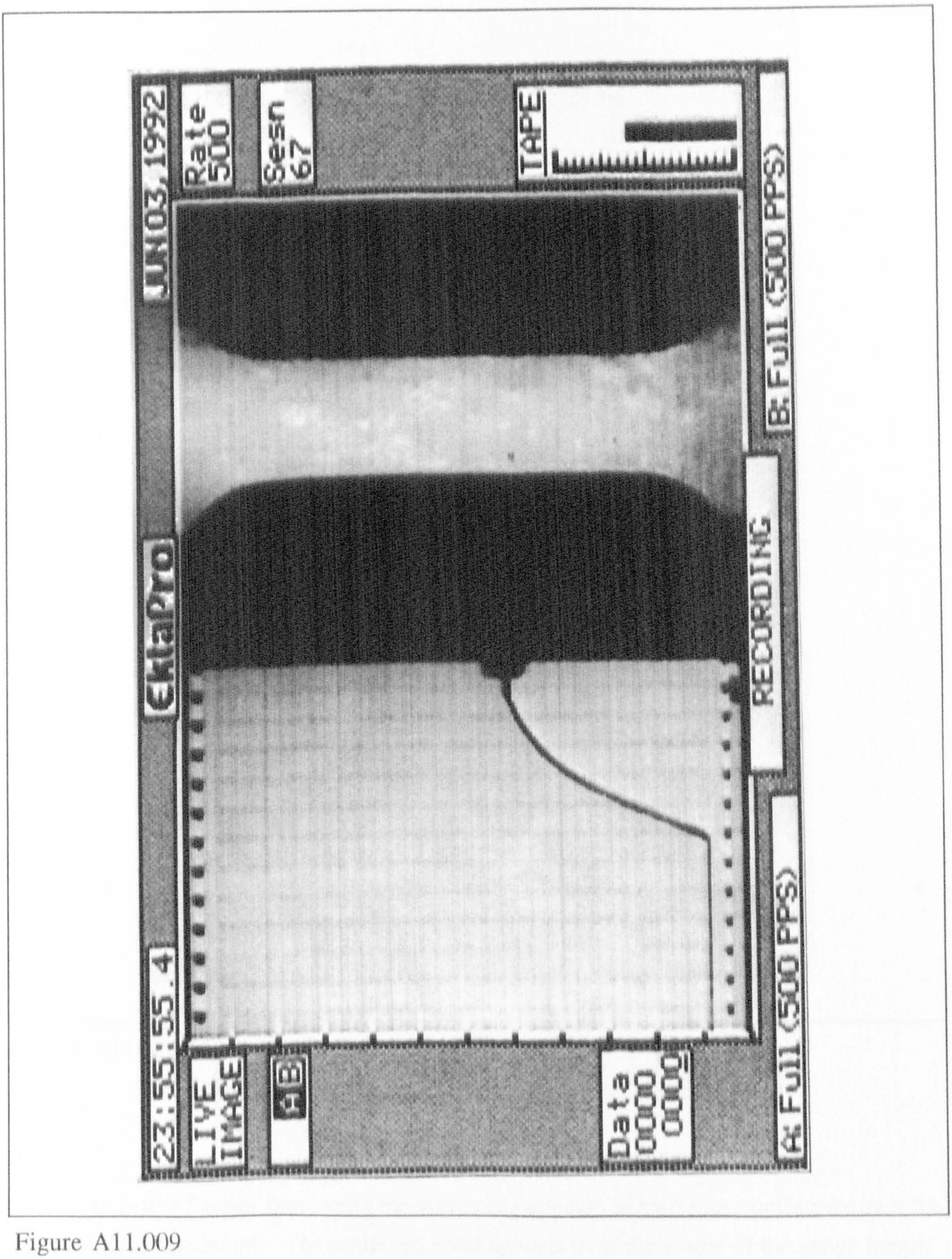

Figure A11.009

Outline of video image 4 (session 67): tensile test of antler

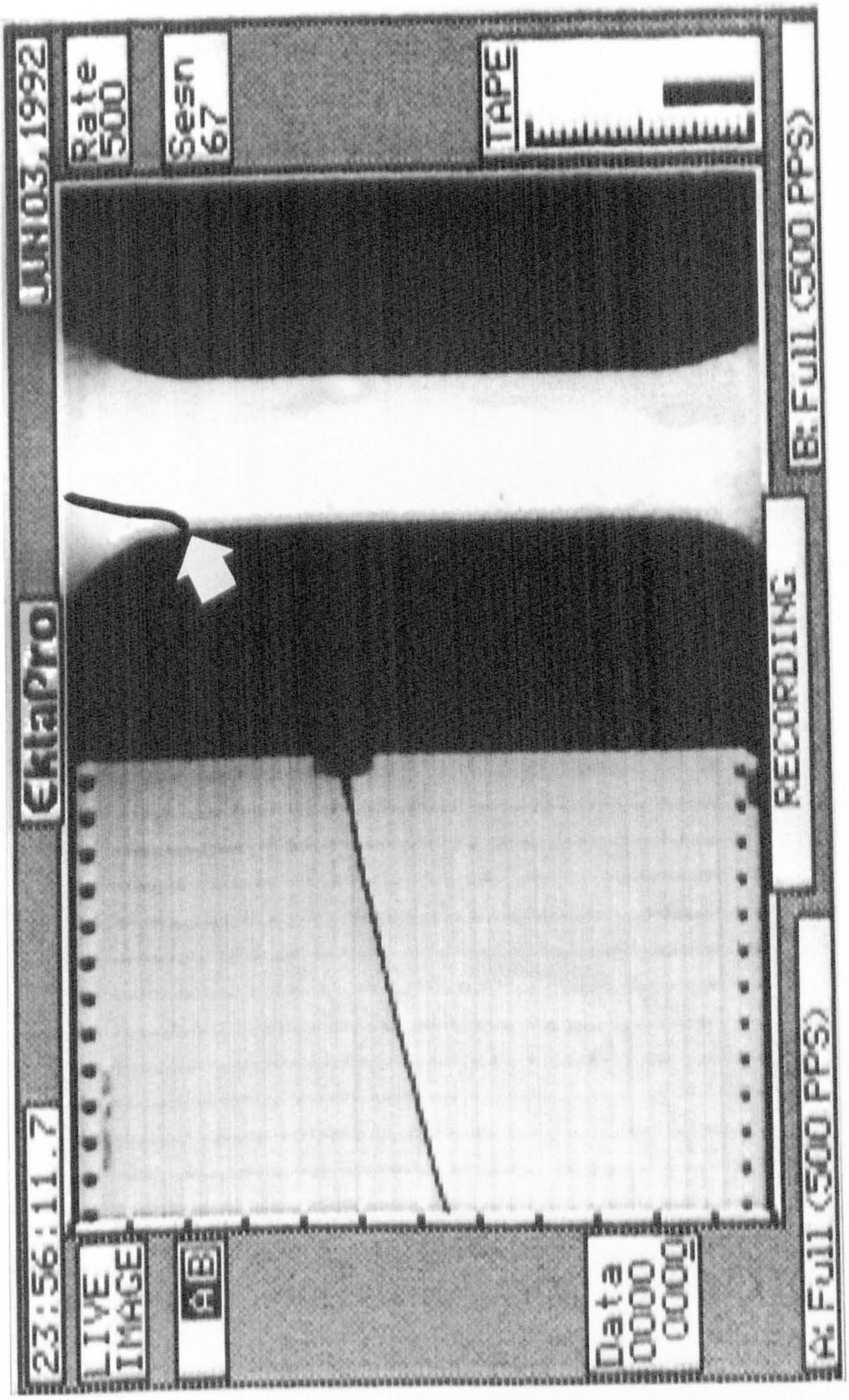

Figure A11.010

Outline of video image 4 (session 67): tensile test of antler

In tests of antler specimens the whitening appears to start more uniformly over the specimen's gauge length. The whitened zone spreads over the whole of the gauge length when the load is increased, but not into the shoulders. The shape of the whitened zone at the shoulders gives some indication of the changing stress field.

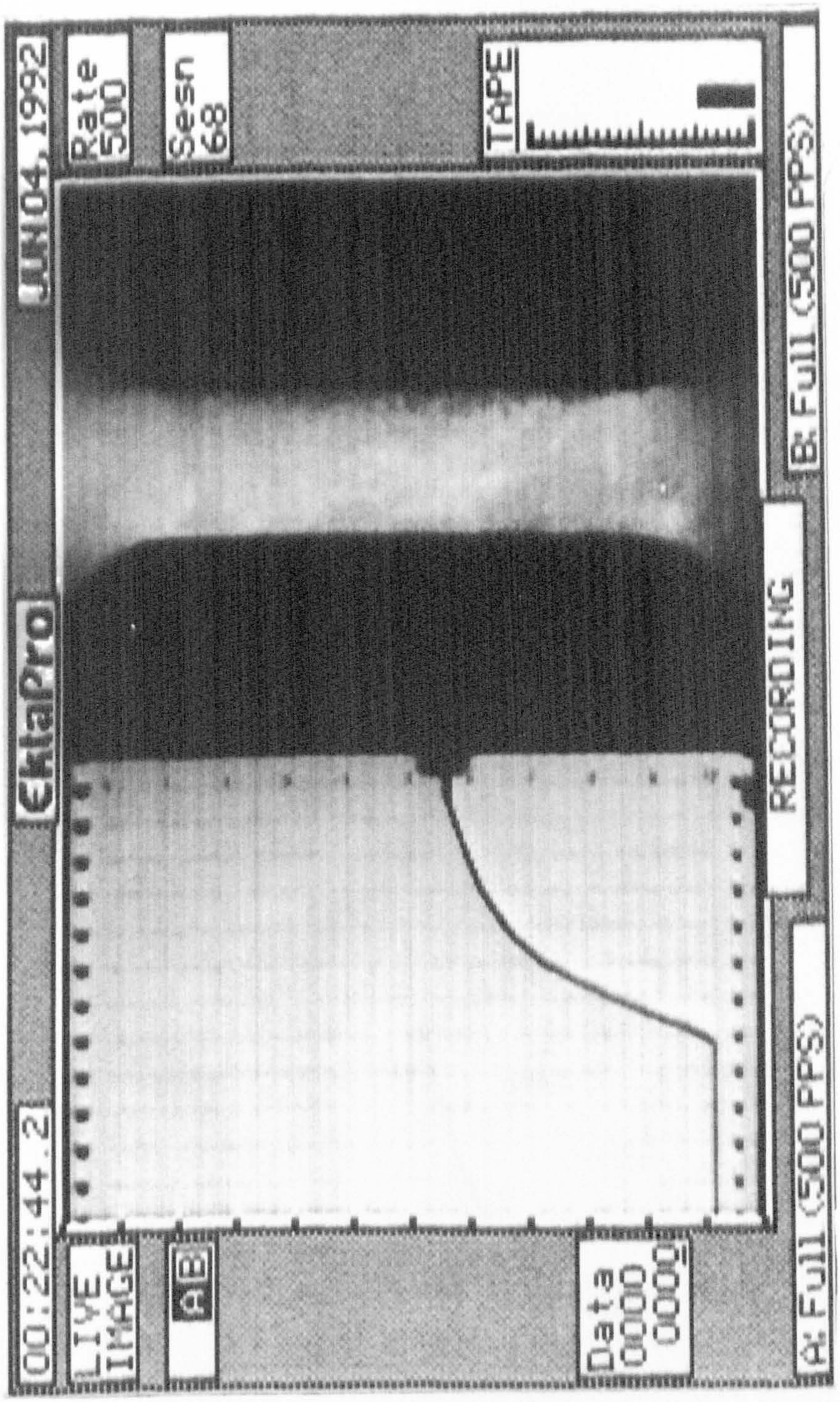

Figure A11.011

Outline of video image 5 (session 68): tensile test of antler

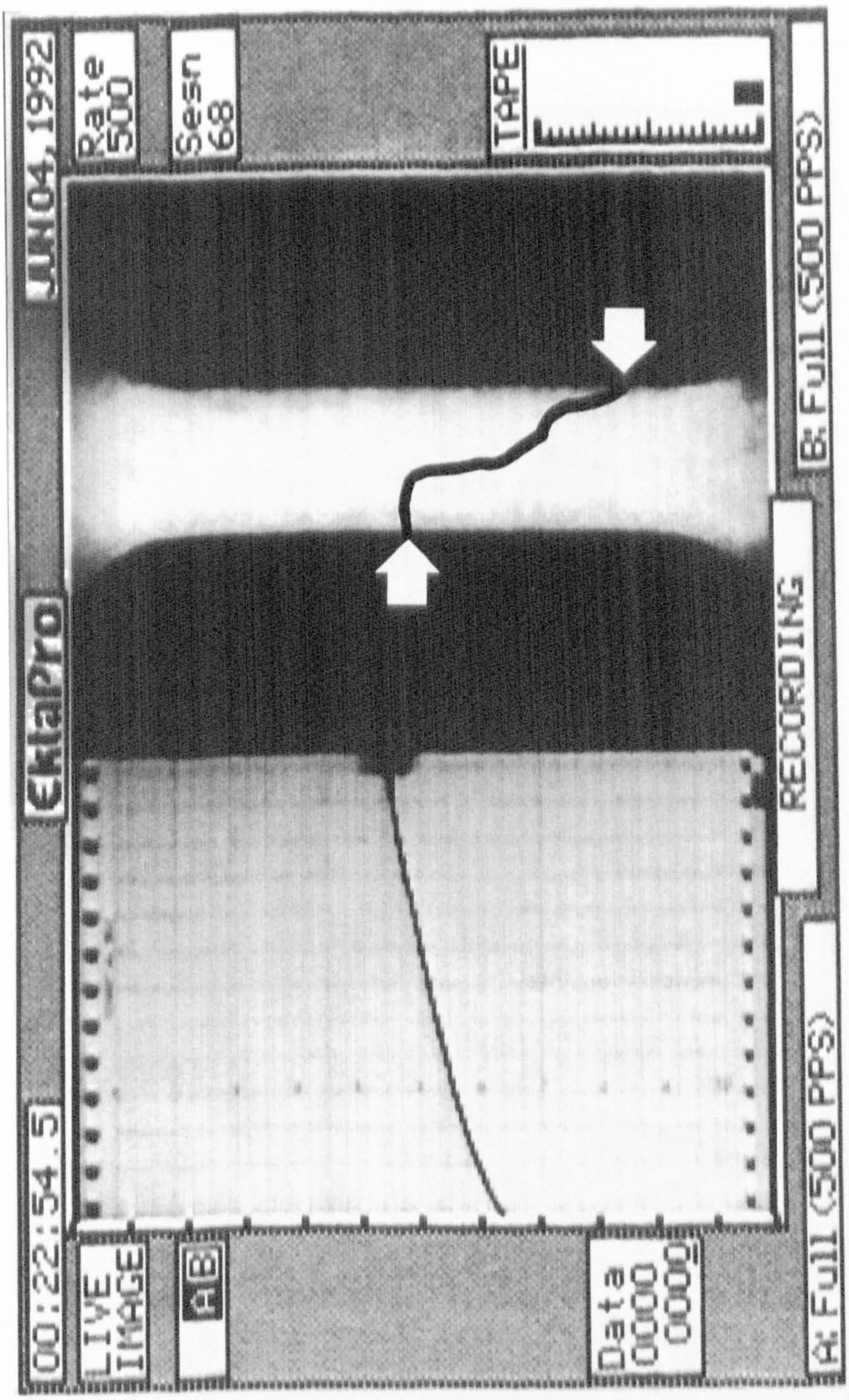

Figure A11.012

Outline of video image 5 (session 68): tensile test of antler

Again the whitening was seen to be more uniform than in the bovine bone tests. The darker initial appearance of the antler is a real effect.

A11.2.1.3. LOADING-UNLOADING UNTIL FAILURE: BOVINE BONE

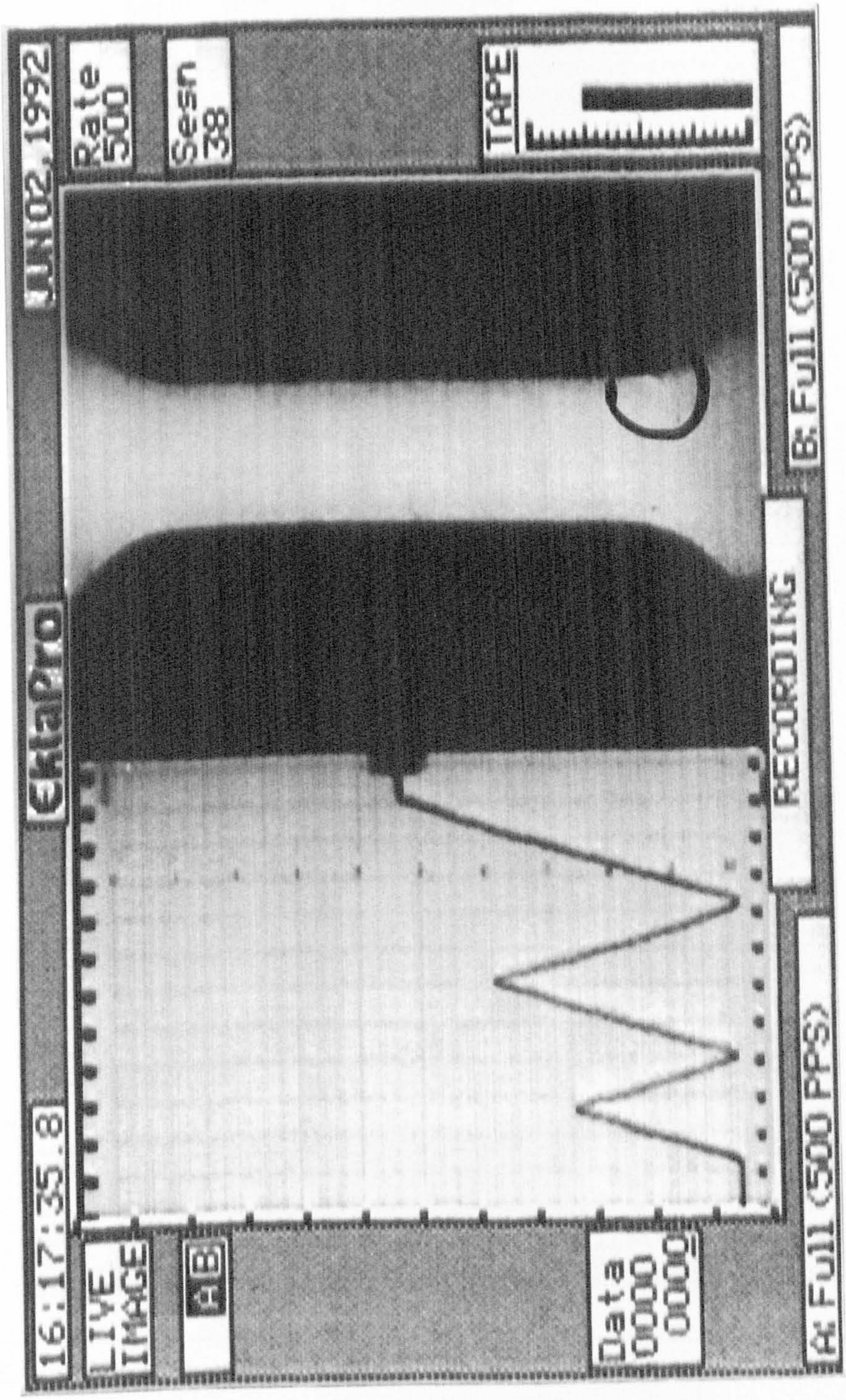

Figure A11.013

Outline of video image 6 (session 38): loading-unloading test of bovine bone

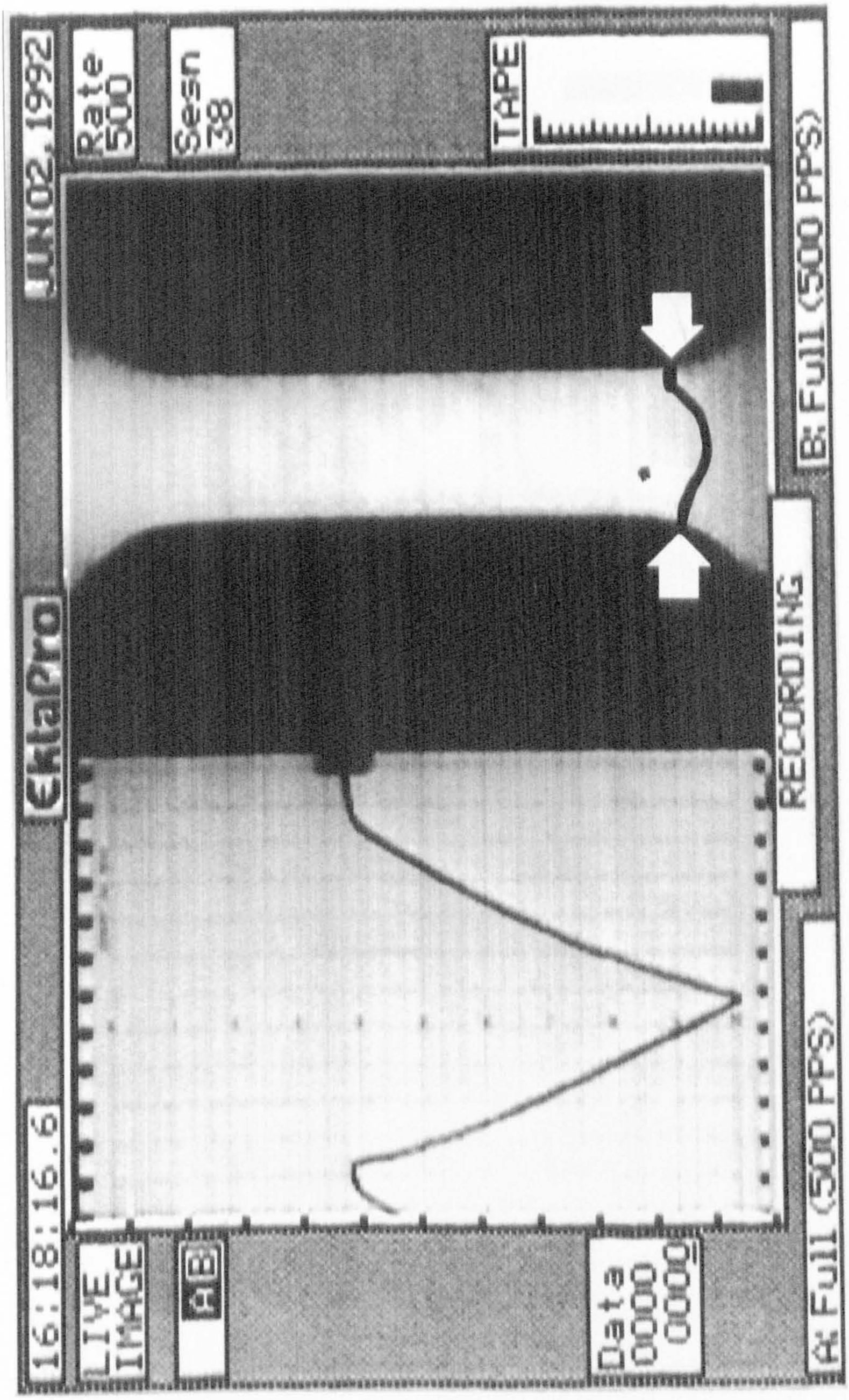

Figure A11.014

Outline of video image 6 (session 38): loading-unloading test of bovine bone

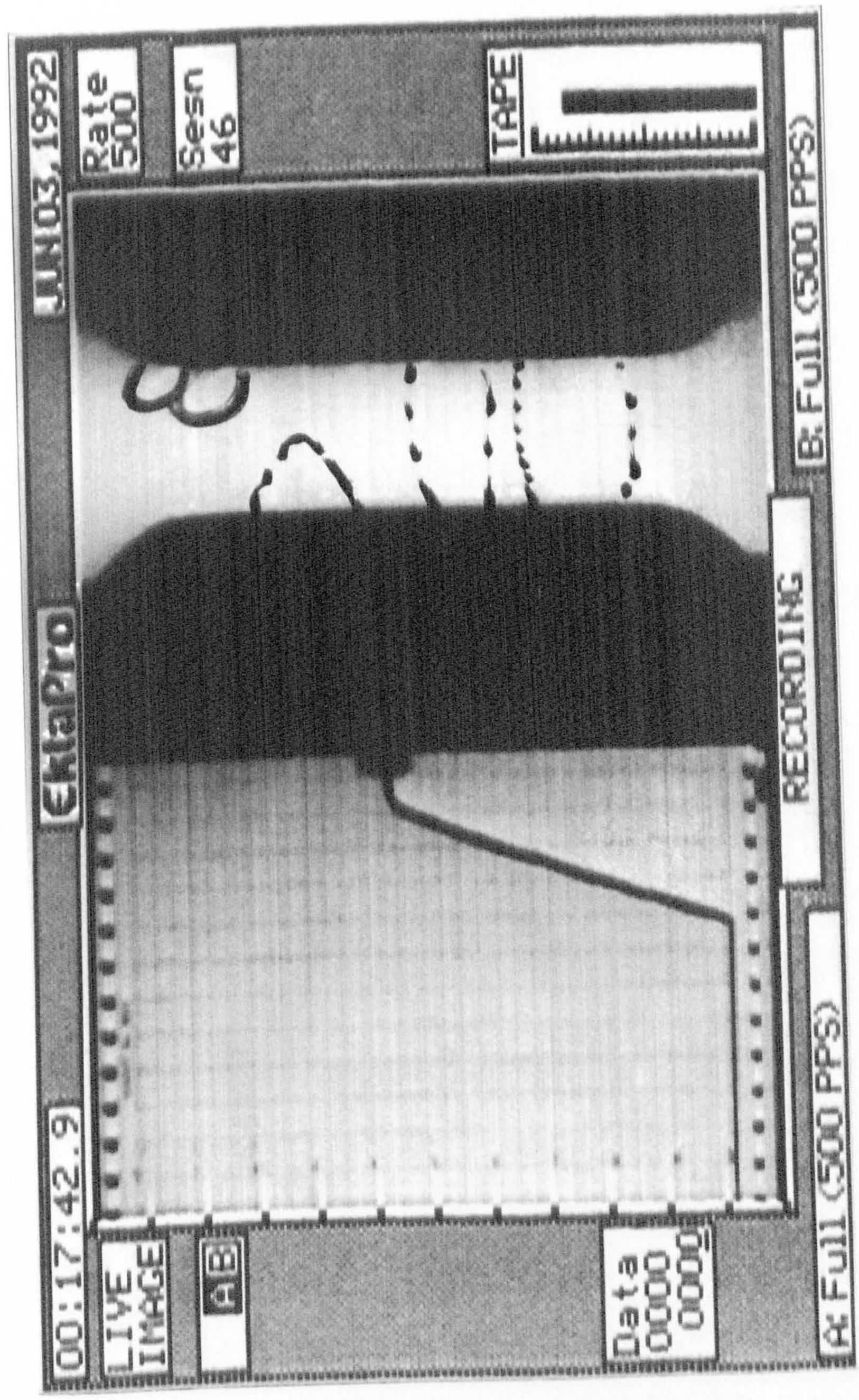

Figure A11.015

Outline of video image 7 (session 46): loading-unloading test of bovine bone

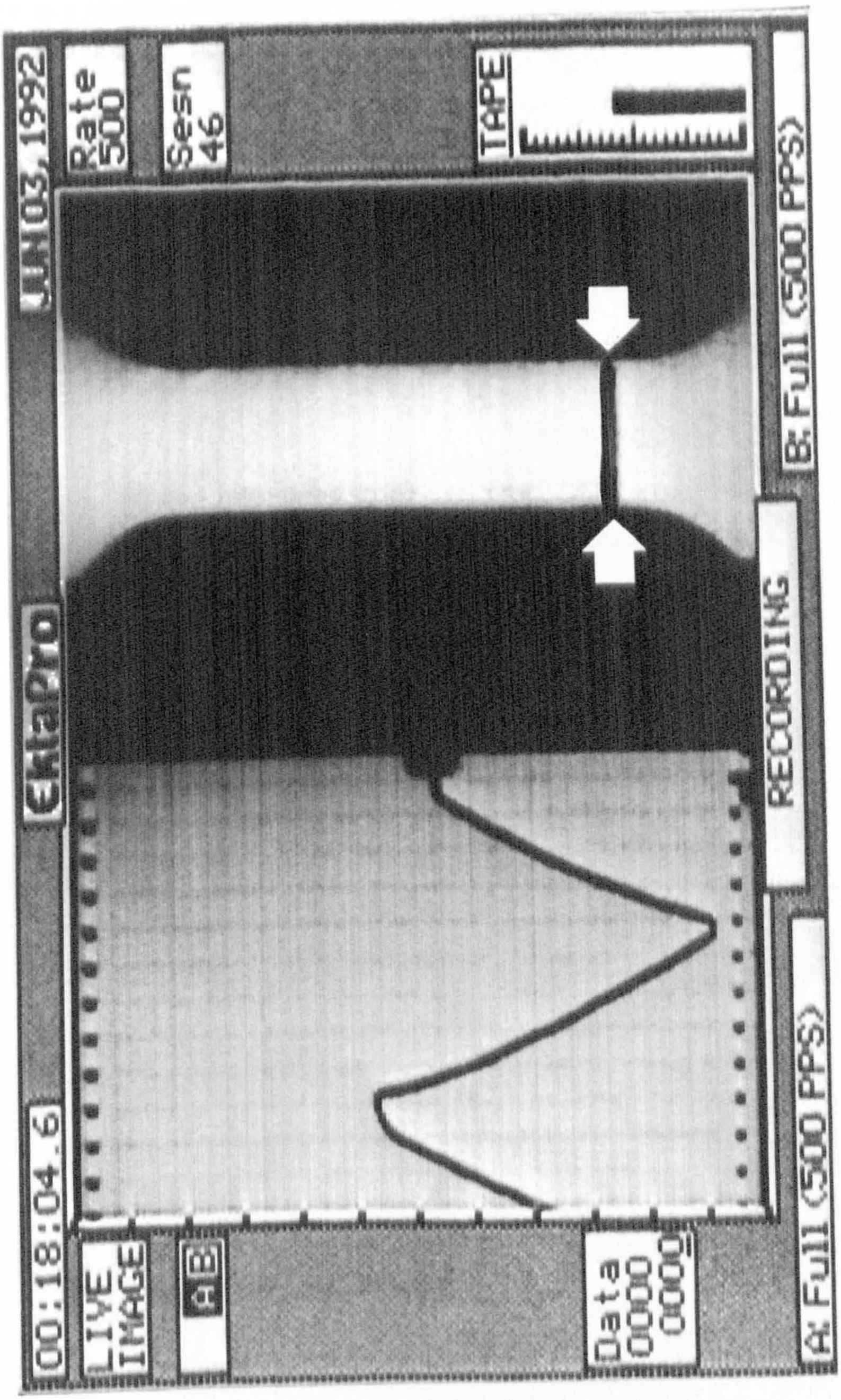

Figure A11.016

Outline of video image 7 (session 46): loading-unloading test of bovine bone

In the first loading-unloading tests that was shown (session 38) the occurrence of whitening appeared to correspond to the changes in nominal stress level. The whitening becomes more uniform with each progressive cycle. Fracture finally occurred where the whitening first appeared. The next set of images (session 46) displays the optical changes

observed in another specimen subjected to the same type of test. The loading curve is also displayed in a slide 5.

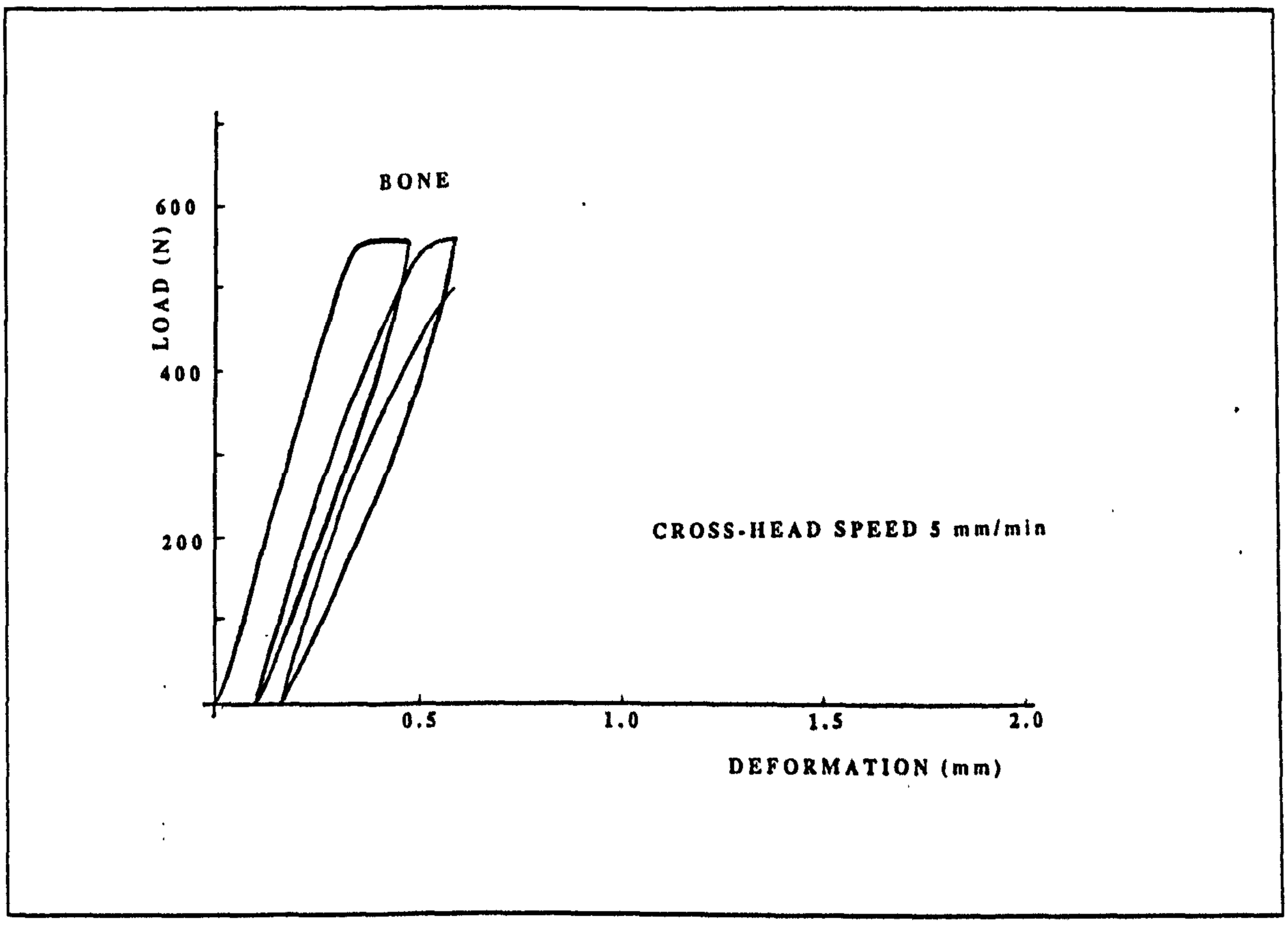

Figure A11.017

Slide 5: load-extension plot of bovine bone (shown in video session 46)

A11.2.1.4. LOADING-UNLOADING UNTIL FAILURE: ANTLER

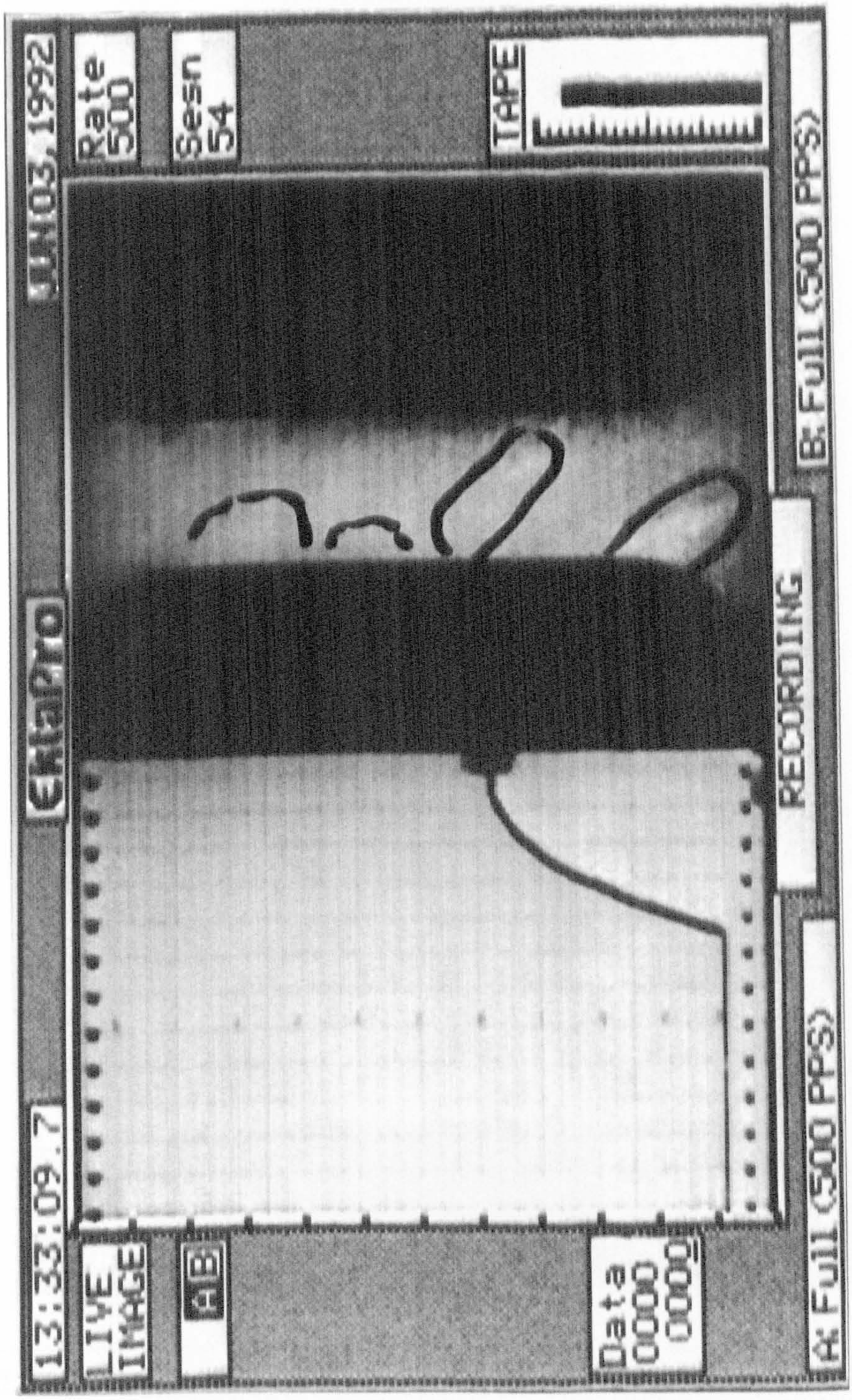

Figure A11.018

Outline of video image 8 (session 54): loading-unloading test of antler

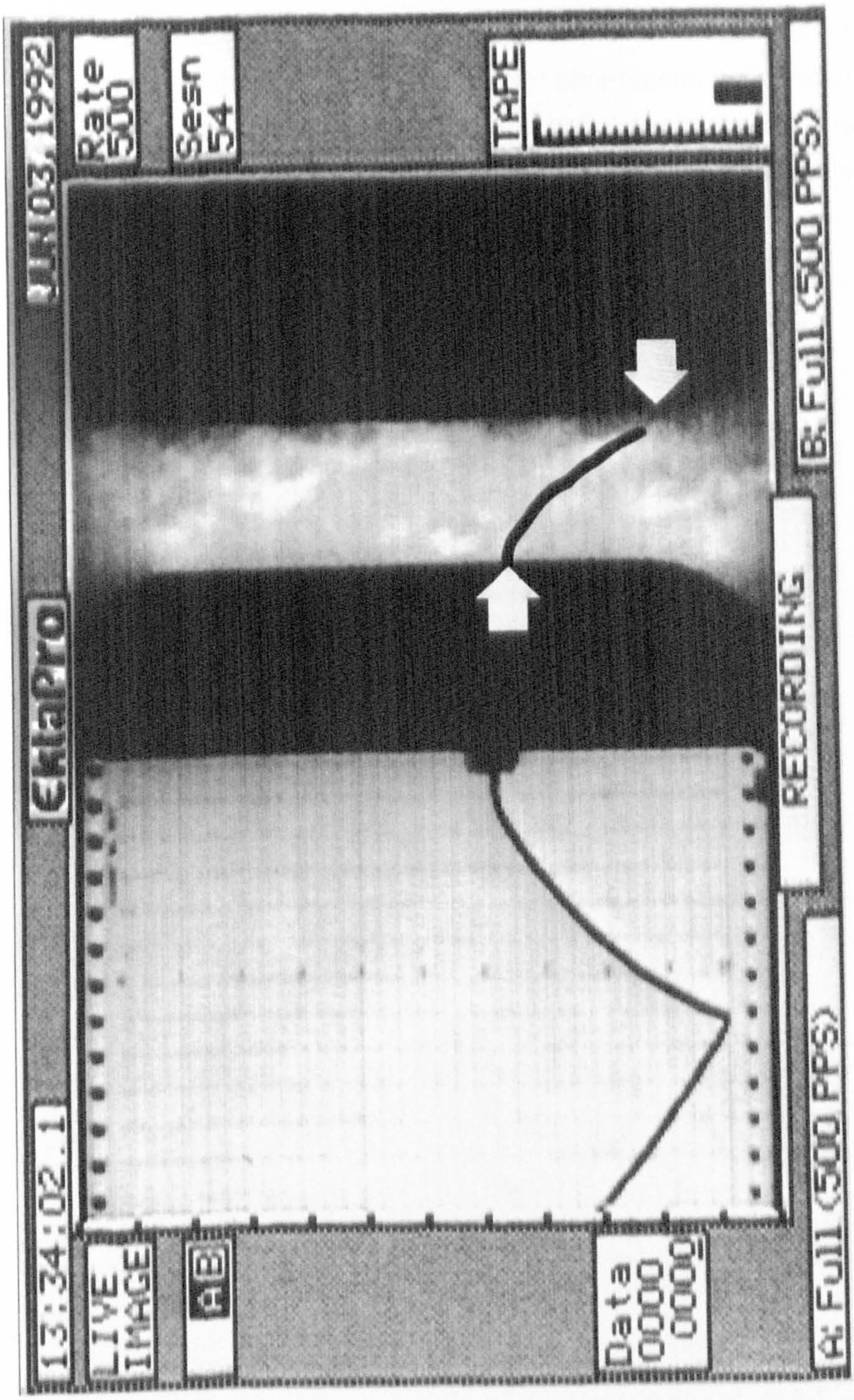

Figure A11.019

Outline of video image 8 (session 54): loading-unloading test of antler

In the loading-unloading tests of antler specimens, as in the tensile tests, the whitening is more uniform than in those of bovine bone. This antler specimen (session 54) exhibits large extensions as in the tensile tests. The whitening appears to be almost in the form of bands running diagonally across the specimen, from top-left to bottom-right. (The final fracture follows a similar path.) The extent of the whitening is related to nominal stress level, but on returning to zero stress some whitening persists. From

experiments where an extensometer was used to measure strain directly it has been found that the whitening in both materials occurs at a similar strain level, thus this residual whitening may be related to the residual strain, the two phenomena both reducing with time. This is what would be expected if the whitening is due to cracks in the material. This result is shown again with another specimen, the loading curve of which was shown on a slide (6).

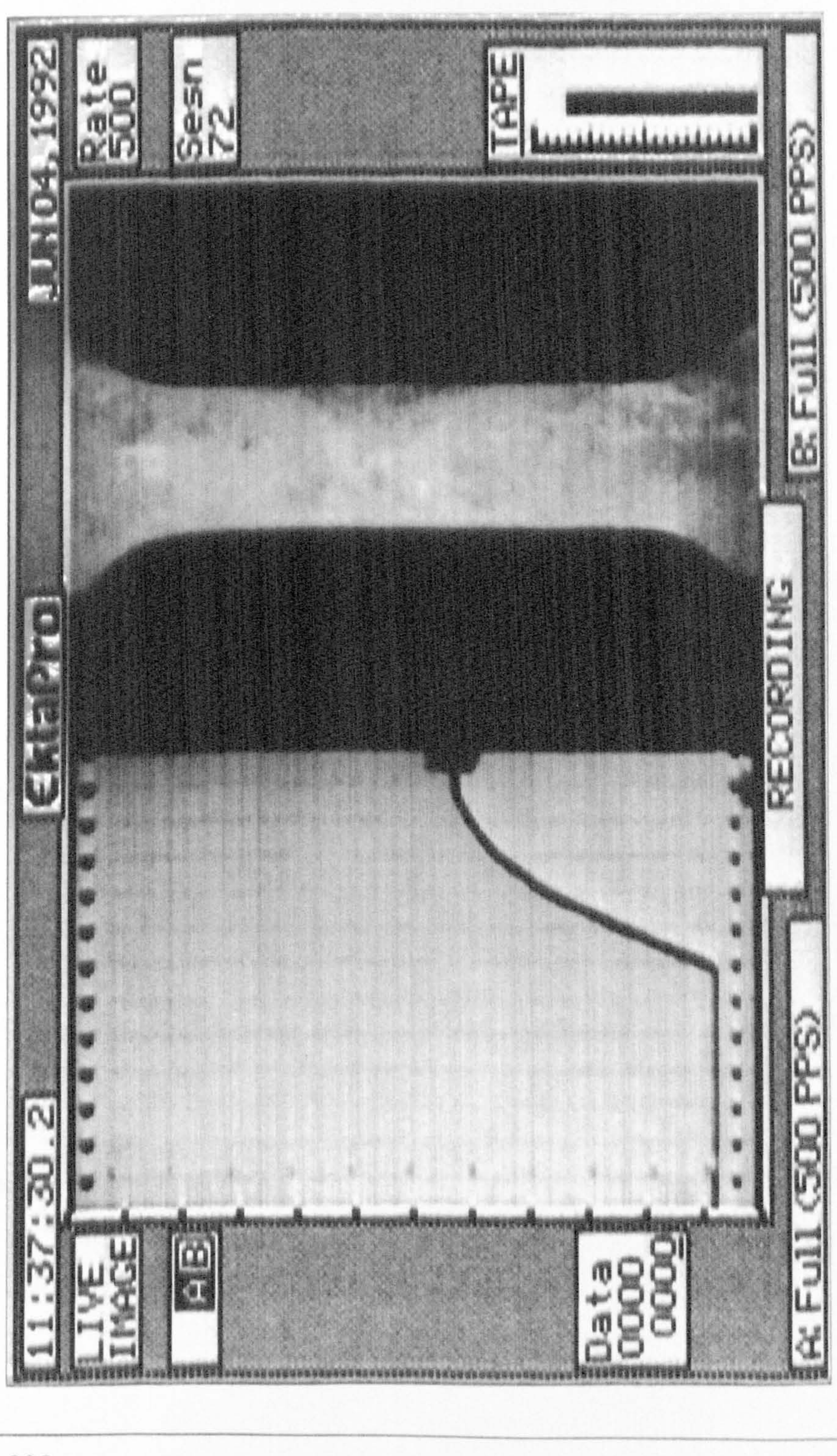

Figure A11.020

Outline of video image 9 (session 72): loading-unloading test of antler

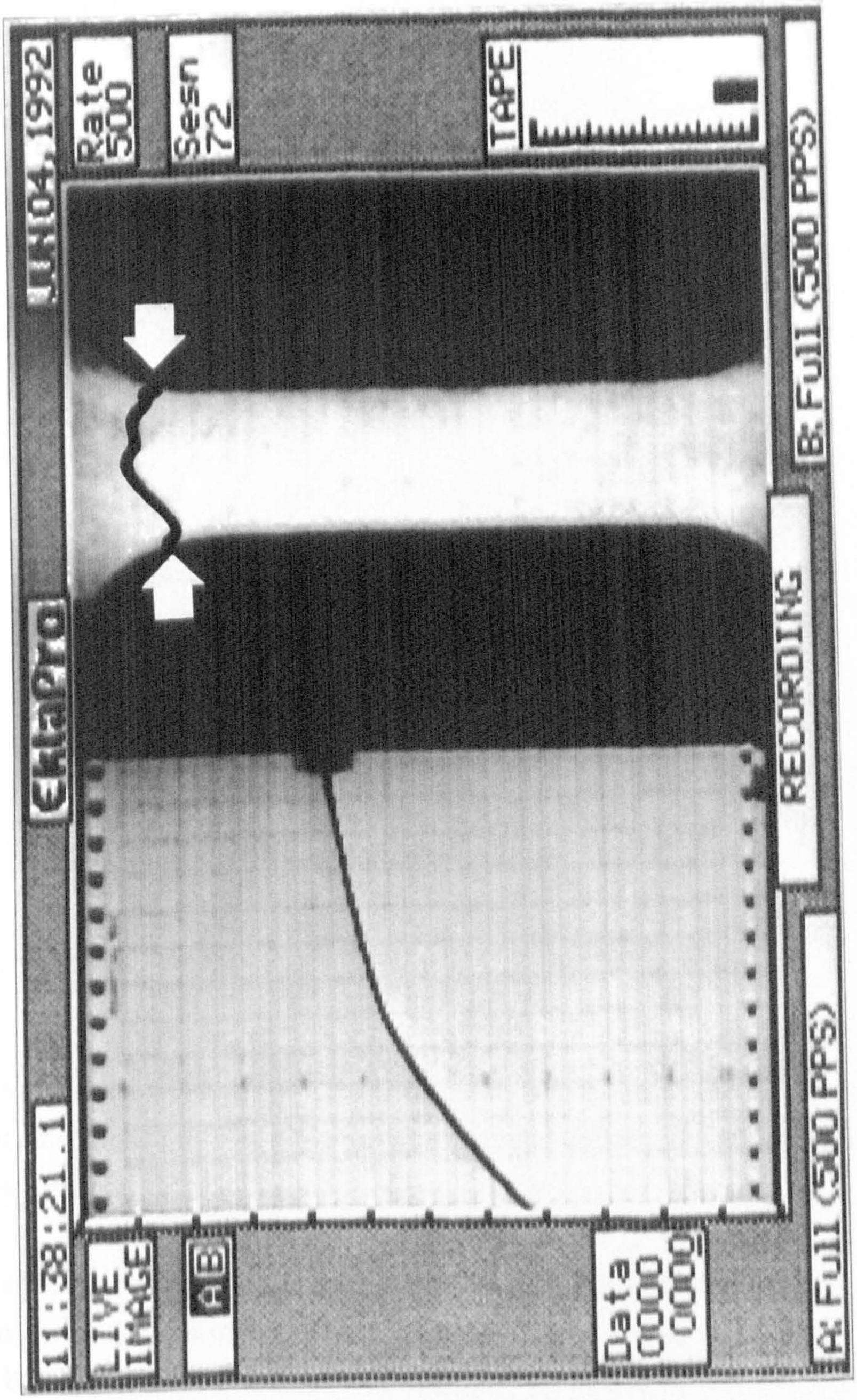

Figure A11.021

Outline of video image 9 (session 72): loading-unloading test of antler

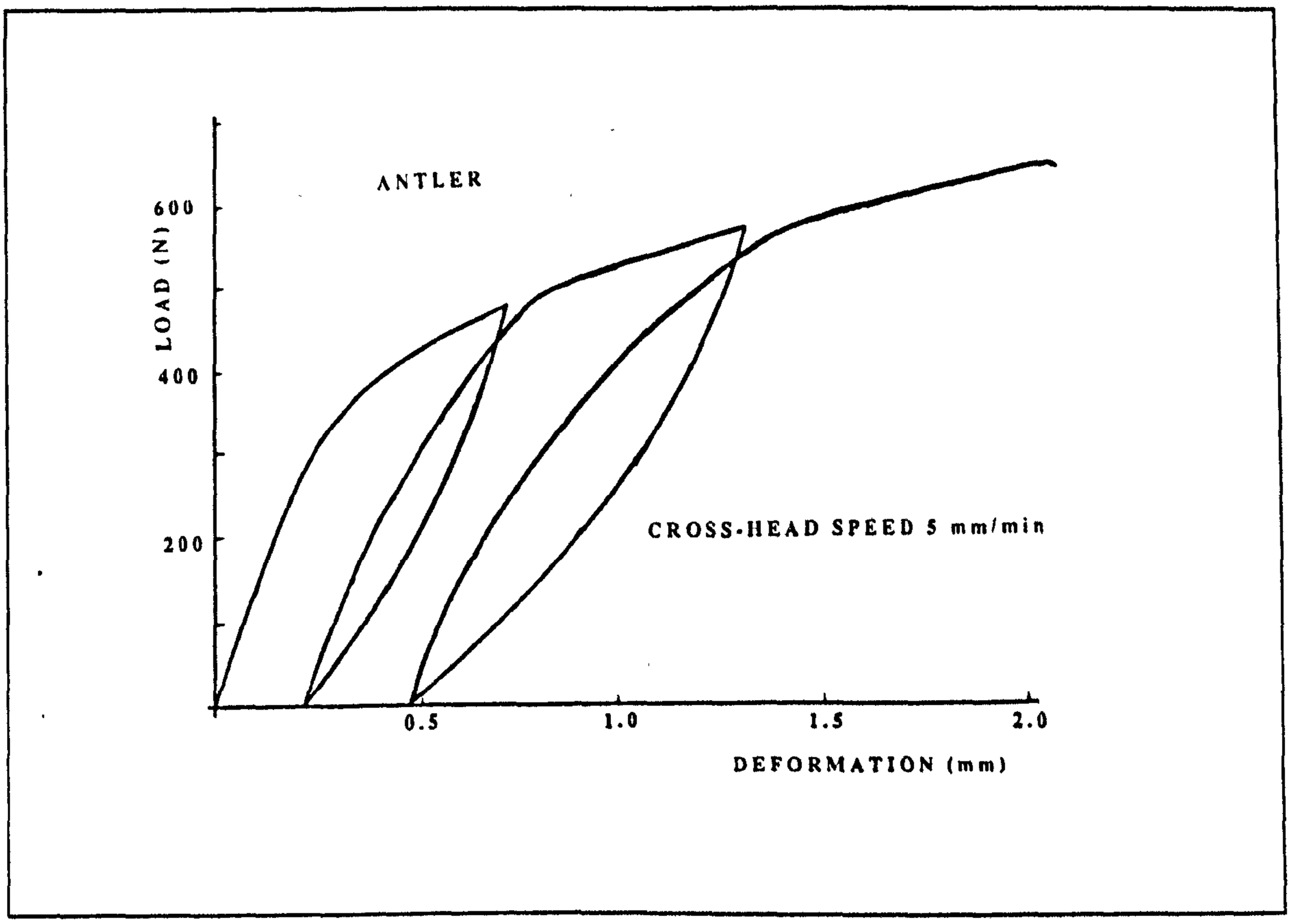

Figure A11.022

Slide 6: load-extension plot of antler (shown in video session 72)

A11.2.2. NOTCH SENSITIVITY TESTS

The whitening, when viewed as damage, can be used it to help explain some basic fracture mechanics results. The whitened area showing the damage region ahead of the notch or in some cases the moving crack.

The specimens shown in the images of tests on notched specimens are of the same overall dimensions as those in tensile tests. However, they appear larger as the area of interest has been enlarged, by using a zoom lens.

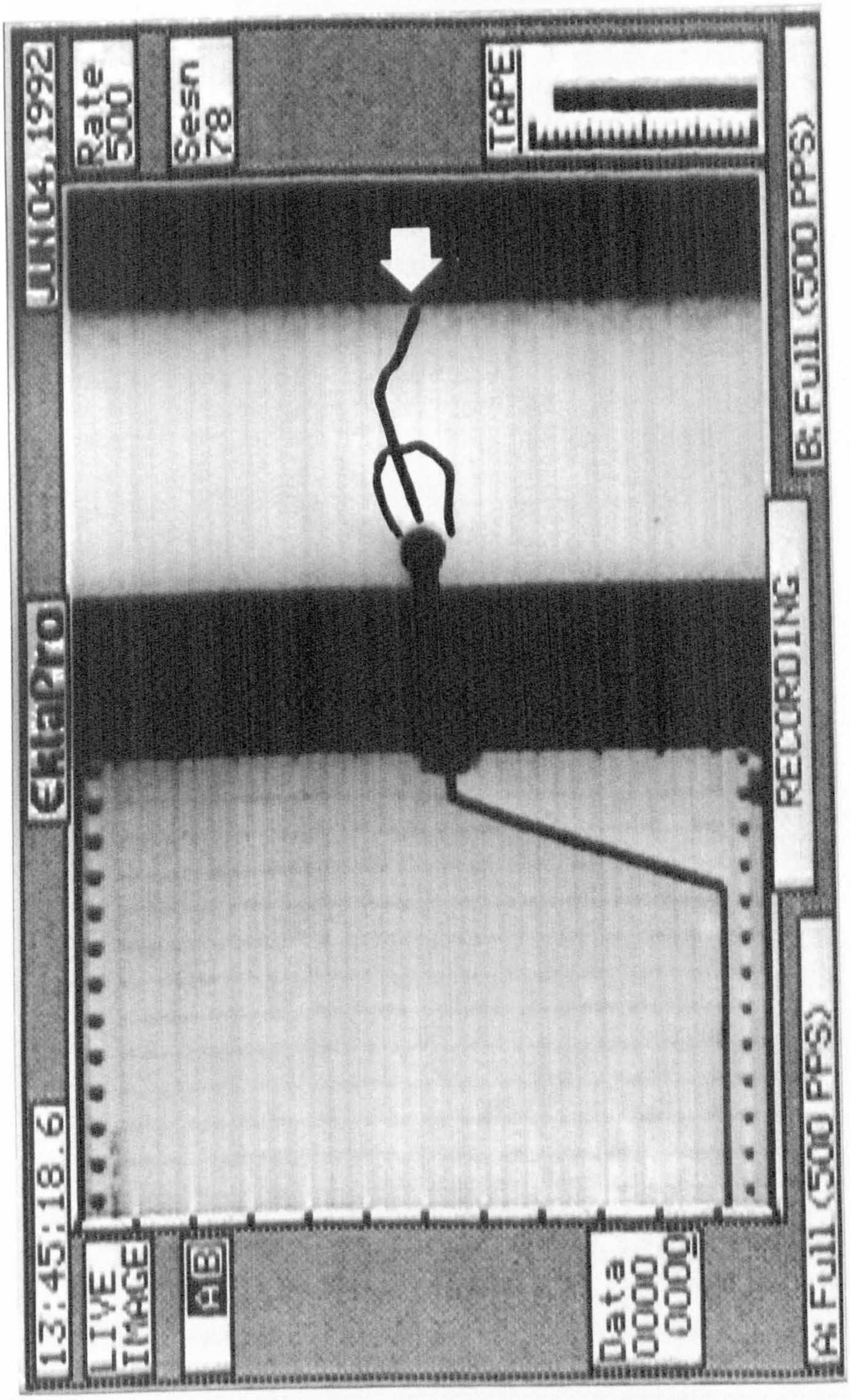

Figure A11.023

Outline of video image 10 (session 78): notch sensitivity test of bovine bone

The whitening is seen to be concentrated at the tip of the notch. The images show that as the load is increased the area of the white zone increases. There is then a very fast final fracture. A very similar result is displayed in the next set of images (session 79).

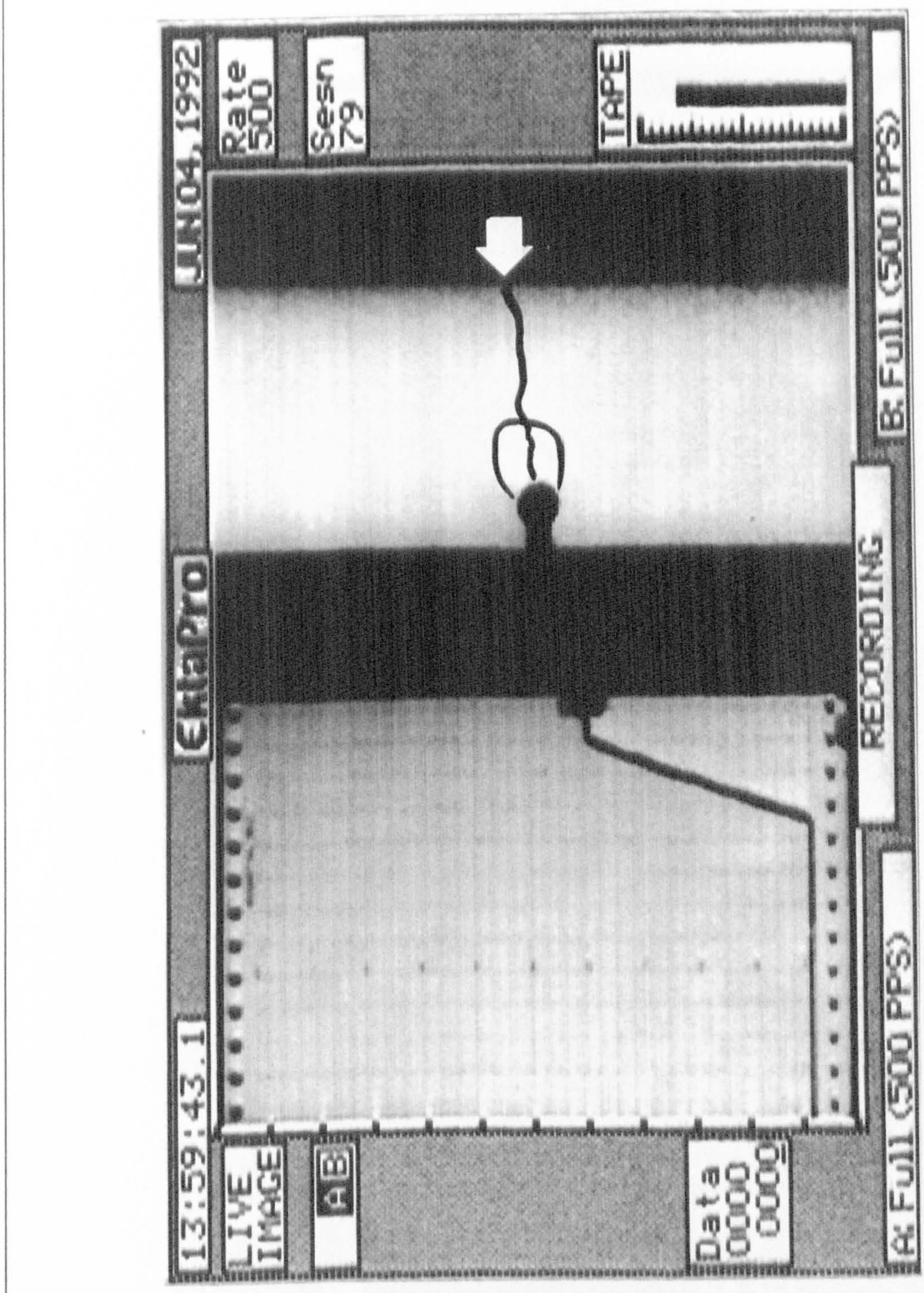

Figure A11.024

Outline of video image 11 (session 79): notch sensitivity test of bovine bone

A11.2.2.2. NOTCH SENSITIVITY TESTS: ANTLER

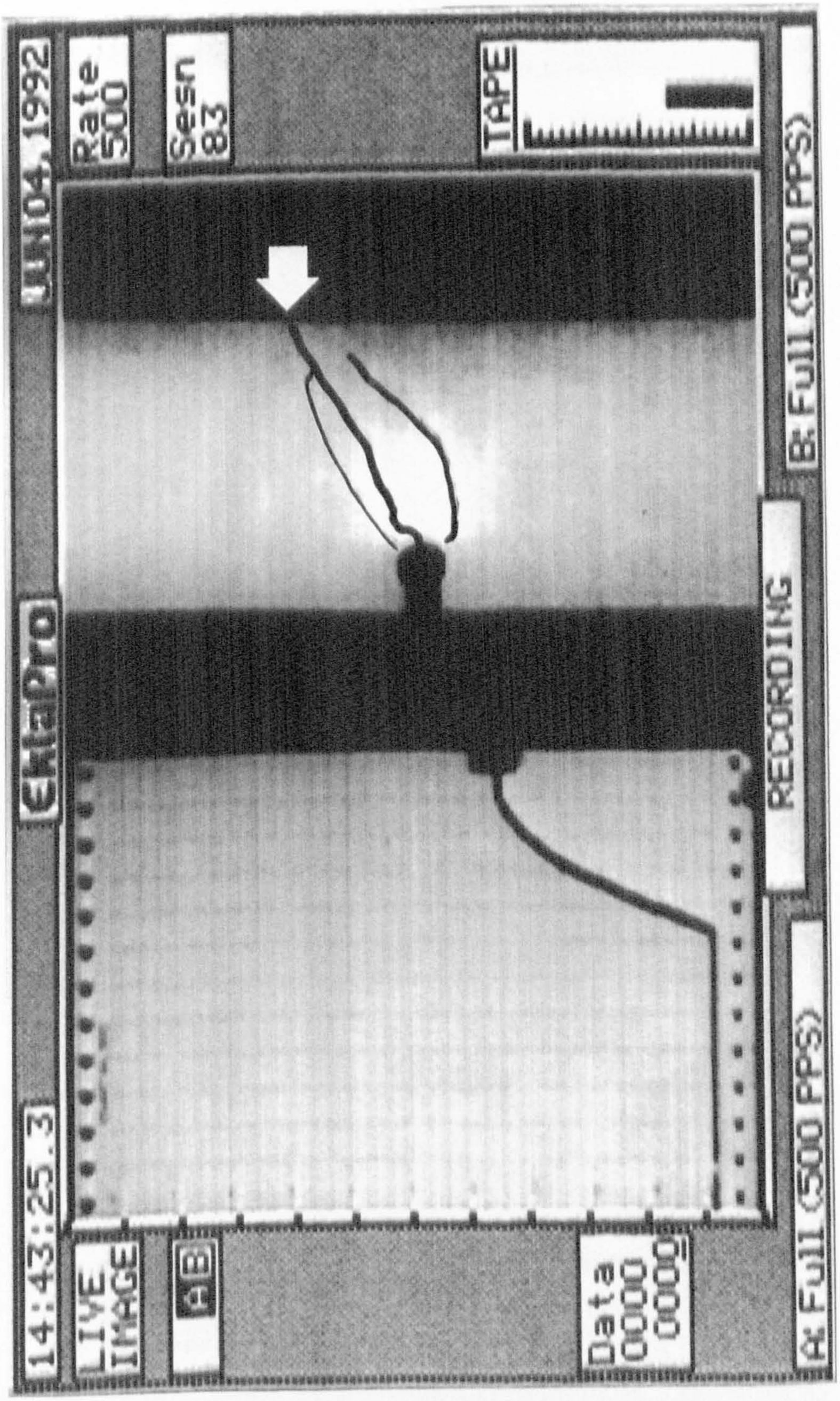

Figure A11.025

Outline of video image 12 (session 83): notch sensitivity test of antler

It was reported that there had been a general observation that the damage zone is clearer and larger in notched antler specimens than the notched bovine specimens. The fracture process also takes a greater time from initiation to failure in antler. The images of the antler test show the failure was not due to a fast brittle fracture, but like a slow rip.

A11.2.3. WHITENING IN TENSILE TEST OF BOVINE BONE WHICH FAILED AT A HIGH STRAIN

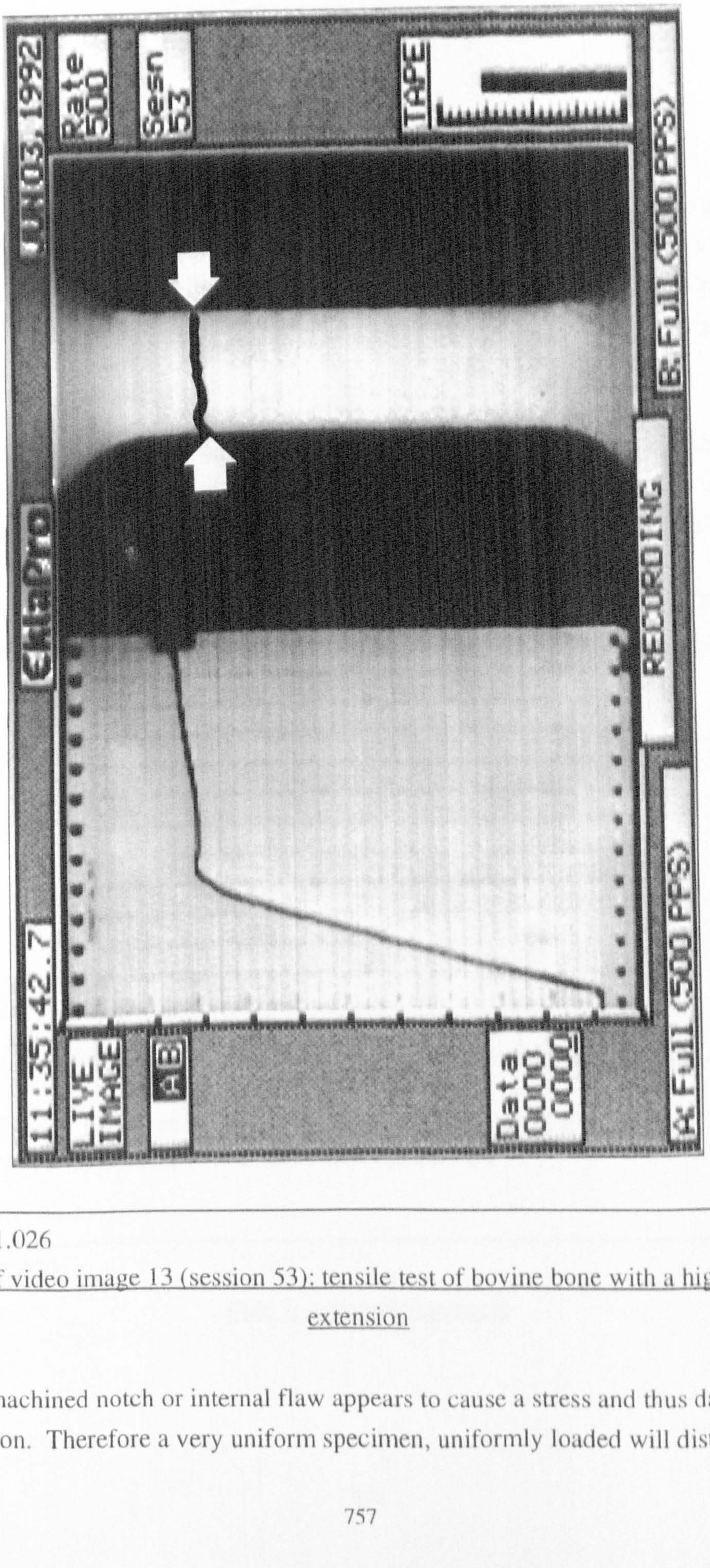

Figure A11.026

Outline of video image 13 (session 53): tensile test of bovine bone with a high ultimate extension

A machined notch or internal flaw appears to cause a stress and thus damage concentration. Therefore a very uniform specimen, uniformly loaded will distribute the

damage more widely and thus exhibit a larger strain at failure, as shown for bovine bone. The whitening in the specimen shown in session 53 is more uniform than that in the previously shown images of bovine bone in tension. This specimen also exhibits a larger failure strain. Thus the recorded strain in tensile tests can be shown to be very dependent on the specimen being free from flaws or other stress concentrating effects.

A11.2.4. CLOSING REMARKS

The recording of the occurrence of optical changes can be used to map the position of material that has yielded within a specimen. This can be put to a number of uses, including a check on the loading conditions. Optical changes at diagonally opposite shoulders (not shown here) highlight a non-uniform stress field due to poor alignment of the specimen.

The occurrence of damage ahead of the machined notch in bone explains the lack of dependence of the critical stress intensity factor used in fracture mechanics on the radius of the notch tip, and suggests that some correction to the crack length is needed.

Thanks were given to the Science and Engineering Research Council (for funding me during this study and for the use of the video camera). Thanks were also given to the Scientific Committee of the meeting for giving me a studentship.

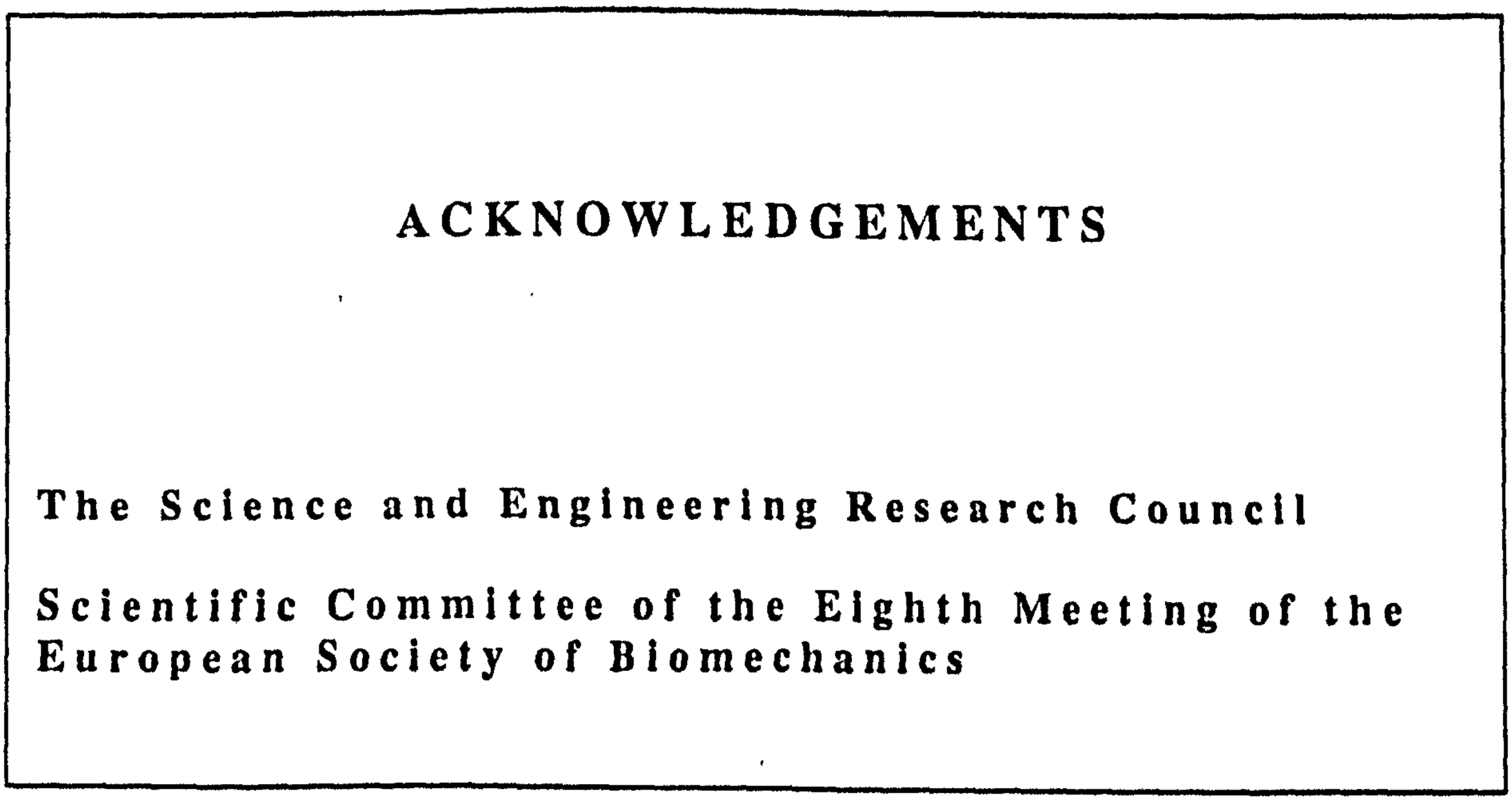

Figure A11.027

Slide 7: acknowledgements

APPENDIX 12

STUDENT'S t-DISTRIBUTION

This appendix provides a table showing the relationship of the three significance levels used in this work (significant, highly significant, very highly significant) and the value of the Student's t-distribution. In the regression equations presented in this work the t values have been given. In many cases the *p* value or the significance level has been given in the relevant section of the text. To use the following table the degrees of freedom, d.f., needs to be established. For a regression equation this is given by

d.f. = number of data sets used - number of explanatory variables - one

By way of an example the first equation and part of table 3.001 is repeated below

Type of specimens	Regression equations and t values, for the data published by Currey (1975).	R^2 %	
35 Bovine femoral	$\sigma_{ult} = 115 + 306\,\dot{\varepsilon}$ t: 18.17 2.79	16.6	*a*
.	.	.	.
.	.	.	.
Units: σ_Y, MPa.	σ_{ult}, MPa. $\dot{\varepsilon}$, s^{-1}. E, GPa.		

Table A12.001 Reproduced, in part, from table 3.001

The relationship of various mechanical properties to strain rate exhibited by the data published by Currey in 1975

In this example there is data from 35 specimens. This data is analysed using one explanatory variable. Thus there are 33 degrees of freedom. Therefore on consulting table A12.002 it is seen that the associated *p* value falls between 0.01 and 0.001. I have chosen the following descriptions of the levels of significance;

$p > 0.05$	Non-significant
$p \leq 0.05$	Significant
$p \leq 0.01$	Highly significant
$p \leq 0.001$	Very highly significant

Therefore in this case the variable, $\dot{\varepsilon}$, is highly significant.

Degrees of freedom	Value of p		
	0.05	0.01	0.001
1	12.706	63.657	636.619
2	4.303	9.925	31.598
3	3.182	5.841	12.941
4	2.776	4.604	8.610
5	2.571	4.032	6.869
6	2.447	3.707	5.959
7	2.365	3.499	5.408
8	2.306	3.355	5.041
9	2.262	3.250	4.781
10	2.228	3.169	4.587
11	2.201	3.106	4.437
12	2.179	3.055	4.318
13	2.160	3.012	4.221
14	2.145	2.977	4.140
15	2.131	2.947	4.073
16	2.120	2.921	4.015
17	2.110	2.898	3.965
18	2.101	2.878	3.922
19	2.093	2.861	3.883
20	2.086	2.845	3.850
21	2.080	2.831	3.819
22	2.074	2.819	3.792
23	2.069	2.807	3.767
24	2.064	2.797	3.745
25	2.060	2.787	3.725
26	2.056	2.779	3.707
27	2.052	2.771	3.690
28	2.048	2.763	3.674
29	2.045	2.756	3.659
30	2.042	2.750	3.646
40	2.021	2.704	3.551
60	2.000	2.660	3.460
120	1.980	2.617	3.373
∞	1.960	2.576	3.291

Table A12.002

Values of student's t-distribution associated with three percentage point values for significance tests

LIST OF SYMBOLS USED

Most of the symbols and accompanying nomenclature are defined locally in the text, so some of them are not included in this list. However, those that more generally applicable are listed here. (Some of the locally defined symbols are reused elsewhere.) In this list I do not include symbols used to represent constants in equation and so on. When the rate of change of a quantity is being expressed with respect to time I have generally used the dot notation. Therefore if the quantity is represented by B its rate with respect to time is presented by $\dot{B}$. (In some reviews I have used $^{d B}/_{d t}$.) In some cases (t) has been placed after a quantity to indicate that it a function of time. Generally the failure of specimens during tensile tests is referred to as the ultimate (normally maximum) value thus the subscript 'ult' is used. The failure of creep specimens is referred to as rupture, so the subscript 'r' is used. Those specimens that fail due to the effect of a notch are referred to as fractured, thus the subscript 'f' is used.

a	Half the length of an internal through the thickness crack
a_{int}	Intrinsic edge notch length
A	Instantaneous cross-sectional area of the specimen (at time t)
A	Crack area
A_{eff}	Effective area of the specimen (cross-section accounting for damage)
A_0	Initial cross-sectional area of the specimen (at time t = 0)
Ca^{++}	Calcium content
d_w	The length of the whitened zone
d_y	Length of the crack tip plastic zone
D	Damage
E	Young's modulus of elasticity
E_b	Material stiffness in three-point-bending
E_M	Measured stiffness of the material
E_s	Secant modulus (stress/strain at one point on loading curve)
E_t	Material stiffness in tension
E_U	Stiffness of the undamaged material
E^*	For a material under conditions of plane stress Young's modulus, E
E^*	For a material under conditions of plane strain $E^* = E/(1 - \nu^2)$
F	External work supplied to the system (Griffith)
G	Potential energy release rate
G_c	Critical potential energy release rate
H(t)	Unit or Heaviside step function.

$J(t)$	Creep compliance
K	Stiffness of spring or specimen
K	Stress intensity factor
K_C	Critical stress intensity factor
K_{IC}	The plane strain critical stress intensity factor for opening mode one
K_{IQ}^{I}	Infinite sheet stress intensity factor (experimentally derived value)
K_{IQ}^{P}	Pin-jointed finite sheet stress intensity factor (experimentally derived value)
K_{IQ}^{U}	Un-flexing finite sheet stress intensity factor (experimentally derived value)
K_{IQ}^{*}	K_{IQ}^{I}, K_{IQ}^{P} or K_{IQ}^{U}
L	Instantaneous gauge length of the specimen (at time t)
L_0	Initial gauge length of the specimen (at time $t = 0$)
P	Load (also P1, P2, etc.)
r_w	Half the length of the whitened zone
r_y	Half the length of the crack tip plastic zone
R	Work-of-fracture (energy divided by one surface area)
R^2	Coefficient of determination, adjusted for degrees of freedom
$\Re$	Resilience
S	Final slope
t	Specimen thickness
t	Time
t_{fail}	Time-to-fail (any stress history)
$t_R\ [\sigma]$	Time-to-rupture in a creep test, with stress level σ.
t_R	Time-to-rupture (experimental results)
t_1	Time-to-rupture by a purely ductile creep process (Kachanov)
t_2	Time-to-rupture by a purely brittle creep process (Kachanov)
t_3	Time-to-rupture some combined ductile and brittle creep process (Kachanov)
t_4	Time-to-rupture under creep conditions if $n = m$ (Kachanov)
t_5	Time-to-rupture by a purely brittle allowing for damage localisation
t_{1P}	Time-to-rupture by a purely ductile process allowing for primary creep (Odqvist)
t_{3P}.	Time-to-rupture by a ductile and brittle process allowing for primary creep
U_e	Energy released due to the crack (Griffith)
U_s	Surface energy due to the crack (Griffith)
U_o	Elastic energy of the loaded system without a crack (Griffith)
w	Width of specimen
W	Work
$\dot{x}$	Cross-head speed
Y	Shape correction factor

$Y(t)$	Relaxation modulus
γ_s	Surface free energy of a material.
γ_p	Energy consumed by crack tip plastic zone
Δ_y	Dugdale strip yield model plastic zone length
ε	Nominal strain, extension normalised by initial length
$\dot{\varepsilon}_i$	Strain rate measured during the initial region of the loading curve, s^{-1}
ε_K	Knee strain
ε_{nom}	Nominal strain (used where clear differentiation from true stress is needed)
ε_{peak}	Peak strain in first loading cycle of loading-unloading test
$\dot{\varepsilon}_{pk}$	Measures strain rate in the post knee region of the curve, s^{-1}
ε_{py}	Post-yield strain, the strain accumulated between yield and final failure
ε_R	Rupture strain (creep tests)
$\dot{\varepsilon}_s$	Secondary creep rate
ε_{true}	True strain
ε_{ult}	Ultimate strain (tensile tests)
ε_y	Yield strain
ε_0	Instantaneous strain (assuming step load input)
ε_1^*	Steady state instantaneous strain
ε_3	Steady state rupture strain
$\varepsilon_{0\rightarrow R}$	Creep strain
$\varepsilon_{1*\rightarrow 3}$	Steady state creep strain
$\varepsilon_{1*\rightarrow R}$	Approximate creep strain
$\dot{\varepsilon}_{0\rightarrow R}$	Average creep rate
$\dot{\varepsilon}_{total}$	Total strain rate (creep tests)
η	Viscosity (visco elastic models)
λ	Ratio of instantaneous and initial specimen length L/L_0
ν	Poisson's ratio
ρ	Radius of curvature of notch or ellipse tip
ρ_C	Critical value of the tip radius
σ	Nominal stress, load normalised by initial cross-sectional area
σ_{cr}	Critical stress level (Griffith)
σ_{eff}	Effective stress, load normalised by effective area
σ_f	fracture stress (notch specimens)
σ_{fr}	fracture stress used in literature review section (notch specimens)
σ_K	Knee stress
σ_{lig}	Ligament stress
σ_{peak}	Peak stress in first loading cycle of loading-unloading test

σ_{pred} Predicted failure stress

σ_{py} Strain increase occurring between yield and fracture

σ_{tip} Tensile stress at the tip of the ellipse (Inglis equation)

σ_{true} True stress

σ_{ult} Ultimate stress (un-notch specimens)

σ_{y} Yield stress

σ_{Y} Yield stress

σ_{0} Creep stress

σ_{1} Largest principal stress

σ_{2} Intermediate principal stresses

σ_{3} Smallest principal stresses

σ_{∞} Tensile stress at a distance not effected by the hole (Inglis equation)

ψ_{R} Continuity at failure accounting for damage localisation

ψ Continuity

ω Damage 1 - ψ

GLOSSARY

Curvilinear Co-ordinates

In two dimensions the position of a set of points can be described by the intersection of two functions

$$F_1(x,y) = \xi$$

$$F_2(x,y) = \eta$$

In the general case they are referred to as curvilinear co-ordinates. In the specific case referred to as polar co-ordinates the functions are

$$F_1(x,y) = \sqrt{x^2 + y^2} = r$$

$$F_2(x,y) = \arctan\left(\frac{y}{x}\right) = 0$$

In the Cartesian co-ordinate system the functions are

$$F_1(x,y) = x$$

$$F_2(x,y) = y$$

Heaviside step function

The Heaviside or unit step function is defined as follows:

$$H(t - a) = \begin{cases} 1 & \text{if } t > a \\ 1/2 & \text{if } t = a \\ 0 & \text{if } t < a \end{cases}$$

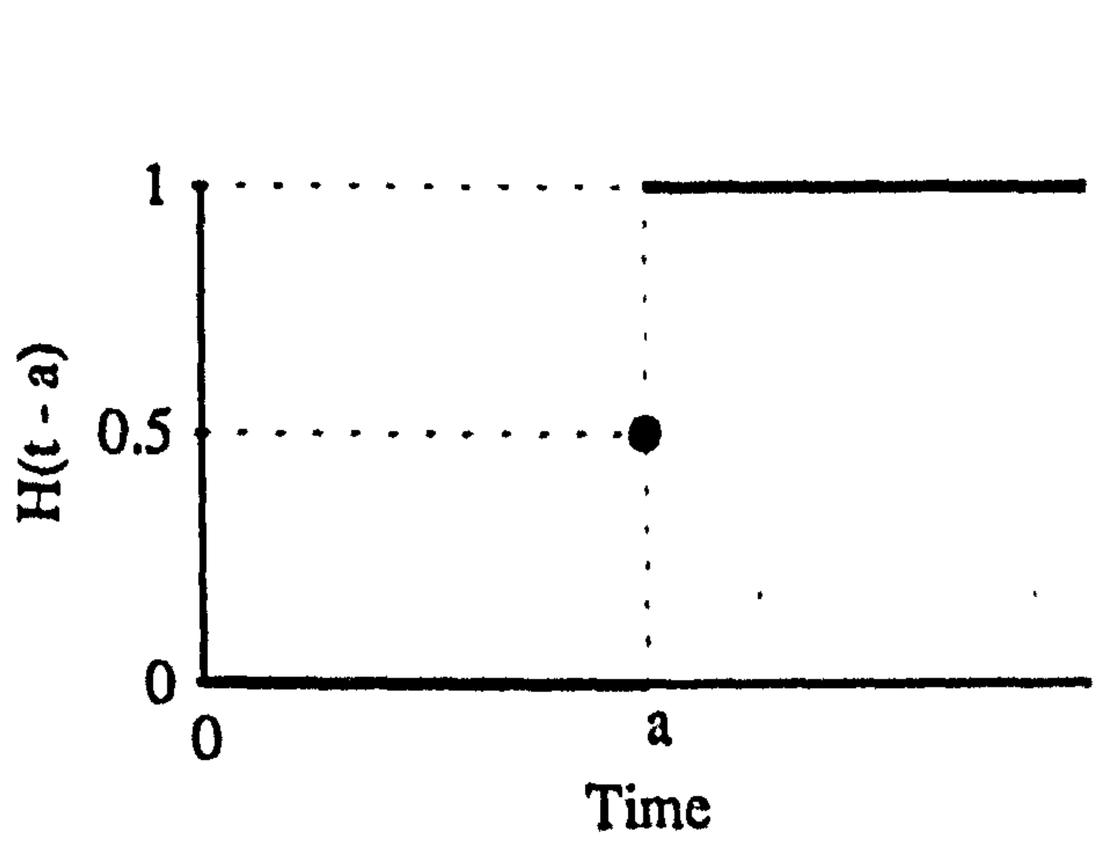

where a is an arbitrary number and t is the time. Any function f(t) multiplied by H(t - a) will have a value of zero for $t < a$, and a value of f(t) in the region $t > a$. Thus a step change in stress from $\sigma = 0$ to $\sigma = \sigma_0$ at $t = a$ may be expressed as $\sigma(t) = \sigma_0 H(t - a)$.

Tresca yield criterion

The Tresca criterion assumes that yielding occurs when the maximum shear stress, $(\sigma_1 - \sigma_3)/2$, is greater than the maximum shear stress in uniaxial tension, $\sigma_y/2$. So yielding just occurs when $\sigma_1 - \sigma_3 = \sigma_y$

Von Mises criterion

In this case the maximum shear strain energy per unit volume is assumed to be equal to that which causes yielding in uniaxial tension

$$(\sigma_1 - \sigma_2)^2 + (\sigma_2 - \sigma_3)^2 + (\sigma_3 - \sigma_1)^2 = 2\,\sigma_y^2$$

Plane stress

When a material is under conditions described as 'plane stress' the through the thickness stress in negligible compared to the other stress, i.e. $\sigma_z = \tau_{zx} = \tau_{zy} = 0$. This is approximately the situation for a thin sheet of material.

Plane strain

Plane strain assumes that the strain through the thickness of the material compared to thus in the other directions are negligible, i.e. $\varepsilon_z = \varepsilon_{zx} = \varepsilon_{zy} = 0$.

Trapezium rule

An approximation to the area under a curve is calculated by marking a series of discrete points on the curve. The whole area is calculated by summation of the amount of the required area that is contained within the trapeziums formed by lines parallel to the Y-axis passing through adjacent pairs of these points [$(x_1, y_1), (x_2, y_2)$], the line between the pair of points [$X = x_1, X = x_2$], and the X-axis [$Y = 0$]. The area being of one trapezium being

$$\frac{y_1 + y_2}{2} (x_2 - x_1)$$

In the case of the experimental data to which this rule was applied the points were paired in the order in which they were collected. Thus the influence of noise on the calculated area is limited. For example if two strain values are in the 'wrong' order then one will result in the calculation of a larger area and the other a negative one.

REFERENCES

Alexander, R. McN. (1982)
Optima for animals
Edward Arnold, London

Anderson, J. E. (1979)
Mechanical Properties of Equine Femoral Cortical Bone.
M.Sc. thesis, Clemson University.
(Cited by Rogers and Moyle (1988))

ASTM Standards E399-70T (1970)
Tentative method of test for plane-strain fracture toughness of metallic materials.
Book of ASTM Standards, Part 31, pp .911 - 927
ASTM, Philadelphia, PA.
(Cited by Wright and Hayes (1977))

ASTM Standard E399-78a (1980)
(Cited by Charalambides (1988))

Atkins, A. G. and Mai, Y. W. (1988)
Elastic and Plastic Fracture.
Ellis Horwood, Chichester.

Van Ballenberghe, V. (1983)
Growth and development of moose antlers in Alaska.
Antler Development in Cervidae.
(Edited by Brown, R. D.)
Caesar Kelberg Wildl. Res. Inst., Texas A & I University, Kingsville (in press).
(Cited by Goss (1983))

Bao, G., Hutchinson, J. W. and McMeeking, R. M. (1991)
Particle reinforcement of ductile matrices against plastic flow and creep.
Acta. Metall. Mater.. **39,** 1871-1882.

Beaumont, P. W. R. (1990)
The failure of fibre composites: an overview.
In *The Failure of Reinforced Plastics*
(Edited by Matthews, F. L.), pp. 1-17.
Mechanical Engineering Publication, Ltd., London.

Behiri, J. C. (1982)
Fracture Mechanics of Bone.
Doctoral thesis, Queen Mary College, University of London, UK.

Behiri, J. C. and Bonfield, W. (1980)
Crack velocity dependence of longitudinal fracture in bone,
J. Mater. Sci. **15,** 1841-1849.

Behiri, J. C. and Bonfield, W. (1989)
Orientation dependence of the fracture mechanics of cortical bone.
J. Biomechanics. **22,** 863-872.

Berry, J. P. (1972)
Fracture of polymeric glasses.
In *Fracture, Volume VII,*
(Edited by Liebowitz, H.), pp. 37-92.
Academic Press, New York and London.

Bonfield, W. (1981)
Mechanisms of fracture in bone.
In *Mechanical Properties of Bone*
(Edited by Cowin, S. C.), pp. 163-170.
ASME., New York.
Bonfield, W. (1987)
Advances in the fracture mechanics of cortical bone,
J. Biomechanics **20,** 1071-1081.
Bonfield, W. and Datta, P. K. (1974a)
Young's modulus of compact bone,
J. Biomechanics. **7,** 147-149.
Bonfield, W. and Datta, P. K. (1974b)
Impact fracture of compact bone in a shock tube,
J. Materials Science. **9,** 1609-1614.
Bonfield, W. and Datta, P. K. (1976)
Fracture toughness of compact bone,
J. Biomechanics. **9,** 131-134.
Bonfield, W., Grynpas, M. D. and Young, R. J. (1978)
Crack velocity and the fracture of bone,
J. Biomechanics. **11,** 473-479.
Bonfield, W. and Li, C. H. (1966)
Deformation and fracture of bone,
J. Applied Physics **37,** 869-875.
Bonfield, W. and O'Connor, P. (1978)
Anelastic deformation and friction stress of bone,
J. Mater. Sci. **13,** 202-207.
Brown, W. and Srawley, J. (1966)
Plane strain crack testing of high strength metallic materials,
Spec. Publ. No. 410, ASTM. Philadelphia.
(Cited by Bonfield and Datta (1976), see below)
Brown, W. and Srawley, J. (1966)
Plane strain crack toughness testing of high strength material,
Spec. Publ. No. 410, ASTM. Philadelphia.
(Cited by Charalambides (1988) see above)
BS 5447. (1977)
Methods of tests for plain strain fracture toughness (K_{IC}) of metallic materials.
British Standards Institution, London.
BS 5762. (1979)
Crack opening displacement (C.O.D.) testing.
British Standards Institution, London.
BS 4618. (1970)
Recommendations for the presentation of plastics design data.
British Standards Institution, London.
Bubenik, A. B. (1983)
The behavioural aspects of antlerogenesis.
Antler Development in Cervidae (Edited by Brown, R. D.), pp. 389-449.
(Cited by Watkins (1987))
Bundy, K. J. (1989)
Composite Material Models For Bone.
Bone Mechanics. (Edited by Cowin, S. C.), pp. 197-210.
CRC Press, Inc. Boca Raton, Florida.

Burdekin, F. M. and Stone, D. E. W. (1966)
The crack opening displacement approach to fracture mechanics in yielding.
J. Strain Analysis. **1,** 145-153.
Burr, D. B. and Stafford T. (1990)
Validity of the bulk-staining technique to separate artifactual from in vivo bone microdamage.
Clinical Orthopaedics and Related Research. **260,** 305-308.
Burstein, A. H., Currey, J. D., Frankel, V. H. and Reilly, D. T. (1972)
The ultimate properties of bone tissue: The effects of yielding,
J. Biomechanics **5,** 35-44.
Burstein, A. H., Reilly, D. T. and Frankel, V. H. (1973)
Failure characteristics of bone and bone tissue.
In *Perspectives in Biomedical Engineering*
(Edited by Kenedi, R. M.), pp. 131-134.
Macmillan, London.
Caler, W. E. and Carter, D. R. (1989)
Bone creep-fatigue damage accumulation,
J. Biomechanics **22,** 625-635.
Carter, D. R. and Caler, W. E. (1983)
Cycle-dependent and time-dependent bone fracture with repeated loading.
J. Biomech. Eng. **105,** 166-170.
Carter, D. R. and Caler, W. E. (1985)
A cumulative damage model for bone fracture.
J. Orthop. Res. **3,** 84-90.
Carter, D. R., Hayes, W. C. (1976)
Fatigue life of compact bone-I. Effects of stress amplitude, temperature and density.
J. Biomechanics. **9,** 27-34.
Carter, D. R. and Hayes, W. C. (1977a)
Compact bone fatigue damage: a microscopic examination.
Clinical Orthopaedics and related research. **10,** 325-337.
Carter, D. R. and Hayes, W. C. (1977b)
Compact bone fatigue damage-I. Residual strength and stiffness.
J. Biomechanics. **10,** 325-337.
Carter, D. R., Hayes, W. C. and Schurman, D. J. (1976)
Fatigue life of compact bone-II. Effects of microstructure and density.
J. Biomechanics. **9,** 211-218.
Cartwright, A. G. (1975)
The effect of histological variation on the tensile strength of cortical bone.
Biomedical Engineering. **10,** 442-446.
Chapman, D. I. (1975)
Antlers-bone of contention.
Mammal Rev.. **5,** 121-172.
Chapman, D. I. (1981)
Antlers structure and function - a hypothesis.
J. Biomechanics. **14,** 195-197.
Charalambides, B. (198*)
Comparison of Fracture in Cortical Bone and Analogue Composites.
Doctoral. thesis, Queen Mary College, University of London, UK.

Clutton-Brock, T. H., Albon, S. D., Gibson, R. M. and Guinness, F. E. (1979)
The logical stag: adaptive aspects of fighting in red deer (*Cervus elaphus* L.).
Animal Behaviour. **27**, 211-225.
(Cited by Putman (1988))

Clutton-Brock, T. H. and Albon, S. D. (1980)
Antlers, body size and breeding group size in the cervidae.
Nature. **285**, 565-567.

O'Connor, P. (1976)
Deformation and Fracture Behaviour of Compact Bone.
Doctoral thesis, Queen Mary College, University of London, UK.

Conway, J. B. (1967)
Numerical Methods for Creep and Rupture Analysis,
Gordon and Breach, New York.

Crowninshield, R. D. and Pope, M. H. (1974)
The response of compact bone in tension at various strain rates
Annals of Biomedical Engineering **2**, 217-225.

Currey, J. D. (1960)
Differences in the blood-supply of bone of different histological type.
Quarterly Journal of Microscopical Science. **101**, 351-370.

Currey, J. D. (1962)
Stress concentrations in bone.
Quarterly Journal of Microscopical Science. **103**, 111-133.

Currey, J. D. (1965)
Anelasticity in bone and echinoderm skeletons,
J. Exp. Biol.. **43**, 279-292.

Currey, J. D. (1975)
The effects of strain rate, reconstruction and mineral content on some mechanical properties of bovine bone,
J. Biomechanics **8**, 81-86.

Currey, J. D. (1977)
Mechanical properties of mother of pearl in tension,
Proc. R. Soc. Lond. B., **196**, 443-463.

Currey, J. D. (1979a)
Mechanical properties of bone tissues with greatly differing functions,
J. Biomechanics **12**, 313-319.

Currey, J. D. (1979b)
Changes in the Impact Energy Absorption of Bone with Age,
J. Biomechanics **12**, 459-469.

Currey, J. D. (1981)
What is bone for ? Property - function relationships in bone.
In *Mechanical Properties of Bone*.
(Edited by Cowin, S. C.), pp. 13-26.
ASME, New York.

Currey, J. (1984a)
The Mechanical Adaptations of Bone.
Princeton University Press, New Jersey.

Currey, J. D. (1984b)
Effects of differences in mineralization on the mechanical properties of bone.
Phil. Trans. R. Soc. Lond. B. **304**, 509-518.

Currey, J. D. (1988a)
The effect of porosity and mineral content on the Young's modulus of elasticity of compact bone,
J. Biomechanics **21,** 131-139.

Currey, J. D. (1988b)
The effects of drying and re-wetting on some mechanical properties of cortical bone.
J. Biomechanics **5,** 439-441.

Currey, J. D. (1988c)
Strain rate and mineral content in fracture models of bone.
J. Orthop. Res. **6,** 32-38.

Currey, J. D. (1989)
Strain rate dependence of the mechanical properties of reindeer antler and the cumulative damage model of bone fracture,
J. Biomechanics **22,** 469-475.

Currey, J. D. (1990)
Physical characteristics affecting the tensile failure properties of compact bone,
J. Biomechanics **23,** 837-844.

Currey, J. D. and Brear, K. (1974)
Tensile yield in bone,
Calc. Tiss. Res. **15,** 173-179.

Currey, J. D. and Brear, K. (1992)
Fractal analysis if compact bone and antler fracture surfaces,
Biomimetic **1,** 103-118.

Currey, J. D., Unsworth, A. and Hall, D. A. (1981)
Properties of bone, cartilage, and synovial fluid: A bone.
In *Introduction to the Biomechanics of Joints and Joint Replacement.*
(Edited by Dowson, D. and Wright, V.), pp. 103-107.
Mechanical Engineering Publications Ltd., London.

Duck, F. A. (1990)
Physical Properties of Tissue, A Comprehensive Reference Book.
Academic Press, London.

Dunne, F. P. E., Othman, A. M., Hall, F. R. and Hayhurst, D. R. (1990)
Representation of uniaxial creep curves using continuum damage mechanics.
Int. J. Mech. Sci. **32,** 945-957.

McElhaney, J. H. and Byars, E. F. (1965)
Dynamic response of biological materials
ASME 65-WA/HUF-9
(Cited by Burstein *et al.* (1973))

Evans, F. G. (1957)
Stress and Strain in Bones.
Charles C Thomas, Springfield.

Evans, F. G. (1958)
Relations between the microscopic structure and the tensile strength of human bone
Acta Anat. **35,** 285.
(Cited by Burstein *et al.* (1973))

Evans, F. G. (1973)
Mechanical Properties of Bone.
Charles C Thomas, Illinois.

Ewalds, H. L. and Wanhill, R. J. H. (1986)
Fracture Mechanics.
Edward Arnold, London.
Felbeck, D. K. and Atkins, A. G. (1984)
Strength and Fracture of Engineering Solids.
Prentice-Hall, New Jersey.
Findley, W., Lai, J. S. and Onaran, K. (1989)
Creep and Relaxation of Nonlinear Viscoelastic Materials: With an Introduction to Linear Viscoelasticity.
Dover Publications, Inc., New York.
Fischer, R. A., Arms, S. W., Pope, M. H. and Seligson D. (1986)
Analysis if the effect of using two different strain rates on the acoustic emission in bone.
J. Biomechanics. **19,** 119-127.
Flügge, W. (1975)
Viscoelasticity.
Springer-Verlag, Berlin.
Fondrk, M., Bahniuk, E., Davy, D. T. and Michaels C. (1988)
Some viscoplastic characteristics of bovine and human cortical bone.
J. Biomechanics. **21,** 623-630.
Freudenthal, A. M. (1950)
The Inelastic behaviour of Engineering Materials and Structures.
Chapman and Hall, London.
Gordon, J. E. (1976)
The New Science of Strong Materials :or Why You Don't Fall Through the Floor.
Penguin Books Ltd, Harmondsworth.
Gordon, J. E. (1978)
Structures: or Why Things Don't Fall Down.
Penguin Books Ltd, Harmondsworth.
Goss, R. J. (1983)
Deer Antlers: Regeneration Function, and Evolution.
Academic Press, New York.
Griffith, A. A. (1920)
The phenomena of rupture and flow in solids.
Proc. Roy. Soc. A. **221,** 163-198.
Griffith, A. A. (1924)
(Title not known)
In *Proceedings of the 1st International Congress for Applied Mechanics, Delft, 1924.*
(Edited by Biezeno, C. B. and Burgers, J. M.), p. 55.
J. Waltman, Jr., Delft, Holland
(Cited by Berry (1972))
Harris, B., Dorey, S. E. and Cooke, R. G. (1988)
Strength and toughness of fibre composites.
Comp. Sci. Technol. **31,** 121-141.
Harris, D. O. (1967)
J. bas. Engng. **89,** 49.
(Cited by Rooke and Cartwright (1976))
Hayhurst, D. R., Brown, P. R. and Morrison, C. J. (1984)
The role of continuum damage in creep crack growth,
Phil. Trans. R. Soc. Lond. A., **311,** 131-158.

Henshaw, J. (1971)
Antlers-the unbrittle bones of contention.
Nature. **231,** 469.
Hodgskinson, R. A. G. (1991)
High Resolution Imaging of the Apatite Phase in Bone Tissue.
Doctoral thesis, Queen Mary and Westfield College, University of London, UK.
Hoff, N. (1953)
The necking and rupture of rods, subjected to constant tensile loads
J. Appl Mech.. **20,** 1
(Cited by Kachanov (1960))
Honeycombe, R. W. K. (1981)
Steels Microstructure and Properties.
Penguin Books Ltd, Harmondsworth.
Howard, I. C. and Found, M. S. (1986)
Size effects in the fracture of notched fibre-reinforced plastics.
In *Size Effects In Fracture.*
pp. 17-24.
Mechanical Engineering Publications Limited, London.
Howatson, A. M., Lund, P. G. and Todd, J. D.
Engineering Tables and Data
Chapman and Hall, London
Hull, D (1981)
An Introduction to Composite Materials.
Cambridge University Press, Cambridge.
Hülsen, K. K. (1896)
Specific gravity, resilience and strength of bone.
Bull. Biol Lab (St Petersburg), **1,** 7-35
(Cited by Evans(1973))
Inglis, C. E. (1913a)
Stresses in a plate due to the presence of cracks and sharp corners.
Trans. Inst. Naval Architects. **55,** 219-230
Inglis, C. E. (1913b)
Stresses in a plate due to the presence of cracks and sharp corners.
Engineering. **95,** 415-
(Report of meeting at which he presented this paper.)
Irwin, G. R. (1948)
Fracturing of Metals.
Cleveland, Ohio: ASM
(Cited by Stevens and Guiu (1991))
Irwin, G. R. (1957a)
Analysis of stresses and strains near the end of a crack traversing a plate.
J. Appl. Mech. **24,** 361-364
Irwin, G. R. (1957b)
Proc. 9th Int. Congr. Appl. Mech.. **VIII,** Paper 101(II),
University of (Brussels), Brussels
(Cited by Atkins and Mai (1988))
Kachanov, L. M. (1958)
Time of fracture process under creep.
Izv. Akad. Nauk. SSSR. Otd. Teck. Nauk. **8,** 26-31
(In Russian)

Kachanov, L. M. (1960)
The Theory of Creep.
Nauka, Moscow.
(Translation by Kennedy (Ed.), National Lending Library, Boston Spa, 1967)
Kachanov, L. M. (1986)
Introduction to Continuum Damage Mechanics.
Kluwer Academic Publishers, Dordrecht.
Katz, J. L. (1971)
Hard tissue as a composite material: I, bounds on the elastic behaviour
J. Biomechanics. 4, 455.
(Cited by Burstein *et al.* (1975))
Katz, J. L. (1980a)
Anisotropy of Young's modulus of bone.
. *Nature.* 283, 106-107.
Katz, J. L. (1980b)
The structure and biomechanics of bone.
In *The Mechanical Properties of Biological Materials*
Symposia of the Society for Experimental Biology, XXXIV
Cambridge University Press, Cambridge.
Katz, J. L. (1981)
Composite material models for cortical bone.
In *Mechanical Properties of Bone.*
(Edited by Cowin, S. C.), pp. 171-184.
ASME, New York.
Kitchener, A. C. (1991)
The evolution and mechanical design of horns and antler.
In *Biomechanics in Evolution.*
(Edited by Rayner, J. M. V. and Wootton, R. J.), pp. 229-253.
Cambridge University Press, Cambridge.
Knets, I. V. and Melnis, A. E. (1982)
Peculiarities of the Fracture of Dry and Wet Compact Bone Tissue.
In *Fracture of Composite Materials.*
(Edited by Sih, G. C. and Tamuzs, V. P.), pp. 451-463.
Martinus Nijhoff, The Hague.
Knott, J. F. (1973)
Fundamentals of Fracture Mechanics.
Butterworths, London.
Koenczoel, L., Hilitner, A and Baer, E. (1986)
Crazing and fracture in polystyrene studied by acoustic emission,
J. Appl. Phys.. 60, 2651-2654.
Kolossof, G. (1909)
Doctoral Thesis, Dorpat
(Cited by Timoshenko and Goodier (1982))
Krajcinovic, D. (1984)
Continuum Damage Mechanics,
Applied Mechanics Reviews. 37, 1-6.
Krajcinovic, D., Trafimow, J. and Sumarac, D. (1987)
Simple constitutive model for a cortical bone.
J. Biomechanics. 20, 779-784.
Kraus, H. (1980)
Creep Analysis.
John Wiley and Sons, New York.

Lanyon, L. E., Goodship, A. E. and Bagott, D. G. (1976)
The significance of bone strain (in vivo).
Acta. Orthop. Belg., **42**, suppl. I, 109-123.
Lakes, R. S. and Katz, J. L. (1984)
Viscoelastic properties of bone.
In *Natural and living Biomaterials.*
(Edited by Hastings, G. W. and Ducheyne, P.), pp. 61-87.
C.R.C. Press, Florida.
Lakes, R. S., Nakamura, S., Behiri, J. C. and Bonfield, W. (1990)
Fracture mechanics of bone with short cracks.
J. Biomechanics. **23**, 967-975.
Leckie, F. A. and Hayhurst, D. R. (1974)
Creep rupture of structures.
Proc. R. Soc. Lond. A. **340**, 323-347.
Lees, S. (1982)
Ultrasonic measurements of deer antler, bovine tibia and tympanic bulla.
J. Biomechanics **15**, 867-874.
Lincoln, G. A. (1992)
Biology of antlers,
J. Zool., Lond. **226**, 517-528.
Lorrain, M. and Loland, K. E. (1983)
Damage theory applied to concrete.
In *Fracture Mechanics of Concrete*
(Edited by Wittmann, F. H.), pp. 341-369.
Elsevier, Amsterdam.
Martin, B. R. and Burr, D. B. (1989)
Structure, Function, and Adaptation of Compact Bone.
Raven Press, New York.
Martin, R. B. and Ishida, J. (1989)
The relative effects of collagen fibre orientation, porosity, density, and mineralization on bone strength,
J. Biomechanics **22**, 419-426.
Martin, R. B. (1991)
Determinants of the mechanical properties of bones.
J Biomechanics. **24**, 79-88.
Martin, R. B. (1992)
A theory of fatigue damage accumulation and repair in cortical bone.
J Orthopaedic Research. **10**, 818-225.
Mauch, M., Currey, J. D. and Sedman, A. J. (1992)
Creep fracture in bones with different stiffnesses,
J. Biomechanics **25**, 11-16.
Melvin, J. W. and Evans, F. G. (1973)
Crack propagation in bone,
ASME Biomaterials Symposium, Detroit, 87-89
Messerer, O. (1880)
Über Elastizität und Festigkeit der menschlichen Knochen.
J. G. Cotta'sche Buchhandlung, Stuttgart.
(Cited by Roesler (1987))
Milne, A. A. (1928) (14th edition used 1941)
Winnie-the-Pooh.
Methuen and Co. Ltd., London.

Milne, A. A. (1974)
The House at Pooh Corner.
McClelland and Stewart Ltd., Toronto.
Moyle, D. D. and Bowden, R. W. (1984)
Fracture of human femoral bone,
J. Biomechanics **17**, 203-213.
Moyle, D. D., Cooke F. W. and Welborn, J. W. (1975)
Fracture toughness of canine bone,
Proc. 28 ACEMB. 173
Moyle, D. D. and Gavens, A. J. (1986)
Fracture properties of bovine tibial bone,
J. Biomechanics **19**, 919-927.
Moyle, D. D., Welborn, J. W. and Cooke, F. W. (1978)
Work to fracture of canine femoral bone,
J. Biomechanics **11**, 435-440.
Murakami, S. (1990)
A continuum mechanics theory of anisotropic damage..
In *Yielding, Damage, and Failure of Anisotropic Solids.*
(Edited by Boehler, J. P.), pp. 465-482.
Mechanical Engineering Publications, London.
Nash, C. D. (1966)
Fatigue of self-healing structures: a generalised theory of fatigue failure
ASME 66-WA/BHF-3
Newaz, G. M. and Walsh, W. J. (1989)
Interrelationship of damage and strain in particulate composites,
Journal of Composite Materials. **23**, 326-336.
Norman, T. L., Vashishth, D. and Burr, D. B. (1992)
Effect of groove on bone fracture toughness,
J. Biomechanics **25**, 1489-1492.
Odqvist, F. K. G. (1966)
Mathematical Theory of Creep and Creep Rupture.
Oxford University Press, Oxford.
Orowan, E. (1952)
In *Fatigue and Fracture of Metals*
(Edited by Murray, W. M.), p 139.
John Wiley, London.
(Cited by Stevens and Guiu (1991)
Pattin, C. A., Carter, D. R. and Caler, W. E. (1990)
Cortical bone modulus reduction in tensile and compressive fatigue
36th Annual meeting of the Orthopaedic Research Society
New Orleans, Louisiana
Pattin, C. A. (1993)
Crack closure estimation
39th Annual meeting of the Orthopaedic Research Society
San Francisco, California
Piekarski, K. (1970)
Fracture of bone
J. Applied Physics. **41**, 215-223.
Piekarski, K. (1973)
Analysis of bone as a composite material.
Int. J. Engng. Sci. **11**, 557-565.

Piekarski, K. (1978)
Structure, Properties and Rheology of Bone.
In *Orthopaedic mechanics, procedures and devices*
(Edited by Ghista, D. N.), pp. 1-20.
Academic Press, London.
Piekarski, K. (1984)
Fractography of bone.
In *Natural and Living Biomaterials,*
(Edited by Hastings, G. W. and Ducheyne, P.), pp. 99-117.
C.R.C. Press, Florida.
Pope, M. H. and Outwater, J. O. (1972)
The fracture characteristics of bone substance,
J. Biomechanics **5,** 457-465.
Powell, P. C. (1983)
Engineering With Polymers
Chapman and Hall, London.
Purslow, P. (1991)
Notch-sensitivity of non-linear materials.
J. Mater. Sci. **26,** 4468-4476.
Putman, R. (1988)
The Natural History of Deer.
Christopher Helm, London.
Rabotnov, Yu, N. (1980)
Elements of Hereditary Solid Mechanics.
Mir, Moscow.
(Cited by Fondrk *et al.* (1988))
Rajaram, A. and Ramanathan, N. (1982)
Tensile properties of Antler bone,
Calcif. Tissue. Int. **34,** 301-305.
Rauber, A. A. (1876)
Über Elastizität und Festigkeit der Knochen.
Wilhelm Engelmann, Leipzig.
(Cited by Roesler (1987))
Reilly, D. T. and Burstein, A H. (1975)
The elastic and ultimate properties of compact bone tissue,
J. Biomechanics **8,** 393-405.
Rimnac, C. M., Petko, A. A., Santner, T. J. and Wright, T. M. (1993)
The effect of temperature, stress and microstructure on the creep of compact bovine bone,
J. Biomechanics **26,** 219-228.
Robertson, D. M., Robertson, D. and Barrett, C. R. (1978)
Fracture toughness, critical crack length and plastic zone size in bone,
J. Biomechanics **11,** 359-364.
Roesler, H. (1987)
The history of some fundamental concepts in bone biomechanics,
J. Biomechanics **20,** 1025-1034.
Rogers, L. L. and Moyle, D. D. (1988)
Effect of specimen size on work-of-fracture measurements,
J. Biomechanics **21,** 919-926.
Rooke, D. P. and Cartwright, D. J. (1976)
Compendium of Stress Intensity Factors,
Her Majesty's Stationary Office, London.

Sarkhar, B. C. and Chauhan, U. P. S. (1967)
A new method for the determining micro quantities of calcium in biological materials,
Anal. Biochem. **20,** 155-156.
(Cited by Currey (1988c))
Schulte, K. (1986)
Fatigue damage development in carbon fibre reinforced composites
In *Fatigue of Engineering Materials and Structures Volume II*
Proceedings of the Institution of Mechanical Engineers
Mechanical Engineering Publications, London.
Sedlin, E. D. (1965)
A rheological model for cortical bone.
Acta Orthop Scand. **36,** Sup 83.
Sedman, A. J., Currey, J. D. and Zioupos, P. (1992)
Optical Changes as an Indicator of Mechanical Damage in Bone and Antler.
VIII Meeting of the European Society of Biomechanics
Rome, Italy.
Sedman, A. J., Currey, J. D. and Zioupos, P. (1993)
Optical Changes as an Indicator of Mechanical Damage in Bone and Antler.
J. Biomechanics **26,** 777.
(Short abstract of Sedman *et al.* (1992))
Sih, G. C., Paris, P. C. and Irwin, G. R. (1965)
On cracks in rectilinear anisotropic bodies,
Int. J. Fracture. Mech. **1,** 189-202.
(Cited by Wright and Hayes (1977))
Silva, F. C. and Fortes, A. M. (1987)
Compartmento a fracturea de osso compacto da tibia de boi,
Mareriais 87 - 3 Encontro nacional da Sociedade Portugesa de Materiais,
pp. 345-357.
(Cited by Bonfield (1987))
Smith, J. W. (1960)
Collagen fibre patterns in mammalian bone,
J. Anat. **94,** 329-344.
(Cited by Carter *et al.* (1976))
Smith, R. N. L. (1991)
BASIC fracture mechanics,
Butterworth-Heinemann, Oxford.
Stevens, R. N. and Guiu. (1991)
Energy balance concepts in the physics of fracture,
Proc. R. Soc. Lond. A. **435,** 169-183.
Tanabe, Y., Tanaka. S., Samamoto, M. and Hara, T. (1991a)
The evaluation of mechanical properties of bone under compressive impact loading.
Proc, 44th Japan Congress on Materials Research. 233-237.
Tanabe, Y., Tanaka. S., Samamoto, M. and Hara, T. (1991b)
Determination of a viscoelastic model of bone.
Proc, 40th Japan National Congress for Applied Mechanics 1990. 259-266.
Tanabe, Y., Tanaka. S., Samamoto, M., Hara, T., Takahashi, H. and Koga, Y. (1991c)
Influence of loading rate on anisotropy of compact bone.
J. De Physique. 4, C3.305-C3.310.

Tattersall, H. G. and Tappin, G. (1966)
The work of fracture and its measurement in metals, ceramics and other materials,
J. Mater. Sci. **1**, 296-301.
Tennyson, R. C., Ewert. R. and Niranjan, V. (1972)
Dynamic viscoelastic response of bone.
Experimental Mechanics. **12**, 502-507.
Timoshenko, S. P. (1953)
History of Strength of Materials,
McGraw-Hill, New York.
Timoshenko, S. P and Goodier, J. N. (1982)
Theory of Elasticity,
McGraw-Hill, London.
Tortora, G. J. and Anagnostakos, N. P. (1987)
Principles of Anatomy and Physiology,
Harper and Row, New York.
Tse, A., Shin. E., Hiltner, A. and Baer, E. (1991)
The stress-whitened damage zone of PVC blends.
J. Mater. Sci. **26**, 2823-2832.
Turner, I. G. (1981)
A Study of the Spatial Organization of the Mineral Component in Bone.
Doctoral. thesis, University College of Swansea, UK.
Viano, D. C. (1986)
Biomechanics of bone and tissue: A review of material properties and failure characteristics.
Proceedings - Society of Automotive Engineers. **P-186**, 33-63.
Watkins, M. R. (1987)
The Development of a Tough Artificial Composite Based on Antler Bone.
Doctoral thesis, University of Reading, UK.
Weiss, V. and Yukawa, S. (1964)
Critical appraisal of fracture mechanics.
In *Fracture Toughness Testing and its Applications: a symposium presented at the sixty-seventh annual meeting of ASTM*, pp. 1-22.
ASTM, Philadelphia
Wertheim, M. G. (1847)
Mémoite sur l'élasticité et la cohésion des principeaux tissues du corps humaine.
Annls Chim. Phys. **21**, 385-453
(Cited by Roesler (1987) after Evans, (1957))
Williams, J. G. (1990)
Fracture mechanics of composites failure,
Proc. Instn. Mech. Engrs. **C204**, 209-218.
Wintringham, C. (1740)
An Experimental Inquiry on some parts of the Animal Structure,
J Walthoe, London.
Wolff, J. (1892)
Die Lehre von der funktionellen Knochengestalt
Virchows Arch. path. Anat. Physiol. **155**, 256-315.
(Cited by Roesler (1987))
Wood, J. L. (1970)
Tensile Properties of Bone at High Strain Rates
ASTM 70-WA/BHF-10
ASTM, New York

Wood, J. L. (1971)
Dynamic Response of Human Cranial Bone,
J. Biomechanics **4**, 1-12.
Wright, T. M. and Hayes, W. C. (1976)
Tensile testing of bone over a wide range of strain rates: effects of strain rate, microstructure and density.
Medical and Biological Engineering. **14**, 671-680.
Wright, T. M. and Hayes, W. C. (1977)
Fracture mechanics parameters for compact bone - effects of density and specimen thickness,
J. Biomechanics **10**, 419-430.
Wright, T. M., Vosburgh, F. and Burstein, A. H. (1981)
Permanent deformation of compact bone monitored by acoustic emission.
J. Biomechanics. **14**, 405-409.